ORNL-3176
UC-4 – Chemistry

CHEMISTRY DIVISION

ANNUAL PROGRESS REPORT

FOR PERIOD ENDING JUNE 20, 1961

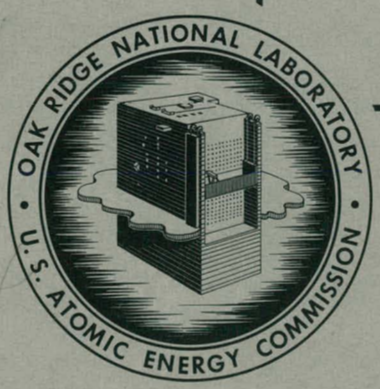

OAK RIDGE NATIONAL LABORATORY
operated by
UNION CARBIDE CORPORATION
for the
U.S. ATOMIC ENERGY COMMISSION

DISCLAIMER

Printed in USA. Price $2.50. Available from the

Office of Technical Services
Department of Commerce
Washington 25, D.C.

ORNL-3176
UC-4 – Chemistry

Contract No. W-7405-eng-26

CHEMISTRY DIVISION ANNUAL PROGRESS REPORT

for Period Ending June 20, 1961

E. H. Taylor, Director
M. A. Bredig, Associate Director

DATE ISSUED

OCT 10 1961

OAK RIDGE NATIONAL LABORATORY
Oak Ridge, Tennessee
operated by
UNION CARBIDE CORPORATION
for the
U. S. ATOMIC ENERGY COMMISSION

THIS PAGE

WAS INTENTIONALLY

LEFT BLANK

SUMMARY

1. NUCLEAR CHEMISTRY

Upper limits were measured for the thermal-neutron-capture cross sections of Po^{210} to form the isomers 0.52-sec Po^{211} and 27-sec Po^{211} as 30 and 0.5 mb respectively. The low cross section of Po^{210} can be understood on the basis of the closed shell of 126 neutrons and the energetics and spin states of the system.

By irradiating samples of U^{233} with neutrons and measuring the U^{234} formed mass-spectrographically, the thermal cross section and resonance integral for capture were measured directly. Together with the resonance integral for fission, a value of α for epithermal neutrons is reported as $\alpha_{epi}(U^{233}) = 0.170$.

A program was written for the IBM 7090 computer to calculate the reaction rate and effective cutoff energy E_c for a $1/v$ absorber inside a spherical, cylindrical, or double-slab filter containing boron, cadmium, gadolinium, or samarium. Results to data indicate that effective cadmium cutoffs are very nearly independent of the lower limit of the $1/E$ flux; that gadolinium filters afford lower cutoffs but are less efficient than cadmium filters.

The thermal-neutron-capture cross section and capture resonance integral of Ce^{144} were found to be 0.96 ± 0.1 and 2.6 ± 0.2 barns.

The nuclide Re^{184} was shown to have a long-lived isomeric state and to decay with half-lives of 33 ± 4 and 169 ± 9 days. A decay scheme is proposed, based primarily on single-crystal and coincidence measurements with NaI spectrometers.

New light was shed on the level structure of Ge^{74} by studying the radiations of As^{74} using single-crystal and coincidence scintillation spectrometry. A new half-life of 17.74 ± 0.05 days was obtained for As^{74}.

Rapid radiochemical separations of Zr, Nb, and Mo from thermal-neutron-irradiated solutions of U^{235} gave evidence for a previously unreported $\sim$10-sec activity, which is a precursor of fission product Mo^{99} and is probably due to an isomer of Nb^{99}. If this is true, the data obtained indicate a fractional cumulative yield of 0.96 ± 0.21 for Nb^{99}, and imply that a suggested effect of the 50-proton shell on fission-yield distributions may not be great.

The ranges of 2.736-Mev tritons produced by the reaction $Li^6(n, \alpha)H^3$ were measured in xenon, krypton, nickel, argon, aluminum, air, nitrogen, and polystyrene. Values of range and energy loss were obtained for triton energies up to 2.7 Mev.

The conceptual design of a "three-dimensional" pulse-height analyzer for storing information from coincidence experiments is described. A ferrite core memory with 20,000 channels, with a storage capacity of $(10^6 - 1)$ counts per channel, is arranged into a basic 200×100 channel sorting and storage array.

The precision attained in beta-ray polarization measurements was increased as a result of alterations in experimental equipment. The longitudinal polarization of P^{32} beta rays at 615.6 kev was found to be $(98.8 \pm 0.9)\%$ of the theoretical value, $-v/c$.

2. ISOLATION AND CHEMICAL PROPERTIES OF SYNTHETIC ELEMENTS

Isopiestic vapor-pressure measurements on aqueous solutions of $NaClO_4$, $NaTcO_4$, and $NaReO_4$ over the concentration range 0.1 to 5.2 m showed that the latter two salts behaved as strong electrolytes, as was expected. The sequence of the computed molal osmotic coefficients was $NaClO_4 > NaTcO_4 > NaReO_4$ at all concentrations.

Absorption bands or groups of absorption bands of ReX_6^{2-} and TcX_6^{2-} ions (X = F, Cl, Br, I) were assigned to certain energy levels expected to arise from a ligand field of octahedral symmetry surrounding the Re^{4+} or Tc^{4+}. However, the numbers of bands in two of the groups give evidence for a ligand field of lower than cubic symmetry. The fundamental crystal-field splittings, $10Dq$, are linear functions of the atomic number of the halogen for each of the ReX_6^{2-} and TcX_6^{2-} complex ions.

Two equilibria were demonstrated to be involved in the reduction by stannous sulfate of heptavalent rhenium in concentrated sulfuric acid to hexavalent rhenium. The hexavalent rhenium is present as a monomer and a dimer, with

$$K_1 = \frac{[\text{dimer}]}{[\text{monomer}]^2} = 140 .$$

The hexavalent rhenium also disproportionates into penta- and heptavalent rhenium:

$$K_2 = \frac{[\text{Re(V)}]\,[\text{Re(VII)}]}{[\text{Re(VI)}_{\text{monomer}}]^2} = 3.1 .$$

The calculated spectra of the hexavalent monomer and dimer are presented for the spectral range 4000 to 8000 A.

3. CHEMICAL SEPARATION OF ISOTOPES

Ion exchange studies were made in nonaqueous solvents to compare these systems with aqueous systems previously examined. Rates of swelling of resins in organic solvents, rates of exchange of alkali-metal ions between salts dissolved in the solvents and ions on cationic resins, and distribution coefficients were measured. The water contents of Decalso exchangers and Dowex 50-X16 in the NH_4^+, Li^+, and K^+ forms were also compared.

Characterization of BF_3–organic complexes continued. Single-stage separation factors, BF_3 solubility, and vapor pressures of selected complexes were studied. Labeled complexes of B^{10} and B^{11} were prepared for infrared and Raman spectral studies.

The separation factor for oxygen isotopes in the gas/liquid system paraldehyde-acetaldehyde is 1.017 ± 0.002 at 26°C.

The single-stage separation factor for oxygen isotopes (O^{18}/O^{16}) for the dimethyl ether–HCl system was found to be 1.004 at –32°C, with O^{18} enriching in the liquid phase. The vapor pressure and the extent of dissociation of the complex were also studied.

Nitrogen isotope separation with $(CH_3)_4N{\cdot}Hg$ vs $(CH_3)_4N^+$ and NO vs $K_2SO_3(NO)_2$ was not possible because of unstable systems. Gaseous NO did not exchange with the NO in $(C_2H_5)_2NH_2^+$-$(C_2H_5)_2N(NO)_2^-$.

Exchange of calcium between calcium amalgam and aqueous calcium formate gave a separation factor of 1.0013 per mass unit. The solubility of calcium in mercury and the heat of reaction were determined.

More than 70 g of 95 to 99% N^{15} were separated in the Nitrox cascade. Operation of this facility was suspended until a need for additional N^{15} develops.

Construction of the O^{17} cascade was completed during fiscal year 1961. Preoperational testing of the water distillation cascade is nearing completion. Productive operation is expected to begin soon.

A nuclear-magnetic-resonance structural study of alkyl carbamates is in progress. A number of configurations were eliminated and some tentative structures assigned. No single structure seems to apply to all the species studied.

The observation of the infrared and Raman spectra of the boron trifluoride–dimethyl ether complex was continued with the use of B^{10} and B^{11}, and deuterated molecules were prepared. Isotopic partition-function ratios for various nitrogen-containing molecules and ions were calculated. A general computer program for computing the vibrational force constants for molecules containing up to 15 atoms was written. The mass spectrum of N_2O was studied, using various N^{15}-containing species.

Boron trifluoride samples were analyzed mass-spectrometrically by peak-height measurements at masses 10 and 11 and also at 48 and 49. Samples of CO, CO_2, N_2, and O_2 were assayed by dual collection. Two test samples of CO_2 were compared over a period of several months and showed a ratio of 46/44 ratios of 1.0155 ± 0.0002 at the 95% confidence level.

4. RADIATION CHEMISTRY

Radiation yields from deuterated silica gel exchange with methane and with hydrogen were determined as a function of gel pretreatments, reaction temperature, and purity. The results suggest a charge-transfer mechanism initiated by ions formed in the gel. Thermoluminescence studies were initiated.

Rates and activation energies for hydrogen-deuterium exchange and formic acid decomposition were measured on a series of doped germanium

catalysts covering the range from highly *p*- to highly *n*-type.

The radiolytic stability of the alkali-metal bromates toward Co^{60} gamma rays was found to decrease from $LiBrO_3$ to $CsBrO_3$, to increase only slightly with temperature between −195 and 85°C, and, for $CsBrO_3$, to be almost independent of the dose rate for a change in this variable of nearly two orders of magnitude. The initial 100-ev yields for the decomposition of bromate ion appeared to increase exponentially with the "free space" in the crystal. Bromite, hypobromite, bromine, bromide, and oxygen gas were formed as radiolytic products. Almost all the oxidation states higher than bromide could be removed by thermal annealing.

Yields were measured for decomposition of various nitrate crystals by 3.4-Mev alpha particles, cobalt gamma rays, and ultraviolet light at several temperatures. The fact that the increase in yield with increase in stopping power (alpha particles compared with gamma rays or ultraviolet light) roughly parallels the increase in yield with increased temperature (for decomposition by gamma rays or ultraviolet light) suggests that thermal effects along alpha-particle tracks are an important factor in the radiolysis.

The study of the radiolysis by transferred energy of substances suspended in alkali halides was continued, with special attention to the decompositions of NO_3^- and NO_2^- in potassium bromide. No equilibrium is attained between NO_3^- and its radiolysis products; the nitrite ion found in an aqueous solution of irradiated KNO_3 exists in the solid prior to dissolution and does not arise by reaction of stabilized intermediates with water. The solubilities of KNO_3 and KNO_2 in KBr (0.21 and 0.082 mole % respectively) were determined by a new method. The kinetics of the decompositions of NO_3^- and NO_2^- in KBr are being studied.

From a study of the $G(H_2)$, $G(O_2)$, $G(Ce^{3+})$, and $G(Ce^{3+})_{Tl^+}$ from Co^{60} gamma-irradiated concentrated aqueous HNO_3 and Ce^{4+}–0.4 *M* H_2SO_4–HNO_3 solutions and a comparison of these yields with those determined in comparable $NaNO_3$ solutions, it may be concluded that HNO_3 decomposes by two mechanisms: a molecular process, $HNO_3 \rightsquigarrow HNO_2 + \frac{1}{2}O_2$, and a radical process, $HNO_3 \rightsquigarrow OH + NO_2$. The increased $G(OH)$ from HNO_3 solutions is directly proportional to the HNO_3 concentration.

The 100-ev yields of the radiolytic products produced by Co^{60} gamma irradiation of sulfuric acid solutions are presented graphically as a function of the stoichiometric sulfuric acid concentration. The postirradiation reaction occurring in Ce(IV)-H_2SO_4 solutions has been shown to be a reaction between H_2SO_5 and Ce(IV) ions. The mechanism probably involves the hydrolysis of H_2SO_5 to H_2O_2, which then reacts with Ce(IV).

By means of low-temperature cells and absorption spectrophotometry, the formation of ozone in liquid oxygen has been observed, *in situ*, by alternate gamma irradiation and UV absorption measurement. Ozone formation was found to be linear with dose for five increments of 5.4×10^{17} ev/g. Preliminary *G* values for ozone formation in liquid oxygen at 77°K are 14 to 16 molecules of ozone per 100 ev.

Alpha radiolysis of biphenyl produced higher (a factor of less than 10) yields of gas (mostly hydrogen) and "polymer" than have been reported for electron and gamma-ray radiolysis. The average molecular weight of the polymer was about three times that of biphenyl, and evidence was obtained for hydrogenation.

Ionic complexes, $[XeC_2H]^+$ and $[XeC_2H_2]^+$, were observed in a C_2H_2-Xe mixture irradiated by 90-ev electrons in a mass spectrometer. The complex $[XeC_2H]^+$ results from a second-order process, whereas $[XeC_2H_2]^+$ is formed by a third-order process. No complexes were observed in mixtures of C_2H_2 and the other noble gases.

The yield obtained for the alpha radiolysis of C_2H_4 agrees with the previously reported value. The main products of this radiolysis are H_2 and polymer. The H_2 comes from irradiation of the polymer.

5. ORGANIC CHEMISTRY

The benzilic acid rearrangements of alloxan and several of its derivatives were studied with isotopic tracer methods. It was unambiguously established that the nitrogen-carbon shift takes place to the exclusion of the carbon-carbon shift. The migratory aptitude of N-CH_3 vs N-H is about 4:1.

The differential method developed at the Laboratory for studying isotope effects was used in determining the values of some secondary isotope effects of C^{14} and deuterium during the formation of the 2,4-dinitrophenylhydrazones of several isotopically substituted ketones.

The compound *erythro*-1-amino-1-phenyl-2-*p*-methoxyphenylpropanol-2 was resolved, and the (+) and (–) forms were subjected to deamination. The fractions of ketonic product of inverted and retained configurations are nearly identical with those previously determined during deamination of sterically similar compounds.

The study of interactions in aqueous systems that are in equilibrium with organic solvents continued. Tributyl phosphate supported on Celite 545 (a free-flowing solid) has the same solubility in aqueous solutions as does liquid tributyl phosphate. The polyvalent electrolyte is accompanied by water when it is extracted into tributyl phosphate; strong specific interactions were indicated by high molecular weight and high viscosity. Equilibria between aqueous nitric acid and butyl *p*-toluene sulfonate (a weaker solvent than tributyl phosphate) show that water (0.7 mole per mole of sulfonate) accompanies nitric acid into this system.

6. CHEMISTRY OF AQUEOUS SYSTEMS

Equilibrium ultracentrifugations of hydrolyzed U(VI) chloride solutions indicated that the "core-link" mechanism proposed on the basis of pH measurements is not tenable. A scheme involving a hydrolyzed monomeric, dimeric, and trimeric species was found to be compatible both with acid-base titration data and with the molecular weight measurements. A test of equilibrium ultracentrifugation in the determination of solute activity coefficients in the "known" three-component system $BaCl_2$-HCl-water indicates possible value of the technique for this purpose. Rules were found for correlating volumes and refractive-index increments for the same system with the values for the two-component systems $BaCl_2$-water and HCl-water.

In continuation of studies of ion exchange resins and their application to separations, the cation exchange behavior of 53 elements in concentrated HCl-$HClO_4$ mixtures was investigated. The mixed-acid system was particularly useful for group separations of elements by column techniques.

Boric acid is useful as a complexing agent for HF in anion exchange separations involving concentrated HCl-HF media.

Adsorbabilities of a number of divalent and trivalent elements in acid media were determined for zirconium phosphate and zirconium oxide. A number of separations of trivalent elements from divalent elements were demonstrated. Mercuric sulfide was found to exhibit rather unusual adsorptive properties. Small columns of HgS adsorbed large amounts of $Hg(NO_3)_2$ from aqueous solutions, forming a white double salt. This double salt showed a high selectivity for halide ions.

Liquid ion exchangers have been found especially useful for researches on the mechanisms of ion exchange, because the nature of the ions they take up from aqueous electrolyte mixtures may be studied by spectrophotometric, magnetic susceptibility, and other physical methods more readily than is the case with resinous exchangers. The nature of the chloro- and bromo-complex anions formed by some of the metals in the 3*d* transition series was determined by examining their optical absorption bands when they were present in a liquid anion exchanger prepared by dissolving small amounts of tertiary alkylamine in toluene. The typical "ligand field" spectra of the complexes of Fe, Co, Cu, and Mn were observed, and it was concluded that the species selectively taken up by anion exchangers were four-coordinated: $FeCl_4^-$, $FeBr_4^-$, $CoCl_4^{2-}$, $CuCl_4^{2-}$, $CuBr_4^{2-}$, and $MnCl_4^{2-}$. The preference of the exchanger for four- rather than for six-coordinated anions from aqueous solutions was considered to be a consequence of the fact that usually the latter contain water as a ligand and because, for the same ionic charge, octahedral anions are larger than the tetrahedral or square planar types.

Relative apparent molal heat-content differences derived from measurements of heats of solution and dilution on aqueous solutions of quaternary ammonium halides structurally analogous to the exchange groups in Dowex 1 and Dowex 2 ion exchange resins were found to agree well with previously measured heats of anion exchange on the more highly cross-linked exchangers. However, with the lightly cross-linked resins, the exchange heat was significantly larger than the

electrolyte heat-content difference. Heat-of-mixing measurements with linear cationic polyelectrolyte (i.e., linear Dowex 1, etc.) showed that even in dilute solutions these compounds reacted with ions as if they were effectively at a high concentration. This observation is consistent with the behavior of weakly cross-linked exchangers whose molecular chains must also be at an effectively high concentration.

A nonlinear least-squares method for fitting osmotic coefficient data to a semiempirical equation was investigated. From the coefficients so obtained, it is possible to compute activity coefficients over a wide range of concentrations. The method is greatly to be preferred over graphical integration if a high-speed computer is available to perform the calculations.

The bisulfate acid constant was computed from 25 to 225°C from data on the solubility of Ag_2SO_4 in H_2SO_4 solutions. The value of K_2 at 25°C agrees very well with the values reported by other investigators. The thermodynamic constants ΔF^0, ΔH^0, and ΔS^0 for the reaction $HSO_4^- = H^+ + SO_4^{2-}$ were also computed over the same temperature range.

A beginning was made on writing an IBM 7090 computer program for solvent extraction involving an aqueous-nitrate and a TBP-containing organic phase.

A second prototype high-temperature aqueous spectrophotometric cell, designed to allow gas-liquid equilibration, has been used to study the system UO_2SO_4-$CuSO_4$-D_2SO_4-D_2O-H_2O in the wavelength range from 0.34 to 1.2 μ as a function of time, temperature, and overpressure of hydrogen and/or oxygen.

7. ELECTROCHEMISTRY OF CORROSION

Polarization measurements on the relative rates of reduction of oxygen and reducible inhibitors on the surface of passive iron provided important data on the mechanism of maintenance of passivity. The rate of reduction of the pertechnetate ion is much smaller than that of oxygen, but the reduction product [presumably $Tc(OH)_4$] catalyzes the reduction reactions of both oxygen and the pertechnetate ion. The rate of reduction of the chromate ion is also smaller than that of oxygen, but its reduction product does not function as a catalyst. In contrast, the reduction of osmium(VIII) oxide is very much faster than that of oxygen, and very small amounts of the reduction product catalyze cathodic processes in the system.

Studies on carbonyl iron powder passivated in chromate solutions showed that chromate ions are retained on the passive surface after water washing and may be displaced by hydroxide or sulfate ions. Extractions with NH_4OH and NaOH, followed by analysis with diphenylcarbazide, showed that unreduced chromate is removed and indicated that the surface is nonuniform with respect to the adsorption of chromate ion. Similar experiments with the pertechnetate ion gave no evidence of exchangeable technetium after water washing.

Studies on the effects of SCN^-, OH^-, SO_4^{2-}, and Cl^- on the reduction of cupric ion on passive stainless steel showed that adsorption of these ions on the surface affects the reduction kinetics. The adsorption reactions follow a potential-dependent Langmuir isotherm to a good approximation. In simple cases, it is possible to calculate enthalpies and entropies of adsorption from the data.

The rate of reduction of hydrogen ions on passive zirconium was determined as a function of film thickness, thus providing a basis for assessing the merits of several alternative theories of the distribution of potential and the nature of the rate-controlling steps in processes occurring at the oxide-solution interface. The kinetics of oxygen reduction was investigated as a function of electrode potential and pH, together with a determination of the amount of hydrogen peroxide produced as a reaction intermediate.

A detailed study was made of transient and steady-state polarization characteristics of iron actively corroding in benzoate solutions. The great variety of Tafel slopes reported in the literature for the iron system is easily explained as a result of neglect of the effect of slow transients by previous investigators. The phenomenon of hysteresis in the polarization of iron is a straightforward consequence of the existence of very slow processes in the iron system.

8. NONAQUEOUS SYSTEMS AT HIGH TEMPERATURE

A comparison was made of the extent of fission product release from UO_2-containing reactor fuels by the following mechanisms: oxidation in air, high-temperature diffusion in the solid, and melting in air, helium, or CO_2. These might be operative

in loss-of-coolant accidents under various conditions. Release experiments demonstrating the effect of irradiation level or burnup conform to the expected pattern in that generally increased releases were observed in highly irradiated samples over the values at tracer irradiation level.

The specific electrical conductivity in the melts of three rare-earth and two alkaline-earth metal–metal chloride systems was determined. The increase in conductivity in La-$LaCl_3$ and Ce-$CeCl_3$ on addition of metal to the normal chloride is essentially due to electronic contribution from $M^{2+} \longrightarrow M^{3+} + e^-$, but in Nd-$NdCl_3$, where the increase is much smaller, Nd dissolves as a stable Nd^{2+} ion. The results in the systems Ca-$CaCl_2$ and Sr-$SrCl_2$ are interpreted in terms of partially electronic conductance and formation of $(Ca_2)^{2+}$ and $(Sr_2)^{2+}$ ions.

The increase in the resistivity of liquid potassium on dissolution of potassium halides was found to be roughly proportional to the cross section as well as the number of the halide ions which act as scattering centers for mobile electrons.

9. CHEMICAL PHYSICS

In a paramagnetic resonance study of irradiated potassium nitrate single crystals, the spectra for two species having N^{14} hyperfine splittings were measured.

In gamma-irradiated single crystals of sodium nitrite and of sodium nitrite containing silver nitrite, the same paramagnetic resonance spectrum was seen, but with much higher intensity in crystals containing $AgNO_2$. The spectra are attributed to oriented molecules of NO_2 in the lattice of $NaNO_2$.

In gamma-irradiated single crystals of potassium chlorate, one paramagnetic species exhibiting chlorine hyperfine structure was tentatively identified as chlorine dioxide.

Anomalous neutron scattering from CdI_2 and enriched $Cd^{113}I_2$ single crystals was observed. The magnitudes and energy dependence of the real and imaginary components of the scattering amplitude of cadmium are quantitatively predictable from the appropriate resonance parameters, using the Breit-Wigner single-level formulation.

Neutron diffraction patterns of powder specimens and rotating single crystals were recorded photographically by means of a device that utilizes high-speed Polaroid film and a neutron-sensitive phosphor (ZnS-Li^6F-Lucite). The time for most exposures is a fraction of the time required previously, and the development time is 10 sec.

A neutron diffraction study of $Li_2SO_4 \cdot H_2O$ showed the water molecule to be very weakly hydrogen-bonded to the oxygen atom (O_5) of an equivalent water molecule (O_5-O_5 = 2.95 A) and to an oxygen atom (O_1) of the sulfate ion (O_5-O_1 = 2.86 A). The O_5-$H_2 \cdot\cdot O_5$ and O_5-$H_1 \cdot\cdot O_1$ angles are 150.9 ± 1.1° and 151.8 ± 2.8° respectively. The dimensions of the water molecule are: O_5-H_1 = 0.94 ± 0.02 A, O_5-H_2 = 0.97 ± 0.04 A, H_1-H_2 = 1.56 ± 0.04 A, and $\angle H_1$-O_5-H_2 = 110.4 ± 2.1°. The R-factor (for F^2) based on 240 ($h0l$) and ($0kl$) reflections is 7.1%.

A neutron diffraction study to determine the crystal structure and molecular geometry of hydrazine is in progress. An x-ray study of hydrazine hydrate indicates that it has a cubic structure, with freely rotating or disordered H_2O and N_2H_4 molecules.

The coherent neutron scattering cross sections of Rb^{85} and Rb^{87} were found to be essentially alike, 6.1 ± 0.3 barns. The total cross sections of these isotopes and those of Cl^{35} and Cl^{37} were found to be 7.45, 8.7, 47.45, and 3.9 barns respectively.

In connection with a study of hydrogen bonding, the cell parameters and space groups of potassium, rubidium, and cesium acid chloromaleate single crystals were determined by x-ray diffraction.

The structure of the cubic, high-temperature form of calcium carbide is discussed in terms of various models based on x-ray and neutron diffraction measurements.

Of the four cooperative transitions exhibited by K_2ReCl_6 with heat capacity maxima at 11.9, 76, 103, and 111°K, only the one at the lowest temperature is the result of a magnetic transition. It is estimated that an entropy of R ln 2 is associated with each of the remaining transitions. At 25°C the entropy of $K_2ReCl_6(c)$ is 88.84 cal deg^{-1} $mole^{-1}$, the entropy of $ReCl_6^{2-}(aq)$ is 59.8, and the entropy of formation is −140.2.

It was found possible to calculate the liquid-soluble, solid-insoluble impurity content of Li_3ThF_7 from careful heat-content measurements with the Bunsen ice calorimeter in the premelting region.

Progress in the study of reactive collisions of hydrogen atoms and of alkali atoms is discussed.

It was demonstrated that beta particles from Ni^{63} can be used as an ionization source in a mass spectrometer. The relative proportions of the primary and secondary ions produced in ethylene were investigated as a function of pressure in the ionization chamber.

When 3.1-kev electrons were used to bombard either argon or krypton in a mass spectrometer, positive ions ranging in charge from one through eight were observed in both gases, and the relative proportions of the ionic species bear a marked similarity to those of the multiply charged ions resulting from β^- nuclear transitions.

THIS PAGE

WAS INTENTIONALLY

LEFT BLANK

CONTENTS

SUMMARY iii

1. NUCLEAR CHEMISTRY 1
   - Reactor Neutron Cross Sections 1
     - The Effective Capture Cross Section of Po^{210} for Thermal Neutrons 1
     - Thermal Cross Section and Resonance Integral for Capture of U^{233}, and $\alpha(U^{233})$ for Resonance Neutrons 1
     - Neutron Energy Filters 2
     - Thermal-Neutron-Capture Cross Section and Capture Resonance Integral of Ce^{144} 3
   - Decay of Re^{184} Isomers 3
   - Decay of As^{74} 5
   - Fission Yields in the Mass-99 Decay Chain 6
   - Ranges and Energy Loss of Tritons in Various Substances 8
   - Three-Dimensional Pulse-Height Analyzer 9
   - Beta-Ray Polarization 11

2. ISOLATION AND CHEMICAL PROPERTIES OF SYNTHETIC ELEMENTS 12
   - Chemistry of Technetium 12
     - Measurement of Osmotic and Activity Coefficients for $NaTcO_4$ and $NaReO_4$ Solutions 12
     - Crystal-Field Analysis of the Spectra of ReX_6^{2-} and TcX_6^{2-} Ions in Aqueous Hydrogen Halide Solution 12
     - Hexavalent and Pentavalent Rhenium in Sulfuric Acid 14

3. CHEMICAL SEPARATION OF ISOTOPES 17
   - Ion Exchange Studies in Nonaqueous Solvents 17
   - Separation of Boron Isotopes 18
   - Oxygen Isotope Separation in the System Paraldehyde-Acetaldehyde 19
   - Studies of the Dimethyl Ether–Hydrogen Chloride Complex 20
   - Nitrogen-Containing Compounds 21
   - Separation of Alkali-Metal and of Alkaline-Earth Isotopes 22
   - Nitrogen-15 Separation 22
   - Oxygen-17 Separation 23
   - Chemical Structural Studies by Nuclear Magnetic Resonance 23
   - Spectroscopic Investigations of Isotopic Molecules 23
     - Vibrational Spectra and Isotopic Partition-Function Ratios 23
     - Study of Force Fields of Selected Molecules 24
     - Isotopic-Mass Spectral Studies 25
   - Isotopic-Mass Spectroscopy 25

4. RADIATION CHEMISTRY 26
   - Radiation Damage of Silica Gel 26

Catalytic Reactions on Semiconductors 27
Radiolysis of Crystalline Alkali-Metal Bromates with Co^{60} Gamma Rays 27
Thermal Spikes in the Alpha-Particle Radiolysis of Nitrate Crystals 27
Radiolysis by Transferred Energy of Compounds Dispersed in Alkali Halide Matrices 28
The OH Radical Yield in the Co^{60} Gamma Radiolysis of Aqueous Nitric Acid Solutions 31
Radiation Chemistry of Sulfuric Acid Solutions 33
Radiolysis of Liquid Oxygen 33
Radiolysis of Biphenyl 34
Energy Transfer Through Transient Species in the Radiolysis of Binary Mixtures of Acetylene and the Noble Gases 36
Alpha Radiolysis of Ethylene 36

5. ORGANIC CHEMISTRY 39
Evidence for Nitrogen Migration in the Benzilic Acid Rearrangement of Alloxan and Its Derivatives 39
Studies of Carbon-14 and Deuterium Isotope Effects 41
The Deamination Reaction 42
Rearrangement of *erythro*-1-Amino-1-phenyl-2-*p*-methoxyphenylpropanol-2 42
Solubility of Tributyl Phosphate (TBP) Supported on Celite 42
The System Tributyl Phosphate (TBP), Phosphoric Acid, and Water 43
The System Butyl *p*-Toluene Sulfonate, Nitric Acid, and Water 44

6. CHEMISTRY OF AQUEOUS SYSTEMS 45
Ultracentrifugation Studies of Inorganic Solutions 45
Hydrolysis of U(VI) 45
Activity Coefficients of Three-Component Systems as Determined with the Ultracentrifuge 45
Mixture Rules for Molal Volumes and Refractive Index Increments 46
Ion Exchange Studies 47
Adsorption of Metals from Concentrated HCl-$HClO_4$ Mixtures 47
Use of Boric Acid as a Complexing Agent for HF in Concentrated HCl Solutions 48
Adsorption on Inorganic Materials 48
Separations with Zirconium Oxide and Zirconium Phosphate 48
Adsorptive Properties of Mercuric Sulfide 48
Physical Chemistry of Ion Exchangers 49
Spectrophotometric Investigations of Liquid Anion Exchange Systems 49
Calorimetric Measurements of the Heat of Ion Exchange and Related Reactions 50
Calculation of Activity Coefficients from Osmotic Coefficient Data 52
The Bisulfate Acid Constant from 25 to 225°C, as Computed from Solubility Data 55
Method of Calculation 55
Results and Discussion 56
A Computer Program for Solvent Extraction Calculations 57
Aqueous Spectrophotometry at Elevated Temperatures and Pressures 58

7. ELECTROCHEMISTRY OF CORROSION 60

Studies on the Mechanism of Passivation 60
Ion Exchange Properties of the Passive Film on Iron 60
Effect of Adsorbed Anions on Reduction Processes on Passive Stainless Steel 61
Electrochemistry of Zirconium 63
Hysteresis Effects in the Corrosion of Iron 65

8. NONAQUEOUS SYSTEMS AT HIGH TEMPERATURE 68
Fission Product Release from Reactor-Grade UO_2 by Oxidation, Diffusion, and Melting 68
Introduction 68
Oxidation of UO_2 to U_3O_8 in Air 68
Release of Fission Products by High-Temperature Diffusion into Pure Helium 68
Release of Fission Products on Melting UO_2 in Impure Helium, in Air, and in CO_2 71
Size of Particles Released from UO_2 Melted in Air and Helium 72
Electrical Conductivity of Solutions of Some Alkaline- and Rare-Earth Metals in Their Molten Chlorides 72
Electrical Conductance of Solutions of Salts in Liquid Metals: KF-K, KBr-K, KI-K 75

9. CHEMICAL PHYSICS 77
Microwave and Radio-Frequency Spectroscopy 77
Paramagnetic Resonance Study of Irradiated Single Crystals of Potassium Nitrate 77
Paramagnetic Resonance Study of Gamma-Irradiated Single Crystals of Sodium Nitrite and of Sodium Nitrite Containing Silver Nitrite 78
A Paramagnetic Resonance Study of Irradiated Potassium Chlorate 78
Studies of Anomalous Neutron Scattering 78
Photographic Techniques in Neutron Diffraction 79
Neutron Diffraction Study of $Li_2SO_4 \cdot H_2O$ 80
A Single Crystal Neutron Diffraction Study of Hydrazine 82
The Crystal Structure of Hydrazine Hydrate, $N_2H_4 \cdot H_2O$ 83
Coherent and Total Thermal Neutron Cross Sections of Rubidium and Chlorine Isotopes 83
Cell Parameters and Space Groups of Potassium, Rubidium, and Cesium Acid Chloromaleates 84
The Structure of Calcium Carbide at High Temperature 85
Calorimetry 86
Thermodynamic Properties of Potassium Hexachlororhenate(IV) 86
High-Temperature Heat-Content Measurements 87
Molecular Beam Studies of Chemically Reactive Collisions 88
Reactions of Atomic Hydrogen 88
Reactions of Alkali Metals 89
Collision Mechanics in Crossed Maxwellian Molecular Beams 89
Mass Spectrometry and Related Techniques 89
Positive-Ion Intermediate in the Beta-Particle Radiolysis of Ethylene 89
Ionization Processes in Argon, Krypton, and the C_2 Hydrocarbons Produced by 3.1-kev Electrons and Other Modes of Excitation 91

PUBLICATIONS 94

PAPERS PRESENTED AT SCIENTIFIC AND TECHNICAL MEETINGS 98

1. NUCLEAR CHEMISTRY

REACTOR NEUTRON CROSS SECTIONS

The Effective Capture Cross Section of Po^{210} for Thermal Neutrons

J. Halperin J. H. Oliver
R. W. Stoughton

Measurements were carried out to determine thermal-neutron-capture cross sections for the formation of both isomers of 138-day Po^{210}. Although large quantities of Po^{210} have been widely used for many years and although it would be formed in large quantities by radiative capture in any reactor using bismuth or its compounds as a reactor coolant or fuel carrier, no measurement of its cross section seems to have been made.

The 0.52-sec isomer of Po^{211} emits primarily 7.43-Mev alpha particles and the 27-sec isomer largely 7.14-Mev alpha particles, with several more energetic alphas in low abundance. These alpha groups are all sufficiently energetic to be readily distinguishable from the 5.30-Mev alphas of Po^{210}. The irradiations were carried out in the pneumatic tube facility of the ORR, where a maximum thermal flux of about 8×10^{13} neutrons cm^{-2} sec^{-1} is available and where the ratio of thermal flux to resonance flux per ln E interval is about 50. The alpha particles were measured with a solid-state detector and counted through a filter sufficiently thick to just absorb the Po^{210} alphas. The energy calibration was made with a radium source using Ra C′ (7.68 Mev) and Ra A (6.00 Mev) alphas. Transit time from the face of the reactor to the detector is about 2 sec; no chemical separations are required.

In this work the thermal cross sections were shown to be <30 mb for the 0.52-sec isomer and <0.5 mb for the 27-sec isomer. A low cross section for Po^{210} is not unexpected, since it contains a closed shell of 126 neutrons and one pair of protons beyond the closed shell of 82. The isotones of ${}_{84}Po^{210}_{126}$, ${}_{82}Pb^{208}_{126}$ and ${}_{83}Bi^{209}_{126}$, have similarly low cross sections: 0.6 mb and 0.034 barn respectively. This enhanced stability of the closed shell leads to a wider level spacing and, consequently, to the lower thermal cross sections. The excitation curves[1] for the formation of Po^{211} by the $Pb^{208}(\alpha,n)$ reaction show yields for the formation of the 0.52-sec isomer higher by a factor of 100 than the yields for the 27-sec isomer for alpha energies in excess of threshold by some 3 to 6 Mev. These energies are comparable to and greater than the Q value for the $Po^{210}(n,\gamma)Po^{211}$ reaction. It is of interest to note that radiative capture is exoergic by 4.5 Mev for the 0.52-sec isomer and 3.2 Mev for the 27-sec isomer. These low energies for radiative capture reflect the enhanced stability of the closed-shell nuclide. The 1.3-Mev difference between the ground states of the two nuclides suggests the greater difficulty of forming the upper state. In fact, the beta decay of Bi^{211} and the electron capture of At^{211}, both parents of Po^{211}, lie at levels below Po^{211m}, so that decay to that level is not possible. Although the spin states of Po^{211} are not well identified, the 27-sec level is thought to be unusually high,[2] possibly 25/2, whereas the 0.52-sec level is probably 9/2. There thus appears to be good reason for finding a particularly low cross section for the $Po^{210}(n,\gamma)Po^{211m}$ reaction.

Thermal Cross Section and Resonance Integral for Capture of U^{233}, and $\alpha(U^{233})$ for Resonance Neutrons

J. Halperin E. L. Blevins
R. W. Stoughton R. E. Druschel
F. J. Johnston[3] A. L. Harkness[4]
J. H. Oliver B. A. Swarz[4]

The thermal-neutron cross section and resonance integral for capture of U^{233} were measured by

---

[1] F. N. Spiess, *Phys. Rev.* 94, 1292 (1954).

[2] W. Jentschke, A. C. Juveland, and G. H. Kinsey, *Phys. Rev.* 96, 231 (1954).

[3] ORINS summer participant, University of Georgia, Athens.

[4] Argonne National Laboratory, Argonne, Ill.

irradiating microgram quantities of U^{233} (essentially free of U^{234}) in the ORR at fluxes of $\sim 1.3 \times 10^{14}$ neutrons cm^{-2} sec^{-1} and using a cadmium-filter technique with 0.040 in. cadmium. The samples were monitored with cobalt in a dilute Co-Al alloy (containing 0.151% Co). The U^{234} formed during the course of the irradiation was determined by mass-spectrographic analyses of the uranium samples.

The measurement of the capture cross section σ_c of U^{233} at various neutron energies by conventional neutron time-of-flight methods suffers from the inherent difficulty of measuring a relatively small quantity (σ_c) by taking the difference between two relatively large numbers (i.e., $\sigma_{abs} - \sigma_F$, where σ_{abs} is in turn derived from a σ_{tot} measurement and corrected for scattering). The direct determination of the capture cross section for both thermal and resonance energies and the epithermal value of α provides a pertinent check of this measurement by an additional method. The evaluation of these quantities is of particular interest to reactors making use of the Th^{232}-U^{233} cycle.

By using values of 37.0 and 75 barns for the thermal cross section σ_0(Co) and resonance integral I(Co) of cobalt and the peak in the Maxwellian neutron spectrum of $E_m = 0.029$ ev, a ratio for the thermal flux to the resonance flux per ln E interval of 16.45 was found (see ref 5 for conventions used). In addition an integrated thermal flux-time of 3.65×10^{20} neutrons/cm^2 was measured. Under the conditions of the irradiation an effective capture cross section (based upon the Maxwellian flux) of $\sigma_{eff}(U^{233}) = 61.3$ barns was observed. By using Westcott's value[6] of "g" the ratio of $(\sigma_0/I)_c$ for U^{233} was found to be equal to 0.352; this in turn leads to values of $\sigma_0(U^{233})_c = 51.7$ barns and $I(U^{233})_c = \int_{0.54\ ev} \sigma\, dE/E = 147$ barns. The lower limit for the integral is determined primarily by the filter thickness but also by other parameters of the irradiation.[7] By using the definition $\alpha_{epi}(U^{233}) \equiv I_c/I_F$ (i.e., the ratio of the capture resonance integral to the fission resonance integral),[8] we find $\alpha_{epi}(U^{233}) = 147/865 = 0.170$.

The uncertainties in the values of both $\sigma_0(U^{233})_c$ and $I(U^{233})_c$ are about 5%, assuming that the reaction-rate model and the cross-section values of the standards are exact. The value of $\alpha_{epi}(U^{233})$ is probably uncertain to about 10%, due to the larger uncertainty in $I_F(U^{233})$. The presently reported value of $\sigma_0(U^{233})_c = 51.7$ barns may be compared to the World Consistent Set value of $\sigma_0(U^{233})_c = 53 \pm 5.5$ barns or the U.S. value of 51 ± 5.5 barns as quoted in BNL-325.[9] Westcott[6] quotes a value of $I_{abs}(U^{233}) - I_F(U^{233}) = 117$ barns – considerably lower than the presently reported measurement. His low value is probably due to the indirect nature of that measurement. Chernick and Moore[10] have estimated $\alpha_{epi}(U^{233}) = 0.153$ from absorption and fission vs energy data, whereas Westcott[6] quotes 0.145. These values are to be compared with the presently reported value of $\alpha_{epi}(U^{233}) = 0.170$.

The effect of this value of α_{epi} on thermal breeding may be seen by making the assumption that about 10% of the absorptions in U^{233} occur at epithermal energies. The World Weighted Average and the U.S. value for the 2200 m/sec value of α are both very close to 0.100.[9] An effective value of α would thus be about 0.107 based on 10% epithermal absorption. Even for an epithermal absorption of 20%, the effective α would be only 0.114.

Neutron Energy Filters

R. W. Stoughton J. Halperin

A program has been written for the IBM 7090 computer to calculate the reaction rate and effective cutoff energy E_c for a $1/v$ absorber inside a spherical, cylindrical, or double-slab

[5] R. W. Stoughton and J. Halperin, *Nuclear Sci. and Eng.* 6, 100–18 (1959); in this report the subscript 0 has been dropped from the symbol I_0 for the infinitely dilute resonance integral.

[6] C. H. Westcott, *Effective Cross Section Values for Well-Moderated Thermal Reactor Spectra*, AECL-1101 (3rd Edition Corrected) (November 1960).

[7] R. W. Stoughton, J. Halperin, and M. P. Lietzke, *Nuclear Sci. and Eng.* 6, 441–47 (1959).

[8] The measurement of the fission resonance integral had been carried out previously as a part of this experiment but had been completed and reported earlier; the value was $I_F = 865$ barns. See *Chem. Div. Ann. Progr. Rept. June 20, 1960*, ORNL-2983, p 6.

[9] *Neutron Cross Sections*, BNL-325, 2d ed., 1st suppl (1960).

[10] J. Chernick and S. O. Moore, *Nuclear Sci. and Eng.* 6, 537–44 (1959).

filter containing boron, cadmium, gadolinium, or samarium. A Maxwellian plus a $1/E$ epithermal flux is assumed. The parameters which may be varied are the Maxwellian temperature, the ratio of the Maxwellian flux to the epithermal flux, the lower limit of the $1/E$ flux, the thickness of filter, and, in the case of the cylindrical filters, the height/diameter ratio.

The program computes the effective cutoff energy [i.e., the cutoff of a perfect (infinitely sharp) filter which allows the same reaction rate as the actual filter], the fraction *FRACT* of total reactions occurring below the cutoff, the ratio of Maxwellian reactions occurring below the cutoff to total reactions at all energies, the ratio of Maxwellian to $1/E$ flux reactions occurring above the cutoff, and the total reaction rate. In the case of spherical filters, the program also computes as functions of energy the transmission factor, the differential Maxwellian and $1/E$ rates, the integrated Maxwellian, $1/E$, and total rates, and the corresponding rates for an unfiltered sample. With a point $1/v$ sample at its center, a spherical filter allows the same reaction rate as does a slab filter in a beam flux, since in the former case only neutrons going along a diameter will strike the sample at the center.

From the calculations to date the following conclusions may be drawn:

1. The values of both the effective cutoff and the fraction of reactions below the cutoff are insensitive to the lower limit of the $1/E$ flux for cadmium filters. Westcott[11] discusses four different expressions for the lower limit and states that it lies between about 3 and 5 times the energy E_m corresponding to the Maxwellian temperature. The maximum deviation in E_c and *FRACT* on varying the lower limit from 3 to 5 times E_m occurred at the higher values of E_m and the lower values of thickness. However, even for a Maxwellian temperature of 600°C and a thickness of 10 mils of cadmium, the changes in E_c and *FRACT* were only slightly over 1%.

2. As expected from the lower resonance energy of gadolinium (0.03 ev) compared with cadmium (0.178 ev), the former provided lower effective cutoffs, that is, around 0.2 ev compared with around 0.5 ev for cadmium for reasonable thicknesses. Unfortunately, however, while cadmium afforded values of 0.05 to 0.10 for *FRACT* for reasonable values of the parameters, the gadolinium *FRACT*'s were in the range of 0.1 to 0.3.

[11] C. H. Westcott, *Effective Cross Section Values for Well-Moderated Thermal Reactor Spectra*, AECL-1101 (3rd Edition Corrected) (November 1960).

Thermal-Neutron-Capture Cross Section and Capture Resonance Integral of Ce^{144}

P. M. Lantz

Measurements of the thermal-neutron-capture cross section and capture resonance integral of Ce^{144} were completed, using cadmium-ratio techniques. Samples of purified fission-product cerium containing 1 to 7 mc of Ce^{144} were irradiated in the LITR. The separation of 5.9-hr Pr^{145}, daughter of 3-min Ce^{145}, from the cerium isotopes, the identification, and the determination of yield have been previously[12] described. The average thermal-neutron-capture cross section and capture resonance integral, based on results from seven experiments, are 0.96 ± 0.1 and 2.6 ± 0.2 barns, respectively. Since Ce^{144} has two pairs of neutrons beyond the closed 82 shell, a low cross section for radiative capture is to be expected.

Samples of initially pure Ce^{140}, which have been in the MTR for 100- and 200-day periods for the production of Ce^{142} by the reaction $Ce^{140}(n,\gamma)Ce^{141}(n,\gamma)Ce^{142}$, are being prepared for determination of the Ce^{142} by neutron activation and the mass spectrometer.

DECAY OF Re^{184} ISOMERS[13]

N. R. Johnson

Both natural rhenium and rhenium enriched with Re^{185} were irradiated in the LITR to form Re^{184} by an $(n,2n)$ reaction. After intensive chemical purification the decay of the activity was followed with an end-window proportional counter and with an NaI scintillation spectrometer. This decay, followed for over four years, revealed Re^{184} isomers with half-lives of 33 ± 4 and 169 ± 9 days. In the source prepared from natural rhenium there is an additional weak component with a half-life greater than ten years, which is thought to result from Re^{189} formed by double neutron capture on

[12] P. M. Lantz, *Chem. Div. Ann. Progr. Rept. June 20, 1960*, ORNL-2983, p 5.

[13] Abstract published in *Bull. Am. Phys. Soc.* **6**, 73 (1961).

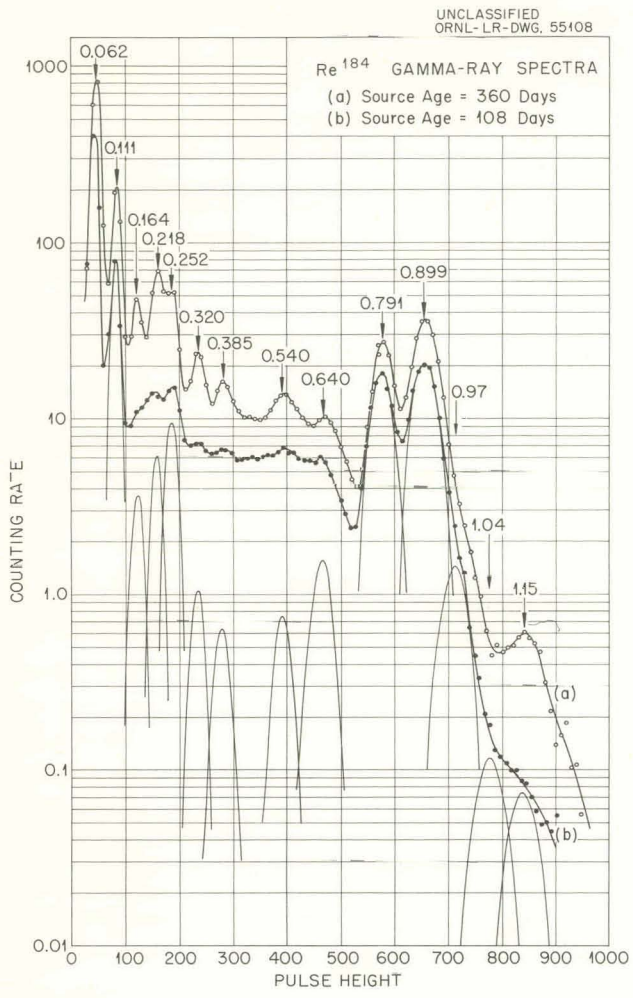

Fig. 1.1. Re 184 Gamma-Ray Spectra Taken 252 Days Apart. The analyzed photopeaks are for spectrum (b). Energies are in Mev.

Re^{187}. Repurification of the source after four years confirmed that these new activities are indeed due to rhenium.

Gamma-ray spectra taken with a 3 × 3 in. NaI scintillation spectrometer over the four-year period showed peaks at 0.062, 0.111, 0.164, 0.186, 0.218, 0.252, 0.320, 0.385, 0.450, 0.540, 0.640, 0.791, 0.899, 0.97, 1.04, and 1.15 Mev. (The 0.186- and 0.450-Mev gamma rays were observed only in coincidence measurements.) All of these gamma rays, except the peak at 164 kev, exhibited a complex decay with half-lives of about 30 and 170 days. The 164-kev transition appeared to follow only the longer period and is assumed to represent an isomeric transition between the two Re^{184} isomers. Figure 1.1 shows two gamma-ray spectra taken 252 days apart. These spectra point out the change in relative population of W^{184} levels as the Re^{184} isomers decay.

Gamma-gamma coincidence measurements have been made gating on the peaks at 0.111, 0.252, 0.320, 0.540, 0.791, and 0.899 Mev. Part of these coincidence measurements were repeated at different stages of decay, in order to further elucidate the manner in which the Re^{184} isomers populate W^{184} levels.

These data have led to the proposed decay scheme shown in Fig. 1.2. This level scheme in W^{184} is somewhat similar to those proposed by

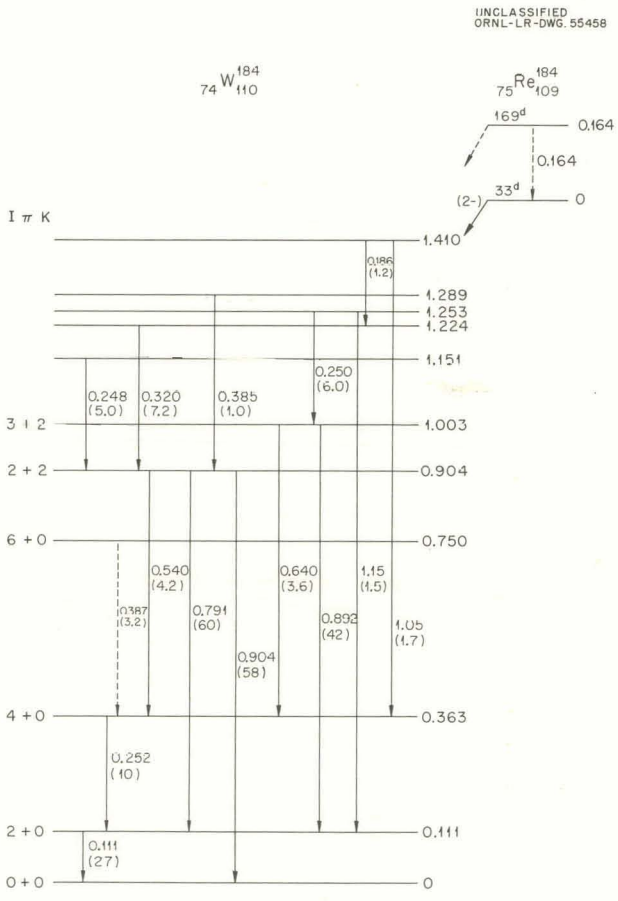

Fig. 1.2. Decay Scheme of Re 184. Energies are in Mev, and the relative gamma-ray intensities are given in parentheses.

Gallagher, Strominger, and Unik[14] and by Harmatz, Handley, and Mihelich.[15] It does differ from the proposals by these investigators in that it contains several additional levels, which were concluded from the results of the coincidence experiments.

The four low-lying levels in W^{184} are members of the ground-state rotational band, and thus have spin and parity assignments of 0+, 2+, 4+, and 6+. The levels at 0.904 and 1.003 Mev are members of a gamma-vibrational band. This is concluded since the reduced transition probabilities from the 0.904-Mev level to the 4+, 2+, 0+ member of the ground-state rotational band agree with the theoretically expected ratio of $\frac{1}{2}$:10:7.

DECAY OF As^{74}[16]

E. Eichler
R. L. Robinson[17]
G. D. O'Kelley
N. R. Johnson

New light was shed on the level structure of Ge^{74} by studying the radiations from As^{74}. Although the As^{74} half-life is conveniently long, the low intensity of most of the gamma rays and the continuum from the annihilation in flight of the positrons makes analysis of the single-crystal gamma-ray spectrum difficult (Fig. 1.3). However, by subtracting an arbitrary but reasonable annihilation-in-flight continuum from the singles spectrum the following gamma-ray peaks (and relative intensities) were resolved: 0.60 (100), 0.635 (30), 1.20 (0.4), 1.59 (0.02), 2.18 (0.04), and 2.53 (0.01) Mev. These results are in good agreement with those of recent investigators of this nuclide.[18] In an attempt to reduce the effect of the annihilation-in-flight continuum, a number of experiments were performed: triple coincidences of the types (gamma–x ray–0.60 Mev) and (gamma–0.511 Mev–0.511 Mev); gamma coincidences with x rays; and gamma coincidences with 0.60 Mev. The last experiment succeeded to some extent in verifying the presence of several gamma-ray groups, as can be seen in Fig. 1.4. Combining the earlier results from Ga^{74} measurements[19] with these new data, we obtain the decay scheme of Fig. 1.5. By following the decay of two As^{74} samples for more than a year, a new value, 17.74 ± 0.05 days, was obtained for the half-life.

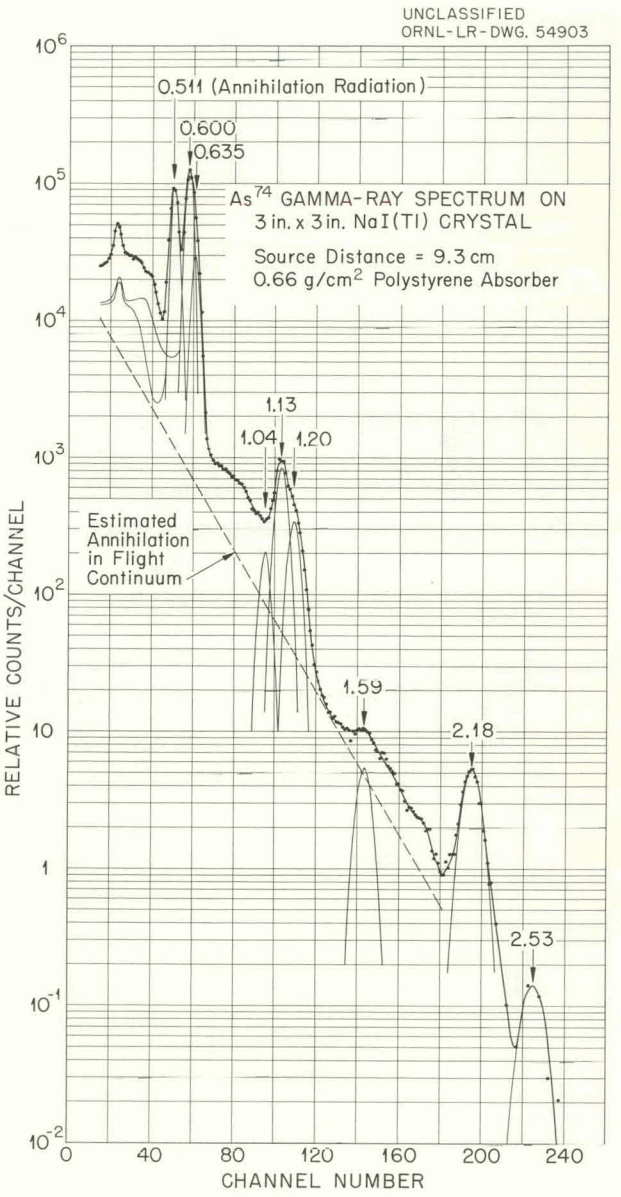

Fig. 1.3. Gamma-Ray Spectrum of As^{74} Taken with a 3 × 3 in. NaI(Tl) Crystal.

[14] C. J. Gallagher, Jr., D. Strominger, and J. P. Unik, *Phys. Rev.* **110**, 725 (1958).

[15] B. Harmatz, T. H. Handley, and J. W. Mihelich, submitted for publication in the *Physical Review*.

[16] Abstract published in *Bull. Am. Phys. Soc.* **6**, 228 (1961).

[17] Physics Division.

[18] D. J. Horen *et al.*, *Phys. Rev.* **113**, 875 (1959); R. K. Girgis and R. Van Lieshout, *Physica* **25**, 688 (1959); T. Yamazaki, H. Ikegami, and M. Sakai, *J. Phys. Soc. Japan* **15**, 957 (1960).

[19] E. Eichler *et al.*, *Chem. Div. Ann. Progr. Rept., June 20, 1960*, ORNL-2983, p 2.

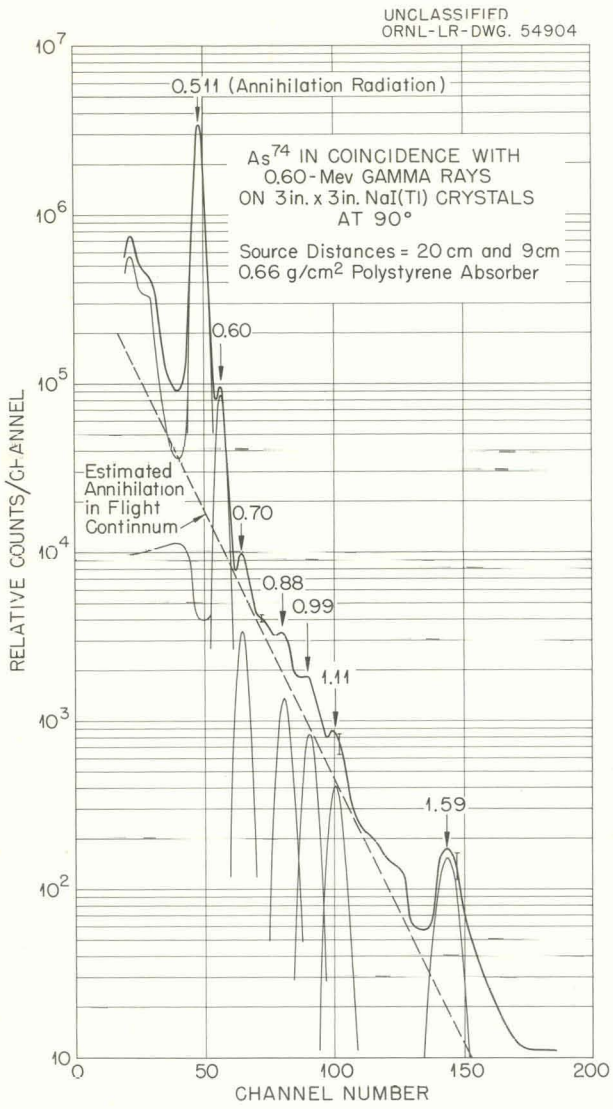

Fig. 1.4. Gamma-Ray Spectrum of As^{74} in Coincidence with 0.60-Mev Gamma Rays Taken with Two 3 × 3 in. NaI(Tl) Crystals at 90°.

FISSION YIELDS IN THE MASS-99 DECAY CHAIN

D. E. Troutner[20] R. L. Ferguson

Attempts were made to measure fission yields of individual members of the mass-99 fission-product decay chain and to determine the genetic relationships along the chain. Rapid separations of Zr, Nb, and Mo from one another following brief thermal-neutron irradiations of U^{235} solutions gave evidence for the existence of previously unreported isomers of Zr^{99} and/or Nb^{99}. Figure 1.6 summarizes data obtained from experiments in which Zr and Nb were separated from Mo by coprecipitation of the former with $Fe(OH)_3$.[21] The ordinate values give the ratios of Mo^{99}, which grows in from the quickly separated Zr and Nb to the total Mo^{99} present after complete decay of its precursors. Separation times are indicated on the abscissa. Thus, the curve represents the decay of Mo^{99} precursors. Preliminary experiments have been performed in which the fission-product Zr was allowed to pass through an ion exchange column which retained Nb and Mo. These experiments indicate that less than ~5% of the Mo^{99} produced in fission arises from the known 35-sec Zr^{99}.[22]

It has been assumed that the curve of Fig. 1.6 represents the sum of two independently decaying radioactivities. This "decay curve" has been resolved into two half-life components of 10 ± 4 sec and 130 ± 20 sec, using a least-squares program on the IBM 7090.[23] Assignments of these activities to isomers of Nb^{99} would be consistent with the reported existence of a (2.4 ± 0.3)-min Nb^{99} activity[22] and with the apparently small fraction of the chain passing through 35-sec Zr^{99}. In addition, the expected[24] fractional cumulative yield of Nb^{99} is in good agreement with the value obtained by extrapolating the "decay curve" components to zero time and adding together the ordinate intercepts. This extrapolation was performed by the computer, and gave values of 0.61 ± 0.20 and 0.35 ± 0.05 for the 10-sec and 130-sec components respectively.

If this interpretation is correct, and if the distribution of yields along the chain is normal,[24] there must also exist a very short-lived, high-yield isomer of Zr^{99}. Furthermore, the fractional independent yield of Mo^{99} obtained (approximately

[20] ORINS research participant, 1960. Permanent address: University of Missouri, Columbia.

[21] The authors are grateful to G. D. O'Kelley for assistance with some of these experiments, as well as for his continued interest and support of this work.

[22] C. J. Orth and R. K. Smith, *J. Inorg. & Nuclear Chem.* 15, 4 (1960).

[23] The authors are indebted to P. B. Wood, ORGDP, for programming and supervising this calculation.

[24] A. C. Wahl, R. L. Ferguson, D. R. Nethaway, D. E. Troutner, and K. Wolfsberg (to be published).

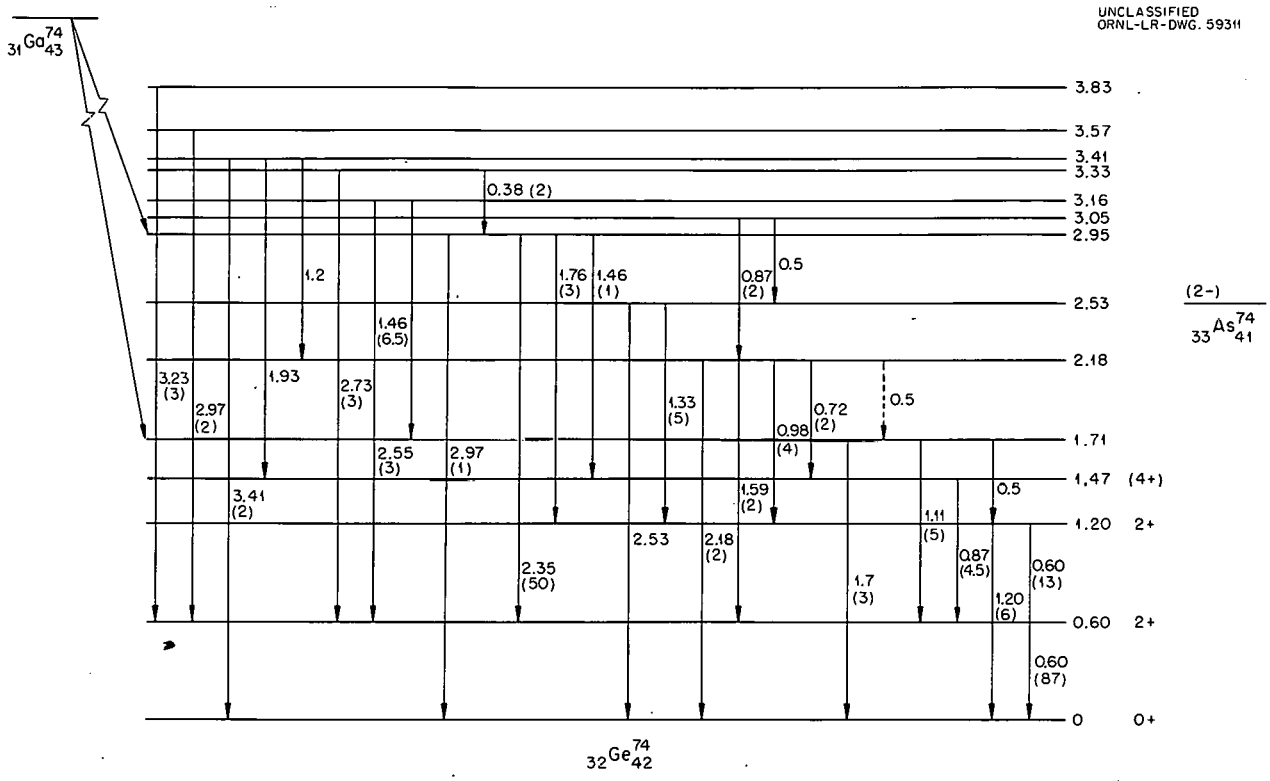

Fig. 1.5. Level Scheme of Ge^{74}. Numbers in parentheses are relative intensities with the total 0.60-Mev intensity taken as 100.

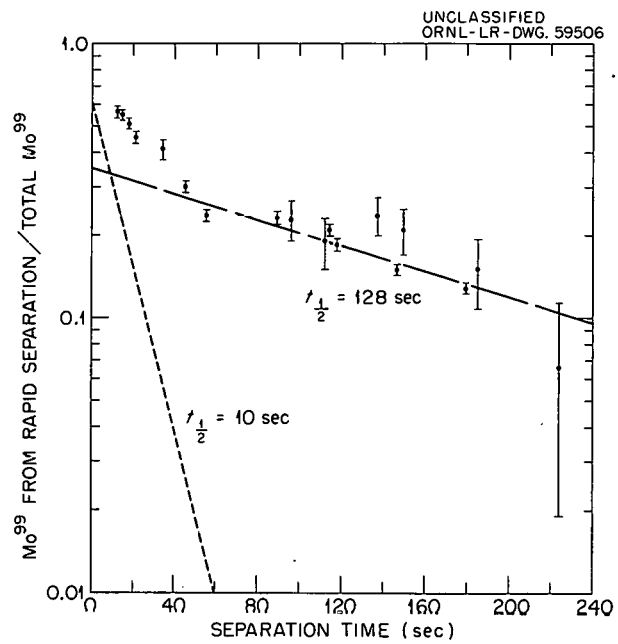

Fig. 1.6. Decay of Mo^{99} Precursors.

one minus the fractional cumulative yield of Nb^{99}) would indicate that the 50-proton shell effect suggested by Wahl[25] is not great. The results presented here do not preclude the possibility that the 10-sec activity is an isomer of Zr^{99} which decays partly through an unknown, very short-lived Nb^{99} isomer; in this case, the yield distribution along the chain would not be normal.

RANGES AND ENERGY LOSS OF TRITONS IN VARIOUS SUBSTANCES [26]

W. N. Bishop[27] E. Eichler
R. L. Wolke[28] N. R. Johnson
G. D. O'Kelley

Studies were made of the range and energy loss of tritons in a variety of materials. The tritons were produced by the reaction $Li^6(n,\alpha)H^3$, using the neutron beam from hole HB-1 of the LITR. Interference from the intense gamma-ray background was considerably reduced by using silicon surface-barrier diodes for detecting the charged particles. The remaining background effects were eliminated by demanding a coincidence between the tritons and associated alpha particles, which are correlated at 180°.

The mean ranges of 2.736-Mev tritons were determined in the following materials (values are in mg/cm^2): xenon, 20.36 ± 0.20; krypton, 17.83 ± 0.18; nickel, 15.15 ± 0.15; argon, 11.40 ± 0.09; aluminum, 10.10 ± 0.10; air, 7.34 ± 0.06; nitrogen, 7.26 ± 0.06; polystyrene, 6.12 ± 0.10. The only experimental triton range data previously reported in the literature are for air at 2.736 Mev. The results of Bøggild and Minnhagen,[29] 7.36 ± 0.07 mg/cm^2, and of Cooper, Crocker, and Walker,[30] 7.32 ± 0.06 mg/cm^2, are in excellent agreement with the present work.

Table 1.1. Values of Parameters in the Triton Range-Energy Equation, $R = aE^b + C$, Where R is in mg/cm^2 and E is in kev

Substance	Z	Energy Span (Mev)	a	b	C
			× 10^5		
Xenon	54	0–1.4	49.3	1.33	0.57
		1.3–2.7	8.43	1.55	1.66
Krypton	36	0–0.8	40.6	1.33	0.41
		0.8–2.7	24.0	1.42	0.31
Nickel	28	0–1.4	62.6	1.27	0.40
		1.4–2.7	12.0	1.47	1.27
Argon	18	0–1.2	1.96	1.67	0.41
		1.0–2.7	4.98	1.56	0.13
Aluminum	13	0–1.1	40.7	1.26	0.19
		1.0–2.7	7.17	1.49	0.51
Air	7.2	0–1.2	6.34	1.44	0.23
		1.2–2.7	2.81	1.57	0.12
Nitrogen	7	0–1.2	5.78	1.46	0.20
		1.3–2.7	2.61	1.59	0.06
Polystyrene	3.5	0–1.4	11.2	1.35	0.10
		1.4–2.7	0.67	1.72	0.44

By measuring the triton energy as a function of absorber thickness, the range and energy loss were obtained. The range data for each absorbing material were fitted to the equation $R = aE^b + C$ by means of a least-squares program[31] on the IBM 704 computer. Here, R is the mean range in mg/cm^2; E is the triton energy in kev; and a, b, and C are empirical constants. Table 1.1 lists the values obtained for the parameters, and the energy regions for which they are valid. The estimated error of the ranges in the table increases from ~1% at 2.7 Mev to 3% at the lowest

[25] A. C. Wahl, *J. Inorg. & Nuclear Chem.* 6, 263 (1958).

[26] Abstract published in *Bull. Am. Phys. Soc.* 6, 36 (1961). This is a partial report of research performed for a Ph.D. dissertation, "The Interaction of Tritons with Matter," submitted by W. N. Bishop to the University of Florida, June 1961.

[27] ORINS graduate Fellow from the University of Florida, Gainesville, Fla. Present address: Brookhaven National Laboratory, Upton, N.Y.

[28] ORINS research participant, summer, 1958, 1959; Permanent address: University of Pittsburgh, Pittsburgh, Pa.

[29] J. K. Bøggild and L. Minnhagen, *Phys. Rev.* 75, 782 (1949).

[30] P. N. Cooper, V. S. Crocker, and J. Walker, *Proc. Phys. Soc.* 66, 660 (1953).

[31] The authors are indebted to Marjorie P. Lietzke and M. H. Lietzke for programming these calculations.

energies. It was possible in these experiments to make the first extensive measurements of the energy loss of tritons. The results, expressed as atomic stopping cross sections in ev-cm^2, are given in Figs. 1.7 and 1.8. The error estimated for these data is 5%. Literature values for other charged particles, when converted to the equivalent triton energy, show gratifying agreement with the range and energy-loss data reported here.

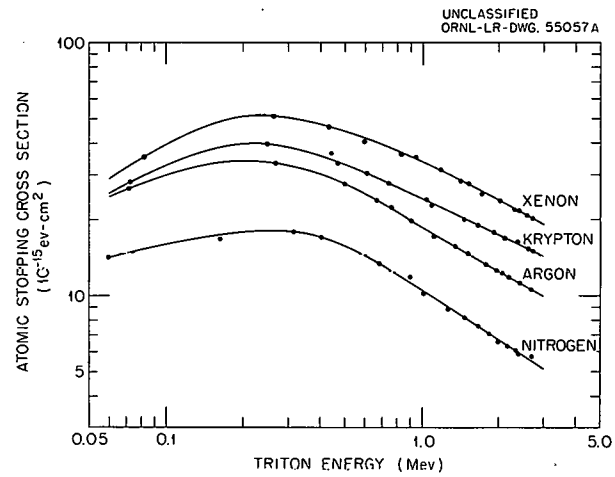

Fig. 1.7. Atomic Stopping Cross Sections for Tritons in Xenon, Krypton, Argon, and Nitrogen.

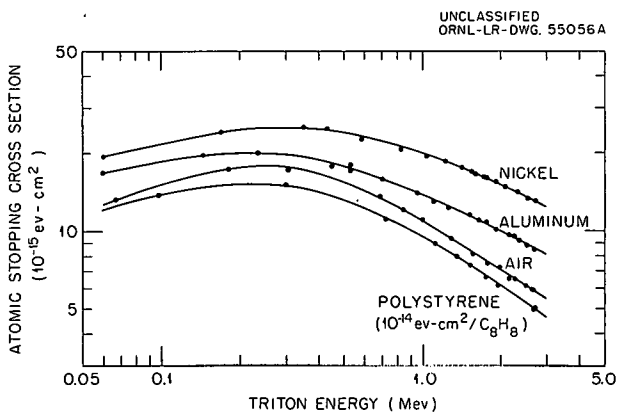

Fig. 1.8. Atomic Stopping Cross Sections for Tritons in Nickel, Aluminum, Air, and Polystyrene.

THREE-DIMENSIONAL PULSE-HEIGHT ANALYZER[32]

G. D. O'Kelley C. D. Goodman[33]
D. A. Bromley[34]

Conventional coincidence spectrometry of radioactive nuclides is performed by selecting a narrow pulse-height interval from a detector; the pulses falling within this "window" are used to gate a multichannel analyzer, which records the pulse-height distribution from another detector. Such a procedure can be very time-consuming, because it is necessary to perform a new experiment for each gating energy of interest. When short-lived nuclides are involved, this requires the preparation of at least one new source for each experiment. In these circumstances, it is very difficult to reproduce conditions from one measurement to another.

An enormous saving in effort and an accompanying improvement in the quality of the data would result if all coincidence events from a particular detector configuration were recorded in the same experiment. An instrument to perform this function can be termed a "three-dimensional" pulse-height analyzer, because it records Z, the number of events which fall at each pair of coincident pulse heights, X and Y. Such a scheme is very attractive for a variety of experiments in which two coincident events can be converted to a pulse height. Examples of quantities which may be expressed as pulse heights are: beta- or gamma-ray energy; neutron time-of-flight; heavy-charged-particle energy; and charged particle dE/dx.

The requirements of decay-scheme and nuclear-reaction investigations lead to the following specifications for a three-dimensional analyzer:

Memory Size. – Available detector resolution dictates that at least one pulse-height coordinate should have 200 channels; a 100 × 200 array appears reasonable. Storage capacity of each channel depends upon the application.

---

[32] Abstract submitted for presentation at the Symposium on Nuclear Instruments, Atomic Energy Research Establishment, Harwell, England, Sept. 11–12, 1961.

[33] Electronuclear Research Division.

[34] Yale University.

Access Time. – In studies of short-lived activities, coincidence rates up to 2500 counts/sec may be encountered; therefore, the average dead time for processing a pulse should not exceed about 400 μsec. Nuclear reaction studies, in which large peak-intensity ratios are common, require a similar access time.

Storage of Ungated Spectra. – Quantitative coincidence spectrometry requires that a three-dimensional analyzer be capable of storing in its memory the ungated, or "singles," pulse-height spectra in both detectors. This also requires a low dead time.

Display. – It is felt that in the experiments for which this analyzer is intended, the data must always be in a meaningful arrangement for examination, so that it is unnecessary to process the data in a computer before they can be examined. A display of the entire memory should be provided to give the operator a means of checking on the progress of an experiment.

These stringent specifications can only be met by a pulse-height analyzer with a very large ferrite core memory.[35] A contract has been awarded for construction of three such analyzers, which will be used at the authors' institutions. Each analyzer contains a 20,000-channel memory with a storage capacity of $(10^6 - 1)$ counts per channel. As shown in Fig. 1.9, the analyzer includes two analog-to-digital converters and two address scalers, arranged into a basic 200 × 100 channel sorting and storage array. This array can be rearranged into 50 × 400 or 20 × 1000 channels. Provision is made for routing of analyzed pulses into selected 100 × 50 channel memory quadrants. The large memory also can be used to store a series of conventional 200-channel spectra (i.e., counts vs pulse height) in 100 successive memory planes, and this feature is expected to be very useful for studies of short-lived activities.

The programmer consists of three scalers which can be connected through a plugboard to provide various modes of operation. For example, they can be arranged to record live time, dead time, or counting loss. In another mode of operation, the programmer will cause the counting time to be shared periodically between the storage of coincidences in the matrix and the storage of X and Y singles spectra in the $Y = 0$ and $X = 0$ planes of the memory. Thus, an accurate sample of the singles spectra will be obtained even during the decay of short-lived samples.

[35] The authors acknowledge contributions to the design by J. B. Davidson, R. A. Eason, T. L. Emmer, and J. W. Woody of the Instrumentation and Controls Division; and E. Eichler and N. R. Johnson of the Chemistry Division.

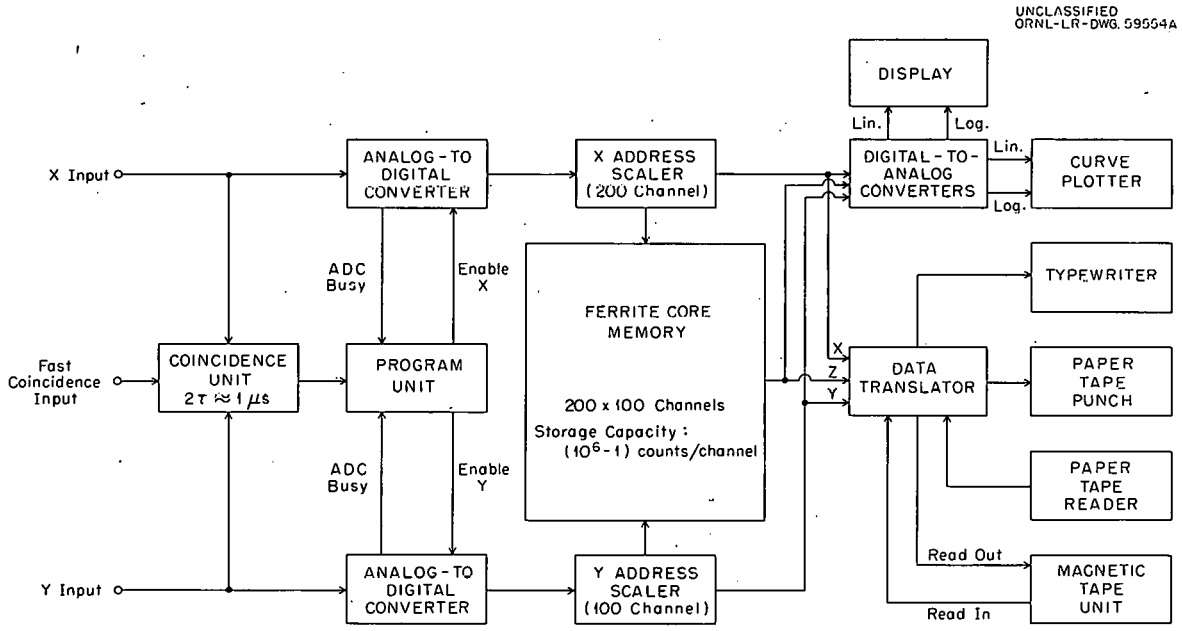

Fig. 1.9. Functional Diagram of a Three-Dimensional Analyzer.

A display is provided which shows simultaneously, on two cathode-ray tubes, an X-Y map of the memory contents with spot brightness as an indication of channel contents, and a conventional counts vs channel number display of any selected memory plane. An adjustable contour line is provided on the map display, as well as an intensified line showing which memory plane is being displayed on the other tube.

The readout system permits a wide choice of media and formats (Fig. 1.9). An in-line curve plotter and an electric typewriter are available for obtaining small portions of the stored information. For high-speed (<2 min) readout of the entire memory, a magnetic-tape unit with 7-channel, IBM 7090 format is provided. The data may also be stored in permanent form on punched paper tape.

BETA-RAY POLARIZATION

A. R. Brosi B. H. Ketelle
H. B. Willard[36]

Instrumental asymmetries are a major difficulty in the determination of beta-ray polarization by measurement of Mott scattering from high-Z foils. Since the Mott-scattering cross section changes rapidly with angle, the scattering asymmetry is strongly affected if the electron beam makes an angle with the axis of rotation of the detectors. In all earlier work, instrumental asymmetries have been measured by replacing the high-Z (gold) scattering foil with a low-Z (aluminum) foil. Since a symmetric polarized beam is scattered nearly symmetrically from low-Z foils at all angles, the asymmetry of the beam can be determined. The chief difficulty with this method is that the scattering cross section for aluminum at 135° is 100-fold smaller than that for gold. This means that a large fraction of the time in any polarization measurement must be spent on the determination of instrumental asymmetry.

A symmetric polarized beam is scattered symmetrically also from a high-Z scatterer at small angles. The beta-ray polarization apparatus was modified to take advantage of this fact for the instrumental asymmetry measurement. The modification involved the addition of three detectors for the scattered electrons to the two at 135° previously used. One of the new counters monitors the undeflected beam and the other two detect electrons scattered either up or down at 30° angles. The new counters make it possible to measure the instrumental asymmetry concurrently with the polarization asymmetry. Since the 30° gold scattering cross section is about 200-fold greater than the 135° gold cross section, the statistical error in the instrumental asymmetry now makes a very small contribution to the over-all error in a polarization measurement.

The modified apparatus was used to measure the effects on electron polarization of scattering in the source and scattering from the electrostatic deflector plates. It was used also to check earlier results on the effect of multiple scattering in gold foils on the observed scattering asymmetry.

For P^{32} at an energy of 615.6 kev, the sum of all corrections amounted to only a few per cent. The final longitudinal polarization was (98.8 ± 0.9)% of $-v/c$, the value predicted by theory.

[36] Physics Division.

2. ISOLATION AND CHEMICAL PROPERTIES OF SYNTHETIC ELEMENTS

CHEMISTRY OF TECHNETIUM

Measurement of Osmotic and Activity Coefficients for $NaTcO_4$ and $NaReO_4$ Solutions

G. E. Boyd Q. V. Larson

The vapor pressures of aqueous solutions of $NaTcO_4$, $NaReO_4$, and $NaClO_4$ were measured over the concentration range 0.1 to 5.2 *m* by means of the isopiestic comparison technique of Sinclair and Robinson, with NaCl solutions being used as standards. The crystalline $NaTcO_4$ and $NaReO_4$ employed were prepared by the NaOH neutralization of the strong acid $HTcO_4$ and Re_2O_7, followed by recrystallization. The solubilities at 25°C were 6.917 and 4.873 *m* respectively. The sequence of osmotic coefficients was $NaClO_4 > NaTcO_4 > NaReO_4$ at all concentrations. A minimum of $\phi = 0.838$ at $m = 2.10$ was observed with $NaTcO_4$.

Crystal-Field Analysis of the Spectra of ReX_6^{2-} and TcX_6^{2-} Ions in Aqueous Hydrogen Halide Solution

R. H. Busey

The recent preparation[1] of K_2ReF_6 and K_2TcF_6 made it possible to complete the near-infrared, visible, and ultraviolet spectral examination of the complex ions ReX_6^{2-} and TcX_6^{2-} (where X represents F, Cl, Br, and I) in aqueous hydrogen halide solution. The near-infrared and visible spectra of $ReBr_6^{2-}$ and ReF_6^{2-} are very similar to that of $ReCl_6^{2-}$ (ref 2). Examination of the near-infrared spectrum of $ReCl_6^{2-}$ (in 1 *N* HCl) beyond 12,000 A (below 8300 cm^{-1}) has revealed the location of the first excited electronic state. The band observed is a partially resolved doublet band, with absorption maxima at approximately 8000 and 7600 cm^{-1}. The principal absorption bands of the ReX_6^{2-} ions exclusive of ReI_6^{2-} are given in Table 2.1. The observed absorption bands (energy levels) are assigned to certain energy levels[3] (first column) expected to arise as a result of a ligand field of octahedral symmetry surrounding the Re^{4+}. The assignment is based upon an approximate fit of the observed energy levels to an extrapolated (to higher values of Dq/B) Tanabe-Sugano[4] energy-level diagram for a d^3 configuration in an octahedral field. The values obtained for the Racah parameter, *B*, were 486, 380, and 370 cm^{-1} for the fluoride, chloride, and bromide complexes respectively.

Table 2.1. Principal Absorption Bands of ReX_6^{2-} Ions, with Location of Bands Given in cm^{-1}

Energy-Level Designation	ReF_6^{2-}	$ReCl_6^{2-}$	$ReBr_6^{2-}$
$^2T_1, {}^2E$	9,090	7,600	7,300
	10,100	8,000(s)[a]	7,600
	10,900	9,090	8,800
	11,400	9,400	9,200
$^2T_2$	18,000	14,200	13,300
	18,900	15,400	14,800
	19,800	15,900	15,300
$^4T_2$	32,800	31,500(s)	28,400
$^4T_1$		35,600	30,800
$^2A_1$		38,100	33,000

[a](s) = shoulder.

The five *d* orbitals of the gaseous Re^{4+} are split by an octahedral ligand field into three low-lying orbitals, designated as $d\epsilon$ orbitals, and two upper orbitals, $d\gamma$ orbitals. The energy separation of

[1]By D. E. LaValle, Analytical Chemistry Division.

[2]R. H. Busey, *Chem. Div. Ann. Progr. Rept. June 20, 1960*, ORNL-2983, p 9, Fig. 8.

[3]For significance of $^2T_1$ etc., see, for example, L. E. Orgel, *An Introduction to Transition-Metal Chemistry*, Methuen, London, 1960.

[4]Y. Tanabe and S. Sugano, *J. Phys. Soc. (Japan)* 9, 753, 766 (1954).

these levels, $10Dq$, is given by the $^4T_2$ band, which represents the transition from $^4A_2(d\epsilon^3)$ to $^4T_2(d\epsilon^2 dy)$. It is seen from Table 2.1 that this separation increases in the order Br < Cl < F, as expected from the spectrochemical series.[3] The appearance of three bands instead of a single $^2T_2$ band and the appearance of four bands instead of two $^2T_1, ^2E$ bands show that a ligand field of lower than cubic symmetry is present.

It was not possible to resolve the visible and near-infrared spectrum of the ReI_6^{2-} ion. This spectrum is complicated by the presence of high-intensity charge-transfer bands which effectively mask the low-intensity ligand-field bands. Between 11,000 and 39,000 cm^{-1}, a total of 15 absorption maxima are observed. It is possible, however, to predict the value of $10Dq$. The fundamental crystal-field splittings ($10Dq = {}^4T_2$) for the ions given in Table 2.1 were found to be approximately a linear function of the atomic number of the halogen in the complex. This relation predicts that $10Dq$ for ReI_6^{2-} should be approximately 25,300 cm^{-1}, provided that the symmetry of the ligand field is still predominantly cubic.

The two highest energy bands in the $^2T_1, ^2E$ group and the lowest energy band of the $^2T_2$ group of ReF_6^{2-} and $ReCl_6^{2-}$ show extensive vibrational fine structure. The average energy separation of the vibrational bands is 150 cm^{-1} for $ReCl_6^{2-}$ and 240 cm^{-1} for ReF_6^{2-}. For $ReBr_6^{2-}$ only the 9200-cm^{-1} band shows extensive vibrational fine structure (average energy separation of 100 cm^{-1}); the 13,300-cm^{-1} band gives only two vibrational bands, with approximately the same separation. Because of this vibrational fine structure, the band locations given in Table 2.1 for these electronic bands are only approximate.

The principal absorption bands of the TcX_6^{2-} ions are given in Table 2.2. No vibrational fine structure was observed. An approximate fit of the observed energy levels was again obtained by using an extrapolated Tanabe-Sugano energy-level diagram for a d^3 configuration. The values obtained for the Racah parameter, B, were 490, 430, 375, and 425 cm^{-1} for the fluoride, chloride, bromide, and iodide complexes respectively. The near-infrared spectra of $TcBr_6^{2-}$ and TcI_6^{2-} were not measured; the wave numbers given in parentheses represent predictions of the center of gravity of the $^2T_1, ^2E$ bands based upon the above analysis. Evidence for a ligand field of lower than cubic symmetry is again indicated by the presence of several absorption bands where only one or two would be expected from a pure octahedral ligand field surrounding Tc^{4+}. The $10Dq$ energy separations are linear functions of the atomic number of the halogen. This relation was utilized to predict the $^4T_2$ energy level of the TcF_6^{2-} ion from those of the chloride, bromide, and iodide complexes before the K_2TcF_6 was synthesized. The prediction of 27,500 cm^{-1} for the $^4T_2$ level was in good agreement with the 28,400 cm^{-1} observed.

Table 2.2. Principal Absorption Bands of TcX_6^{2-} Ions, with Location of Bands Given in cm^{-1}

Energy-Level Designation	TcF_6^{2-}	$TcCl_6^{2-}$	$TcBr_6^{2-}$	TcI_6^{2-}
$^2T_1, ^2E$	10,600(s)[a]	8,600(s)		
	11,000	8,900(s)		
	11,400(s)	9,120	(8,500)	(9,400)
		9,530		
		9,720(s)		
$^2T_2$	17,600	14,180	13,200(s)	
		16,260	13,420	14,600
			13,900(s)	
$^4T_2$	28,400	25,800	22,500	17,700(s)
$^4T_1$	34,500	29,600	26,000	22,000

[a](s) = shoulder.

Hexavalent and Pentavalent Rhenium in Sulfuric Acid

R. H. Busey

Investigators[5,6] have reported the formation of a violet-colored species of rhenium in strong sulfuric acid upon reduction of perrhenate by a variety of reducing agents. They attribute the violet color to a Re(VI) species. The most recent study of oxidation states of rhenium in sulfuric acid below Re(VII) is that of Wehner and Hindman,[7] who made a controlled-potential electrolytic-reduction study of perrhenic acid in various sulfuric acid concentrations. They conclude that the oxidation state of the rhenium giving the violet solution has not been definitely established as Re(VI).

The investigation briefly described in this report is a spectrophotometric study of the violet species formed from perrhenate in concentrated sulfuric acid[8] by reduction with stannous sulfate. The spectrum (4000 to 8000 A) of the violet species formed shows one very broad absorption band with a maximum at 5200 A. Over this spectral range the absorption shows a large deviation from Beer's law. A dilution curve giving the absorbancy at any particular wavelength vs the relative concentration of rhenium is concave upward (dilution by concentrated sulfuric acid). The Beer's law deviation is not the same at all wavelengths, indicating that the absorption is due to more than one species.

With the addition of two or more equivalents of Sn^{2+} per mole of rhenium, the very intense violet color disappears, and a relatively pale sapphire blue solution of Re(V) results, which gives the spectrum shown in Fig. 2.1. The low intensity and relative sharpness of the absorption bands show that they are crystal-field bands. A crystal-field analysis of the spectra by a Tanabe-Sugano[9] energy-level diagram for a d^2 configuration shows that the Re(V) is in octahedral coordination.

Increasing amounts of Sn^{2+} (0.0754 *N*) in H_2SO_4 were added (under a nitrogen atmosphere) with a microburet to a series of $KReO_4$ samples dissolved in H_2SO_4, and the spectra from 4000 to 8000 A were determined. The total rhenium concentration was maintained constant at 6.43×10^{-3} *M* by addition of the required amount of H_2SO_4. The results are presented in Fig. 2.2. Maximum absorption occurs at each wavelength shown at a Sn/Re ratio (equivalents of Sn^{2+} to moles of Re) of 0.90 to 0.95. These curves clearly demonstrate that the violet color arises from formation of hexavalent rhenium. The absence of a sharp change in slope at a Sn/Re ratio of approximately unity is indicative of a disproportionation of the Re(VI), probably into Re(V) and Re(VII). Wehner and Hindman[7] also found evidence for this disproportionation.

The Re(VI) species are stable only in relatively high sulfuric acid concentration. A violet solution

[5] H. Holeman, *Z. anorg. u. allgem. Chem.* **220**, 33 (1934).

[6] O. Tomicek and F. Tomicek, *Collection Czechoslov. Chem. Communs.* **11**, 626 (1939).

[7] P. Wehner and J. C. Hindman, *J. Am. Chem. Soc.* **75**, 2873 (1953).

[8] The sulfuric acid used throughout was sulfuric acid distilled at atmospheric pressure.

[9] Y. Tanabe and S. Sugano, *J. Phys. Soc. (Japan)* **9**, 753, 766 (1954).

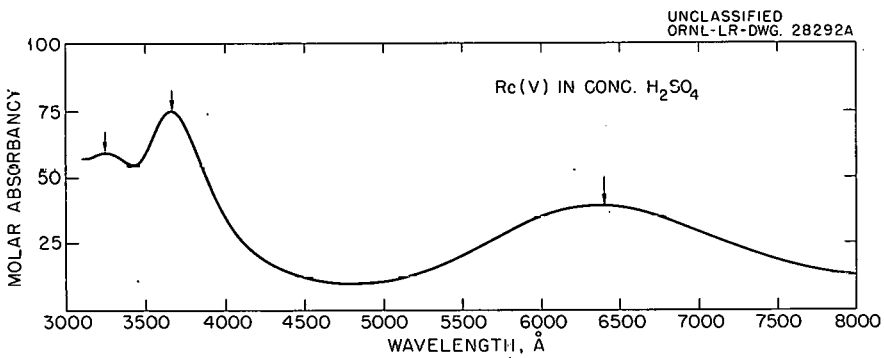

Fig. 2.1. Visible Spectrum of Pentavalent Rhenium Formed from Reduction of Perrhenate Ion in Concentrated Sulfuric Acid by Stannous Sulfate.

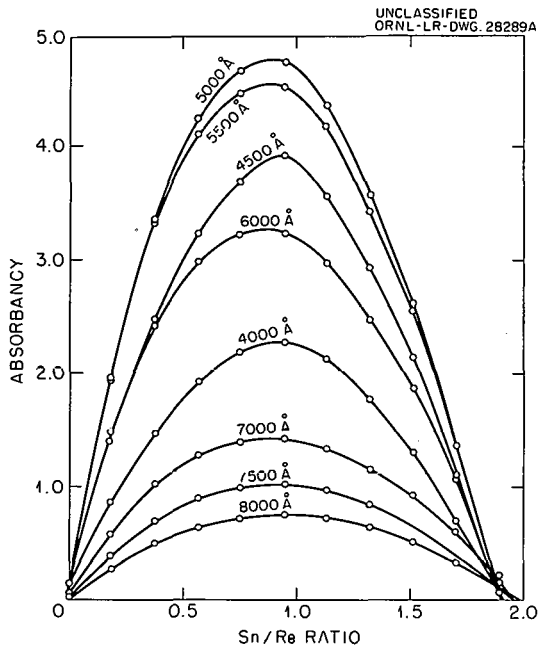

Fig. 2.2. Absorbancy at Several Wavelengths, of Solutions Formed by Reduction of Heptavalent Rhenium in Concentrated Sulfuric Acid with Stannous Sulfate, vs Sn/Re Ratio (Equivalents of Sn^{2+} to Moles of Re). Total Re = 6.43×10^{-3} M.

of Re(VI) in 18 M H_2SO_4 diluted by successive additions of water became essentially colorless at 12 M H_2SO_4. Another sample of Re(VI) in H_2SO_4 (Sn/Re ratio = 0.500) diluted with approximately twice its volume of water precipitated a blue-black solid after a few days. The precipitate separated by centrifugation from the dilute sulfuric acid and dissolved in 12 M HCl gave a solution whose visible and ultraviolet spectra revealed that the predominant rhenium species present was Re(V). The production of Re(V) by dilution with water of the Re(VI) in sulfuric acid lends support to the hypothesis of disproportionation of Re(VI) into Re(V) and Re(VII), water favoring the disproportionation.

All the above information suggests that two equilibria are involved: (1) a monomer-dimer equilibrium,

$$2\mathrm{Re(VI)}_{\mathrm{monomer}} = \mathrm{Re(VI)}_{\mathrm{dimer}} ,$$

giving

$$K_1 = \frac{[\mathrm{Re(VI)}_{\mathrm{dimer}}]}{[\mathrm{Re(VI)}_{\mathrm{monomer}}]^2} ;$$

and (2) a disproportionation equilibrium,

$$2\mathrm{Re(VI)}_{\mathrm{monomer}} = \mathrm{Re(V)} + \mathrm{Re(VII)} ,$$

giving

$$K_2 = \frac{[\mathrm{Re(V)}]\,[\mathrm{Re(VII)}]}{[\mathrm{Re(VI)}_{\mathrm{monomer}}]^2} .$$

A successful analysis of the data, by using these assumed equilibria, is briefly described below.

The dilution data indicate that the dimer is much the stronger absorber, since the dilution curve mentioned above is concave upward. The molar absorbancy at wavelength λ, $\epsilon_1(\lambda)$, of the monomer is given by the expression

$$\epsilon_1(\lambda) = \lim_{c \to 0} \frac{dA(\lambda)}{dc} ,$$

where $A(\lambda)$ is the absorbancy and

$$c = [\mathrm{Re(VI)}_{\mathrm{monomer}}] + 2[\mathrm{Re(VI)}_{\mathrm{dimer}}] .$$

This expression is based on the fact that at infinite dilution all the Re(VI) is present as monomer. The determination of ϵ_1(5200 A) was made by observing the absorbancy of successive dilutions of a dilute solution of Re(VI) that had a high concentration of Re(VII) present. The high concentration of Re(VII) made c = [Re(VI)] = normality of Sn^{2+}; that is to say, essentially no Re(V) was present. Extrapolation of the data to infinite dilution yielded ϵ_1(5200 A) = 500.

Dilution data given in Table 2.3 were used to determine ϵ_2(5200 A), the molar absorbancy of the dimer at 5200 A, and the monomer-dimer equilibrium constant K_1 by use of the equation

$$K_1 = \frac{(A - c\epsilon_1)\,(\epsilon_2 - 2\epsilon_1)}{(c\epsilon_2 - 2A)^2} .$$

Choice of the proper value of c by trial and error gave K_1 and ϵ_2, from which the dilution-curve absorbancy (column 2 of the table) could be calculated (column 3). The values obtained were K_1 = 140 and ϵ_2(5200 A) = 17,300. The absorbancy at 5200 A from Re(V) was sufficiently low to be ignored (Fig. 2.1).

The equilibrium constant for the disproportionation, K_2, was calculated from the A(5200 A), [Sn^{2+}], and total rhenium concentration (Table 2.4), by using data from the experiment described above

Table 2.3. Dilution Data of Hexavalent Rhenium

In initial solution (1.0 relative concentration), [Re] = 7.25×10^{-3} *M* and Sn/Re = 1.057

Relative Concentration	*A*(5200 A), Observed	*A*(5200 A), Calculated
1.0	5.64	5.56
0.9[a]	4.85	4.85
0.8	4.06	4.08
0.7	3.35	3.34
0.6	2.67	2.65
0.5	1.98	2.02
0.4	1.43	1.43
0.3[a]	0.925	0.925
0.2	0.49	0.49
0.1	0.16	0.18

[a]Calculated absorbancy fitted to these points.

Table 2.4. Total Absorbancy vs Concentration of Sn^{2+}

[Re] = 6.43×10^{-3} *M*

Sample Number	Corrected Normality of Sn^{2+}	*A*(5200 A)	K_2
	$\times 10^{-3}$		
1	1.922	2.045	3.3
2	3.164	3.50	2.9
3	4.372	4.34	3.0
4	5.588	4.75	3.1
5	6.533	4.82	3.1
6	8.025	4.44	3.2
7	9.240	3.64	3.3
8	10.462	2.68	3.2
9	11.690	1.43	2.6
10	12.92	0.09	
From dilution sample (Table 2.3)			3.4
		Average K_2	3.1

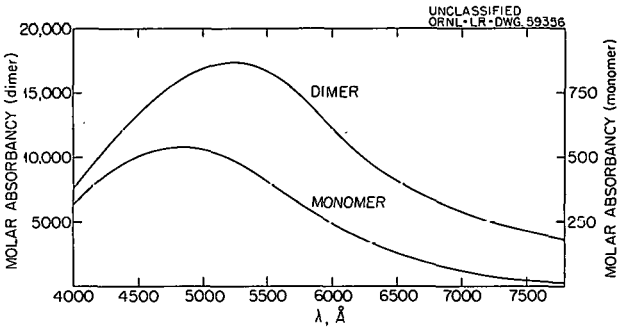

Fig. 2.3. Calculated Absorption Spectra of Monomeric and Dimeric Hexavalent Rhenium. Ordinate at left applies to dimer; ordinate at right to monomer.

(Fig. 2.2) in the following way. The concentration of the dimer is given in terms of K_1 and c by the expression

$$[\mathrm{Re(VI)}_{dimer}] = \frac{(4K_1c + 1) - (8K_1c + 1)^{1/2}}{8K_1},$$

and the concentration of the monomer is

$$[\mathrm{Re(VI)}_{monomer}] = c - 2[\mathrm{Re(VI)}_{dimer}].$$

For each sample, c was calculated by using the expression

$$c = \frac{(4d\epsilon_2 A - \epsilon_1) + (4d\epsilon_2^2 A - 8d\epsilon_1\epsilon_2 A + \epsilon_1^2)^{1/2}}{2d\epsilon_2^2},$$

where $d = K_1/(\epsilon_2 - 2\epsilon_1)$. The concentrations of Re(V) and Re(VII) were calculated from $[Sn^{2+}]$, c, and the total concentration of rhenium. The concentrations of Sn^{2+} given in Tables 2.3 and 2.4 have been corrected to make the maximum absorbancy (Fig. 2.2) fall at a Sn/Re ratio of 1. The spectrum of the stock solution of Re(VII) in sulfuric acid before addition of Sn^{2+} showed the presence of hexavalent rhenium.

The constancy of K_2 given in column 4 of Table 2.4 establishes the equilibria postulated as the correct ones. A small correction for Re(V) absorbancy was made in calculating K_2 for samples 7, 8, and 9. It is now possible to calculate the spectra of the monomeric and dimeric species of hexavalent rhenium from the observed spectra of the dilution experiment. The calculated spectra are given in Fig. 2.3. Note that the ordinate for the dimer is 20 times that of the monomer. A confirmation of the location of the maximum absorbancy at approximately 4850 A for the monomer is afforded by the observed shift of λ_{max} in the dilution-experiment spectra. A plot of λ_{max} against c extrapolates into 4850 A at $c = 0$.

From the magnitude of the molar absorbancy of the dimer it is obvious that the absorption band with a maximum at 5250 A is a charge-transfer band. The absorption band of the monomer with a maximum at 4850 A might be a ligand-field band, although the molar absorbancy would be high for such a band. Ligand-field theory predicts one broad absorption band for a d^1 configuration, which is the electronic configuration of hexavalent rhenium, provided that there is octahedral coordination.

3. CHEMICAL SEPARATION OF ISOTOPES

ION EXCHANGE STUDIES IN NONAQUEOUS SOLVENTS

D. A. Lee

The rate of exchange of alkali-metal ions between ion exchange resins and salts in nonaqueous solvents was studied. Generally, the rate in nonaqueous systems was very slow. Solvents which did not swell the resins were eliminated since the exchange rates would be too slow to be practical. Half-times of swelling, times of half-exchange ($T_{1/2}$) for alkali-metal ions, effective diffusion coefficients (D^i), and distribution coefficients (K_K^{Li}) were determined for several systems. Experiments were made in aqueous solutions for comparison with the data for nonaqueous solutions.

The swelling experiments are summarized in Table 3.1. Dowex 50-X8-Na^+ and IRC-50-K^+ were dried in vacuum over $Mg(ClO_4)_2$. The solvents were used as received from the manufacturer. A large number of organic solvents did not swell the resins. These included *N*-methylacetamide, propylene carbonate, acetic anhydride, *tert*-butylamine, tetrahydrofuran, ethylformate, 4-methyl-2-pentanone, dimethylformamide, and *n*-butylamine. Ethylenediamine would not swell IRC-50-K^+. The effective solvents are shown in Table 3.1.

The rates of exchange in nonaqueous media are summarized in Table 3.2. Batch equilibrations were made. Alkali-metal ions in the solvent and resin phases were analyzed by flame spectrophotometry. By using the theory of Boyd, Adamson, and Myers,[1] the effective diffusion coefficients were calculated. The rate-controlling process in these systems was "particle diffusion." The salt concentrations were >0.1 *N*. Since IRC-50 resin reacted with formamide, no meaningful studies could be made with that combination. For methanol systems the nature of the monovalent anion did not affect the exchange kinetics within experimental error. Reversing the cations in the resin and solution phases caused a change in the exchange rate in the methanol–Dowex 50 system. This effect will be investigated further.

From these studies it can be concluded that lithium isotope separations could be made in the methanol–IRC-50 system and in the Dowex 50–formamide system. However, column efficiencies probably would be poorer than in aqueous systems because exchange rates are approximately an order of magnitude faster in aqueous systems.

The water contents of Decalso exchangers and Dowex 50-X16 in the NH_4^+, K^+, and Li^+ forms were compared. These exchangers were air-dried under identical conditions, and the cation and

[1] G. E. Boyd, A. W. Adamson, and L. S. Myers, *J. Am. Chem. Soc.* 69, 2836 (1947).

Table 3.1. Half-Times of Swelling of Resins in Nonaqueous Solvents

Solvent	Dowex 50-X8-Na^+	IRC-50-K^+
Ethylene glycol	135 min	17 min
Methanol	86 min	5 min
Formamide	1690 min	6 days (reacts)
Formic acid	50 min	Reacts
Ethylenediamine	1030 min	None in 1 month

Table 3.2. Ion Exchange in Nonaqueous Solvents

System	D^i (cm^2/sec)	K_K^{Li}	$T_{1/2}$ (min)	Temperature (°C)
KOH-CH_3OH vs Dowex 50-X8-Li^+	2.7×10^{-9}	0.06	23	25
KBr-CH_3OH vs Dowex 50-X8-Li^+	3.3×10^{-9}		20	25
KI-CH_3OH vs Dowex 50-X8-Li^+	2.4×10^{-9}	0.06	25	25
KCN-CH_3OH vs Dowex 50-X8-Li^+	2.9×10^{-9}	0.05	21	26
KCNS-CH_3OH vs Dowex 50-X8-Li^+	3.2×10^{-9}	0.07	20	25
KPF_6-CH_3OH vs Dowex 50-X8-Li^+	2.7×10^{-9}	0.09	23	26
LiCl-CH_3OH vs Dowex 50-X8-K^+	1.4×10^{-9}	0.02	45	23
LiBr-CH_3OH vs Dowex 50-X8-K^+	1.4×10^{-9}	0.02	45	25
LiCl-CH_3OH vs IRC-50-K^+	1.9×10^{-7}	0.88	4	25
LiBr-CH_3OH vs IRC-50-K^+	1.7×10^{-7}	0.99	4.5	26
LiBr-EDA vs Dowex 50-X8-K^+	1.3×10^{-9}	0.03	48	26
LiBr-formamide vs Dowex 50-X8-K^+	1.4×10^{-8}	0.41	6	28
LiCl-formamide vs Dowex 50-X8-K^+	5.1×10^{-9}	0.44	11	25

Table 3.3. Water Contents in Exchangers [(meq H_2O)/(meq M^+)]

Form	Decalso	Dowex 50-X16
NH_4^+	1.83	2.40
Li^+	4.15	7.67
K^+	2.06	5.00

water contents were determined. The results are summarized in Table 3.3. The lower water content in the Decalso exchanger may account for the larger separation factor found for lithium isotopes separated on this exchanger.

SEPARATION OF BORON ISOTOPES

A. A. Palko

Characterization of the BF_3–organic complexes was continued in an effort to understand better the processes and factors which govern B^{10}-B^{11} isotopic exchange in gas-liquid systems. The methods used in these studies have been described previously.[2–4]

The solubility of BF_3 in $(CH_3)_2O$, $(C_2H_5)_2O$, $(C_2H_5)_2S$, and $(C_2H_5)_3N$ was determined at 400 and 760 mm Hg over the temperature range −20 to +30°C. These organic ligands, with the exception of $(C_2H_5)_3N$, dissolve BF_3 to a greater extent than is necessary to form the 1:1 complex. The presence of excess dissolved BF_3 in a gas-liquid exchange system such as the $BF_3(g)$–BF_3 organic complex(l) system has a tendency to lower the isotopic separation factor by an amount proportional to the amount of dissolved BF_3. Hence it is necessary to know the extent of the dissolved BF_3 present in order that observed separation factors might be corrected. These solubility data are shown in Figs. 3.1–3.3. Triethylamine reacts with only enough BF_3 to form the 1:1 complex. The melting point of the complex is 29.6°C.

Single-stage isotopic separation factors as a function of temperature are now being determined for the systems mentioned above. The data for the $(C_2H_5)_3N \cdot BF_3(l) \rightleftharpoons BF_3(g)$ system have been obtained and may be expressed by the equation $\log \alpha = (7.5667/T) - 0.015195$ from 30 to 50°C.

[2] A. A. Palko, R. M. Healy, and L. Landau, *J. Chem. Phys.* 28, 214 (1958).

[3] A. A. Palko, *J. Chem. Phys.* 30, 1187 (1959).

[4] A. A. Palko and J. S. Drury, *J. Chem. Phys.* 33, 779–81 (1960).

Values at 30°C for ΔS, ΔF, ΔH of exchange, calculated from the above equation, are ΔH = −34.6 cal/mole; ΔS = −0.069 cal deg^{-1} mole^{-1}; $\Delta F \approx -13.7$ cal/mole.

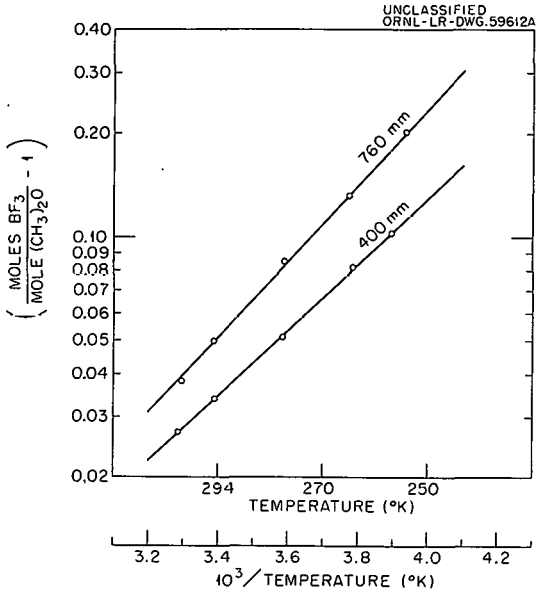

Fig. 3.1. Solubility of BF_3 in $(CH_3)_2O$ at 760 and 400 mm Hg.

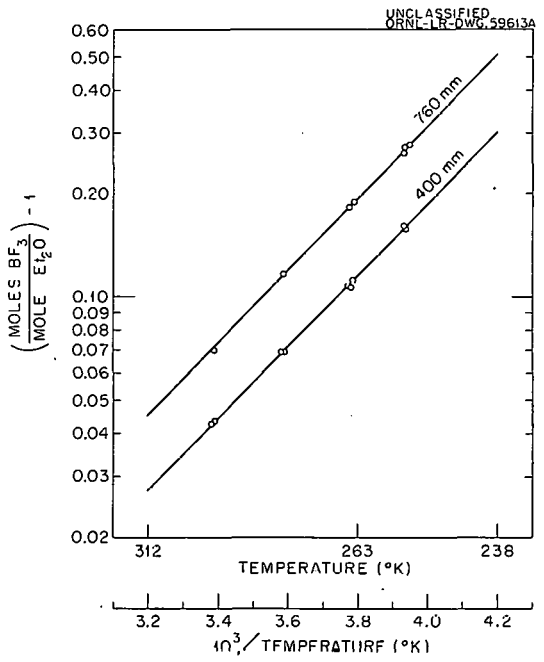

Fig. 3.2. Solubility of BF_3 in Diethyl Ether at 760 and 400 mm Hg.

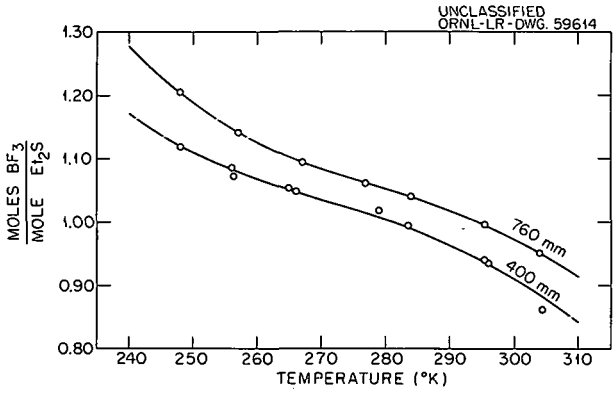

Fig. 3.3. Solubility of BF_3 in $(C_2H_5)_2S$ at 760 and 400 mm Hg.

A series of isotopically labeled BF_3 complexes was prepared in order that spectral shifts for the isotopically substituted molecules could be measured. The $B^{10}F_3$ used for these preparations assayed 96.5% B^{10}, and the $B^{11}F_3$ assayed 98+% B^{11}. The $(CD_3)_2O$ was obtained from Merck Ltd., Montreal, Canada. The labeled BF_3 complexes prepared for infrared and Raman spectral studies are shown below:

Tetrahydrofuran • $B^{10}F_3$	Tetrahydrofuran • $B^{11}F_3$
$Et_2O \cdot B^{10}F_3$	$Et_2O \cdot B^{11}F_3$
$NH_3 \cdot B^{10}F_3$	$NH_3 \cdot B^{11}F_3$
$(CD_3)_2O \cdot B^{10}F_3$	$(CD_3)_2O \cdot B^{11}F_3$
$2H_2O \cdot B^{10}F_3$	
$Et_3N \cdot B^{N}F_3$	

OXYGEN ISOTOPE SEPARATION IN THE SYSTEM PARALDEHYDE-ACETALDEHYDE

L. L. Brown

Acetaldehyde can be catalytically polymerized to a cyclic trimer with alternating C and O bonds:

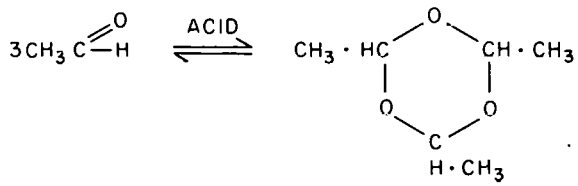

The equilibrium at room temperature favors the polymer (95%), from which the monomer can be recovered by distillation. Acetaldehyde boils at

21°C and freezes at −123.5°C, while the respective values for paraldehyde are 124 and 12.6°C. It is possible to have a gas/liquid equilibrium system that might separate oxygen isotopes and, furthermore, one that could be thermally refluxed.

Good isotopic analyses of O^{18} in CH_3CHO were difficult to obtain. Unsuccessful methods of sample preparation for the mass spectrometer include (1) purification alone, (2) pyrolysis with carbon at 1100°C to give CO, and (3) cracking at a hot filament to give CO. All these methods suffer from extraneous contributions to the mass peaks of principal interest. Spectroscopically clean CO was obtained finally through the use of a modified cracking procedure.

The "cracker" used is the same as described by Lauder[5] for volatile materials. Gas samples of 25 ml of CO (10^{-3} mole) and 0.3 ml of liquid bromine were used. The filament was maintained at 1100°C for 10 min. A departure from Lauder's procedure was necessary because the formation of HBr caused formation of the less volatile trimer. In order to vaporize the paraldehyde, a Glas-Col mantle was used around the lower portion of the cracker to warm it to 125°C. Estimates of sample recovery show the method to be reproducible and nearly quantitative.

A single-stage equilibration was made at 26°C and 1 atm pressure between 50 ml of liquid phase and 50 ml of gas. Phosphoric acid was used to catalyze the polymerization (95% trimer, 5% monomer). Samples of the gas were removed periodically up to 24 hr. An equal number of samples from the feed acetaldehyde was used to represent the liquid phase. Each gas sample was run against two liquid samples on the ratio mass spectrometer, and the average isotope ratio was determined. From ten pairs of samples (20 sets of ratios), the single-stage factor for O^{18}/O^{16} separation was 1.017 ± 0.002 (95% confidence level). The heavy isotope enriched in the liquid phase. The separation factor

$$\alpha\ [\alpha = (O^{18}/O^{16})(l)/(O^{18}/O^{16})(g)]$$

at various times was found to be:

Time (hr)	α
2	1.018
3	1.021
4	1.013
5	1.016
7	1.016
8	1.017
24	1.014

The reflux reaction was performed on a small scale. A steady flow of drops of the liquid phase was added to warm (50 to 60°C) mineral oil. The reflux flow rate of acetaldehyde vapor equaled that of the incoming paraldehyde after the short period that was required to reach a steady state. There was some discoloration of the oil. Reflux without the oil did not work well and resulted in charring of the aldehyde.

Current plans include a temperature study of the separation factor and a run with reflux in a multistage column.

STUDIES OF THE DIMETHYL ETHER–HYDROGEN CHLORIDE COMPLEX

L. L. Brown

Dimethyl ether and hydrogen chloride are known to form complexes in the ratios $1/1$, $1/2$, and $1/3$. The boiling point of the $1/1$ complex is higher than that of pure methyl ether and in the right direction for consideration of the complex for a thermally refluxed oxygen separation system. Measurements have been completed on several properties of interest.

The vapor pressure of the $1/1$ complex was determined over the temperature range −60 to 0°C by using an isoteniscope. The data were plotted as P vs $1/T$ on log paper, with the resulting equation: $\log P$ (cm Hg) $= -1149/T + 6.241$. The observed boiling point was −6°C. By using the isoteniscope of known volume and a weighed amount of complex, a pressure-temperature curve was obtained in the region where all the liquid was vaporized. From the slope of the curve an estimate of the degree of dissociation of the complex was made. For an ether/HCl ratio of 1.03/1, the vapor was 22% complexed between −12 and +10°C; for a ratio of 1.95/1 there was 32% complexing between −5 and +10°C.

[5] I. Lauder and B. Zerner, *Australian J. Chem.* 12, 621–29 (1959).

The single-stage separation factor

$$\alpha\,[\alpha = (O^{18}/O^{16})(l)/(O^{18}/O^{16})(g)]$$

for oxygen isotopes was determined at −32°C at an ether/HCl ratio of 1.21/1. The vapor pressure at this temperature is about 24 cm Hg and is due predominantly to ether. Equilibration was made in a 50-ml bulb with 15 ml of well-stirred complex. The oxygen distribution calculated as (liquid phase)/(gas phase) was 300/1, so that isotopic composition of the complex did not change appreciably during equilibration. Samples of the gas phase were taken periodically and later compared with samples of the complex. The samples were converted to CO for mass analyses by the cracker described previously. The O^{18} enriched in the liquid phase with a single-stage enrichment of 1.004 ± 0.004 (95% confidence interval). The sample times and related separation factors are shown below:

Time (hr)	α
1	1.0086
3	0.9997
4	1.0042
5	0.9997
6	1.0055

The large uncertainty in the α measurement is due to two samples at intermediate times which showed little separation. The direction of enrichment is clear, according to the remaining samples.

NITROGEN-CONTAINING COMPOUNDS

L. L. Brown

Several special nitrogen compounds were studied for possible usefulness in isotope separation. The intent was to measure fractionation between various nitrogen species, but this was not possible for reasons discussed below.

It was not possible to equilibrate NH_3 with ammonium amalgam ($NH_4 \cdot Hg$) because the amalgam was too unstable. An attempt was also made to equilibrate the solid tetramethylammonium amalgam, $(CH_3)_4N \cdot Hg$, with a solution of a tetramethylammonium salt. Electrolysis of $(CH_3)_4NCl$ from alcohol into mercury at −15°C produced an emulsion of mercury, alcohol, and solid amalgam. The emulsion could not be broken, and the solid amalgam was never separated.

Drago[6] has discussed various addition compounds between aliphatic amines and nitric oxide which form in the 2:2 ratio. Their suggested structure is $R_2NH_2{}^+R_2N{-}N(O)NO^-$, where R is an alkyl group. The diethylamine compound was prepared by using normal NO. A chloroform solution was equilibrated at −60°C with an equimolar quantity of $N^{15}O$ (96%). The last equilibration sample of the gas phase was taken after 6½ hr and showed no exchange between the complexed NO and the gaseous NO.

The isotopic values associated with the run are:

% Exchange	% N^{15} in Gas
0 (feed)	96.55, by assay
50 (1 NO)	50.98, calculated
100 (2 NO)	34.68, calculated
Found after 6½ hr	96.69, by assay

There are two distinct NO arrangements in the compound according to Drago's structure. Neither of them exchanged under the experimental conditions.

The well-known salt potassium dinitrososulfite, $K_2SO_3(NO)_2$, is formed by passing NO through a concentrated KOH solution saturated with SO_2. The structure assigned to this salt is $KO \cdot SO_2 \cdot N(OK) \cdot NO$. It was of interest to determine if exchange of nitrogen would occur between this compound and gaseous NO. Some of the salt was prepared from normal NO and was equilibrated in aqueous solution with an equal molar amount of 96% $N^{15}O$ at 25°C. Samples from the gas phase were taken periodically and, after being converted to N_2, were analyzed for % N^{15}. Divergent results were obtained, depending upon the peaks which were chosen for comparison. The discrepancy was traced to decomposition of the salt itself to N_2O, as shown by the normalized spectra of a six-day sample, shown below. The appearance of mass 46 indicates exchange before decomposition, since N_2O and NO are not known to exchange.

[6] B. R. Karstetter and R. S. Drago, *Reactions of Nitrogen(II) Oxides*, O.O.R. Report 2069:2 (May 1960).

Mass	Abundance	Sources
28	25.4	$N_2^{14}O$
29	12.7	$N^{14}N^{15}O$, $N^{15}N^{14}O$
30	70.7	$N^{14}O$, $N^{15}N^{14}O$
31	76.3	$N^{15}O$, $N^{14}N^{15}O$
44	100	$N_2^{14}O$
45	57.1	$N^{15}N^{14}O$, $N^{14}N^{15}O$
46	74.1	$N_2^{15}O$

Examination of the system was discontinued because of the instability of the salt and an apparent slow exchange of nitrogen between the salt and NO under the conditions studied.

SEPARATION OF ALKALI-METAL AND OF ALKALINE-EARTH ISOTOPES

D. Zucker

Calcium formate and calcium amalgam were equilibrated at room temperature for the determination of the separation factor.[7] In the amalgam leg, aqueous phases were prepared by reacting the amalgam with enough formic acid to decompose half the amalgam. In the aqueous leg, amalgam was prepared by electrolysis of the aqueous phase with a mercury cathode. Samples were converted to iodide for assay. A separation factor of 1.0013 ± 0.0003 per mass unit was obtained, with the heavy isotope concentrating in the aqueous phase.

The solubility of calcium in mercury is given in Table 3.4. These data were obtained by carefully filtering pre-equilibrated amalgam solutions containing excess calcium. The values are generally lower than those shown in the literature. It is believed that published data are erroneously high because of the tendency toward formation of finely divided calcium suspension when hot, saturated amalgam is allowed to cool.

The heats of reaction of calcium and mercury are given in Table 3.5 as a function of final calcium concentration. Measurements were made at concentrations of 0.23 to 0.68 mole/liter.

[7] D. Zucker, *Chem. Div. Ann. Progr. Rept. June 20, 1960*, ORNL-2983, p 21.

Table 3.4. Solubility of Calcium in Mercury

Temperature (°C)	Molarity of Calcium in Saturated Solution, 95% Confidence Level
0	0.563 ±0.005
10	0.651 ±0.005
20	0.745 ±0.005
30	0.843 ±0.005
36	0.909 ±0.005

Table 3.5. Heat of Reaction of Calcium and Mercury

Moles Calcium per Liter Mercury	Heat of Reaction, 95% Confidence Level (kcal per mole calcium)
0.0 (by extrapolation)	45.4 ±0.3
0.2	45.3 ±0.2
0.4	45.2 ±0.2
0.6	45.1 ±0.2
0.7	45.0 ±0.2

The exchange time between aqueous NaCl and sodium amalgam was found to be less than 3 sec. A five-stage batch equilibration of NaCl and sodium amalgam was performed by using Na^{22}, but no isotopic fractionation was observed. However, contamination of the distilled water and difficulties with electrolysis in the chloride system made the results uncertain. This work is being repeated, with NaOH being used instead of NaCl.

NITROGEN-15 SEPARATION

J. S. Drury

More than 70 g of 95 to 99% N^{15} were separated in the Nitrox cascade during the first half of this report period. With this latest addition, the accumulated inventory of N^{15} was deemed more than adequate for predictable needs, and operation of the cascade was terminated. The equipment was placed in stand-by condition.

OXYGEN-17 SEPARATION

J. S. Drury

Installation of the oxygen-17 cascade was completed during fiscal year 1961. Preoperational testing of the water distillation unit was begun in April and is continuing. A number of equipment changes became necessary because of the stringent requirements of this unique system. Satisfactory progress is being made in the shakedown operations, and productive operation is expected to begin soon.

CHEMICAL STRUCTURAL STUDIES BY NUCLEAR MAGNETIC RESONANCE

A. C. Rutenberg

A Varian Associates model V4302, dual purpose, nuclear magnetic resonance (NMR) spectrometer was put into operation. The structure of alkyl carbamates is now being studied. The accepted ionic formula

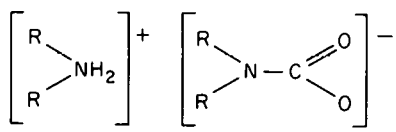

seems at variance with the properties of some of these compounds. Several of the alkyl carbamates are low-melting distillable compounds which are quite soluble in nonpolar solvents. The NMR spectra of the compounds formed by the reaction of two amine molecules with a CO_2 molecule were observed for ethyl, diethyl, *n*-propyl, *n*-butyl, and *t*-butyl amines and the 1:1 ethylenediamine-CO_2 compounds dissolved in CCl_4, benzene, $CHCl_3$, $CDCl_3$, CH_3OH, H_2O, or D_2O.

Only a single peak was observed for the hydrogen atoms that were not bonded to the alkyl carbons, indicating fairly rapid exchange among these hydrogens. This observation eliminates structures in which any of the non-alkyl hydrogens are bonded to the C of the CO_2, since such species would not be expected to exchange readily. Infrared spectra were run of the ethyl, diethyl, and tertiary-butyl amine carbamates dissolved in CCl_4. The spectra showed evidence of OH bonds in the ethyl and diethyl compounds but not in the *t*-butylamine carbamate. The infrared findings were in agreement with the location of the non-alkyl hydrogens in the NMR spectra of these compounds.

Ethylenediamine carbamate is somewhat different from the others. It melts at 170°C and is slightly soluble in organic solvents. Its NMR spectrum is also different from the spectra of the other carbamates studied.

Further work on this problem is in progress, and the present data do not unambiguously assign formulas to any of the alkyl carbamates. The existing data tend to favor a structure of the type

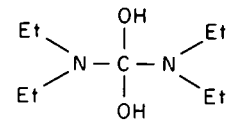

for the diethylamine-CO_2 compound, and the ionic form for the ethylenediamine addition compound.

SPECTROSCOPIC INVESTIGATIONS OF ISOTOPIC MOLECULES

G. M. Begun W. H. Fletcher
L. Landau

The study of the infrared and Raman spectra of isotopic molecules yields data which may be used to calculate isotopic exchange equilibrium constants. In addition, spectral data yield fundamental information concerning the configuration and bonding of the molecules observed. The use of isotopic species in mass spectral observations is very useful to provide unequivocal interpretation of the data.

Vibrational Spectra and Isotopic Partition-Function Ratios

The infrared and Raman spectra of various BF_3-addition complexes are of considerable interest, both theoretically and because of their use for the separation of boron isotopes. For this reason, samples of $BF_3 \cdot (CH_3)_2O$ and $BF_3 \cdot (CD_3)_2O$ were prepared, by using highly enriched B^{10} and B^{11}. The infrared and Raman spectral data of the various isotopic forms of the liquid complex are virtually complete. Assignment of the vibrational frequencies and calculation of partition functions are under way. Table 3.6 gives a summary of the most important observed bands of the complex.

A compilation of partition-function-ratio calculations for molecules containing nitrogen isotopes

Table 3.6. Tentative Vibrational Assignments for Boron Trifluoride–Dimethyl Ether Complexes (cm^{-1})

$BF_3 \cdot O(CH_3)_2$		Assignment[a]	$BF_3 \cdot O(CD_3)_2$	
B^{10}	B^{11}		B^{10}	B^{11}
322	322	$O(CX_3)_2$ wag	295	295
344	344	$O(CX_3)_2$ rock	332	332
499	499	C-O-C deformation	452	452
506	506	BF_3 deformation	503	502
675	662	B-O stretch	668	655
810	805	BF stretch (symmetric)	774	763
925	918	C-O stretch (symmetric)	877	872
1020	1020	C-O stretch (antisymmetric)	944	944
1150	1150	CX_3 rock	856	856
1225	1177	BF stretch (antisymmetric)	1223	1184
1259	1216	BF stretch (antisymmetric)	1260	1215
1459	1459	CX_3 deformation	1064	1063
1471	1471	CX_3 deformation	1129	1128
2850	2850	C-X stretch	2090	2090
2889	2889	CX_3 deformation (overtone)	2130	2130
2927	2927	C-X stretch	2263	2263
2979	2979	C-X stretch	2167	2167
3036	3036	C-X stretch	2280	2280
3069	3069	C-X stretch	2308	2308

[a] X is either H or D.

has been published.[8] In this article the nitrogen isotopic partition-function ratios were recorded for the following molecules and ions: N_2, N_2O, NO, NOCl, NO_2, NO_2^-, NO_3^-, and N_2O_4. All available isotopic and anharmonic data were used, and values of Q^{15}/Q^{14} were tabulated for temperatures at intervals from 100 to 600°K. Isotopic equilibrium constants calculated from the partition-function ratios were compared with those that have been observed experimentally.

Study of Force Fields of Selected Molecules

Calculation of the basic force constants which describe a molecular force field can be a useful tool for indicating electron distributions in molecules and is often helpful in making correct assignments of observed frequencies. Spectroscopic observations made on the oxalate ion in solution and in the crystalline state, as well as the infrared and Raman data previously reported on N_2O_4 (ref 9), are being subjected to mathematical analysis. A general program for computing the force constants for molecules containing up to 15 atoms has been written for use with the IBM 7090 computer. Preliminary results have shown an unexpected and otherwise undetectable error in the assignments made for N_2O_4, and they show the program to be generally useful

[8] G. M. Begun and W. H. Fletcher, *J. Chem. Phys.* 33, 1083–85 (1960).

[9] G. M. Begun and W. H. Fletcher, *J. Mol. Spectroscopy* 4, 388 (1960).

in assigning observed fundamental vibrational frequencies to their correct symmetry species. A systematic study of the force fields of NO_2, NO_2^-, and NO_3^- as well as N_2O_4 is in progress.

The infrared and Raman spectra of the oxalate ion in aqueous solution and in the crystalline state were re-examined because of the similarity of this ion to N_2O_4. Analysis of the spectral data for the $C_2O_4^{2-}$ ion in solution points very strongly to the conclusion that it is not planar, as has frequently been assumed, but has either D_2 or D_{2d} symmetry. Confirmation of this and of our present assignment of the observed spectra is being sought through use of the digital computer program.

Isotopic-Mass Spectral Studies

The study of the mass spectra and metastable transitions in the isotopic nitrous oxides ($N^{14}N^{14}O$, $N^{14}N^{15}O$, $N^{15}N^{14}O$, and $N^{15}N^{15}O$) reported last year[10] has been completed. The $(NO)^+$ fragment produced by electron impact was found to be formed by rearrangement as well as by loss of the end nitrogen. Ions produced by metastable transitions were shown to arise from both spontaneous and collision-induced dissociation of the parent molecule ion $(N_2O)^+$. Calculation of a theoretical cracking pattern for $N^{14}N^{14}O$ (Table 3.7), based upon a Franck-Condon vertical transition followed by immediate decomposition, accounted for the major features of the mass spectrum of nitrous oxide. The observance of delayed decompositions, however, indicates that a semistable excited state of the ion also exists. A possible explanation of the rearranged ions is the formation of triangular activated ions which subsequently decompose.

Table 3.7. Experimental and Calculated Mass Spectra for $N^{14}N^{14}O$

Ion	Experimental	Calculated
N_2O^+	100	100
NO^+	20.4	22.1
N_2^+	8.3	9.0
$N^+ + O^+$	6.1	3.8

[10] G. M. Begun and L. Landau, *Chem. Div. Ann. Progr. Rept. June 20, 1960*, ORNL-2983, p 22.

ISOTOPIC-MASS SPECTROSCOPY

L. Landau

Precise isotopic-mass analyses were made on samples of BF_3, CO, CO_2, N_2, and O_2 by using a Nuclide Analysis Associates RMS-1 ratio mass spectrometer.[11]

The CO, CO_2, N_2, and O_2 samples were run as ratios, with the minor isotope beam and the major isotope beam of a sample being collected simultaneously on different collector plates and then compared by attenuation of the larger current with a set of decade resistors until it matched the smaller. A dual inlet system with viscous leaks and a solenoid-operated valve system allowed the major-to-minor isotopic ratio of a reference sample to be compared with the ratio of the sample under investigation by admitting the two samples alternately to the ionization chamber of the mass spectrometer.

Two CO_2 samples from different sources were compared over a period of several months, and the ratio of ratios, (46/44 for sample 1)/(46/44 for sample 2), was determined. The results average 1.0155, have an average deviation at 95% confidence level of ±0.0002, and are shown below:

Run Number	Ratio of Ratios
224	1.0153
225	1.0157
226	1.0150
233	1.0158
234	1.0159
239	1.0156
307	1.0157
379 a	1.0155
379 b	1.0155
Av	1.0155

[11] L. Landau, *Chem. Div. Ann. Progr. Rept. June 20, 1960*. ORNL-2983, p 24.

4. RADIATION CHEMISTRY

RADIATION DAMAGE OF SILICA GEL

H. W. Kohn

The effects of gamma radiation on silica gel were studied by both physical and chemical means. Equipment for the observation of thermoluminescence[1] was assembled in order to relate it to the chemiluminescence previously observed when hydrogen or water was added to irradiated silica gel. Preliminary results with gamma radiation indicate that (1) no thermoluminescent peaks are produced from silica gel degassed at 300°C or below; (2) two luminescent peaks are produced in gels previously degassed at 400 to 550°C, one in the neighborhood of 100°C and another above the temperature range of the equipment (300°C); (3) a large decrease and slight temperature shift in the low-temperature peak and destruction of the high-temperature luminescence occur when hydrogen is added to the irradiated gel; and (4) destruction of both peaks occurs when oxygen is added to the irradiated gel. Illumination with ultraviolet light produces a broad thermoluminescent continuum.

In addition to the previously reported sharp paramagnetic resonance line at $g = 2.0005 \pm 0.0005$ produced in silica gel irradiated *in vacuo*, a second broad line, stable at −196°C on the low-field side of the sharp line, has also been observed. If oxygen is present during irradiation at −196°C, a third, broad, strong resonance at $g = 2.0061 \pm 0.001$ and an orange color appear.[2]

The study of color centers in synthetic silicas has been extended to minerals,[3] and the dependence of such defects upon impurities and their manner of incorporation in the matrix has been discussed.

[1] G. W. Arnold, *J. Phys. and Chem. Solids* 13, 306 (1960).

[2] H. W. Kohn, *J. Chem. Phys.* 33, 1588 (1960).

[3] H. W. Kohn and B. M. Benjamin, *Am. Mineralogist* 46, 218 (1961).

The gamma-ray-induced exchange of deuterated silica gel with methane and with hydrogen was studied. Ten-gram samples of deuterated gel, previously degassed near 500°C, were irradiated in the presence of small (0.3 to 1.0 mole %) amounts of hydrogen or methane, and the composition of the resultant gas was determined mass spectrometrically. From the amount and composition of the gas, the 100-ev yields of H_2, HD, D_2, and CH_3D, based on energy absorbed by the gel, were calculated.

Hydrogen exchange with gels previously poisoned with oxygen to suppress catalytic H_2-D_2 exchange gave room-temperature yields of 1.5 to 1.8 molecules of HD per 100 ev, and 0.6 to 1.0 molecule of D_2 per 100 ev. The formation of D_2 could be suppressed by degassing the gels at higher temperatures before irradiation or by lowering the temperature of the radiation reaction. These procedures did not appreciably affect the formation of HD.

The radiation reaction of the deuterated gel with methane gave low (<0.4 molecule per 100 ev) yields for all hydrogen species and somewhat greater (0.6 to 1.6) yields for CH_3D. Deuterated-product yield from both the methane and the hydrogen reaction increased as the degassing temperature of the gel was raised from 25 to about 400°C; further increases in the degassing temperature caused the yields to decrease. For impure gels (0.001 to 0.4% Al), the differential yield of deuterated products increased with uninterrupted dose up to the highest dose used, 7×10^{20} ev/g. Independent experiments with deuterium, methane, and silica gel, and with silica gel covered with a monolayer of heavy water, showed that the reactions studied were truly reactions of the gel with the gas, not a series of gaseous exchanges or a variant of water radiolysis.

These data indicate that energy is transferred from the gel to the substrate. Correlation of different preparative procedures for the gel with the

observed radiation yields suggests a charge-transfer process involving ions as the most probable mechanism.

A simple experiment substantiates this postulate. Samples of silica gel on which 1 wt % of triphenylmethane is adsorbed are usually pale yellow. When irradiated with gamma rays, they develop the bright yellow color characteristic of triphenylmethyl carbonium ion, and when illuminated with ultraviolet light, they become the orange color characteristic of the triphenylmethyl free radical.

CATALYTIC REACTIONS ON SEMICONDUCTORS

G. E. Moore E. H. Taylor

In support of investigations on the effects of ionizing radiation on metallic and semiconducting catalysts, a study of the hydrogen-deuterium exchange and formic acid vapor decomposition on unirradiated, chemically doped, elemental germanium was completed. An abstract of these results follows.

Hydrogen-treated powders of chemically doped elemental germanium were used as two-carrier semiconducting catalysts for hydrogen-deuterium exchange and formic acid vapor decomposition over the temperature range 100 to 400°C. Kinetic parameters were related to the electronic chemical potential of the solid; their dependence suggested that the rate-limiting processes involved electronic charge shifts between adsorbate and semiconductor. Two different rate processes appeared to limit the hydrogen-deuterium exchange: a chemisorptive step with electron shift from adsorbate to solid in the region of *n*-type semiconductivity, and a reaction step with electron shift from solid to adsorbate in the region of *p*-type semiconductivity. Dehydrogenation of formic acid vapor appeared to be limited only by an electron shift from adsorbate to semiconductor.

RADIOLYSIS OF CRYSTALLINE ALKALI-METAL BROMATES WITH Co^{60} GAMMA RAYS

G. E. Boyd E. W. Graham Q. V. Larson

The radiolysis of the alkali-metal bromates by Co^{60} gamma rays was effected to decompositions greater than 3 mole %. The amounts of bromate ion decomposed increased linearly with dose at first, but subsequently the dependence became nonlinear for all salts except $LiBrO_3$. The initial 100-ev radiolytic yields or G_0 values were 0.31, 1.46, 1.71, 2.33, 3.40, and 5.1 for $LiBrO_3$, $NaBrO_3$, $KBrO_3$, $RbBrO_3$, $CsBrO_3$, and $TlBrO_3$ respectively. The yields increased only slightly with temperature between −195 and 85°C and for $CsBrO_3$ were almost independent of the dose rate from 8.3×10^{20} to 7.1×10^{22} ev $mole^{-1}$ hr^{-1}.

The radiolysis of bromate ion gave bromite, hypobromite, bromide, and oxygen gas in amounts which varied with the alkali-metal cation in the salt and with the total dose absorbed. Almost all the higher bromine oxidation states formed by radiolysis could be recombined to bromate by thermal annealing.

The radiolytic yields for bromate decomposition could not be correlated with either the thermodynamic stability of the salts or with their isothermal decomposition rates observed in the absence of radiation. However, an exponential dependence of G_0 on the crystal "free space" was found, and a mechanism for the decomposition of the molecular bromate ion could be proposed.

THERMAL SPIKES IN THE ALPHA-PARTICLE RADIOLYSIS OF NITRATE CRYSTALS

C. J. Hochanadel

One of the distinguishing characteristics of the chemical action of ionizing radiation is that energy is deposited in a medium along tracks of charged particles of high velocity. This leads not only to high, localized concentrations of intermediates but also to other extreme, transient conditions along the tracks. Probably the most important of these is transient local heating. However, even though most of the energy deposited in the system is rapidly converted to heat, giving instantaneous "temperatures" of several thousand degrees in these microscopic regions, estimates based on macroscopic thermal conductivity indicate that the heat is dissipated so rapidly that it could have little influence on the processes leading to chemical change. Track effects are therefore generally explained merely on the basis of spatial correlation of the intermediates (e.g., the radiation chemistry of water). However, the number of adjustable parameters is generally so large and the information on any one of them so scanty that no definite evidence for or against thermal effects in tracks can be offered. Comparison of yields for the decomposition of nitrate crystals by alpha particles with yields for

Table 4.1. Summary of Initial 100-ev Yields of Nitrite, $G(NO_2^-)$, Produced in the Decomposition of Various Nitrate Crystals by Radiations of Different Stopping Powers and at Several Temperatures

Salt	3.4-Mev Alpha Particles (~34 ev/A)		Cobalt-60 Gamma Rays[a] (~0.06 ev/A)		44.5-kvp X Rays[b] (~0.8 ev/A)		Ultraviolet Light			
							Published Data[c]		ORNL Data[d]	
	G	Temp (°C)	G	Temp (°C)	G	Temp (°C)	G	Temp (°C)	G	Temp (°C)
$NaNO_3$	1.3	25	0.27	30	0.4	15	0.2		0.2	40
	1.1	120	1.0	150	1.1	150			0.6	150
KNO_3[e]	2.2	25	1.5	30	2.0	15	1.6		1.7	40
			3.0	150	3.0	150			2.7	150
$CsNO_3$	1.4	25	1.6	30	1.4	15	3.0			
			2.3	150	1.2	150				
$Ba(NO_3)_2$	1.6	25	~1.8	30	1.8	15	0.8	30–250		
			~1.6	150	1.8	150				
$LINO_3$	0.7	25	0.02–0.2	30	0.02	15	0.03			
			0.03–0.4	150						

[a]Values at 30°C are in agreement with those of C. J. Hochanadel and T. W. Davis, *J. Chem. Phys.* 27, 333–34 (1957) and with recently reported results of J. Cunningham, *J. Phys. Chem.* 65, 628–35 (1961).

[b]Values selected from results of J. Cunningham and H. G. Heal, *Trans. Faraday Soc.* 54, 1355–69 (1952).

[c]From P. Doigan and T. W. Davis, *J. Phys. Chem.* 56, 764–66 (1952).

[d]This work.

[e]D. Hall and G. N. Walton, *J. Inorg. & Nuclear Chem.* 10, 215–24 (1959), reported $G(NO_2^-) = 6.0$ for decomposition of KNO_3 by fission recoil particles (~730 ev/A).

decomposition by gamma rays, x rays, or ultraviolet light at various temperatures implies directly that thermal effects along alpha-particle tracks are an important factor in the radiolysis.

Initial yields of nitrite are listed in Table 4.1. Yields differ for the various crystals, indicating a sensitivity to the nature of the crystal structure. Also, for decomposition by gamma rays, x rays, or ultraviolet light, the yields generally increase with increased ambient temperature. The yield for sodium nitrate, which is relatively low at room temperature, shows the largest increase with increase in temperature. It also shows the largest increase with increase in LET (linear energy transfer – energy loss per unit track length). In addition, the yield for decomposition by alpha particles is relatively insensitive to the ambient temperature. Trends of product-vs-dosage curves indicate that steady-state concentrations depend qualitatively on structure, temperature, and LET in the same way as do initial yields. The various results suggest that thermal effects in alpha-particle tracks are an important factor and that decomposition is influenced to some extent by the diffusion characteristics of the intermediates.

RADIOLYSIS BY TRANSFERRED ENERGY OF COMPOUNDS DISPERSED IN ALKALI HALIDE MATRICES

A. R. Jones

The investigation of the radiolysis by transferred energy of substances suspended in alkali halides was continued during the past year. The decompositions of nitrate and nitrite ions in potassium bromide were the principal subjects. It was shown (Fig. 4.1) that, although the initial rates for the decomposition of nitrate ion and for the formation of nitrite ion may be equivalent during the radiolysis of nitrate ion dispersed in KBr, no equilibrium is attained because the nitrite ion decomposes with the formation of unidentified products which do not recombine to form an equivalent amount of nitrate ion (Fig. 4.2); it is not possible to equate the amount of nitrite ion found after irradiation with the amount

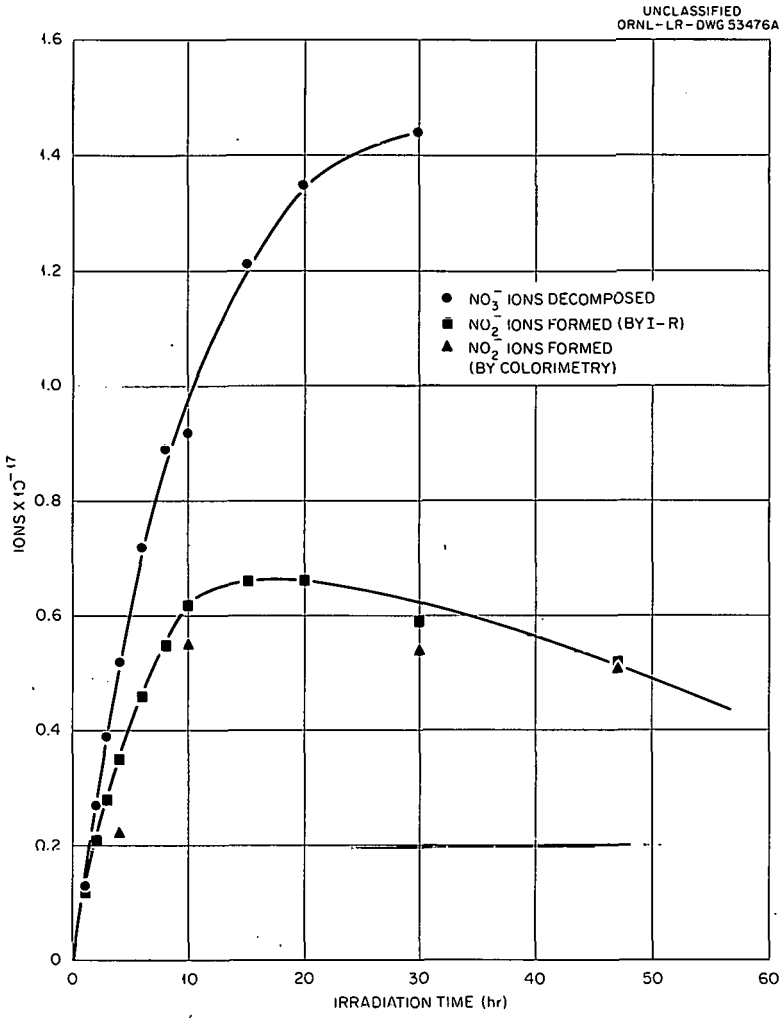

Fig. 4.1. Gamma Radiolysis of Nitrate Ions Dispersed in a KBr Matrix. Infrared data represents averages for four matched disks.

of nitrate ion decomposed, as has been done by investigators of the radiolysis of pure potassium nitrate.

Although the presence of nitrite ions within irradiated crystals of potassium nitrate and in the aqueous solution formed by dissolving the irradiated crystals had been established,[4,5] the equality of these two measures had only been assumed. Such an equality is not self-evident: The dissolution of irradiated sodium carbonate yields different chemical products, depending upon the different heat treatments before solution.[6] The dissolution of irradiated sodium azide yields ammonia as well as nitrogen gas.[7] Even irradiated sodium chloride crystals when dissolved in pure water produce a basic solution that has oxidizing capabilities.[8,9] Moreover, in a set of experiments in which irradiated crystals of potassium nitrate were heated to various temperatures in a vacuum, the yields of evolved oxygen and aqueous nitrite ion obtained upon subsequent dissolution of the crystals decreased as the temperature was increased above 129°C, results which the authors explained by assuming the presence within the irradiated salt of atomic oxygen and free radicals which yield NO_2^-

[4] J. Cunningham and H. G. Heal, *Trans. Faraday Soc.* 54, 1355 (1958).

[5] J. Forten and E. R. Johnson, *J. Phys. and Chem. Solids* 15, 218 (1960).

[6] L. J. Sharman and K. J. McCallum, *J. Am. Chem. Soc.* 77, 2989 (1955).

[7] H. G. Heal, *Can. J. Chem.* 31, 1153 (1953).

[8] M. Hacskaylo and D. Otterson, *J. Chem. Phys.* 21, 552 (1953).

[9] M. Hacskaylo, D. Otterson, and P. Schwed, *J. Chem. Phys.* 21, 1434 (1953).

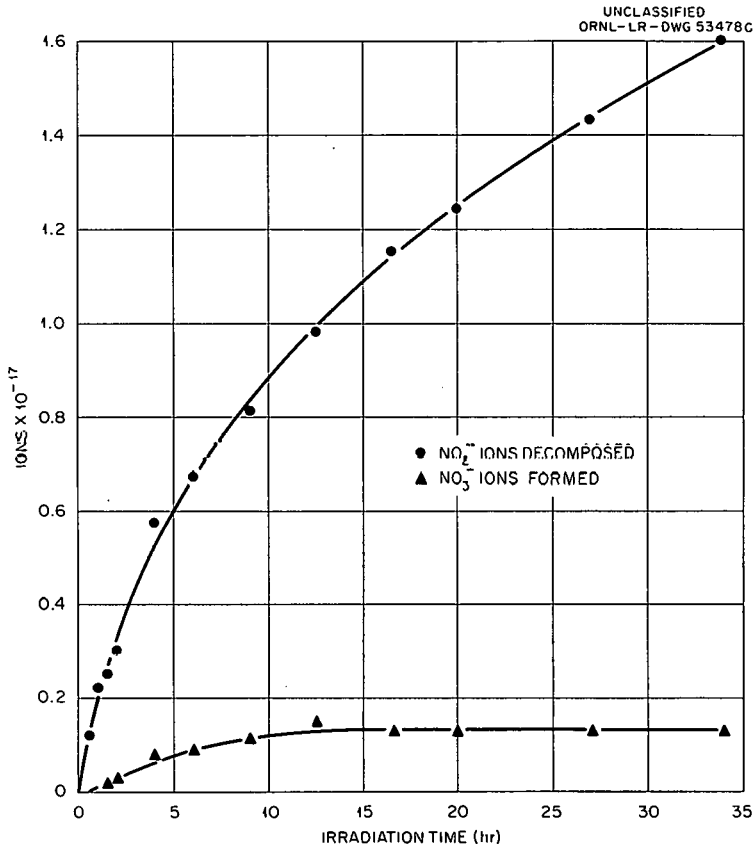

Fig. 4.2. Gamma Radiolysis of Nitrite Ions Dispersed in a KBr Matrix. Data represents averages for four matched disks (analyses by infrared method).

upon dissolution and which are stable in the crystalline lattice below the transition temperature.[10] The data of Table 4.2 show that the nitrite ion found in an aqueous solution of the irradiated solid mixture of KNO_3 and KBr existed in the solid prior to dissolution and thus did not arise by reaction of stabilized intermediates with water. It has been shown[11] that stabilized free radicals can be produced in alkali halide matrices by photolysis. It therefore appears that if the decomposition of nitrate ions produces free radicals or radical-ions stabilizable by a crystalline lattice, then in the system investigated these intermediates should have an equal or better opportunity to maintain their identity than they have in a potassium nitrate lattice.

Table 4.2. Formation of NO_2^- by Radiolysis of NO_3^- In a Potassium Bromide Lattice, as Determined Before and After Dissolution of the Crystals in Water

Time (arbitrary units)	Number of NO_2^- Ions $\pm\sigma$,[a] by Direct Infrared Analysis of Solid	Number of NO_2^- Ions $\pm\sigma$, by Colorimetric Analysis of Water Solution
	$\times 10^{17}$	$\times 10^{17}$
1	0.30 ±0.02	0.30 ±0.03
2	0.87 ±0.04	0.78 ±0.04
3	1.36 ±0.03	1.31 ±0.09
4	2.00 ±0.03	1.80 ±0.08
5	2.65 ±0.04	2.49[b]
6	3.41[c]	3.42 ±0.08

[a] σ = standard deviation.
[b] Two identical values.
[c] One value.

[10] A. S. Baberkin, M. A. Proskurnin, and V. D. Orekhov, "Action of Ionizing Radiation on Inorganic and Organic Systems," *Akad. Nauk S.S.S.R.*, p 186 (1958).

[11] H. T. J. Chilton and G. Porter, *Spectrochim. Acta* 16, 390 (1960).

Plots of the optical densities at 4000 A vs the concentrations of KNO_3 or KNO_2 dispersed in pressed KBr disks show discontinuities which appear to correspond to the respective solubilities of NO_3^- and NO_2^- in KBr (Fig. 4.3). The solubility of KNO_2 is about 0.08_2 mole %, in agreement with the result of Ketelaar[12] (0.1 mole %), obtained by a different method. The solubility of KNO_3 is about 0.21 mole %. The method appears to be generally useful for substances with different indexes of refraction than the alkali halide solvent.

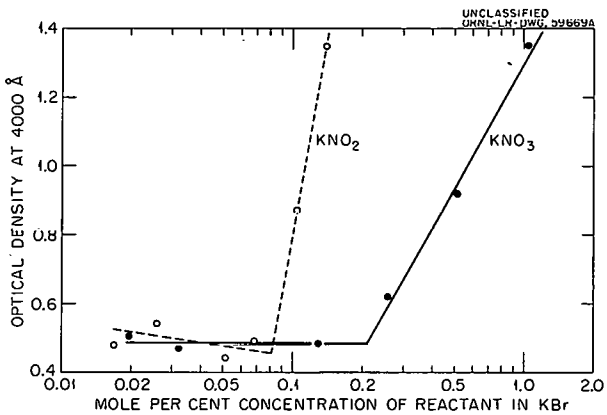

Fig. 4.3. Determination of Solubilities of KNO_2 and KNO_3 in KBr.

The decomposition of nitrate ion in potassium bromide has been studied as a function of the concentration of the reactant and of the energy absorbed by the matrix. The course of the radiolysis is expressed with good precision and to greater than 50% decomposition of the NO_3^- by $C_0 - C = k_1D - k_2D^2$. The values of the constants for each initial concentration of the reactant are listed in Table 4.3.

Table 4.3. Constants for the Equation $C_0 - C = k_1D - k_2D^2$, Which Expresses the Course of the Decomposition of Nitrate Ions in Potassium Bromide[a]

Initial Concentration of Nitrate Ions, C_0 (ions per g of KBr)	$k_1 = G_0$[b]	k_2[c]
$\times 10^{17}$		
0.658	0.124	0.117
1.316	0.225	0.179
2.632	0.227	0.176
3.29	0.233	0.165
6.58	0.553	0.499
9.92	0.688	0.550
16.50	1.051	1.05
32.9	2.19	1.94
66.3	0.652	0.732
131.6	0.373	0.285
263	0.294	0.155
526	0.235	0.147

[a] C is the concentration of NO_3^- per gram of KBr, expressed as ions $\times 10^{17}$. D is the accumulated dose per gram of KBr, expressed as ev $\times 10^{19}$.

[b] G_0 is the initial yield, expressed as ions decomposed per 100 ev.

[c] The units of k_2 are $\dfrac{NO_3^-\text{ ions} \times \text{g of KBr}}{(\text{ev} \times 10^{11})^2}$.

THE OH RADICAL YIELD IN THE Co^{60} GAMMA RADIOLYSIS OF AQUEOUS NITRIC ACID SOLUTIONS[13]

H. A. Mahlman

The Co^{60} gamma-ray radiolysis of concentrated aqueous HNO_3 solutions has been interpreted as the composite of two decomposition mechanisms: a molecular process, $HNO_3 \rightsquigarrow HNO_2 + \frac{1}{2}O_2$, and a radical process, $HNO_3 \rightsquigarrow OH + NO_2$. The existence of these direct-action decomposition mechanisms is suggested by consideration of the molecular and ionic yields generated by the gamma irradiation of HNO_3 and $NaNO_3$ solutions. These yields are reported as G(product), which is defined as the number of molecules or ions produced by 100 ev of absorbed energy.

The hydrogen yields observed from the irradiation of deaerated aqueous HNO_3 solutions, containing 10^{-3} M KBr to protect the molecular

[12] J. A. A. Ketelaar, C. J. H. Schutte, and B. L. Schram, *Spectrochim. Acta* 13, 336 (1959).

[13] H. A. Mahlman, *Journal of Chemical Physics* (to be published).

hydrogen from OH radical attack, were found to be essentially the same as those observed in comparable $NaNO_3$ solutions. Therefore the differences to be discussed cannot be attributed to these small discrepancies in the molecular hydrogen yields. The oxygen yields from the $NaNO_3$ solutions indicate that a decomposition of the nitrate ion to nitrite ion and molecular oxygen also takes place, just as in photochemistry.[14] Since molecular oxygen is a product of the gamma-ray irradiation of deaerated aqueous HNO_3 solution, the equivalent decomposition is assumed.

The mechanisms for the Co^{60} gamma-ray irradiation-induced reduction of ceric ion in a Ce^{4+}–0.4 *M* H_2SO_4 solution[15] and in a Ce^{4+}–0.4 *M* H_2SO_4–Tl^+ solution[16] predict that the difference in cerous yields (5.72) is equal to $2G(OH)$. Sodium nitrate additions to these ceric systems cause the cerous yields to increase as a function of the $NaNO_3$ concentration,[17,18] as illustrated in Fig. 4.4. However, the difference in these cerous yields [the $G(Ce^{3+})_{Tl^+}$ observed in the Ce^{4+}–0.4 *M* H_2SO_4–$NaNO_3$–Tl^+ system less the $G(Ce^{3+})_{no\ Tl^+}$ observed in the Ce^{4+}–0.4 *M* H_2SO_4–$NaNO_3$ system] remained constant and was interpreted as evidence that the $G(OH)$ from solvent decomposition was constant, independent of the $NaNO_3$ concentration (see Fig. 4.5).

As shown in Fig. 4.4, replacing the $NaNO_3$ with comparable concentrations of HNO_3 also caused the cerous yields to increase with increasing HNO_3 concentration. However, in these HNO_3-containing ceric solutions the difference in cerous yields $[G(Ce^{3+})_{Tl^+} - G(Ce^{3+})_{no\ Tl^+}]$ was not constant but increased in direct proportion to the HNO_3 concentration (see Fig. 4.5). The increasing difference in the cerous yields is ascribed to the direct-action decomposition of HNO_3 to give OH and NO_2 radicals. The $G(OH)$ from the direct-action decomposition of HNO_3 may be found by correcting the difference in cerous yields for the amount of OH radicals generated from solvent decomposition, as found from the studies of $NaNO_3$-containing ceric solutions and the amount of NO_2 formed simultaneously with the OH radical in the radical process. Thus, as shown in Fig. 4.5, the $G(OH)$ from HNO_3 decomposition varies from 0 at zero HNO_3 concentration to 1.89 at 7 *M* HNO_3. These data

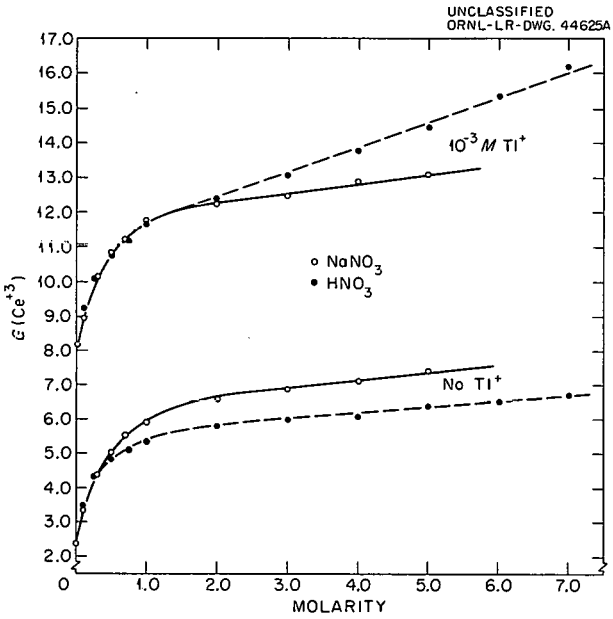

Fig. 4.4. Effect of $NaNO_3$ and HNO_3 on Cerous Yield.

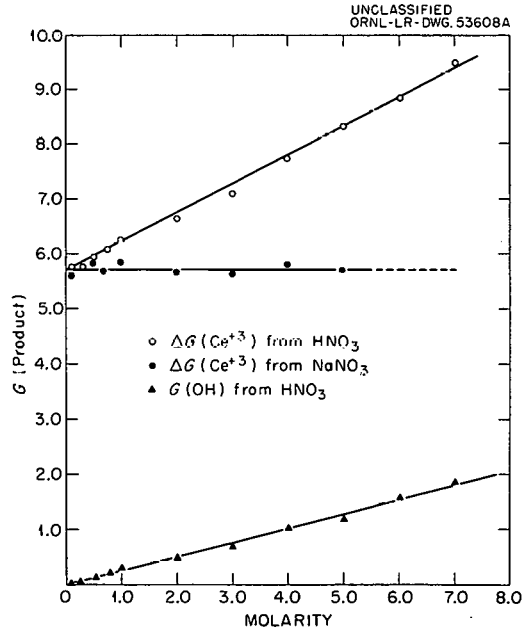

Fig. 4.5. $\Delta G(Ce^{3+})$ and $G(OH)$ in Acidic Ceric Solutions Containing $NaNO_3$ and HNO_3 as a Function of Nitrate Molarity.

[14] E. Warburg, *Sitzber. preuss. Akad. Wiss., Physik.-math. Kl.* 1918, 1228 [*Chem. Abstr.* 14, 1930 (1920)].

[15] A. O. Allen, *Radiation Research* 1, 87 (1954).

[16] T. J. Sworski, *Radiation Research* 4, 483 (1956).

[17] T. J. Sworski, *J. Am. Chem. Soc.* 77, 4689 (1955).

[18] H. A. Mahlman, *J. Phys. Chem.* 64, 1598 (1960).

represent the first evidence that a direct-action effect that is directly proportional to the nitrate concentration takes place in a nitrate solution.

RADIATION CHEMISTRY OF SULFURIC ACID SOLUTIONS

J. W. Boyle

Investigation of the Co^{60} gamma radiolysis of Ce(IV)–sulfuric acid solutions has continued during the past year, with emphasis on concentrated solutions. The results are summarized in Fig. 4.6. Initial yields (molecules produced per 100 ev absorbed) of the various products are presented as a function of the stoichiometric electron fraction (e.f.) of sulfuric acid. This function (e.f. H_2SO_4) is defined by the expression $n_a z_a/(n_a z_a + n_w z_w)$, where, respectively, n_a and n_w are the number of moles of acid and of water per liter of solution, and z_a and z_w are the number of electrons associated with each molecule of H_2SO_4 and of H_2O.

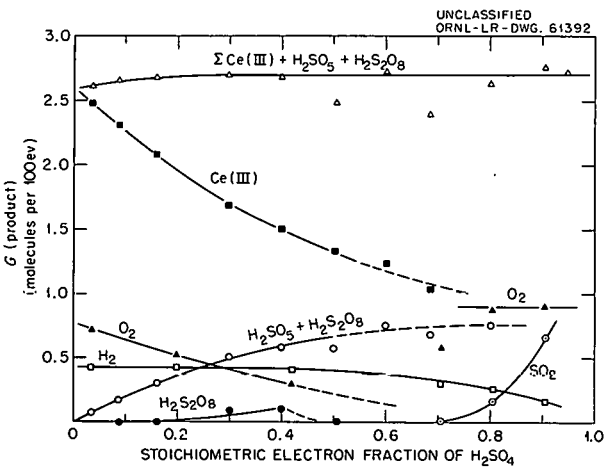

Fig. 4.6. Initial Yields of the Various Products of the Co^{60} Gamma Radiolysis of Ce(IV)–H_2SO_4 Solutions as Functions of the Stoichiometric Electron Fraction of H_2SO_4.

There is a reaction in these solutions, first noted by Sworski[19] in 10 *M* acid solution, which continues after the irradiation has been terminated. This postirradiation reaction has been investigated and shown to be a reaction between H_2SO_5 and Ce(IV):

$$H_2SO_5 + 2Ce(IV) + H_2O \longrightarrow H_2SO_4 + 2Ce(III) + 2H^+ + O_2 \cdot \quad (1)$$

The rate of this reaction increases greatly as the sulfuric acid concentration increases; for example, the rate increases by 10^3 as the acid concentration is changed from 9 to 15 *M*. This change in rate parallels the change in the apparent rate of the hydrolysis of H_2SO_5, as measured by Monger and Redlich:[20]

$$H_2SO_5 + H_2O \longrightarrow H_2SO_4 + H_2O_2 \cdot \quad (2)$$

It is well known that H_2O_2 and Ce(IV) react rapidly and completely; so it is postulated that the mechanism of reaction (1) involves first the hydrolysis of H_2SO_5 (rate-determining step) and then the reaction of H_2O_2 with Ce(IV).

The determination of the initial Ce(III) and H_2SO_5 yields for solutions having >0.5 e.f. H_2SO_4 was possible only through a kinetic treatment of the postirradiation reaction. Yields determined in this way are included in Fig. 4.6 and agree with an extrapolation of the yields from lower acid concentrations, where H_2SO_5 and Ce(III) can be measured without interference from the postirradiation reaction. In solutions having an e.f. H_2SO_4 >0.8, the reaction between H_2SO_5 and Ce(IV) is complete in a matter of seconds. In this region only the sum of the Ce(III) yield plus reaction (1) is observed. These summation yields are in agreement with an extrapolation of the summation yields at lower acid concentrations. The yields of $H_2S_2O_8$ and the gaseous products H_2, O_2, and SO_2 have been measured also and are included in Fig. 4.6. This phase of the study is now complete, and a detailed report is being prepared for publication.

RADIOLYSIS OF LIQUID OXYGEN

J. F. Riley

Gaseous oxygen was the first radiolysis system in which both the amount of ionization and the yield of chemical product were measured.[21] Although the system offered simplicity in products,

[19] T. J. Sworski, *Chem. Div. Semiann. Progr. Rept. June 20, 1955*, ORNL-1940, p 66.

[20] J. M. Monger and O. Redlich, *J. Phys. Chem.* 60, 797 (1956).

[21] S. C. Lind, *J. Am. Chem. Soc.* 47, 397 (1911).

being limited to ozone, yields were erratic and in later work were found[22,23] to depend upon flow rate and radiation intensity, presumably because of a chain back-reaction. The maximum yield, observed at high flow rates, was estimated as 6 molecules of ozone per 100 ev of dose.

There has been very little study of the irradiation of liquid oxygen, even though the electron affinity of oxygen and its consequences[24] offer basic interest. In 1955, Pshezhetsky[25] reported some fragmentary results on the radiolysis of liquid oxygen and nitrogen-oxygen mixtures. In both systems he found $G(O_3) = 15$ molecules per 100 ev. While within theoretical limits, this high yield represents an extremely efficient (22%) energy conversion. Other workers have not confirmed the high yield; Brown[26] and Kircher[27] both report a G value of 6 for ozone formation in liquid oxygen at 77°K.

A major experimental difficulty in the radiolysis of liquid oxygen is the assay of the product, ozone. The usual analysis, by chemical reaction, requires the vaporization and transfer of the ozone-oxygen mixture, without loss by decomposition. We approached the problem by absorption spectrophotometry, which does not require sample transfer or vaporization.

By means of low-temperature cells and quartz Dewars, the absorption spectrum of liquid oxygen has been obtained over the region 8000 to 2700 A. Cells of 2 and 5 cm path length, with pure silica windows, were used with liquid-nitrogen coolant (77°K) in a Cary model 11MS spectrophotometer. The spectrum of liquid oxygen is complex, and still not clearly explained.[28] Fifteen absorption bands of the Ellis-Kneser series were observed between 8000 and 3100 A; below 2900 A, strong, continuous absorption sets in, the edge of which shows vibrational structure. Ozone has an intense, broad absorption band at about 2550 A, with a long tail observed to extend to nearly 3300 A. Because ozone is a much stronger ultraviolet absorber than oxygen, we are able to determine the ozone concentration in liquid oxygen by measurement of the absorption in the 2900–3100 A region.

By alternate gamma irradiation and ultraviolet absorption measurement, we have observed, *in situ*, the formation of ozone in liquid oxygen. Ozone concentrations as low as 2 ppm have been measured by the change in absorbance in the 2900–3100 A region, as described above. The absorbance in this region was found to be a linear function of radiation dose, for five increments of 5.4×10^{17} ev/g.

Our preliminary G values for ozone formation in liquid oxygen are 14 to 16 molecules of ozone per 100 ev of dose. A final value will depend on a proper calibration of ozone absorbancy at 77°K in the spectral region used. However, our preliminary value is a factor of 2 greater than Kircher's and agrees with the high value reported by Pshezhetsky.

RADIOLYSIS OF BIPHENYL

W. H. Baldwin P. S. Rudolph

The study of the radiolysis of biphenyl (ϕ_2) continued. It was reported previously[29] that the alpha radiolysis of solid biphenyl that had been coated on the inside of a glass sphere was complicated by the biphenyl flaking off the glass. The radon-alpha radiolysis has been repeated with the solid biphenyl deposited in the bottom of an oval-shaped Pyrex vessel formed by sealing two watch glasses together.

"Polymer," the product that boils higher than the original biphenyl, is the main product from the radiolysis of biphenyl. For comparative studies polymer was prepared by Co^{60} gamma radiolysis and by the reaction of free radicals in solution that was initiated by the thermal decomposition of di-*t*-butyl peroxide at 150°C.

The yields of products are summarized in Table 4.4. Hydrogen constitutes more than 90% of the gaseous products reported here and by others

[22] J. D'Olieslager, *Bull. acad. roy. med. Belg.* 11, 711 (1925).

[23] S. C. Lind and D. C. Bardwell, *J. Am. Chem. Soc.* 51, 2754 (1929).

[24] J. L. Magee and M. Burton, *J. Am. Chem. Soc.* 73, 523 (1951).

[25] S. Ya. Pshezhetsky *et al.*, *Collection of Papers on Radiation Chemistry, Academy of Sciences, USSR, 1955*, p 133.

[26] D. W. Brown and L. A. Wall, *J. Phys. Chem.* 65, 915 (1961).

[27] J. F. Kircher *et al.*, *Radiation Research* 13, 452 (1960).

[28] V. I. Dianov-Klolov, *Optika i Spektroskopiya* 1, 650, 863 (1956); 4, 448 (1958); and 6, 290 (1959).

[29] W. H. Baldwin and P. S. Rudolph, *Chem. Div. Ann. Progr. Rept. June 20, 1958*, ORNL-2584, p 20.

Table 4.4. Data on Products of Reactions of Biphenyl

Type of Reaction	Energy Absorbed (ev)	$G(H_2)$	$G(CH_4)$	$-G(\phi_2$ Conversion to Benzene-Insoluble Polymer)	$-G(\phi_2$ Conversion to Benzene-Soluble Polymer)	Molecular Weight[a] of Benzene-Soluble Polymer
	$\times 10^{22}$					
Alpha radiolysis	2.4	0.058	0.0078	0.039	0.55	450–500
Alpha radiolysis	4.4	0.03	0.003	0.046	0.45	450
Gamma radiolysis	47.0				0.25	390
Free radicals in solution						490

[a]Determined cryoscopically in cyclohexane or benzene. The calculated value for biphenyl is 154; for quatraphenyl, 306; and for sexaphenyl, 458.

(see Table 4.5). The yield of hydrogen from the alpha radiolysis of biphenyl was higher than from radiolysis with electrons or gamma rays (factors of 2 to 8).

The polymer from the reactions of biphenyl was defined as the material of low vapor pressure that remains after the removal of excess biphenyl under reduced pressure. The distilled, excess biphenyl was examined by means of gas chromatography and infrared absorption spectroscopy. Only in the case of the excess biphenyl from the reaction of free radicals in solution was another product found. This may be a methyl biphenyl formed by the addition of methyl free radicals to a biphenyl residue.

Table 4.5. Yield of Hydrogen from Radiolysis of Biphenyl

Type of Radiation	Temperature of Biphenyl (°C)	$G(H_2)$	Literature Reference
Alpha	25	0.06	
Alpha	25	0.03	*a*
Gamma	82	0.007	*b*
Gamma	100	0.008	*c*
1-Mev e^-	30	0.005–0.01	*d*
1-Mev e^-	250	0.02	*e*

[a]W. H. Baldwin and P. S. Rudolph, *Chem. Div. Ann. Progr. Rept. June 20, 1958*, ORNL-2584, p 20.

[b]K. L. Hall and F. A. Elder, *J. Chem. Phys.* 31, 1420 (1959).

[c]J. G. Burr and J. M. Scarborough, *J. Phys. Chem.* 64, 1367 (1960).

[d]E. L. Colichman and R. H. J. Gercke, *Nucleonics* 14(7), 50 (1956).

[e]W. G. Burns, W. Wild, and T. F. Williams, *Proc. U.N. Intern. Conf. Peaceful Uses Atomic Energy, 2nd, Geneva, 1958*, 29, 266 (1959).

The molecular weight of the polymers was determined cryoscopically in benzene or cyclohexane, as limited by solubility. Polymer from alpha radiolysis was fractionated by its solubility in benzene. The benzene-insoluble fraction was not examined further, but the average molecular weight of the benzene-soluble alpha-radiolysis polymer (450 to 500; see Table 4.4) was slightly higher than that of the gamma-radiolysis polymer (390) and about the same as that obtained from the free radicals in solution (490).

The formation, by alpha particles, of products of higher molecular weight (indicated by direct measurements and by the solubility in benzene) than those formed with gamma rays is consistent with the concept of linear-energy transfer.

Comparative infrared absorption spectra of polymeric products (using biphenyl as the monomer and phenyl cyclohexane as a model of a polymer) were used to seek additional information about the nature of the polymers. The spectra in the region of 3.3 to 3.6 μ, assigned to C-H stretching (Fig. 4.7), show differences. Only one peak (3.3 μ)

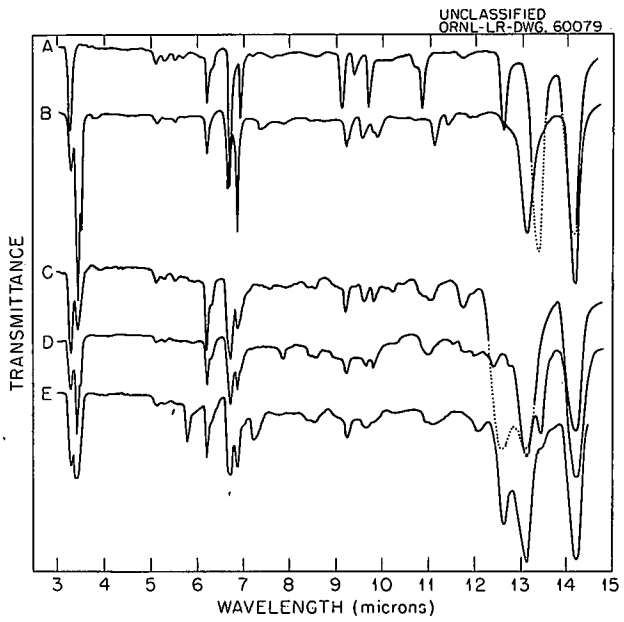

Fig. 4.7. Infrared Absorption Spectra of Alpha-Induced Polymer, Free-Radical-Induced Polymer, and Related Compounds. A, biphenyl; B, phenylcyclohexane; C, alpha polymer; D, gamma polymer; E, F.R.S. polymer.

was obtained with biphenyl. The polymeric products formed from biphenyl, however, show additional peaks in this region and are more nearly like the spectrum of phenyl cyclohexane. The reactions seem to have resulted in the hydrogenation of formerly aromatic rings to produce compounds that contain more than one hydrogen atom per carbon atom. This hydrogenation has already been established during the gamma radiolysis of benzene (Gordon, Van Dykken, and Doumani[30]) and in the reactions of benzene in the presence of free radicals in solution that were initiated by the thermal reactions of dibenzoyl peroxide.[31]

The polymer that was formed from biphenyl by free radicals in solution showed another important spectral difference: An absorption peak at 5.8 μ is probably due to the presence of a carbonyl group that was introduced as an acetone radical, a product formed from di-*t*-butyl peroxide. Products of the acetone radical have been reported by Raley *et al.*[32]

In summary, it can be stated that alpha radiolysis of solid biphenyl results in higher yields of products than does gamma radiolysis. The polymeric products have an average molecular weight about three times that of biphenyl and are partially hydrogenated.

ENERGY TRANSFER THROUGH TRANSIENT SPECIES IN THE RADIOLYSIS OF BINARY MIXTURES OF ACETYLENE AND THE NOBLE GASES

P. S. Rudolph S. C. Lind C. E. Melton

Binary mixtures of acetylene and the noble gases were irradiated by 90-ev electrons in the ionization chamber of a research mass spectrometer. Mixtures of varying proportions were studied as a function of total pressure up to 1.3 mm Hg.

Ionic complexes, $[XeC_2H_2]^+$ and $[XeC_2H]^+$, were observed in the C_2H_2-Xe system (e.g., see Fig. 4.8). In an equimolar mixture, the intensities of those complexes were proportional, respectively, to the third and second powers of the total pressure. Over the ranges studied (10^{-3} to 10^{-2} mm Hg and 0.1 to 0.34 mm Hg), the intensity ratio of $[XeC_2H_2]^+(160)/[XeC_2H]^+(159)$ was linearly proportional to pressure. This indicates that both complexes come from the same precursor, the activated ionic complex $[XeC_2H_2^*]^+$. The complex $[XeC_2H]^+$ results from the spontaneous dissociation of the common precursor, whereas $[XeC_2H_2]^+$ results from a stabilizing collision of the precursor with a neutral molecule and is therefore favored at higher pressures.

No ionic complexes were observed in the other mixtures studied.

ALPHA RADIOLYSIS OF ETHYLENE

P. S. Rudolph W. H. Baldwin

Recent studies by Bardwell[33] indicated that the yield obtained in the x-ray radiolysis of C_2H_4 is

[30] S. Gordon, A. R. Van Dykken, and T. F. Doumani, *J. Phys. Chem.* **62**, 20 (1958).

[31] DeL. F. De Tar and R. A. J. Long, *J. Am. Chem. Soc.* **80**, 4742 (1958).

[32] J. H. Raley, F. F. Rust, and W. E. Vaughn, *J. Am. Chem. Soc.* **70**, 88 (1948).

[33] D. C. Bardwell, unpublished work.

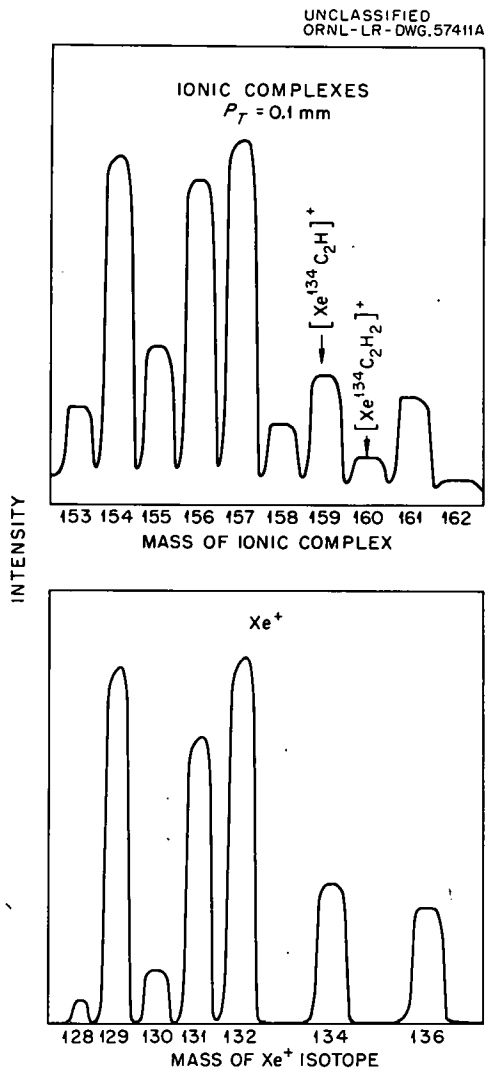

Fig. 4.8. Isotopic Patterns of $[XeC_2H]^+$, $[XeC_2H_2]^+$, and Xe^+ Observed in a $5C_2H_2$:1Xe Mixture at a Total Pressure of 0.1 mm in the Ionization Chamber of a Mass Spectrometer.

higher than the value reported by Lind and Bardwell[34] for the alpha radiolysis. The alpha radiolysis of ethylene was undertaken to clarify this possible discrepancy.

Ethylene was irradiated in a small spherical reaction vessel by the alpha particles from radon. Pressure measurements were made at 25 and −196°C. Calculations of the velocity constant $(k\mu/\lambda)'$ were made, by using the same equation and the same assumptions as in the previous work.[34] However, in the present work 0.123 for the ratio of molecular ionizations is used, compared with 0.139 previously used[34] for these calculations.

The data are presented in Table 4.6. The average value for $(k\mu/\lambda)'$ for over 50% consumption of C_2H_4 is 59.6, compared with the previous value of 66.5 (ref 34). This is good agreement, since different values for molecular ionization were used in the calculations, and use of the older values would give 67.4 for the present measurements.

The alpha radiolysis of C_2H_4 gives mainly noncondensable gases and a polymer. The polymer first appears as a colorless, nonviscous liquid which on continued irradiation turns brown and viscous and finally solidifies. The increasing ratio $(+\Delta P_{nc}/-\Delta P_c)$ indicates that the nc (noncondensable) gas comes primarily from the irradiation of the polymer rather than from the irradiation of the C_2H_4.

The residual gas, after the radon decayed, was analyzed by gas chromatography and mass spectrometry and found to be principally H_2. The mole percentages of the constituent gases were as follows:

H_2	86.7	C_2H_6	4.6
O_2	0.1	C_3H_8	1.9
N_2	0.2	i-C_4H_{10}	0.4
CH_4	6.6	n-C_4H_{10}	<0.1
CO	0.1	C_2H_4	<0.1
		H_2O	0.8

The small amounts of O_2 and N_2 observed presumably arise from air or reaction with the glass.

Insufficient polymer resulted from this irradiation to allow analysis for composition and molecular weight.

[34] S. C. Lind and D. C. Bardwell, *J. Am. Chem. Soc.* 48, 1556 (1926).

Table 4.6. Alpha Radiolysis of C_2H_4

Volume of reaction vessel = 9.636 cc
Diameter of reaction vessel = 2.640 cm
E = 0.1668 curie, initial activity of Rn

Molecular ionizations:
$g(C_2H_4) = 1.71$
$g(H_2) = 0.211$

$e^{-\lambda t}$	Pressures at 25°C[a]			$(k\mu/\lambda)'_{2\ cm}$	$+\Delta P_{nc}/-\Delta P_c$
	P_{tot}	P_c	P_{nc}		
1.0000	783.0	783.0	0		
0.9683	673.3	656.2	17.1	58.1	0.135
0.9318	568.4	528.0	40.4	60.4	0.182
0.8447	406.9	311.5	95.4	59.9	0.254
0.7963	353.2	229.1	124.1	60.1	0.348
0.6638	276.9	99.3	177.6	55.1	0.412
0.5553	272.0	63.1	208.9	29.8	0.865
0.3215	313.4	45.9	267.5	5.33	3.41

[a]Total and noncondensable (P_{nc}) pressures were measured, while P_c (pressure of condensable gases) represents their difference.

EVIDENCE FOR NITROGEN MIGRATION IN THE BENZILIC ACID REARRANGEMENT OF ALLOXAN AND ITS DERIVATIVES

R. W. Spayd[1] C. J. Collins

The benzilic acid rearrangement of alloxan (I) to alloxanic acid[2] (II) has been the subject of a recent[3] kinetic study, on the basis of which it was suggested that three different anions could be formed, any one of which could conceivably be a rearrangement intermediate. These results led to the proposal[3] that not only a carbon-carbon shift but also a nitrogen-carbon shift was possible during the rearrangement I → II. Although both possibilities had been suggested before,[2b,4] the work of Kwart and Sarasohn[3] appears to be the first presumptive evidence that a nitrogen-carbon shift during a benzilic acid rearrangement is possible. Tracer studies with C^{14} have now been carried out which show unambiguously that the nitrogen shift takes place to the exclusion of the carbon shift during rearrangement of alloxan and several of its derivatives under widely differing conditions of pH. Alloxan (I*a*, $R^1 = R^2 = H$) labeled in the 5 position (Chart 1) was prepared by oxidation, with chromic anhydride, of the barbituric acid obtained from urea and methylene-labeled malonic ester.[5] It was then subjected to rearrangement (1) at pH 7 to 10 in KOH solution, (2) at pH 13 in NaOH solution, (3) at pH 9.4 in NaOH-$Na_2B_4O_7$ buffered solution, (4) at pH 7.2 to 7.5 in NaOH-Na_3PO_4 buffered solution, and (5) at pH ~1 in HNO_3. In the experiments performed under alkaline conditions, the alloxanic acid (II*a*) was oxidized to parabanic acid (III*a*) with nitric acid solution, whereas in the acid-catalyzed rearrangement, parabanic acid (III*a*) was formed directly. Radioactivity assay of III*a* and I*a* (or its barbituric acid precursor) or II*a* demonstrated that the samples of III*a* possessed 98.5 to 102.6% of the original radioactivity (see Chart 1). Several derivatives of alloxan labeled in the 4 positions[6] were next prepared; such derivatives, designated I*b* (Chart 2), were subjected to most of the same conditions of rearrangement as was the isotope position isomer I*a*. The values x and $1 - x$ are the mole fractions of product formed through shift of R^1N- or R^2N- respectively. If no isotope effect is exhibited, it would be expected, when $R^1 = R^2$, that $x = 0.500$, whereas if $R^1 \neq R^2$, x could have values of zero to unity. The results of experiments with I*b* are given in Table 5.1.

Although the data of Table 5.1 deviate somewhat from the theoretical values of $x = 0.500$ and $x = 1.00$ (excluding for the moment lines 8 and 9 concerning *N*-methylalloxan-4-C^{14}), the deviations are no greater than those to be expected from the operation of normal intramolecular or intermolecular isotope effects. We therefore conclude that (1) each rearrangement takes place with exclusive

[1]ORINS predoctoral Fellow from the University of Delaware.

[2](*a*) F. Wöhler and J. V. Liebig, *Ann.* **26**, 241 (1838); A. Schlieper, *Ann.* **263**, 55 (1845); (*b*) H. Biltz, M. Heyn, and M. Bergius, *Ann.* **413**, 68 (1916); (*c*) G. M. Richardson and R. K. Cannon, *Biochem. J.* **23**, 68 (1928); (*d*) J. W. Patterson, A. Lazarow, and S. Levey, *J. Biol. Chem.* **177**, 187 (1949).

[3]H. Kwart and I. Sarasohn, *J. Am. Chem. Soc.* **83**, 909 (1961).

[4](*a*) S. Selman and J. F. Eastham, *Quart. Revs. (London)* **14**, 234 (1960); (*b*) F. R. Fisher and R. A. Day, *J. Am. Chem. Soc.* **77**, 4895 (1955).

[5]According to the procedure of A. V. Holmgren and W. Wenner, *Organic Syntheses*, vol 32, p 6, Wiley, New York, 1952.

[6]The route employed in the synthesis of *N*-methylalloxan and of *N*-phenylalloxan starts with the appropriate monosubstituted urea and cyanoacetic-*carboxyl*-C^{14} acid to yield $RNHCONHC^*OCH_2CN$, which undergoes ring closure in the presence of alkali to produce the monosubstituted iminobarbituric acid [W. Traube, *Ber.* **33**, 3039 (1900)]. Hydrolysis of the imine to the barbituric acid with 6 *N* HCl followed by chromic acid oxidation (see ref 5) produced the *N*-methyl- or *N*-phenylalloxan-4-C^{14}. Alloxan-4-C^{14} and *N,N*-dimethylalloxan-4-C^{14} were prepared according to the procedure of ref 5, using carboxyl-labeled malonic ester and urea or dimethylurea as reactants.

CHART I

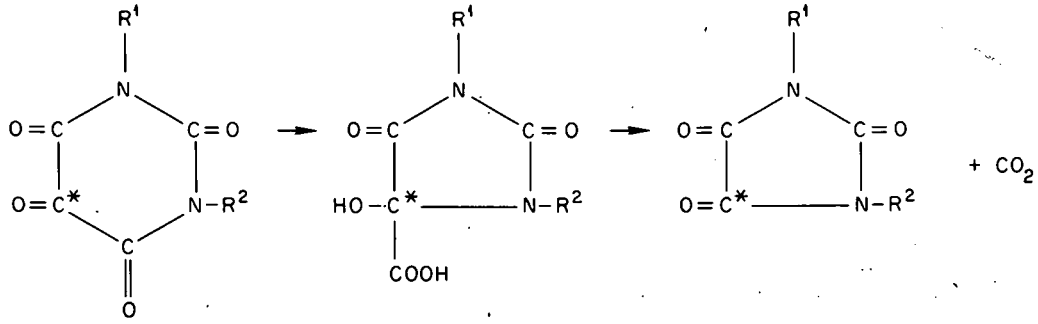

Ia IIa IIIa

CHART II

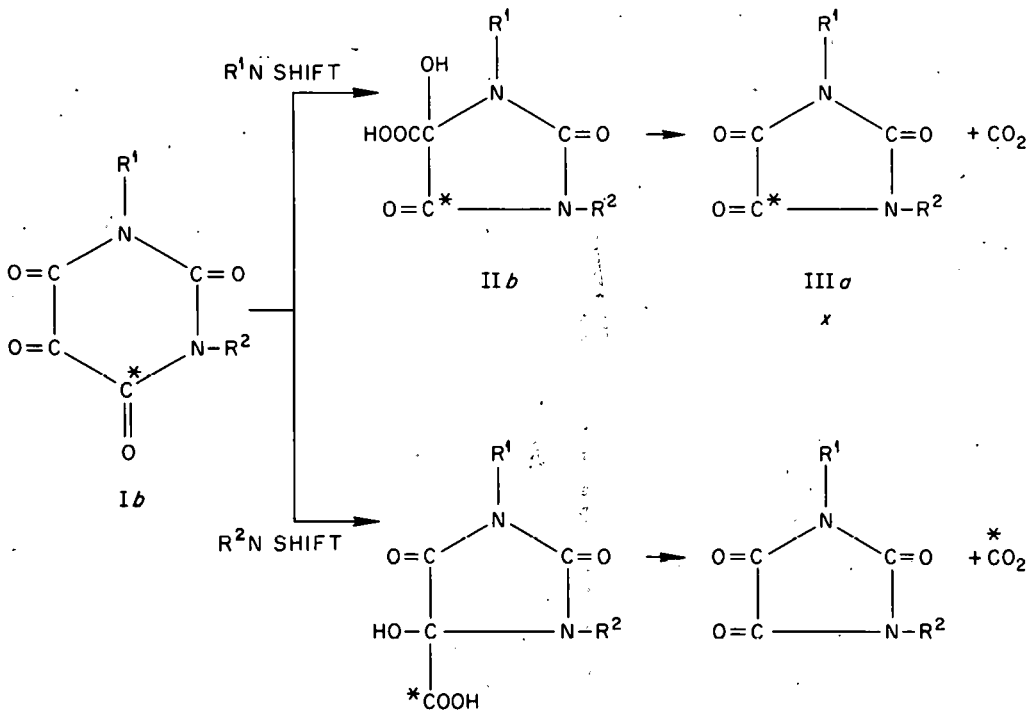

Ib IIb IIIa x IIc III 1 − x

Table 5.1. Radiochemical Results of the Rearrangement of Alloxan-4-C^{14} and Derivatives (I*b*)

Approximate pH	Substituent in I, II, and III		x[a]	$1 - x$[b]
	R^1	R^2		
< 1	H	H	0.533	0.467
7.5	H	H	0.542	0.458
9.4	H	H	0.503	0.497
7–10	H	H	0.498	0.502
> 13	H	H	0.550	0.450
< 1	CH_3[c]	CH_3[c]	0.528	0.472
7–8	CH_3	CH_3	0.529	0.471
< 1	CH_3[d]	H[d]	0.754	0.246
7–8	CH_3	H	0.803	0.197
< 1	Ph[e]	H[e]	0.973	0.027
7–8	Ph	H	0.960	0.040
> 13	Ph	H	0.990	0.010

[a]Based on radioactivity assay of the appropriate parabanic acid (III).

[b]By difference.

[c]I and III, $R^1 = R^2 = CH_3$ [E. Fischer, *Ber.* 14, 1912 (1881); A. Strecker, *Ann.* 118, 174 (1861)].

[d]I, II, and III, $R^1 = CH_3$, $R^2 = H$ [E. Fischer, *Ber.* 15, 455 (1892); H. B. Hill, *Ber.* 9, 1092, 1093 (1876)].

[e]I and III, R^1 = Ph, R^2 = H [N. M. Winslow, *J. Am. Chem. Soc.* 61, 2089 (1939); H. Kammerer, *Ber.* 40, 3741 (1907)].

shift of nitrogen, rather than of carbon; and (2) in the rearrangements of *N*-phenylalloxan-4-C^{14}, the shift of *N*-Ph takes place to the exclusion of unsubstituted nitrogen.[7] Turning now to the data for the rearrangement of *N*-methylalloxan-4-C^{14} (lines 8 and 9, Table 5.1), auxiliary experiments with *N*-methylalloxan-5-C^{14} (I*a*, $R^1 = CH_3$, $R^2 = H$) indicate that the parabanic acid (III*a*, $R^1 = CH_3$, $R^2 = H$) obtained upon rearrangement at pH < 1 contained 93.7% and at pH 7 to 8 contained 96.7% of the original radioactivity of reactant *N*-methylalloxan-5-C^{14}. From lines 8 and 9 it can thus be calculated that the migration ratios, or "migratory aptitudes," of CH_3-N vs H-N under the two reaction conditions studied are 3:1 and 4:1 respectively.

[7]This result is to be contrasted with the observations of W. E. Doering, T. I. Taylor, and E. F. Schoenewaldt, *J. Am. Chem. Soc.* 70, 455 (1948), and of U. K. Neville, *J. Am. Chem. Soc.* 70, 3499 (1948), that in the rearrangement of phenylglyoxal to mandelic acid it is only the hydrogen which undergoes migration.

STUDIES OF CARBON-14 AND DEUTERIUM ISOTOPE EFFECTS

V. F. Raaen
W. B. Guerrant[8a]
D. D. Thompson[8b]
C. J. Collins

The differential method developed at the Laboratory[9] was previously employed in a determination of the secondary isotope effect k^*/k (the value of 1.008 ± 0.001 given in ref 9 was refined by a nonlinear least-squares code[10] to 1.0085 ± 0.0004) for the formation of the 2,4-dinitrophenylhydrazone of acetophenone-β-C^{14} (IV*b*):

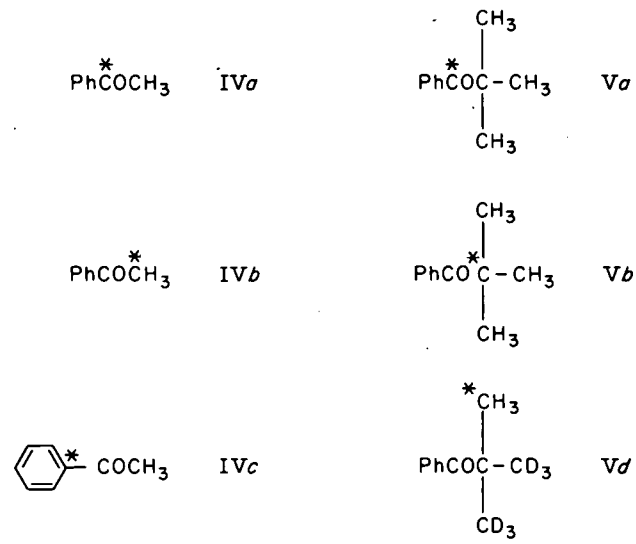

We have now extended the method to include isotope effect determinations during the formation of 2,4-dinitrophenylhydrazones of compounds IV*a*, IV*c*, V*a*, V*b*, and V*d*.

The results are as follows: k^*/k = 0.949 ± 0.002 (IV*a*), 1.0035 ± 0.0003 (IV*c*), 0.951 ± 0.003

[8]ORINS research participant: (*a*) Austin College, summer 1960; (*b*) Sweetbriar College, October 1960–April 1961.

[9]V. F. Raaen, A. K. Tsiomis and C. J. Collins, *J. Am. Chem. Soc.* 82, 5502 (1960); *Chem. Div. Ann. Progr. Rept. June 20, 1960*, ORNL-2983, p 36.

[10]We are indebted to M. H. Lietzke for writing the code.

(V*a*), 1.0041 ± 0.0007 (V*b*), and 1.043 ± 0.0014 (V*d*). In the study of the reaction of V*d*, the C^{14} label was used as a tracer for determining the isotope effect contributed by deuterium substitution in the *tert*-butyl group. All results were obtained by an analysis of the data through a non-linear least-squares code applicable to the IBM 7090 computer.[10] The theoretical relationship between specific radioactivity (A) of product at any fraction (f) of reaction, given a specific isotope effect k^*/k, is given by $\ln A = (k^*/k - 1) \ln (1 - f) + \ln k^*/k + \ln A_0$, where A_0 is the specific radioactivity of reactant at $f = 0$.

It is clear from the results that substitution of acetophenone (IV) or phenyl *tert*-butyl ketone (V) in any position but the carbonyl with a heavier isotope *increases* the reaction rate, whereas C^{14} substitution in the carbonyl of either IV or V *decreases* the reaction rate. The implications of the foregoing results with respect to hydrogen and carbon hyperconjugation are presently under study.

The basic hydrolysis of methyl *p*-benzoyl(carbonyl-C^{14})-benzoate (VI) has also been studied, and an isotope effect k^*/k of 1.0025 ± 0.0005 has been determined:

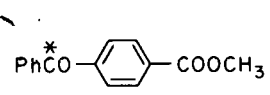

VI

THE DEAMINATION REACTION

Rearrangement of *erythro*-1-Amino-1-phenyl-2-*p*-methoxyphenylpropanol-2

B. M. Benjamin C. J. Collins

In a continuation of the work on the sterochemistry and radiochemistry of the deamination reaction,[11] optically active *erythro*-1-amino-1-phenyl-2-*p*-methoxyphenylpropanol-2 (VII) has been synthesized:

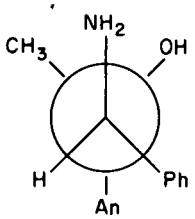

VII

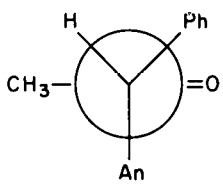

VIII

It was resolved into the (+) and (−) forms, and both forms were subjected to the same conditions of deamination that were previously employed[11] for similar reactions. In two experiments with the (−)-hydrochloride of VII, the ratios of (+)- to (−)-ketone VIII produced were determined by the isotope dilution method as 78.2%:21.8% and 78.5%:21.5% respectively. The total yield of ketone was 81.6% and 93.5% respectively. In another experiment with the (+)-hydrochloride of VII, 87.1% yield of ketone VIII was produced, representing 74.5% of the (−) form and 25.5% of the (+) form. These results are in such close agreement with those previously reported[11] for the deaminations of *erythro*-1-amino-1,2-diphenylpropanol-2 and of *erythro*-1-amino-1-phenyl-2-*p*-tolylpropanol-2 that we conclude there is no driving force for participation of the migrating *p*-methoxyphenyl (i.e., "bridging") during these deaminations.

SOLUBILITY OF TRIBUTYL PHOSPHATE (TBP) SUPPORTED ON CELITE

W. H. Baldwin C. E. Higgins

Recently, the well-known properties of organic phosphorus compounds that are important in solvent extraction have been used for chromatographic separations in columns by supporting the organic phosphorus compounds on inert solids.[12–14]

It is quite obvious that the useful life of such columns will be limited by the solubility of the solvents in aqueous phases that are used in contact with the columns. Furthermore, interactions between the organic phosphorus compound and the solid phase might have some influence on the column separations. The solubility, in aqueous solutions, of TBP (P^{32}) supported on Celite 545 was measured by a method already described[15] to

[11] B. M. Benjamin and C. J. Collins, *Chem. Div. Ann. Progr. Rept. June 20, 1960*, ORNL-2983, pp 32–36.

[12] S. Sekerskii and B. Kotlinskaya, *At. Energ. (U.S.S.R.)* 7, 160 (1959); English abstract, Atom Industry IX(5,6), 17 (1960).

[13] A. G. Hamlin and B. J. Roberts, *Nature* 185, 527 (1960).

[14] J. W. Winchester, *Rare Earth Chromatography Using bis(2-Ethylhexyl)orthophosphoric Acid*, ORNL CF-60-3-158 (Mar. 14, 1960).

[15] C. E. Higgins, W. H. Baldwin, and B. A. Soldano, *J. Phys. Chem.* 63, 113 (1959).

test the extent of interactions between TBP and Celite.

Tributyl phosphate (P^{32}) (ref 15) was deposited on Celite 545 (30 to 50 mesh) by evaporation of an ether solution to give 0.1 or 0.5 g of organic per gram of Celite. Fine particles were removed by flotation with water. The Celite-TBP mixtures (free-flowing solids) were packed into all-glass columns (0.1 cm^2 cross section). Aqueous solutions were allowed to flow downward through these columns at rates that varied from 0.1 to 1.5 ml/min. Batchwise equilibration was obtained by tumbling the solid with aqueous solutions.

The solubility of supported TBP in aqueous solutions (see Table 5.2) was found to be within 5% of the solubility of neat TBP. For practical applications the loss of TBP from such columns and hence the useful life can be calculated from the measured solubility of TBP in aqueous solutions. It is reasonable to assume, also, that the interactions between TBP and Celite are negligible, compared with the interactions in the aqueous phase.

THE SYSTEM TRIBUTYL PHOSPHATE (TBP), PHOSPHORIC ACID, AND WATER

C. E. Higgins W. H. Baldwin

Interactions between TBP, water, and electrolytes are important for the practical separation and purification of certain electrolytes. Valuable knowledge of the interactions in these systems has been obtained from the study of poorly extracted univalent electrolytes.[16] Phosphoric acid was selected as a polyvalent electrolyte for further study in the TBP-H_2O system. It has recently been noted that TBP has an industrial potential for the concentration of phosphoric acid.[17]

Aqueous H_3PO_4 solutions and TBP (equal volumes) were equilibrated at 25°C. The acid concentration in aliquots of the two phases was determined radiometrically with $H_3P^{32}O_4$, or volumetrically with standard NaOH. Water in aliquots of the organic phase was determined volumetrically with Karl Fischer reagent.

The dependence of the distribution coefficient (E_a^o) on the concentration of H_3PO_4 in the aqueous phase (see Fig. 5.1) can be considered in three sections. In the dilute acid region (up to 0.5 *M* H_3PO_4 in the aqueous phase) E_a^o increases linearly, from 0.01 to 0.1, and the concentration of the water in the organic phase was identical to that in TBP that has been equilibrated with pure water.

In the second region, E_a^o increases rapidly with coextraction of water. At 4 *M* H_3PO_4 in the

[16] W. H. Baldwin, C. E. Higgins, and B. A. Soldano, *J. Phys. Chem.* 63, 118 (1959).

[17] B. C. Doumas, "Purification of Phosphoric Acid by Solvent Extraction," University Microfilms, Inc., Ann Arbor, Mich., 1961.

Table 5.2. Solubility of TBP (P^{32}) in Aqueous Solutions at 25°C

Aqueous Phase	Nonaqueous Phase	TBP in Aqueous Phase (mg/liter)	Solubility of TBP, Reported[15]
H_2O	TBP(*l*)[a]	418 ± 1	422
H_2O	0.1 g TBP per gram of Celite	413 ± 5	
H_2O	0.5 g TBP per gram of Celite	415[b] 418[c]	
In KI	0.5 g TBP per gram of Celite	323[b] 316[c]	312
In HBr	0.5 g TBP per gram of Celite	483[c]	506

[a] Liquid TBP.
[b] Column length, 10 cm.
[c] Column length, 30 cm.

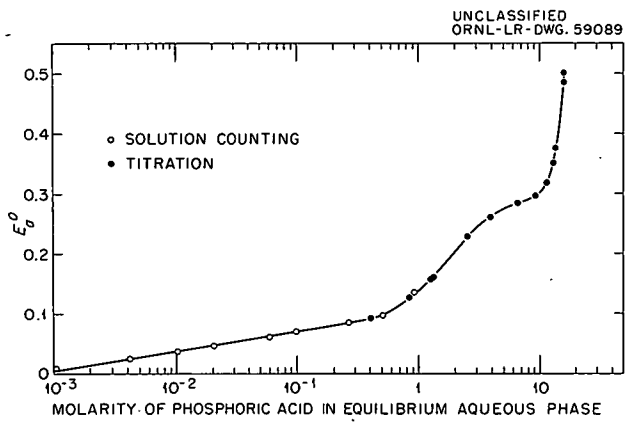

Fig. 5.1. Distribution of Phosphoric Acid Between Tributyl Phosphate and Water at 25°C.

aqueous phase, the composition of the organic phase is $1H_3PO_4$:3TBP:$6H_2O$. Higher concentrations of H_3PO_4 (above 4 *M*) salt out water from the organic phase, and, above 10 *M* aqueous H_3PO_4, the water-to-organic ratio is 1, regardless of the acid-to-organic ratio. Anhydrous H_3PO_4 and TBP are miscible in all proportions at 25°C.

Evidence for a high degree of association in solutions of anhydrous H_3PO_4 in TBP was obtained from ebullioscopic molecular-weight determinations in ether as solvent and from the viscosity of undiluted solutions. The apparent molecular weight of any mixture varied directly with the concentration of the mixture in ether and with the concentration of H_3PO_4 in the mixture.

The viscosity (at 25°C) of mixtures of anhydrous H_3PO_4 and TBP increased rapidly above 33% H_3PO_4 to a maximum at 75%, where the viscosity was about three times that of anhydrous, supercooled H_3PO_4.

THE SYSTEM BUTYL *p*-TOLUENE SULFONATE, NITRIC ACID, AND WATER

W. H. Baldwin C. E. Higgins

The distribution of aqueous HNO_3 between tributyl phosphate (TBP) and water was found to differ from those of the hydrohalogen acids in that HNO_3 displaced water from the solvent, while the hydrohalogen acids were accompanied by about four molecules of water.[18] The behavior of HNO_3 was tested with a poorer solvent (butyl *p*-toluene sulfonate) to determine whether the previously observed equilibrium conditions were general.

Butyl *p*-toluene sulfonate (the Eastman product washed with aqueous sodium carbonate and distilled) was equilibrated with an equal volume of aqueous HNO_3. Aliquots from each phase were titrated potentiometrically with standard NaOH to determine the concentration of HNO_3. Water in the organic phase was determined with Karl Fischer reagent.

The compositions of the two phases that are in equilibrium (see Table 5.3) show that butyl *p*-toluene sulfonate has a lower affinity for HNO_3 than does TBP. The organic solutions in equilibrium with 2 *M* aqueous HNO_3 are 1.7 *M* HNO_3 in TBP and 0.02 *M* HNO_3 in butyl *p*-toluene sulfonate, and with 4 *M* aqueous HNO_3 they are 2.7 and 0.1 *M* respectively.

Furthermore, more water accompanies the HNO_3 in butyl *p*-toluene sulfonate (0.7 mole excess above the solubility of water per mole of solvent) than in TBP.

[18] W. H. Baldwin, C. E. Higgins, and B. A. Soldano, *J. Phys. Chem.* **63**, 118 (1959).

Table 5.3. Distribution of Nitric Acid Between Water and Butyl *p*-Toluene Sulfonate at 25°C

HNO_3 Concentration		Distribution Coefficient, E_a^o	H_2O in Organic Phase	
Aqueous (moles per liter)	Organic (moles per liter)		(moles per liter)	(moles per mole of HNO_3)
0.0	0.0		0.16	
1.95	0.015	0.008	0.16	
3.84	0.11	0.029	0.24	0.7
7.32	0.77	0.105	0.79	0.8
13.8	4.84	0.351	3.67	0.7

6. CHEMISTRY OF AQUEOUS SYSTEMS

ULTRACENTRIFUGATION STUDIES OF INORGANIC SOLUTIONS

R. M. Rush
J. S. Johnson, Jr.
K. A. Kraus
G. Scatchard*

Hydrolysis of U(VI)

Widely varying pictures of uranyl hydrolysis have been presented by different investigators. In an attempt to clarify this situation, equilibrium ultracentrifugations were carried out for hydroxyl numbers **n** [average number of hydroxides bound per U(VI)] up to 1.4. The molecular weight of the uranyl species increased with hydroxyl number, but even at the highest value of **n**, the weight average degree of polymerization, N_w, did not rise above *ca.* 2.7 (Fig. 6.1). These results are in conflict with a "core-link" hydrolytic scheme deduced from pH measurements.[1] Much higher degrees of polymerization are proposed on this basis than we found by ultracentrifugation; although the pH measurements were carried out in perchlorate media, ultracentrifugation of a solution in this medium indicated that the situation is not much different from that in chloride solution (Fig. 6.1).

*Consultant from Massachusetts Institute of Technology.

[1]S. Ahrland, S. Hietenan, and L. G. Sillén, *Acta Chem. Scand.* 8, 1907 (1954).

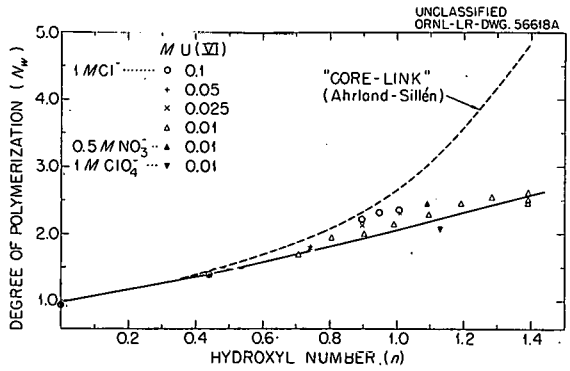

Fig. 6.1. Equilibrium Ultracentrifugation of U(VI). (—— Computed from monomer-dimer-trimer equilibrium, with $K_{11} = 1.7 \times 10^{-5}$, $K_{22} = 0.8 \times 10^{-6}$, $K_{35} = 1.8 \times 10^{-17}$.)

The question arises whether there is a hydrolysis scheme consistent with both the ultracentrifugation results and the pH data. By postulating the hydrolyzed species UO_2OH^+, $(UO_2)_2(OH)_2^{2+}$, and $(UO_2)_3(OH)_5^+$, we have obtained fairly good agreement with our values of N_w; agreement with the pH data is about as good as with the core-link hypothesis and as good as the consistency of results reported with glass and quinhydrone electrodes (Fig. 6.2). This scheme may not be unique. However, it agrees in the most important aspects with the conclusions reached by others in the Laboratory,[2] which they support by titrations in nitrate media.

Activity Coefficients of Three-Component Systems as Determined with the Ultracentrifuge

Lack of knowledge of the behavior of activity-coefficient derivatives in solutions containing two solutes is frequently the limiting factor both in the

[2]C. F. Baes, *Reactor Chem. Div. Ann. Progr. Rept. Jan. 31, 1961*, ORNL-3127, p 64.

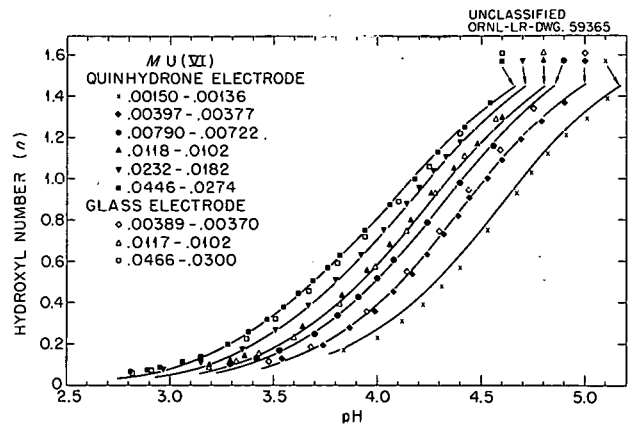

Fig. 6.2. Titration of U(VI) in 1 *M* $NaClO_4$. Experimental data: S. Ahrland, *Acta Chem. Scand.* 3, 374 (1949). Curves computed for each titration, using constants obtained by a least-squares fit of all the data points ($K_{11} = 1.7 \times 10^{-5}$, $K_{22} = 0.8 \times 10^{-6}$, $K_{35} = 1.8 \times 10^{-17}$).

measurement of molecular weights by ultracentrifugation and in the determination of species by other thermodynamic methods. Successful measurement of activity coefficients in two-component systems by equilibrium ultracentrifugation suggests that useful information could also be obtained with three components. The ultracentrifuge has the potential advantage of applicability in cases where lack of reversible electrodes prohibits emf measurements and where presence of a volatile solute precludes the isopiestic method. The principal disadvantage stems from the fact that the only sufficiently accurate techniques available at present for determining concentration are based on the refractive index of the solution, and it is difficult to separate this quantity into the contributions of the individual solutes.

In an attempt to evaluate ultracentrifugation for this purpose, a study was made of the activity coefficients of $BaCl_2$-HCl solutions, at concentrations of *ca.* 0.5 *M* $BaCl_2$–1.5 *M* HCl, or ionic strength 3. Values for these mixed solutes are known from the work of Harned and Gary,[3] and the test has been to find the value of α_{12} as defined by Harned, giving the smallest deviations between computed refractive indices and those measured for the solutions at centrifugation equilibrium. Our results give α_{12} within 0.01 of the Harned value (0.067, common logarithm scale). Agreement here is close enough to indicate possible usefulness of the technique, and the precision suggests that considerably better values could be obtained if systematic errors could be eliminated.

Mixture Rules for Molal Volumes and Refractive Index Increments

Rules relating the volumes and refractive indices of solutions having more than one solute to the volumes and indices of two-component systems are of interest in ultracentrifugation and elsewhere; successful formulas make possible computations of at least first approximations of the values for the more complex systems from the ordinarily more available data for single solutes and tend to reduce the number of measurements on mixtures necessary for more exact values. Young and Smith[4] proposed for apparent molal volumes Φ of electrolyte solutions, containing m_A and m_B moles of components A and B per kilogram of water, the equation

$$\Phi \equiv \frac{V - V_0}{m_A + m_B} = \frac{m_A}{m_A + m_B}\phi_A^0 + \frac{m_B}{m_A + m_B}\phi_B^0 , \quad (1)$$

where V is the volume of solution containing a kilogram of water, V_0 is the volume of a kilogram of pure water, and ϕ_i^0 is the apparent molal volume of component i in a two-component system having the same ionic strength as the mixture. They showed that this equation agreed with literature data for HCl-NaCl and $HClO_4$-$NaClO_4$ solutions well enough to make unnecessary a cross term needed in representing enthalpies.

A similar equation for volumes follows directly from differentiation with respect to pressure of a general equation for free energy of solutions of more than one solute,[5] with neglect of higher terms in the expansion. The cross term obtained in this manner, $b_{AB}[(m_A m_B)/(m_A + m_B)]$ [which is to be added to the right side of Eq. (1)], is a little different from that of Young and Smith.

In the course of ultracentrifugation studies of HCl-$BaCl_2$ solutions, apparent molal volumes and refractive index increments were measured. These data offer an interesting further test of the equation, since the apparent volumes of $BaCl_2$ and HCl in two-component systems are more different than those of the other pairs tested. Furthermore, $BaCl_2$ is a 1,2 electrolyte, and a more definitive test was thus involved, since, unlike the pairs of 1,1 electrolytes, the values of ϕ_i^0 here are different if computed for the total ionic strength of the solutions, rather than, for example, the total molality or total equivalent concentration.

For our measurements, which lie generally in the range of 1 to 4.5 ionic strength, we confirm that much better values of Φ are obtained with Eq. (1) if the values of ϕ_i^0 are for two-component systems having the same ionic strength, rather than the alternatives. We find that to represent the data within experimental precision (about 5×10^{-5} in density), a cross term with $b_{AB} = 0.30$ is necessary.

Our refractive index increments, measured at 436, 546, and 589 mμ, may be represented within

[3] H. S. Harned and R. Gary, *J. Am. Chem. Soc.* **76**, 5924 (1954).

[4] T. F. Young and M. B. Smith, *J. Phys. Chem.* **58**, 716 (1954).

[5] G. Scatchard, *J. Am. Chem. Soc.* **83**, 2636 (1961).

experimental uncertainty (*ca.* 0.2%) by empirical equations of the form:

$$\frac{\Delta n}{c} = \left(\frac{\Delta n}{c_A}\right)^0 \frac{c_A}{c_A + c_B} + \left(\frac{\Delta n}{c_B}\right)^0 \frac{c_B}{c_A + c_B} + r_{AB} \frac{c_A c_B}{c_A + c_B}, \quad (2)$$

n being refractive index; c, concentration in moles/liter; $(\Delta n/c_i)^0$, the value for two-component solutions having the same concentration as the total concentration of the mixture; and r_{AB} (the coefficient of the cross term), a constant.

ION EXCHANGE STUDIES

F. Nelson
K. A. Kraus
D. C. Michelson
J. H. Holloway[6]
R. J. Penick[6]
J. E. Boyden[6]

Work continued on the development of separation schemes for the metallic elements based almost exclusively on ion exchange methods. As a result of these studies, new information was obtained on the use of cation and anion exchange resins for separations. Some typical results are summarized below.

Adsorption of Metals from Concentrated HCl-$HClO_4$ Mixtures

Some elements are unusually strongly adsorbed by cation exchange resins from concentrated perchloric acid solutions; in fact, distribution coefficients as large as 10^5 have been observed[7] for some of the rare earth elements in 12 *M* $HClO_4$. On the basis of this observation, it appeared of interest to investigate systematically the cation exchange adsorbabilities of a number of elements from concentrated $HClO_4$ solutions and from mixtures of concentrated $HClO_4$ and other acids, particularly HCl and HF.

Adsorbabilities were generally determined for tracer concentrations of the elements with a Dowex 50 resin. In experiments involving elements of the fourth and fifth groups, a small amount of HF (0.05 *M*) was added to the solutions to avoid possible difficulties resulting from hydrolytic polymerization reactions. Studies were carried out under various $HClO_4$-HCl concentration ratios with 53 elements. The elements can be divided into "adsorbable" and "nonadsorbable" groups, the relative sizes of which can be adjusted to some extent through proper choice of ionic strength and $HClO_4$-HCl ratio.

With few exceptions, the adsorbed group of elements may be completely separated from the nonadsorbed or weakly adsorbed group by a single pass through a small column of resin, by using as eluent the $HClO_4$-HCl-HF mixtures.

In general, concentrated $HClO_4$-HCl should prove to be a versatile eluent for separations, particularly since many elements have markedly different adsorption functions in this medium. To illustrate, adsorption functions of the alkaline earth elements in 9.0 *M* (total acid concentration) HCl-$HClO_4$ mixtures are shown in Fig. 6.3, a plot of weight distribution coefficients (D) for the alkaline earths vs mole fraction of $HClO_4$ (F_{HClO_4}) in the mixture. With increasing F_{HClO_4}, D increases markedly for Ca(II), moderately for Sr, Mg, and Be, only slightly for Ba, and decreases for Ra(II). Thus for 9 *M* $HClO_4$-HCl mixtures, separation of Ba from Mg, for example, is readily

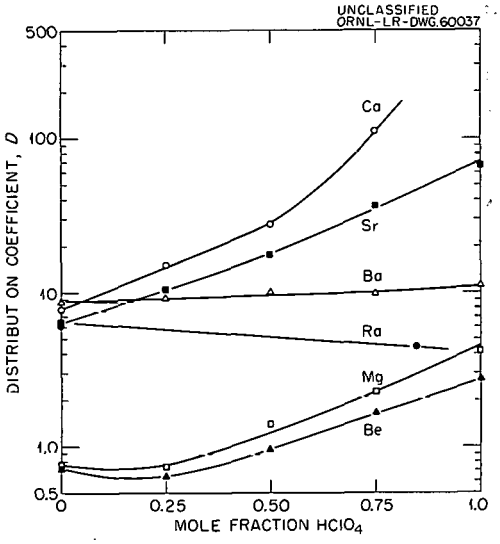

Fig. 6.3. Adsorption of Alkaline-Earth Elements from HCl-$HClO_4$ Mixtures (Dowex 50-X4; Total Acid Conc., 9.0 *M*).

[6]McClellan Air Force Base, Sacramento, Calif.

[7]G. R. Choppin, personal communication.

achieved at low values of F_{HClO_4}; separation of Ba from Sr, on the other hand, is more easily carried out with 9 *M* $HClO_4$.

Use of Boric Acid as a Complexing Agent for HF in Concentrated HCl Solutions

In some anion exchange separations involving HCl-HF solutions, it was believed that the medium would be more versatile for separations if a suitable complexing agent for the HF present could be found. Since B(III) forms relatively stable fluoride complexes, boric acid was considered as a possibility. In column experiments, involving Zr(IV) and Hf(IV) in 9 *M* HCl–0.02 *M* HF solutions, it was found, indeed, that addition of *ca.* 0.1 *M* H_3BO_3 to the solutions sufficiently complexed the fluoride present so that Zr(IV) and Hf(IV) could be adsorbed by strong-base anion exchange resins; in the absence of boric acid, both Zr(IV) and Hf(IV) are essentially non-adsorbable from 9 *M* HCl–0.02 *M* HF. Use of boric acid as a masking agent for HF should find a number of applications in both anion and cation exchange separations.

ADSORPTION ON INORGANIC MATERIALS

H. O. Phillips K. A. Kraus

Investigations of ion exchange properties of inorganic materials were continued. The general behavior of these materials was evaluated, with special emphasis on their use for the concentration of ions from dilute or relatively concentrated solutions and for the separation of difficultly separable ions. Some typical results are summarized below.

Separations with Zirconium Oxide and Zirconium Phosphate

Adsorbabilities of a number of divalent and trivalent elements in acid media were determined for zirconium phosphate and zirconium oxide adsorbents. In general, trivalent ions were considerably more strongly adsorbed by zirconium phosphate than were divalent ions. Separation of several trivalent elements from divalent elements by column techniques was demonstrated. A typical separation of Sr(II), Y(III), and Sc(III) by a zirconium phosphate column is shown in Fig. 6.4. Small columns of zirconium oxide were used to separate Zn(II) and Hg(II) in chloride media. Zinc(II) was eluted with 0.1 *M* HCl in about two column volumes, while Hg(II) was eluted with 1 *M* HCl in slightly less than two column volumes. The elution bands were nearly symmetrical.

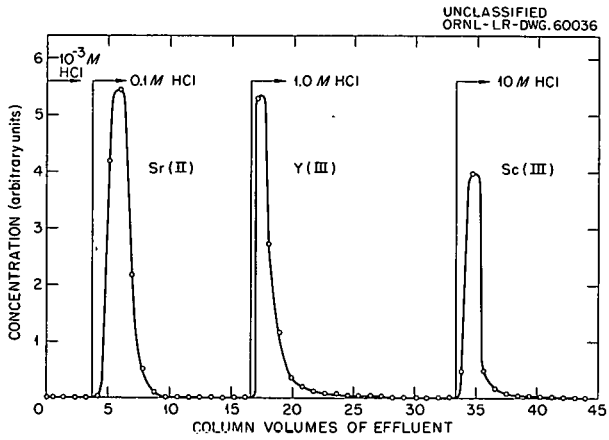

Fig. 6.4. Separation of Sr(II), Y(III), and Sc(III) in HCl Solutions with Zirconium Phosphate (Column 0.19 cm^2 × 2.8 cm; Temperature, 25°C).

Adsorptive Properties of Mercuric Sulfide

Several insoluble sulfides were prepared and their ion exchange properties investigated. Of the sulfides studied, HgS was found to exhibit rather unusual adsorptive properties under some conditions. It was found that small columns of HgS strongly adsorbed $AgNO_3$, $HgCl_2$, and $Hg(NO_3)_2$ from aqueous solution, presumably through formation of "double salts" of the type $Hg(NO_3)_2 \cdot 2HgS$. These double salts showed capacities for adsorption of halide ions of the order of five moles per liter of bed. A typical column experiment is shown in Fig. 6.5, illustrating adsorption of bromide from 0.5 *M* NaBr solution at 115°C. As may be seen in the figure, significant breakthrough of bromide occurred only after approximately 12 column volumes of effluent had passed through the column. After a water wash, the adsorbed bromide was removed by elution with a 5% ammonium sulfide solution (regeneration).

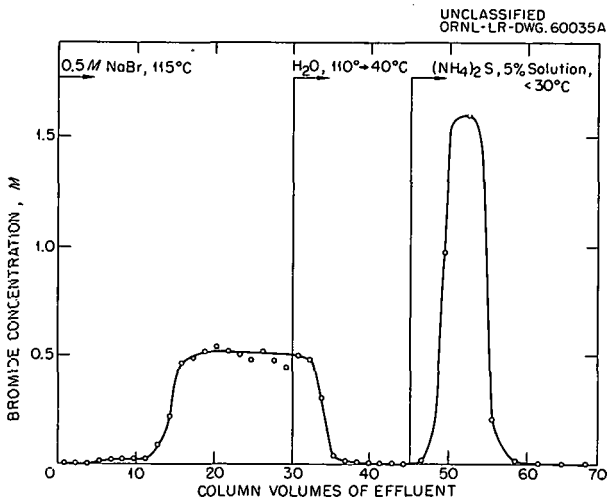

Fig. 6.5. Adsorption of Br^- by HgS at 115°C (0.058 cm^2 × 5.5 cm Column Pretreated with Conc. HNO_3).

PHYSICAL CHEMISTRY OF ION EXCHANGERS

Spectrophotometric Investigations of Liquid Anion Exchange Systems

S. Lindenbaum G. E. Boyd

Visible and ultraviolet absorption spectra of equilibrium aqueous and organic phases were measured in the extraction of Fe(III) from solutions of hydrochloric and hydrobromic acids (Figs. 6.6 and 6.7), Co(II) from hydrochloric acid (Fig. 6.8), and Cu(II) from hydrochloric and hydrobromic acids (Figs. 6.9 and 6.10) by triisooctylamine dissolved in toluene. The "ligand-field" spectrum of the extracted complex in the organic phase in each case is similar to the spectrum observed in the concentrated acid solution. Spectral data in the literature[8-11] indicate that the species for which these spectra are characteristic are the $FeCl_4^-$, $FeBr_4^-$, $CoCl_4^{2-}$, $CuCl_4^{2-}$, and $CuBr_4^{2-}$ complex ions respectively. There is evidence that the $FeCl_4^-$ and $CoCl_4^{2-}$ ions are tetrahedrally coordinated[8,10] and that the $CuCl_4^{2-}$ and $CuBr_4^{2-}$ ions have a configuration intermediate between a tetrahedron and a square plane. The species extracted by the organic phase was independent of the coordination in the aqueous phase. In dilute acid and in pure water solutions, the spectra shown are those of the octahedrally coordinated species. The complex ion extracted even from these solutions has a coordination number of four.

The spectra of $MnCl_2$ dissolved in water and in concentrated hydrochloric acid are shown in Fig. 6.11, together with the spectrum of the species extracted from concentrated hydrochloric acid. The organic phase in this case consisted of Alamine (a mixture of isomeric tertiary amines) dissolved in toluene. The spectrum of the organic phase is similar to the spectrum found by Gill and Nyholm[10] for $(\phi_3CH_3As)_2MnCl_4$ dissolved in nitromethane. The authors showed evidence that

[8] H. F. Friedman, *J. Am. Chem. Soc.* **74**, 5 (1952).

[9] D. E. Metzlar and R. J. Myers, *J. Am. Chem. Soc.* **72**, 3776 (1950).

[10] N. S. Gill and R. S. Nyholm, *J. Chem. Soc.* **1959**, 3997.

[11] L. Helmholtz and R. F. Kruh, *J. Am. Chem. Soc.* **74**, 1176 (1952).

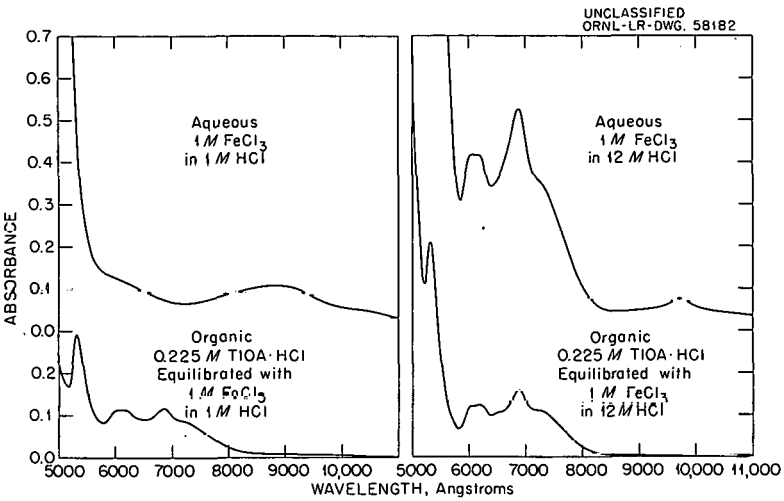

Fig. 6.6. Absorption Spectra of Aqueous and Organic Phases for the Extraction of $FeCl_3$ by Triisooctyl Amine in Toluene.

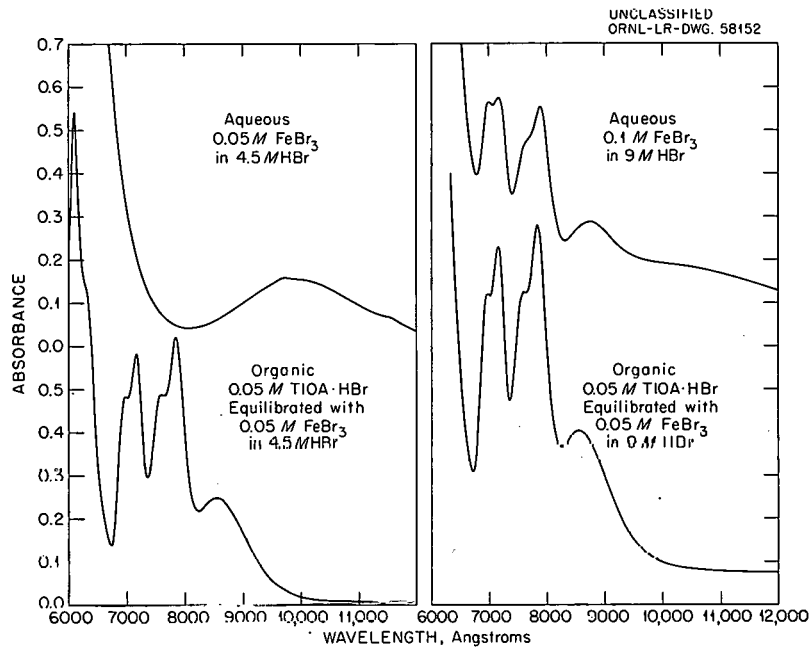

Fig. 6.7. Absorption Spectra of Aqueous and Organic Phases for the Extraction of $FeBr_3$ by Triisooctyl Amine in Toluene.

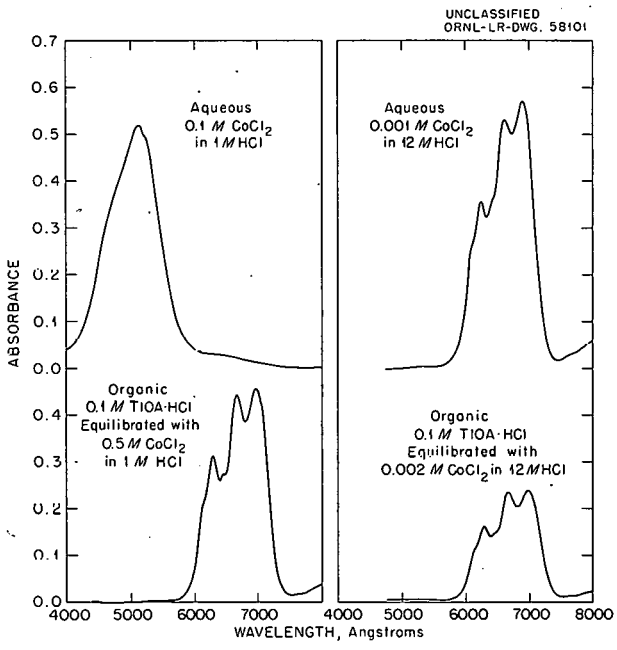

Fig. 6.8. Absorption Spectra of Aqueous and Organic Phases for the Extraction of $CoCl_2$ by Triisooctyl Amine in Toluene.

the species responsible for this spectrum was $MnCl_4^{2-}$ and that its structure was tetrahedral. Evidently this species does not exist in appreciable concentrations even in concentrated hydrochloric acid.

It is of interest that divalent nickel, which is not extracted by liquid or resinous anion exchangers, also does not form four-coordinated complexes in the presence of water, even in concentrated acid solution.

Calorimetric Measurements of the Heat of Ion Exchange and Related Reactions

F. Vaslow G. E. Boyd

Calorimetric measurements were made of the heats of solution and dilution of a number of quaternary ammonium halide salts structurally analogous to the exchanging groups in Dowex 1 and Dowex 2 ion exchange resins. Heats of dilution and solution of linear cationic polyelectrolyte salts corresponding in composition to non-cross-linked exchangers were also determined.

The standard heats measured in the anion exchange reactions were comparable to the differences in relative apparent molal heat contents of the corresponding ammonium halide salt solutions taken at the same concentration as in the resin. There was a reasonably good agreement between the heats of exchange and the differences in heat content at higher concentrations (i.e., higher cross-linkings), but at lower concentrations the electrolyte heat-content differences were much

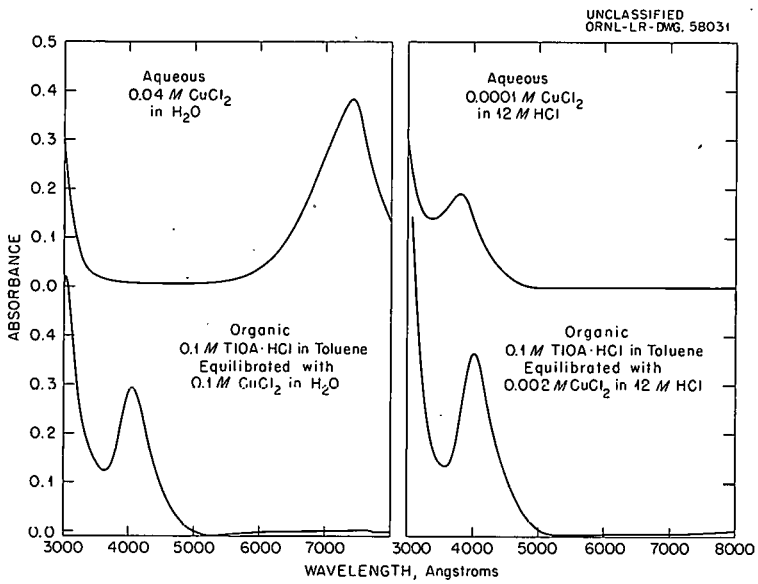

Fig. 6.9. Absorption Spectra of Aqueous and Organic Phases for the Extraction of $CuCl_2$ by Triisooctyl Amine in Toluene.

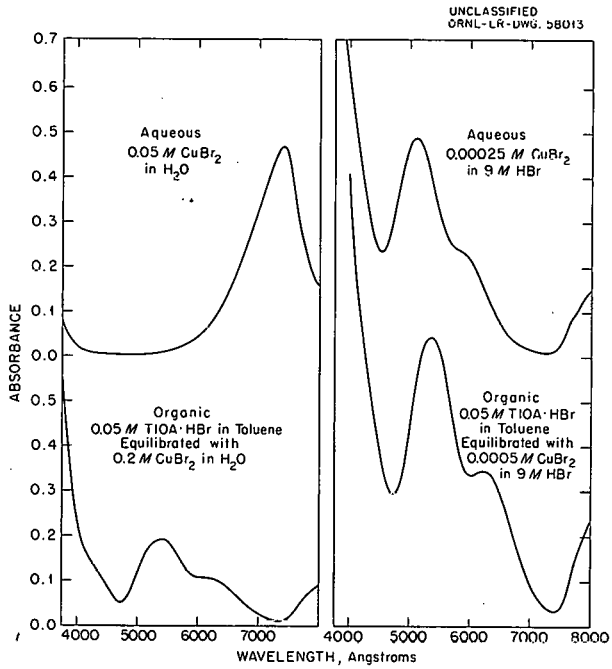

Fig. 6.10. Absorption Spectra of Aqueous and Organic Phases for the Extraction of $CuBr_2$ by Triisooctyl Amine in Toluene.

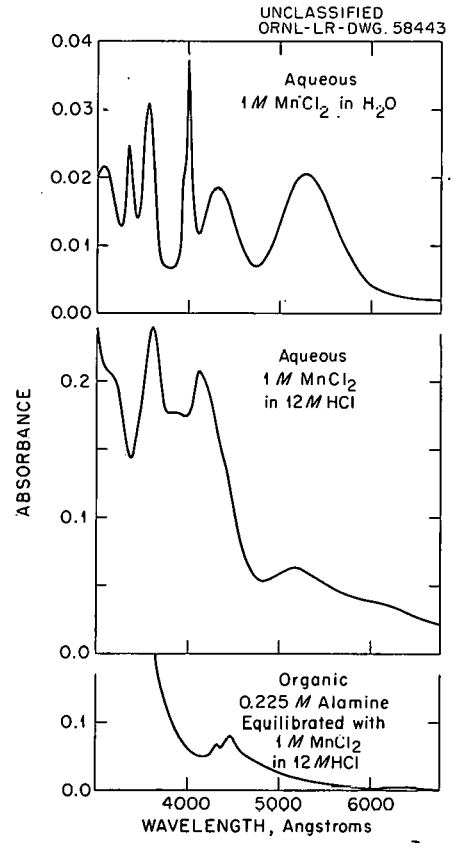

Fig. 6.11. Absorption Spectra of Aqueous and Organic Phases for the Extraction of $MnCl_2$ by Alamine in Toluene.

the smaller and no correlation of the heat of anion exchange with the heat-content differences for the alkali halides could be obtained.

Heat was evolved when bromide ion was added to dilute solutions of the fluoride and chloride salts of the linear polyelectrolyte, indicating that the latter compounds are effectively at relatively high concentration. The molecular chains in an ion exchanger are also at an effectively high concentration, and this fact may explain the lack of correlation of the heat of exchange with the heat-content differences of the corresponding quaternary ammonium halides at lower concentrations, as noted above.

The enthalpies of solution of the linear cationic polyelectrolyte salts were all negative, in contrast to the ammonium halides, where the ΔH of solution for the bromide and chloride salts were positive. The iodides were not sufficiently soluble for heat-of-dilution measurements to be made.

CALCULATION OF ACTIVITY COEFFICIENTS FROM OSMOTIC COEFFICIENT DATA

M. H. Lietzke R. W. Stoughton

Several semiempirical equations were considered for representing the logarithm of an activity coefficient over a wide range of concentration. Each equation involves a one-parameter Debye-Hückel term plus two or three higher terms, each of which is the product of a parameter and a simple function of the ionic strength I. When any one of the activity-coefficient equations is substituted into the Gibbs-Duhem relation and integrated analytically, a corresponding equation may be obtained for the osmotic coefficient in which each of the parameters retains its identity. Thus the parameters may be evaluated, by a nonlinear least-squares method, from osmotic coefficient data, and then used to calculate activity coefficients vs concentration, or vice versa. Since it is relatively difficult to get accurate osmotic coefficient data at low concentrations, and since an integration from zero concentration is required to evaluate activity coefficients therefrom, the possibility of obviating some of the difficulty usually encountered in such graphical integrations has been investigated by the use of analytical methods, using computing machines.

When a single-parameter Debye-Hückel expression for the activity coefficient of an electrolyte

$$\ln \gamma_{\pm} = -\frac{\mathring{A}\sqrt{I}}{1 + A\sqrt{I}}$$

is differentiated and substituted into

$$\phi = 1 + \frac{1}{m}\int_0^m m \, d \ln \gamma_{\pm}$$

and the integration performed analytically, then the following expression for the osmotic coefficient ϕ is obtained:

$$\phi = 1 - \frac{\mathring{A}}{A^3 I}\left[(1 + AI^{1/2}) - 2 \ln (1 + AI^{1/2}) - \frac{1}{1 + AI^{1/2}}\right] .$$

For use at higher concentrations, linear, quadratic, and cubic terms may be added as shown:

$$\phi = 1 - \frac{\mathring{A}}{A^3 I}\left[(1 + AI^{1/2}) - 2 \ln (1 + AI^{1/2}) - \frac{1}{1 + AI^{1/2}}\right] + BI + CI^2 + DI^3 . \quad (1)$$

The corresponding equation for the activity coefficient then becomes

$$\ln \gamma_{\pm} = -\frac{\mathring{A}\sqrt{I}}{1 + A\sqrt{I}} + (2B)I + (\tfrac{3}{2}C)I^2 + (\tfrac{4}{3}D)I^3 . \quad (2)$$

In Eq. (1) the parameters A, B, C, and D for any particular electrolyte may be evaluated by the method of least squares, and the corresponding activity coefficients may be computed immediately from Eq. (2).

In Table 6.1 are shown the parameters obtained by fitting the osmotic coefficients of NaCl (as listed by Robinson and Stokes[12]) with Eq. (1). The fit was performed both with and without a cubic term added. At 25 and 100°C, the inclusion of the cubic term produces a significantly better fit; at 60°C, the three- or the four-parameter equation fits about equally well.

[12] R. A. Robinson and R. N. Stokes, *Electrolyte Solutions*, Academic Press, New York, 1955.

Table 6.1. Parameters Describing the Concentration Dependence of the Osmotic Coefficients of NaCl

t	A	$B \times 10^2$	$C \times 10^3$	$D \times 10^4$	$\sigma^2_{fit} \times 10^{7(a)}$
25	1.31029	3.76085	4.00031		31.2
	1.45397	2.23565	9.30838	−5.36209	1.24
60	1.44563	4.51852	2.76704		12.7
	1.42563	4.81027	1.28089	2.21078	13.3
100	1.49439	4.56788	1.67320		12.2
	1.55510	3.64784	6.43661	−7.13179	7.33

(a) Variance of fit.

In Table 6.2 are shown activity coefficients calculated from the parameters in Table 6.1 by means of Eq. (2), including the cubic term.

Table 6.2. Activity Coefficients of NaCl as a Function of Temperature and Concentration

t	m	$\gamma_\pm$
25	0.1	0.7792
	1.0	0.6570
	4.0	0.7837
60	0.1	0.7659
	1.0	0.6542
	4.0	0.7993
100	0.1	0.7466
	1.0	0.6241
	4.0	0.7392

The values given in Table 6.2 are merely representative – complete tables have been computed.

In Table 6.3 are shown the parameters obtained by fitting the osmotic coefficients of several other salts by this method. With the parameters in Table 6.3 the activity coefficients for the salts shown may be computed at any ionic strength by means of Eq. (2).

In Table 6.4 are given the parameters obtained by fitting the osmotic coefficients of several salts at 99.6°C computed from the osmotic coefficient ratios reported by Patterson, Gilpatrick, and Soldano.[13]

The corresponding calculated activity coefficients for these salts at 99.6°C are shown at several representative concentrations in Table 6.5. Also included for comparison are values of the activity coefficients at 25°C (ref 12).

The activity coefficients of KCl, CsCl, and Na_2SO_4 appear to show relatively little change with temperature. The activity coefficients of LiCl, $MgSO_4$, and UO_2SO_4 (at least at the higher concentrations) show a definite decrease at the higher temperature and have their minimum value at a higher concentration than at 25°C. The activity coefficients of $BaCl_2$ show a decrease at the higher temperature in the small concentration range in which the measurements were made.

Hence the nonlinear least-squares method of fitting osmotic coefficient data in order to calculate activity coefficients appears to be very powerful. In fact, calculations with 25°C data and Eqs. (1) and (2) have shown that osmotic coefficients in the range 1 to 3 m can be used to calculate values of both osmotic and activity coefficients at lower concentrations with good accuracy. Thus activity coefficients may readily be calculated over a wide range of concentrations from relatively few osmotic coefficient data. Moreover, the method is greatly to be preferred over graphical integration if a high-speed computer is available to perform the nonlinear least-squares fits.

[13] C. S. Patterson, L. O. Gilpatrick, and B. A. Soldano, *J. Chem. Soc.* **1960**, 2730.

Table 6.3. Parameters Describing the Concentration Dependence of the Osmotic Coefficients of Several Salts at 25°C[a]

Salt	A	$B \times 10^2$	$C \times 10^3$	$D \times 10^4$	$\sigma^2_{fit} \times 10^6$
KBr	1.29231	0.994831	4.34095	−3.50742	0.24
Na_2SO_4	1.24072	−6.58044	7.26282	−1.94540	4.41
$CaCl_2$	1.61291	4.56577	8.57310	−2.73800	4.03
$BaCl_2$	1.59925	1.23161	8.81121	−6.92099	0.84
$BaBr_2$	1.62543	3.81918	8.02100	−5.19535	1.90

[a]R. A. Robinson and R. N. Stokes, *Electrolyte Solutions*, Academic Press, New York, 1955.

Table 6.4. Parameters Describing the Concentration Dependence of the Osmotic Coefficients of Several Salts at 99.6°C

Salt	A	$B \times 10^2$	$C \times 10^2$	$D \times 10^3$	$\sigma^2_{fit} \times 10^6$
LiCl	1.36704	4.62413	2.09758	−2.50075	8.03
CsCl	1.40727	−1.45738	1.01090	−0.877824	18.53
KCl	1.87392	−2.83699	1.95070	−2.17686	6.64
Na_2SO_4	2.18824	−11.0123	1.52961	−0.704151	0.55
UO_2SO_4	1.11309	−2.11182	0.252142	−0.0580834	40.99
$MgSO_4$	1.58747	−6.80762	0.651886	−0.115772	10.90
$BaCl_2$	1.17244	6.81811	−0.760404	0.547538	17.97

Table 6.5. Activity Coefficients of Several Salts at 25 and 99.6°C

	LiCl		KCl		CsCl		$BaCl_2$		Na_2SO_4		$MgSO_4$		UO_2SO_4	
m	25°C	99.6°C	25°C	99.6°C	25°C	99.6°C	25°C	99.6°C	25°C	99.6°C	25°C	99.6°C	25°C	99.6°C
0.1	0.790	(0.739)[a]	0.770	(0.752)	0.756	(0.732)	0.500	(0.406)	0.445	(0.464)	0.150[b]	(0.1596)	0.150[b]	(0.1210)
0.5	0.739	(0.635)	0.649	(0.637)	0.606	(0.600)	0.397	(0.290)	0.266	(0.295)	0.0675	(0.0675)	0.0611	(0.0419)
1.0	0.774	0.621	0.604	0.594	0.544	0.548	0.395	0.276	0.201	0.223	0.0485	(0.0449)	0.0439	(0.0269)
2.0	0.921	0.673	0.573	0.568	0.496	0.509	0.449[c]	0.295	0.152	0.168	0.0417	0.0317	0.0367	0.0186
3.0	1.156	0.775	0.569	0.571	0.479	0.500		(0.354)	0.137	0.146	0.0492	0.0301	0.0383	0.0162

[a]Parentheses indicate calculated values outside the range of measurement.

[b]These values have been normalized to 0.150 at 0.1 m.

[c]1.8 m.

THE BISULFATE ACID CONSTANT FROM 25 TO 225°C, AS COMPUTED FROM SOLUBILITY DATA

M. H. Lietzke R. W. Stoughton

In a previous series of papers, a study of the solubility of Ag_2SO_4 in a variety of electrolyte media has been described.[14] In this work it was shown that the concentration dependence of the logarithms of the equilibrium quotients and solubility products could be expressed by single-parameter expressions of the type $\mathring{A}\sqrt{I}/(1 + A\sqrt{I})$, where $\mathring{A}$ is the appropriate Debye-Hückel limiting slope, I is the ionic strength of the solution, and A is an adjustable parameter. These expressions were shown to hold for ionic strengths as high as 4.0 and from 25 to 275°C. In the present paper the data on the solubility of Ag_2SO_4 in H_2SO_4 solutions are used to compute values of the bisulfate dissociation constant K_2 for the reaction

$$HSO_4^- = H^+ + SO_4^{2-}$$

from 25 to 225°C.

Method of Calculation

In carrying out the calculations it was assumed that only the species Ag^+, SO_4^{2-}, and HSO_4^- existed in a solution of Ag_2SO_4 dissolved in H_2SO_4. If s is the molal solubility of Ag_2SO_4 in H_2SO_4 of molality m, and x and y are taken as the SO_4^{2-} and H^+ concentrations, then the molality solubility product of the Ag_2SO_4 is given by

$$S = 4s^2x \tag{1}$$

and the bisulfate dissociation quotient by

$$Q_2 = \frac{xy}{2m - y} . \tag{2}$$

The equation for the conservation of total sulfate is

$$m + s = 2m - y + x ,$$

or,

$$s + y - x - m = 0 . \tag{3}$$

In accordance with previous calculations[14] it was assumed that

$$\ln Q_2 = \ln K_2 + 4\mathring{A}_T \left(\frac{\sqrt{I}}{1 + A\sqrt{I}}\right) \tag{4}$$

and

$$\ln S = \ln 4s_0^3 + 6\mathring{A}_T \left(\frac{\sqrt{I}}{1 + P\sqrt{I}} - \frac{\sqrt{3s_0}}{1 + P\sqrt{3s_0}}\right), \tag{5}$$

where K_2 is the bisulfate acid constant, $\mathring{A}_T$ is the Debye-Hückel limiting slope at temperature T for a singly charged ion, s_0 is the solubility of Ag_2SO_4 in water at temperature T, P and A are adjustable parameters, and I is the ionic strength of the solution, given by

$$I = m + s + 2x . \tag{6}$$

The criterion adopted in solving the above set of equations with iterative adjustments of $\ln K_2$, A, and P was that $\sum_i (s_{obs} - s_{calc})_i^2$ be a minimum. Accordingly, a series expansion of s was made in terms of the partial derivatives with respect to the three adjustable parameters, K_2, P, and A as follows:

$$s_{obs} = s_{calc} + \frac{\partial s}{\partial \ln K_2} \Delta \ln K_2 + \frac{\partial s}{\partial P} \Delta P + \frac{\partial s}{\partial A} \Delta A . \tag{7}$$

(In taking the partial derivatives with respect to one parameter, the other two parameters would be held constant.) Since, however, the solubility of Ag_2SO_4 had been measured as a function of temperature in only three different concentrations of H_2SO_4, it was decided to omit the evaluation of $\partial s/\partial P$ directly. Rather, values of $\ln K_2$ and A were obtained over a selected range of values of P. Then that value of P was chosen for the final calculations which gave a most nearly temperature-independent value of A (consistent with previous calculations,[14] in which it was shown that temperature-independent values of P and A could be used to describe the system).

In carrying out the calculations, Eqs. (1), (2), and (3) were solved by the Newton-Raphson method at each temperature with estimates of the parameters $\ln K_2$ and A and a fixed value of P. Then the partial derivatives $\partial s/(\partial \ln K_2)$ and

[14] M. H. Lietzke and R. W. Stoughton, *J. Phys. Chem.* 63, 1183, 1186, 1188, 1190, 1984 (1959); 64, 133, 816 (1960).

$\partial s/\partial A$ were evaluated numerically. The usual matrix technique was used to evaluate $\Delta \ln K_2$ and ΔA, correction factors which were used to modify the original estimates of $\ln K_2$ and A. The procedure was repeated with the new values of $\ln K_2$ and A and with the most recently calculated values of s, x, and y [Eqs. (1), (2), and (3)] until two successive values of both $\ln K_2$ and A differed by less than 0.1%. Then the entire calculation was repeated with a series of values of P.

The computations were repeated for 25°C intervals from 25 to 225°C (the highest temperature at which solubility data were available). Then the values of $\ln K_2$ were chosen corresponding to that value of P for which the value of A was most nearly temperature independent; that is, $P = 0.72$. (Actually the values of $\ln K_2$ and A were not particularly sensitive to the values of P. A variation in the value of P from 0.6 to 0.8 caused a maximum deviation in the value of $\ln K_2$ of only 2%.)

The values of $\ln K_2$ obtained as a function of temperature were fitted by the method of least squares to give Eq. (8):

$$\ln K_2 = -\frac{1283.108}{T} + 12.31995 - 0.04223215T , \quad (8)$$

where T is the absolute temperature.

Results and Discussion

The values of $\ln K_2$ obtained in this work were compared with those of previous investigators. The value of K_2 at 25°C, as calculated from Eq. (8), is 0.01032, which compares very well with reported values.[15] The only previous work as a function of temperature was that of Young, Klotz, and Singleterry[16] in which K_2 was determined over the range of 5 to 55°C by an indicator technique, and an equation (9) was obtained for K_2 vs temperature to 155°C by utilization of the conductivity data of Noyes:[17]

$$\ln K_2 = -\frac{1785.390}{T} + 15.99658 - 0.0489236T . \quad (9)$$

In Table 6.6 are summarized the values of log K_2 vs temperature (t) as calculated from Eq. (8) and as obtained from Eq. (9).

Table 6.6. Values of log K_2 as a Function of Temperature

t (°C)	$-\log K_2$ [Eq. (8)]	$-\log K_2$ [Eq. (9)]
25	1.987	1.988
50	2.301	2.318
75	2.636	2.677
100	2.987	3.059
125	3.352	3.460
150	3.728	3.876
175	4.113	
200	4.506	
225	4.905	

In Table 6.7 are summarized the thermodynamic constants for the reaction $HSO_4^- = H^+ + SO_4^{2-}$ from 25 to 225°C as computed by using Eq. (8). All calculations were carried out on an IBM 7090 computer.

It is interesting to note that the entropy of dissociation of HSO_4^- is negative and attains a higher negative value the higher the temperature. A similar effect was found[16] for the dissociation of UO_2SO_4 into UO_2^{2+} and SO_4^{2-} and for the dissolution of Ag_2SO_4. Thus it appears that the formation of SO_4^{2-} in water increases the amount of "structure" shown by the solvent at any temperature and that this effect is much greater the higher the temperature.

[15] R. A. Robinson and R. H. Stokes, p 374 in *Electrolyte Solutions*, Academic Press, New York, (1955).

[16] I. M. Klotz and C. R. Singleterry, Theses, University of Chicago (1940); R. A. Robinson and R. H. Stokes, p 376 in *Electrolyte Solutions*, Academic Press, New York, 1955; T. F. Young, L. F. Maranville, and H. M. Smith, chap. 4 of *The Structure of Electrolytic Solutions*, ed. by W. J. Hamer, Wiley, New York, 1959; T. F. Young, unpublished work.

[17] A. A. Noyes, *The Electrical Conductivity of Aqueous Solutions*, The Carnegie Institution of Washington, Washington, D.C., 1907.

Table 6.7. Thermodynamic Constants for the Reaction $HSO_4^- = H^+ + SO_4^{2-}$

t (°C)	ΔF^0 (cal)	ΔH^0 (cal)	ΔS^0 (eu)
25	2,712	−4,911	−25.6
50	3,403	−6,214	−29.8
75	4,200	−7,623	−34.0
100	5,102	−9,136	−38.2
125	6,108	−10,750	−42.4
150	7,219	−12,480	−46.5
175	8,436	−14,310	−50.7
200	9,757	−16,240	−54.9
225	11,183	−18,280	−59.1

A COMPUTER PROGRAM FOR SOLVENT EXTRACTION CALCULATIONS

M. H. Lietzke R. W. Stoughton

At the suggestion of R. H. Rainey of the Chemical Technology Division, a beginning was made on a general IBM-7090 computer program for solvent extraction calculations involving an aqueous-nitrate and a TBP (tributyl phosphate)–organic-diluent phase. The procedure adopted is to write programs in which each successive one will involve more complications – that is, take into account more components or higher concentrations of the same components in the organic phase, such that the volumes of the two phases would change during extraction. Equilibration of the following aqueous systems with TBP-diluent will be considered in roughly the following order:

1. NH_4NO_3–dilute $UO_2(NO_3)_2$
2. NH_4NO_3–higher concentration of $UO_2(NO_3)_2$
3. HNO_3
4. NH_4NO_3-HNO_3
5. HNO_3-$UO_2(NO_3)_2$
6. $Al(NO_3)_3$-HNO_3
7. $Al(NO_3)_3$-HNO_3-$UO_2(NO_3)_2$
8. NH_4NO_3-$Th(NO_3)_4$
9. HNO_3-$Th(NO_3)_4$
10. $Al(NO_3)_3$-HNO_3-$Th(NO_3)_4$
11. HNO_3-$UO_2(NO_3)_2$-$Th(NO_3)_4$
12. $Al(NO_3)_3$-$UO_2(NO_3)_2$-$Th(NO_3)_4$
13. $Al(NO_3)_3$-HNO_3-$UO_2(NO_3)_2$-$Th(NO_3)_4$
14. Systems involving fission products and plutonium.

In the case of system 1, the following equilibria were assumed to be sufficient:

Aqueous: $UO_2^{2+} + 2NO_3^- = UO_2(NO_3)_2$, Q_1, (1)

Two-phase: $UO_2(NO_3)_{2(a)} + 2TBP_{(o)} = UO_2(NO_3)_2 \cdot 2TBP_{(o)}$, Q_d, (2)

where the subscripts (a) and (o) represent aqueous and organic phases respectively, and Q_1 and Q_d represent the molarity quotients for the equilibria indicated. The equilibrium quotients (Q_1 and Q_d) were assumed to be expressible in terms of the equilibrium constants (K_1 and K_d) and the aqueous ionic strength I (in the range 0.7 to 6.0 of the latter) by

$$\ln Q_1 = \ln K_1 + B_1 I , \quad (3)$$

$$\ln Q_d = \ln K_d + B_d I . \quad (4)$$

Since the first case considered involved low concentrations of $UO_2(NO_3)_2$ compared with both the $TBP_{(o)}$ and the $NH_4NO_{3(a)}$ concentrations, activity-coefficient changes in the organic phases were not considered, and I was set equal to the NH_4NO_3 concentration. The $TBP_{(o)}$ concentration was set equal to its initial value T_0 less twice the $UO_2(NO_3)_2 \cdot 2TBP_{(o)}$ concentration UO. The NO_3^- concentration can be seen to be equal to M, the molality of NH_4NO_3, plus twice the UO_2^{2+} concentration, by conservation of nitrate ion. Thus equilibria (1) and (2) may be expressed by

$$Q_1 = \frac{[UO_2(NO_3)_2]}{[UO_2^{2+}][M + 2(UO_2^{2+})]^2} , \quad (5)$$

and

$$Q_d = \frac{[UO]}{[UO_2(NO_3)_2][T_0 - 2(UO)]^2} , \quad (6)$$

where the brackets indicate molar concentrations. A third equation in the variables $[UO_2^{2+}]$, $[UO_2(NO_3)_2]$, and $[UO]$ may be obtained from the conservation of uranium; that is,

$$\text{Total original uranium} = [UO_2^{2+}] + [UO_2(NO_3)_2] + [UO] . \quad (7)$$

The distribution ratio D is given by

$$D(o/a) = [UO]/\{[UO_2^{2+}] + [UO_2(NO_3)_2]\}. \quad (8)$$

The data are from Kent and Rohde.[18] The criterion set for fitting the data by a nonlinear least-squares method was that $\sum_i (D_{obs} - D_{calc})_i^2$ be a minimum. The method used was similar to that described in the preceding subsection "The Bisulfate Acid Constant from 25 to 225°C, as Computed from Solubility Data." Thus Eqs. (5), (6), and (7) were to be solved [after linearizing Eqs. (5) and (6) for ease in computation according to the Newton-Raphson method] successively by iteration on estimates of ln K_1, ln K_d, B_1, and B_d, subject to the least-squares restriction on the D's.

It was found that no solution could be obtained unless B_1 was set identically equal to zero. This means that within the accuracy of the data and under the existing conditions no unique linear term (other than zero) in Eq. (3) was obtainable. Interestingly enough then, Q_1 must vary but little with I from 0.68 to 4.7 in NH_4NO_3 media. With $B_1 = 0$, the other parameters were ln $K_d = 3.18$, $B_d = 0.578$, and ln $K_1 = 0.445$.

The experimental and calculated distribution ratios are shown in Table 6.8.

[18] R. A. Kent and K. L. Rohde, IDO-14501, Table 3 (July 1960).

Table 6.8. Observed and Calculated Distribution Ratios D(Organic/Aqueous) for Uranyl Nitrate Between Aqueous-NH_4NO_3 and TBP-Diluent Phases

M NH_4NO_3	Initial M $UO_2(NO_3)_2$	$D(o/a)_{obs}$	$D(o/a)_{calc}$
0.68	0.0098	0.180	0.178
1.37	0.0102	0.680	0.649
2.00	0.0112	1.22	1.24
2.74	0.0109	2.17	2.21
3.42	0.0111	3.50	3.46
4.70	0.0158	6.83	6.83

AQUEOUS SPECTROPHOTOMETRY AT ELEVATED TEMPERATURES AND PRESSURES

W. C. Waggener A. J. Weinberger
R. W. Stoughton

A second prototype high-temperature aqueous spectrophotometric cell, designed to allow gas-liquid equilibration, was tested with favorable results, and construction of a redesigned chamber and cell assembly having both sample and reference cells controllable over the ranges 0 to 280°C and 0 to 2000 psia is 40% completed. This equipment, which is used with the standard Cary model 14 monochromator and detector, should extend the spectral range for study of aqueous solutions at elevated temperatures from 0.7 to 1.2 μ for H_2O and 1.2 to 1.8 μ for D_2O (ref 19).

The revised absorption cell incorporates a reservoir space above the cylindrical cavity of the original design.[20] Tests have indicated that an overpressure of gas (e.g., Ar, H_2, or O_2) can be essentially equilibrated with the liquid phase in the cell in a matter of minutes even at 25°C, due to convective stirring from the axial heat input (0.1 to 0.2 w) of the infrared source. Conditions of temperature and pressure under which bubble nucleation occurs were observed and studied photometrically, and the results give confidence that this problem can be controlled.

The same solution (UO_2SO_4, 0.0123 m; $CuSO_4$, 0.0085 m; D_2SO_4, 0.0072 m; D_2O, 98.5 at. % D) which was studied "degassed" in the original cell with separate reservoir[21] was studied in the wavelength range 0.34 to 1.2 μ as a function of temperature, time, and overpressure of hydrogen and/or oxygen.

At 25°C and a hydrogen pressure of 750 psi, the Cu(II) and U(VI) were reduced successively to Cu(I) or (0) (during the first 19 hr) and U(IV) (during the next 28 hr). The disappearance of the copper spectrum occurred without detectable turbidity, and it is presumed that the reduction of copper occurred at the surface of the titanium cell wall. The U(IV) species (unhydrolyzed and

[19] W. C. Waggener, *Anal. Chem.* 30, 1569 (1958).

[20] W. C. Waggener, *Rev. Sci. Instr.* 30, 788 (1959).

[21] W. C. Waggener, A. J. Weinberger, and R. W. Stoughton, *Chem. Div. Ann. Progr. Rept. June 20, 1960*, ORNL-2983, p 44.

hydrolyzed) appeared to be essentially soluble at room temperature, and their spectra were identified and followed subsequently as a function of temperature over the range 4 to 130°C. The spectral data indicated that the UOH^{3+}/U^{4+} ratio increases monotonically with temperature, while the total U(IV) in the reduced solution slowly decreases due to hydrolytic precipitation.

Aggregation of the U(IV) hydrolytic species appeared to occur preferentially at the surface of the cell walls, because the changing spectrum of the system was uncomplicated by turbidity when the temperature was raised slowly (i.e., <0.1°C per minute). At higher rates of heating turbidity did occur; for example, during a 1°C per minute rise from room temperature, the absorbance at 7150 A increased from ~0 to >2.4 in 2 min at 37 to 39°C. At 130°C not more than 15% U(IV) remained in solution. This hydrolysis was found to be completely, though slowly, reversible with temperature.

Reoxidation of the solution at 25°C with an overpressure of 180 psi oxygen was rapid. The conversion, U(IV) → U(VI), was 96% complete within 5 to 6 min. Oxidation and re-solution of the copper proceeded more slowly, approximately 3¾ hr being required for its completion.

Reduction of the solution with hydrogen at 150°C and higher resulted in complete elimination of all species absorbing in the wavelength range studied (0.34 to 1.2 μ). Upon reoxidation at high temperature, unidentified absorbing species were sometimes observed which could be copper and/or uranium intermediates and/or titanium corrosion products.

Recently, solutions of each component (0.0123 *m* UO_2SO_4 in 0.0072 *m* D_2SO_4, and 0.0085 *m* $CuSO_4$ in 0.0072 *m* D_2SO_4, as well as the solvent solution, 0.0072 *m* D_2SO_4) were subjected to a hydrogen overpressure of 50 psi at 200°C for a day for comparison with the solution containing both uranium and copper, which was treated similarly. In the case of the latter, 95% of the copper was reduced in the first 15 min, the remaining 5% being reduced concurrently with the uranium, which disappeared slowly over 60 to 70 min. Reduction of the $CuSO_4$ solution was somewhat more rapid than that of the UO_2SO_4-$CuSO_4$ solution (95% in <10 min, 100% in <20 min), while the rate of reduction of the UO_2SO_4 solution appeared not to be different. Spectral monitoring of the reoxidation of the UO_2SO_4-$CuSO_4$ solution was generally complicated, both by unidentified absorbing species and by turbidity (the latter persisted for several hours). However, the reoxidation process was clearly more rapid than the reduction process. Oxidation of both the reduced UO_2SO_4 and the reduced $CuSO_4$ solutions was uncomplicated by turbidity or unidentified species and occurred in competition with the recombination of oxygen and hydrogen. Addition of oxygen in amounts less than that required for reaction with the hydrogen resulted in rapid reoxidation of the order of 0.5% of the uranium in the UO_2SO_4 solution and 60% of the copper in the $CuSO_4$ solution, after which slow reduction by the excess hydrogen took place. Addition of oxygen in excess of that required for $2H_2 + O_2 \rightarrow 2H_2O$ resulted in complete and relatively rapid reoxidation of uranium in the UO_2SO_4 solution (30 min) and of copper in the $CuSO_4$ solution (<1 min). The spectrum of the solvent solution was unaffected by treatment with hydrogen and oxygen. Interestingly enough, the rate of the recombination reaction (of hydrogen and oxygen) was about the same whether the mixture was in contact with the solvent (0.0072 *m* D_2SO_4), the UO_2SO_4 solution, the $CuSO_4$ solution, or the UO_2SO_4-$CuSO_4$-D_2SO_4 solution. This fact strongly suggests that the observed recombination reaction was heterogeneous, occurring at the cell walls.

7. ELECTROCHEMISTRY OF CORROSION

STUDIES ON THE MECHANISM OF PASSIVATION

G. H. Cartledge

In the last progress report,[1] reference was made to a series of studies of the passivation process for iron in the presence of oxygenated solutions of inhibitors of different functional types. The first study dealt with inhibitors that have no oxidizing character and necessarily depend upon oxygen for the formation of the passive film. Polarization measurements made it clear that the rate of reduction of oxygen alone on the passive film is adequate for maintenance of passivity, provided that a suitable nonoxidizing inhibitor is present under proper conditions of acidity and concentration. The results for benzoate, phthalate, and phosphate ions as inhibitors have been published.[2]

In further studies, cathodic polarizations were made in order to compare the rates of reduction of oxygen and reducible inhibitors on passive iron. The measurements and other observations with the pertechnetate ion led to the following conclusions.

1. The rate of reduction of the pertechnetate ion under the prevailing conditions is so much smaller than that of oxygen that reduction of oxygen is the principal cathodic process at passive potentials.

2. The pertechnetate ion reacts with active iron areas, but the resulting film of mixed corrosion products does not lead to passivation unless some minimum concentration of pertechnetate remains in solution, even when oxygen is present.

3. Technetium(IV) hydroxide deposited on the surface catalyzes the reduction processes for both oxygen and the pertechnetate ion.

4. The inhibitory process is counteracted by low concentrations of anions which apparently act by competitive adsorption of a labile type.[3]

Experiments with the chromate ion as inhibitor gave the following results.

1. Reduction of oxygen on the passive surface under the conditions in effect is about two orders of magnitude faster than that of chromate ions at potentials near the Flade potential.

2. The reduction product of the chromate ion does not accelerate cathodic processes, as $Tc(OH)_4$ does.

3. The estimated exchange-current densities of the oxygen and chromate processes under the conditions assumed are of similar magnitude, so that the greater contribution of oxygen to the total cathodic process derives chiefly from its more noble reversible potential under these conditions.

4. There is some evidence that the fully passivated surface contains a persistently held reducible constituent other than the passive film itself and not dependent upon the chromate ion for its formation.[4]

A similar series of measurements with osmium(VIII) oxide as inhibitor showed that its reduction is very much faster than that of oxygen under inhibiting conditions. Further, the reduction product, $Os(OH)_4$, has a marked accelerating effect on cathodic processes, even when very small amounts are present. The results of the entire series of measurements have been summarized and discussed in relation to theories of the passivation process in a forthcoming paper.[5]

ION EXCHANGE PROPERTIES OF THE PASSIVE FILM ON IRON

D. H. Spahrbier G. H. Cartledge

The ability of certain inorganic oxides or hydrous oxides to function as ion exchange materials has been shown both by direct measurements of

[1] G. H. Cartledge, *Chem. Div. Ann. Progr. Rept. June 20, 1960*, ORNL-2983, p 58.

[2] G. H. Cartledge, *J. Phys. Chem.* 64, 1877 (1960).

[3] G. H. Cartledge, *J. Phys. Chem.* 64, 1882 (1960).

[4] G. H. Cartledge, *J. Phys. Chem.* 65, 1009 (1961).

[5] G. H. Cartledge, *Journal of Physical Chemistry* (in press).

exchange[6] and, indirectly, by observations of the effects of various anions on their cataphoretic properties.[7] The specific interactions of solute species with the surface of a metal or surface oxide are shown also by measurements of the capacity of electrodes as a function of potential. In view of the importance of the surface state for an understanding of electrode kinetics, particularly in connection with the passivation phenomena, studies on the ion exchange properties of the passive iron surface were initiated.

The experiments involve the passivation of iron or low-carbon steel in an oxygenated inhibitor solution, after which the metal is treated with water and a variety of electrolytes. By use of carbonyl iron powder with the chromate ion as passivator, it was shown that chromate ions are retained on the thoroughly washed material in a form that is readily susceptible to displacement by hydroxide or sulfate ions. The carbonyl iron permitted use of a sufficiently large surface for a spectrophotometric procedure to be used for analysis of the extracted chromium. The reagent, diphenylcarbazide, is sensitive only to Cr(VI), thus demonstrating that unreduced chromate was being removed. After four extractions with 3 *N* NH_4OH in one experiment, extraction with 1 *N* NaOH at 24° removed another considerable amount of chromate. When four such extractions were followed by additional washings with boiling 1 *N* NaOH, the first of these again removed a considerable amount. The results apparently indicate that the surface is nonuniform with respect to the firmness with which the chromate ions are held.

In other chromate experiments, low-carbon steel sheet (0.1% C) was used with $Cr^{51}O_4^{2-}$. The measurements showed clearly that Cr^{51} was displaced very slowly by water alone, but after extensive extraction with water, either hydroxide or sulfate ions quickly removed an amount equivalent to probably about a monolayer (if a roughness factor of ~2 to 4 is assumed for the abraded surface). Very little Cr^{51} was removed by 0.10 *f* KCl, and probably none by 0.01 *f* NH_4TcO_4. The process was shown to be reversible, in that the extraction by hydroxide ions could be repeated after the specimen was again soaked in the $Cr^{51}O_4^{2-}$ solution.

When the pertechnetate ion was used as inhibitor, there was no evidence that exchangeable TcO_4^- was present after a brief washing with water, the limit of accuracy of the extraction and counting procedure being about 3% of a monolayer of TcO_4^-. On the contrary, some extractable Mo(VI) species was observed spectrophotometrically after passivation of carbonyl iron in oxygenated molybdate solutions.

EFFECT OF ADSORBED ANIONS ON REDUCTION PROCESSES ON PASSIVE STAINLESS STEEL

F. A. Posey R. F. Sympson[8]

It was established earlier[9-11] that the electrode potentials and polarization characteristics of passive iron and stainless steel electrodes are markedly affected by the addition of certain anions to the solution. Subsequent experiments[12,13] showed that SCN^- catalyzes the reduction of Cu^{2+} on passive stainless steel, and an attempt was made to interpret these data in terms of a mechanism involving complex ion formation in solution between Cu^{2+} and SCN^-. Further work demonstrated that adsorption of anions on the surface of passive stainless steel is far more important than complexing effects in affecting the rates of reduction reactions, although the data are described by equations of the same general form as those used in the complexing explanation. In addition to work on the effect of SCN^-, studies were conducted on the effects of OH^-, SO_4^{2-}, and Cl^- on the reduction of Cu^{2+} on passive stainless steel, and a unified theory was developed which accounts for the observations.

[6]K. A. Kraus *et al.*, *Proc. U.N. Intern. Conf. Peaceful Uses Atomic Energy, 2nd, Geneva, 1958* **28**, 3 (1958).

[7]See, for example, P. J. Anderson, p 67 in *Proceedings of the Second International Congress on Surface Activity*, Butterworth's, London, 1957; also *Trans. Faraday Soc.* **54**, 130 (1958).

[8]Summer employee from Ohio University, Athens.

[9]R. F. Sympson and G. H. Cartledge, *J. Phys. Chem.* **60**, 1037 (1956).

[10]G. H. Cartledge and R. F. Sympson, *Chem. Div. Semiann. Progr. Rept. Dec. 20, 1955*, ORNL-2046, p 10.

[11]G. H. Cartledge, *Chem. Div. Semiann. Progr. Rept. June 20, 1956*, ORNL-2159, p 66.

[12]R. F. Sympson and F. A. Posey, *Chem. Div. Ann. Progr. Rept. June 20, 1959*, ORNL-2782, p 57.

[13]R. F. Sympson and F. A. Posey, *Chem. Div. Ann. Progr. Rept. June 20, 1960*, ORNL-2983, p 54.

Some results of experiments on the effects of SCN^-, OH^- (acidity), SO_4^{2-}, and Cl^- on cupric ion reduction are shown in Figs. 7.1–7.4 respectively. Here, the logarithm of the rate constant for reduction of Cu^{2+} is plotted against the logarithm of the concentration of added ion. Since the reduction reaction is first order with respect to cupric ion concentration, the rate constant is equal to the current density divided by $[Cu^{2+}]$, which was generally in the range 10^{-6} to 10^{-5} *f*. Sigmoidal curves are obtained in every instance, and they obey a relation having the form of Eq. (1):

$$k = \frac{A + BC[X]}{1 + C[X]} \quad (1)$$

The constants *A* and *B* are rate constants for zero and for very large concentrations of the added ion, $[X]$, respectively. Electrochemical kinetic theory shows that the constant *C*, for simple cases, is the equilibrium quotient for adsorption of the added ion onto the electrode surface. For situations where several anions compete for adsorption, the theoretical form of *C* is very complex. The solid lines in Figs. 7.1, 7.2, and 7.4 are least-squares fits to the data at each potential. The relatively good fit in most cases argues for the correctness of the assumption that use of a potential-dependent Langmuir isotherm is a sufficiently good approximation in treating anion adsorption in the passive systems studied.

It follows from Eq. (1) that the coordinates of the inflection point (infl) of the curve, in a log-log

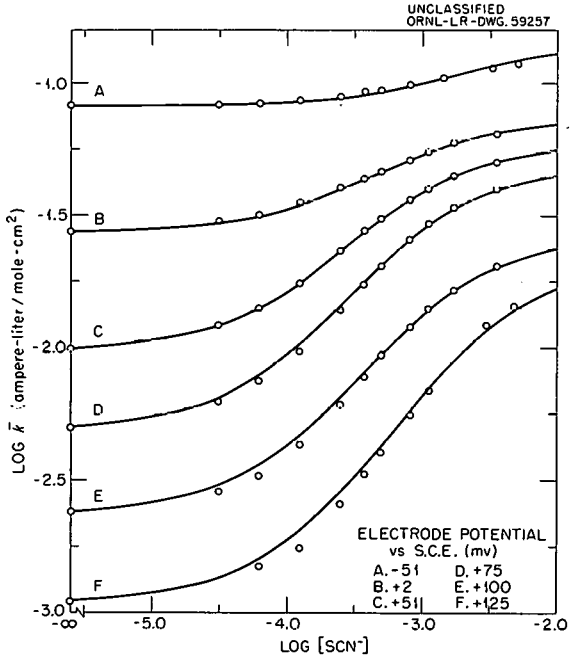

Fig. 7.1. Effect of SCN^- on the Reduction of Cu^{2+} on Passive Stainless Steel in 1×10^{-3} / H_2SO_4 plus 9×10^{-2} / Na_2SO_4; 65°C, Nitrogen Atmosphere.

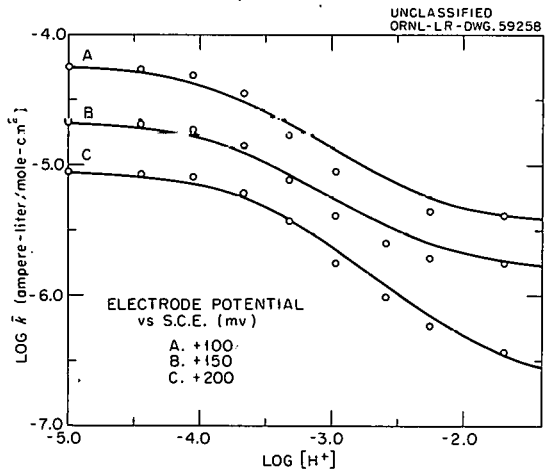

Fig. 7.2. Effect of Acidity on the Reduction of Cu^{2+} on Passive Stainless Steel in 3×10^{-1} / $NaClO_4$; 65°C, Helium Atmosphere.

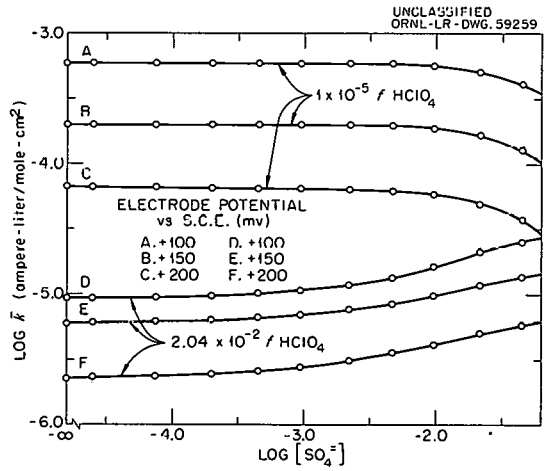

Fig. 7.3. Effect of SO_4^{2-} on the Reduction of Cu^{2+} on Passive Stainless Steel in 3×10^{-1} / $NaClO_4$; 85°C, Helium Atmosphere.

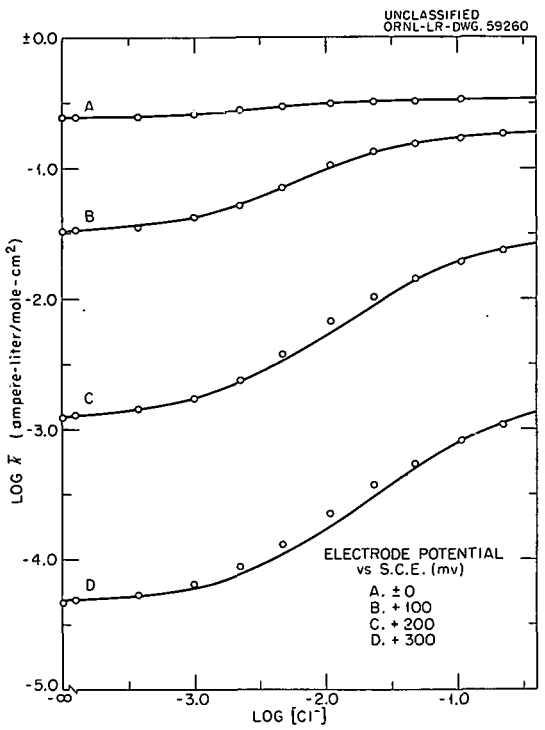

Fig. 7.4. Effect of Cl^- on the Reduction of Cu^{2+} on Passive Stainless Steel in 1×10^{-5} / $HClO_4$ plus 3×10^{-1} / $NaClO_4$; 85°C, Helium Atmosphere.

plot, are related to the several constants by Eqs. (2):

$$\bar{k}\ (\text{infl}) = \sqrt{AB}\ ,$$
$$[X]\ (\text{infl}) = \frac{1}{C}\sqrt{\frac{A}{B}}\ . \qquad (2)$$

Hence the fact that the equilibrium quotient for anion adsorption generally depends on potential is evident on visual inspection of graphs of this type. In the case of SCN^- adsorption, the constant C exhibits a maximum with potential. For OH^- adsorption, C increases exponentially with potential; while for Cl^- adsorption, C decreases exponentially with potential. This behavior is understandable on the basis of the kinetic theory. The interpretation is simplest in the case of adsorption of OH^-, where theory predicts an increase of adsorption constant with increasing potential, in agreement with experiment. However, for the cases of SCN^-, Cl^-, and SO_4^{2-} adsorption, these ions may displace either adsorbed OH^- or (presumably) adsorbed H_2O at the interface, so that the number of reaction paths is greatly increased. The theoretical form of the constant C becomes much more complicated, and the exact variation of C with potential depends on which of several reaction paths predominates in any given system. As an example of the specificity shown in anion adsorption, it is found that SCN^- prefers to displace OH^- from the surface rather than H_2O, whereas SO_4^{2-} exhibits the opposite effect.

The equilibrium quotient for adsorption of OH^- on passive stainless in perchlorate medium has been determined from data similar to those in Fig. 7.2 as a function of both potential and temperature, and the following energetic quantities for the adsorption reaction have been calculated: $\Delta H_{ads}(\text{av}) = -4.3$ kcal/mole; $\Delta S_{ads} = +29.8$ eu. Because the adsorption reaction depends on potential, the apparent enthalpy of adsorption varies with potential, and the value reported here is the average of several values over the potential range +100 to +200 mv vs the S.C.E.

Reducible species other than Cu^{2+} also show anion effects similar to those reported here. However, hydrolysis and complexing effects may vitiate any attempt to apply a similar analysis. Nevertheless, potentiostatic studies have considerable value in delimiting mechanistic choices, even in the more complex situations.

ELECTROCHEMISTRY OF ZIRCONIUM

R. E. Meyer

Zirconium and its alloys normally corrode at very low rates despite their great thermodynamic instability with respect to aqueous environments. Although it is generally accepted that a thin film of corrosion product (probably ZrO_2) accounts for this behavior, the mechanism of this process is the subject of current investigation and debate.

Kinetic analysis of reduction experiments on passive zirconium led to the proposal of a dual-barrier model[14] in which considerable film resistance was assumed. The nature of this film resistance, however, is not clear. Zirconium oxide in bulk is an excellent insulator and is the stable reaction product, but it must be remembered that these films are quite thin and that the structure

[14] R. E. Meyer, *J. Electrochem. Soc.* **107**, 847 (1960).

and composition of the films at these low temperatures will be determined by the kinetics rather than the thermodynamics. It is therefore not correct, as is frequently done, to extrapolate the bulk properties of ZrO_2 to the 50- to 100-A films found on the zirconium specimens investigated here. In fact, although appreciable resistance is predicted by applying the known resistivity of bulk ZrO_2 to the usual passive film, negligible resistance is found when these specimens are taken out and tested with metal contacts. In an effort to determine, if possible, some of the conduction properties of the film, the effect of film thickness upon reduction rate was investigated. Figure 7.5 shows the effect of anodizing (electrolytically producing oxide) upon the reduction of hydrogen ions (pH = 3.18, 75°C, 0.1 / Na_2SO_4). The films of Fig. 7.5 are probably very thin, since they were formed immediately after removal of the specimens from a vacuum system. In comparing the various thicknesses, it must be remembered that one should compare the various rates at constant potential, that is, along a vertical line on the graph. For oxygen reduction on films formed by natural corrosion, the current at constant potential seems to decrease very rapidly initially and then reach a region of almost constant rate as the film thickens. This effect is not yet clear, for it is very difficult to estimate the film thickness when the film is corroding at open circuit. A tentative explanation for these observations can, however, be proposed. First, it seems that the insertion of these specimens in solution drastically modifies the system so that there is appreciable film resistance when they are in solution. Second, the conduction properties of very thin films, such as those of Fig. 7.5, may be explained by the tunnel effect, for it is one of the few possible effects which shows such a large thickness dependence. (For many cases the tunnel effect predicts that the rate will decrease exponentially with thickness, all other factors being equal.) Because of this enormous thickness dependence, the tunnel effect will soon cease to operate as the film thickens. For the thicker films, such as are formed by exposure to oxygen, the electrons must then surmount any barrier presented by the film. For films which are not too thick, this will lead to a rate expression in which the current varies exponentially with the potential and in which the current is almost independent of thickness. This expression will lead

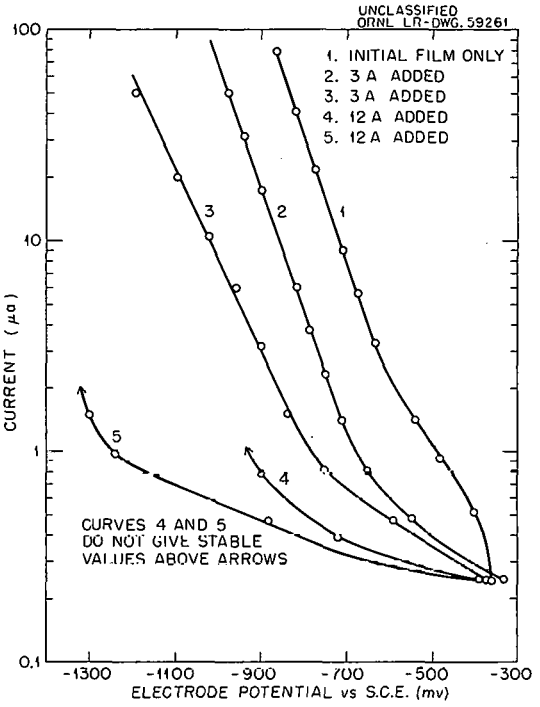

Fig. 7.5. Effect of Anodized-Film Thickness on Reduction of Hydrogen Ions on Passive Zirconium in 0.1 / Na_2SO_4; 75°C, pH = 3.18.

to very low rates, which are, in fact, observed. An extensive discussion of these ideas was presented in an invited paper at the October 1960 meeting of the Electrochemical Society.

The semiconducting properties of these films are sometimes proposed as being important factors in film conduction. If this is so, one might expect drastic modifications of conductivity if foreign atoms of different valence are introduced. Two alloys were investigated (Zr–15 wt % Nb and Zircaloy-2), but there was no significant change in the reduction kinetics.

During the past several years, the kinetic parameters of a variety of reduction processes were characterized. The results were published.[14] Of those systems reported, oxygen reduction was singled out for detailed investigation because of its importance to the corrosion of zirconium.

Experiments were conducted to determine the reaction products of oxygen reduction. In many electrode systems, oxygen is reduced to hydrogen peroxide, and, if conditions are right, significant quantities of hydrogen peroxide can be found in solution. At low current densities (less than 10^{-6} amp/cm^2) only about 10% or less of the

theoretical amount of hydrogen peroxide was found in solution. At higher current densities, up to 40% was found. This was quite interesting, since both the decomposition rate and the reduction rate of hydrogen peroxide were found to be negligible. The fact that some hydrogen peroxide is found indicates that H_2O_2 is always formed at one stage of the reduction (unless one assumes a dual mechanism). Only a slight pH effect is observed on oxygen reduction, but there is a slight tendency for increasing acidity to increase the rate of reduction. These facts suggest the following mechanism of oxygen reduction:

$$O_2 + e^- \longrightarrow O_2^- \text{ (slow step)}, \quad (1)$$

$$O_2^- + e^- + H^+ \longrightarrow HO_2^- \text{ (adsorbed)}, \quad (2)$$

$$HO_{2_{ads}}^- + H^+ \longrightarrow H_2O_2 \text{ (solution) or}$$

$$2HO_2^- + 2H^+ \longrightarrow 2H_2O + O_2. \quad (3)$$

It is further suggested that negative potentials favor the desorption of HO_2^-, while, at more positive potentials, the HO_2^- tends to remain adsorbed and, eventually, to decompose to O_2 and H_2O.

HYSTERESIS EFFECTS IN THE CORROSION OF IRON

E. J. Kelly

Numerous papers in the literature purport to have arrived at the mechanism(s) whereby iron dissolves in deoxygenated solutions of various acids.[15-17] The customary approach to the problem has been to utilize potentiostatic and/or galvanostatic techniques to determine the slopes of the anodic and cathodic Tafel lines (logarithm of the current density vs potential) and the shifts in the positions of these lines accompanying changes in pH. The reports frequently include direct measurements of the corrosion potential and corrosion rate as functions of the pH. These data are analyzed on the basis of the theory of electrode kinetics in an attempt to determine the nature of the partial anodic and cathodic reactions and, consequently, the over-all mechanism of the corrosion process. Unfortunately, Hurlen[18] found that different investigators, even when studying the same solutions under apparently identical conditions, have reported anodic Tafel slopes ranging from 30 to 100 mv/decade, $[OH^-]$ orders for the anodic process ranging from 1 to 2, corrosion rates that are either independent of pH or vary linearly with pH, and corrosion potentials which shift anywhere from 45 to 60 mv per pH unit. Little effort has been expended on the investigation of the cathodic process (the hydrogen-evolution reaction) on iron.

One common observation is found in the majority of these papers. Electrode potentials change with time in galvanostatic studies, and currents vary with time in potentiostatic studies. However, the time effects have been universally ignored; each investigator has selected an arbitrary time of observation of electrochemical variables, ranging from fractions of a second to several minutes. As a result, experimental points obtained on increasing current or potential do not coincide with those obtained on decreasing these variables, and plots of the data exhibit hysteresis loops.

It was felt that neglect of these time effects might account for the wide variety of values assigned to the diagnostic criteria mentioned above. Consequently, a study was undertaken to elucidate the effects of prolonged polarization on the anodic and cathodic polarization characteristics of iron. The solution chosen for this study was 0.1 *f* benzoic acid at a pH of 5.0. This medium is particularly well suited to these studies, since the currents needed to polarize the iron are rather low, and the solution is buffered against pH variations during the necessarily prolonged polarizations. The results are summarized in Fig. 7.6, where the logarithm of the net current density is plotted against the potential of the test electrode with respect to the S.C.E.

The open-circuit or corrosion potential is marked by the vertical line through 1 at −685 mv. If one starts at this potential and suddenly drops

[15] M. Stern, *J. Electrochem. Soc.* 102, 609 (1955).

[16] G. Okamoto, M. Nagayama, and N. Sato, *International Committee on Thermodynamics and Electrochemical Kinetics (C.I.T.C.E.)*, p 72, vol VIII, Butterworth's, London, 1958.

[17] A. C. Makrides, *J. Electrochem. Soc.* 107, 869 (1960).

[18] T. Hurlen, *Acta Chem. Scand.* 14, 1533, 1555 (1960).

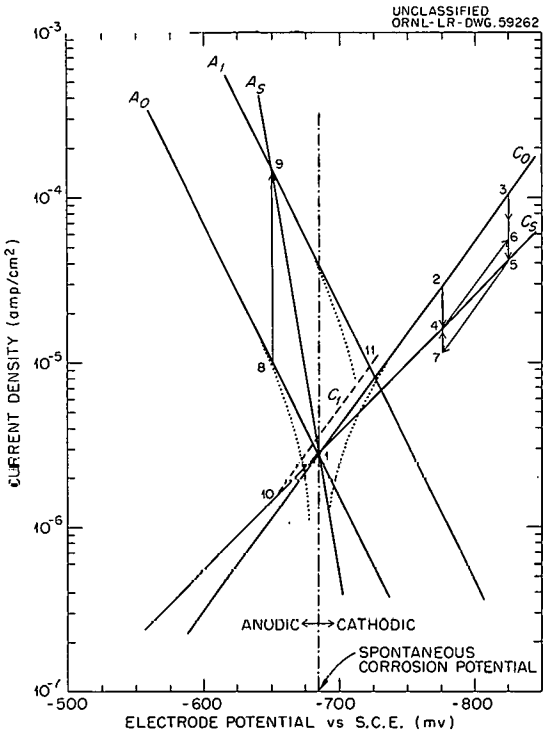

Fig. 7.6. Transient and Steady-State Polarizability of Iron in 0.1 *f* Benzoic Acid at 30°C; pH = 5.0.

the potential to the more cathodic value of –775 mv, the net cathodic current immediately assumes the value given at 2. Immediately changing the potential to –825 mv then gives the instantaneous current value shown at 3. In this manner, the "fast" cathodic polarization curve C_0 is obtained. The linear section of the curve, that is, the cathodic Tafel line, has a slope of about 90 mv/decade. In a similar fashion, A_0, the "fast" anodic polarization curve, is obtained. The slope of the anodic Tafel line is 60 mv/decade. The extrapolated anodic and cathodic Tafel lines intersect at the open-circuit potential to give a corrosion rate of 2.8×10^{-6} amp/cm^2. The deviations from linearity of the anodic and cathodic polarization curves near the open-circuit potential result from the contributions of the cathodic and anodic processes, respectively, to the net current densities.

The anodic and cathodic curves A_0 and C_0 do not correspond to stable states. Focusing on the cathodic process, one finds that if the electrode potential is suddenly changed from the open-circuit potential to the more cathodic potential of –775 mv and held at this potential, the net cathodic current density decreases from the initial value at 2 to the steady-state value at 4. Similarly, if the potential is changed from the open-circuit value to –825 mv and held there, the current drops from its initial value at 3 to the steady-state value at 5. The steady-state-current values give rise to the steady-state cathodic Tafel line C_s, the slope of which is about 120 mv/decade. If the electrode is in a steady state at 4 and the potential is suddenly shifted and held at –825 mv, the cathodic current immediately moves along a 90 mv/decade line to the initial value at 6, and then drops to the steady-state value at 5. Upon restoring the original potential of –775 mv, the current drops along a 90 mv/decade line to the initial value at 7 and then increases to the steady-state value at 4. The transition from an initial cathodic current to the steady-state value, for example, from 2 to 4 or 3 to 5, is a very slow process requiring roughly 20 hr. An analysis of this transient behavior indicates that, after a short induction period, the current-time relationship is given by Eq. (1), in which i_t represents the current at any time t:

$$\log (i_t - i_{ss}) = \log (i_0 - i_{ss}) - kt \,, \qquad (1)$$

where i_0 is the initial current, i_{ss} is the steady-state current, and k is the slope, having a value of about 0.10 hr^{-1}.

On the anodic side, an even more pronounced time effect is observed. If the potential is shifted from the open-circuit potential to the more anodic potential of –650 mv, the initial current shown at 8 on the A_0 curve slowly increases to the steady-state value shown at 9. This transient behavior, like the cathodic transient, is characterized by an induction period after which Eq. (1) is followed, the value of k being about 0.03 hr^{-1}. The steady-state anodic polarization curve is given by A_s, the slope of which is approximately 20 mv/decade. If the electrode is in a steady state at 9, a fast anodic polarization gives the transient Tafel line, A_1, having the usual 60 mv/decade slope. It might be mentioned here that if the experiments described above are carried out galvanostatically rather than potentiostatically, the picture remains the same, except that in the

former case, increases and decreases in the anodic and cathodic overvoltages with time substitute for the decreases and increases, respectively, in the current densities.

While the preceding studies are not yet complete, it can already be seen how the time effects or slow transients might deceive the researcher who adopts the arbitrary time-basis approach. On the cathodic side, depending upon the time basis chosen, one might obtain reasonably straight Tafel lines having slopes anywhere between 90 and 120 mv/decade. On the anodic side, the variations in slope could range from 20 to 60 mv/decade. Hysteresis effects follow directly from Fig. 7.6, a typical cathodic hysteresis loop being formed by the cyclic process 4, 6, 5, 7. An examination of Fig. 7.6 shows that even greater hysteresis effects are to be expected on the anodic side. Another common statement in the literature is that after anodic or cathodic polarization, the electrode potential fails to return directly to the original open-circuit potential, but instead it overshoots the open-circuit potential and then slowly returns. This "overshoot" phenomenon can also be explained by Fig. 7.6. Let the electrode be in a steady state at −650 mv. At this potential the partial anodic and cathodic current densities are given at 9 and 10 respectively. Upon breaking the circuit, the initial open-circuit potential will be given by the intersection, 11, of the transient anodic and cathodic Tafel lines, A_1 and C_1. It is seen that this potential overshoots the original open-circuit potential by about 35 mv. As the transients decay back to the steady-state Tafel lines A_s and C_s, the open-circuit potential moves from 11 back to its original value at 1. Finally, experiments designed to give [OH^-] orders, corrosion-potential-vs-pH relationships, etc., have failed because the slow transient behavior described above has not been previously taken into account. For example, recent studies by this investigator on the corrosion-potential-vs-pH relationship for iron in sulfate and in perchlorate solutions showed that when the pH is suddenly changed, the corresponding change in the corrosion potential is such as to give the frequently cited value of 60 mv per pH unit for $dE(\text{corr})/d\text{pH}$. However, by waiting for steady states, this value is reduced to approximately 45 mv per pH unit, the other most commonly cited value. Again depending upon time, any of the reported values lying between these limits are attainable.

At this stage in the investigation, a clear-cut decision regarding the nature of the process producing the time effects cannot be made. Certainly, to attribute these effects to changes in the electrode surface, impurities in solution, etc., would seem implausible in light of the preceding discussion. The experimental results suggest that the slow reaction responsible for the observed time effects is the reversible transfer of the atomic hydrogen adsorbed on the electrode surface to the bulk interior of the iron.[19] A kinetic analysis on this basis shows that when the electrode potential is made more cathodic, the activity of the adsorbed hydrogen is less at any time t than in the new steady state, and, corresponding to the increasing activity of the adsorbed hydrogen, the cathodic current decreases to the new steady-state current. The increases in the anodic current, with time, accompanying a shift in potential to a more anodic value may then be attributed to the increasing $(FeOH)^0$ catalyst[20] activity on the electrode surface paralleling the decreasing absorbed hydrogen activity. A less likely mechanism assumes the time behavior to result from the slow electrochemical adsorption-desorption of benzoate ions on the electrode surface. In either mechanism, changing surface concentrations of reaction intermediates or catalyst species with time produce the time effects. Further study will be devoted to the mechanisms of the reactions responsible for the effects described above.

[19] L. Cavallaro, G. P. Bolognesi, and L. Felloni, *Korrosion* 12, 131 (1961).

[20] K. E. Heusler, *Z. Elektrochem.* 62, 582 (1958).

8. NONAQUEOUS SYSTEMS AT HIGH TEMPERATURE

FISSION PRODUCT RELEASE FROM REACTOR-GRADE UO_2 BY OXIDATION, DIFFUSION, AND MELTING

G. W. Parker G. E. Creek
W. J. Martin

Introduction

An important aspect of nuclear reactor safety hinges on a knowledge of the diffusion and dispersal of fission products from various types of nuclear accidents. The experimental demonstration of fission product release from overheated reactor-type UO_2 has been the subject of an extensive program[1] intended to serve as a guide in hazards evaluations according to the maximum-credible-accident analysis of a particular reactor.

A comprehensive review of the status of fission product release from UO_2 by Cottrell and others[2] points out the need for experimental data on the diffusion of fission products other than the rare gases but omits consideration of the diffusion effect of the simultaneously oxidizing UO_2. A study of fission product release by the oxidation of UO_2 in air was therefore one of the primary objectives of the present investigation. Since most clad UO_2 fuels are designed with a helium gas filling for heat removal, diffusion of fission products out of elements heated in this medium is also pertinent to the hazards evaluation. Accordingly, results of the melting of UO_2 in impure helium, in air, and in CO_2 are reported.

In part, the present report summarizes a comparison of the release rates observed as a function of a new variable, the extent of burnup or fission density in the fuel. This reported effect is only the initial phase of a more extensive series of parametric studies.

Oxidation of UO_2 to U_3O_8 in Air

Previous investigations[3–5] have shown the oxidation rate of UO_2 at various temperatures, including an induction period for temperatures up to 600°C, which suggests nucleation followed by growth of U_3O_8. The rate after induction is controlled by diffusion through a thin layer of U_3O_8 which cracks upon accumulation of sufficient stress from the large change in density. At higher temperatures, the accumulated oxidized layer is more plastic and leads to a slowly decreasing oxidation rate to 900°C. Above 900°C, the oxidation is rapidly completed but results in a nonstoichiometric U_3O_8.

Considerable controversy exists over the exact rate of UO_2 oxidation at a given temperature. A few recent experiments have shown this to be largely an effect of variations in density, method of manufacture, and specific surface area. Figure 8.1 illustrates the effects of surface area and density, showing the areas of agreement and nonagreement with similar data of Peakall and Antill.

Fission product release as a result of this multiple process is reflected in the summary of release data shown in Fig. 8.2. The results show a curious difference in release, with ruthenium exhibiting the highest volatility above 1000°C and with both iodine and the rare gases significantly suppressed. These results apply only to trace concentrations of fission products and may not resemble the rate at high fission density.

Release of Fission Products by High-Temperature Diffusion into Pure Helium

In a previous report,[1] the enhancement of fission product release by oxidation in *impure* helium has been clearly demonstrated. In order to relate the diffusion parameter to the results obtained by

[1] G. W. Parker, G. E. Creek, and W. J. Martin, *Fission Product Release from UO_2 by High Temperature Diffusion and Melting in Helium and Air*, ORNL CF-60-12-14 (February 1961).

[2] W. B. Cottrell *et al.*, *Fission Product Release from UO_2*, ORNL-2935 (September 1960).

[3] K. A. Peakall and J. E. Antill, *J. Nuclear Materials* 2(2), 194 (1960).

[4] D. T. Livey and P. Murray, *Progr. in Nuclear Energy, Ser. V* 1, 473 (1956).

[5] S. Aronson *et al.*, *J. Chem. Phys.* 27, 137 (1957).

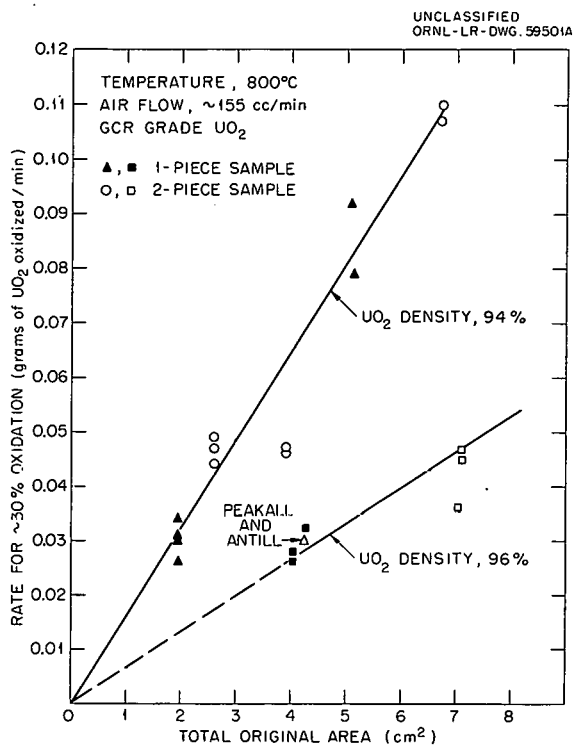

Fig. 8.1. Effects of Surface Area and Density on the Oxidation Rate of UO_2.

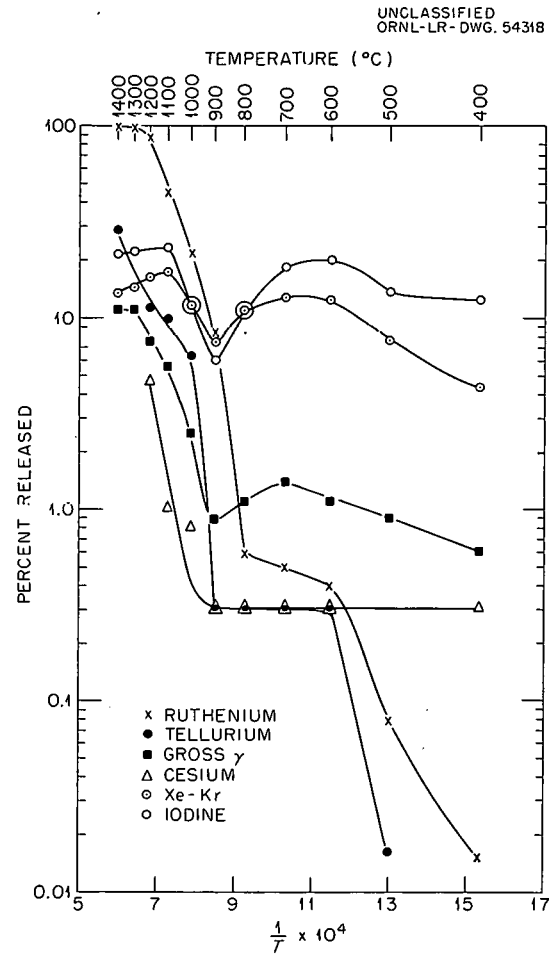

Fig. 8.2. Fission Product Release by the Oxidation of UO_2 to U_3O_8 in Air, Showing Discontinuity Between 600 and 900°C.

others,[6,7] exhaustive care was expended in pretreating the helium by passing it over hot zirconium in order to remove traces of oxygen. Under these conditions, diffusion constants in flowing gas correlated well with results obtained by the average experimenter using the high-vacuum anneal method. The significant results of the helium diffusion experiments are shown in Figs. 8.3 and 8.4. Figure 8.3 is a complete set of diffusion release curves for the volatile fission products to temperatures approaching those of melting UO_2. These are applicable only to trace fission product concentrations. It is of interest that both iodine and tellurium exceed rare-gas diffusion by a factor of 3 to 5. In Fig. 8.4, a derivation of the apparent diffusion coefficient D' for the fission gases shows a two-step process with distinctly different energies of activation. The second slope is apparently associated with UO_2 sublimation as well as grain growth.

In order to illustrate the burnup parameter as it affects diffusion in helium, a series of studies is compared in Table 8.1. At all temperatures above 1400°C, a decided increase in release accompanies a higher irradiation. However, at 1400°C, the opposite seems to be the case, especially with iodine and tellurium. Even higher burnup levels may not produce this dual effect. A significant difference in the rate-of-release curves for trace-irradiated UO_2 and for a 1000-Mwd specimen is illustrated in Fig. 8.5. The initial "burst" effect is characteristic of all diffusion curves; however,

[6] H. H. Booth and G. T. Rymer, *Determination of the Diffusion Constant of Fission Xenon in UO_2 Crystals and Sintered Compacts*, CRDC-720 (August 1958).

[7] J. L. Scott, *Analysis of ORNL Data on the Release of Fission Gases from UO_2*, ORNL CF-60-8-15 (September 1960).

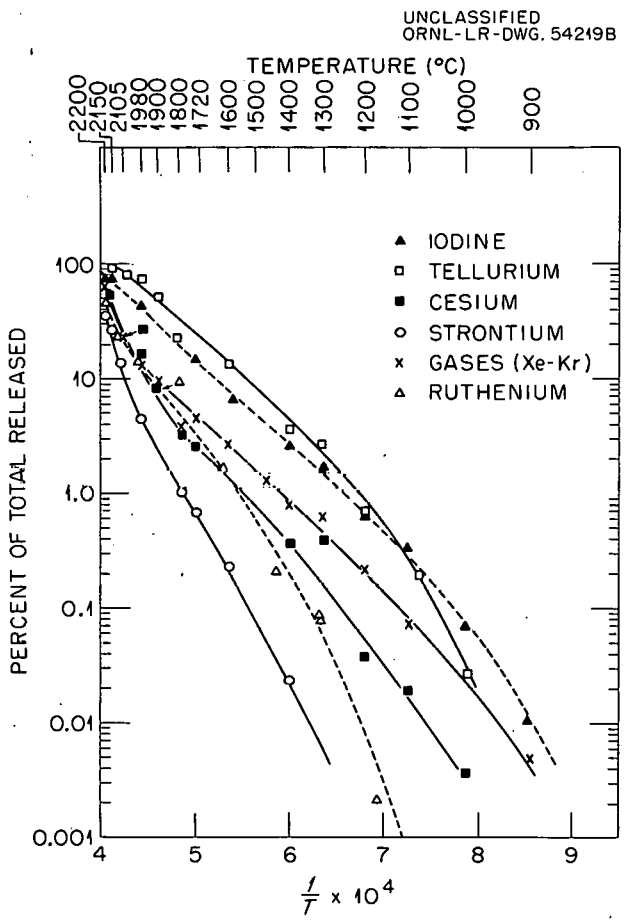

Fig. 8.3. Release of Fission Products by Diffusion from Sintered UO_2 Heated ~5 hr in Purified Flowing Helium.

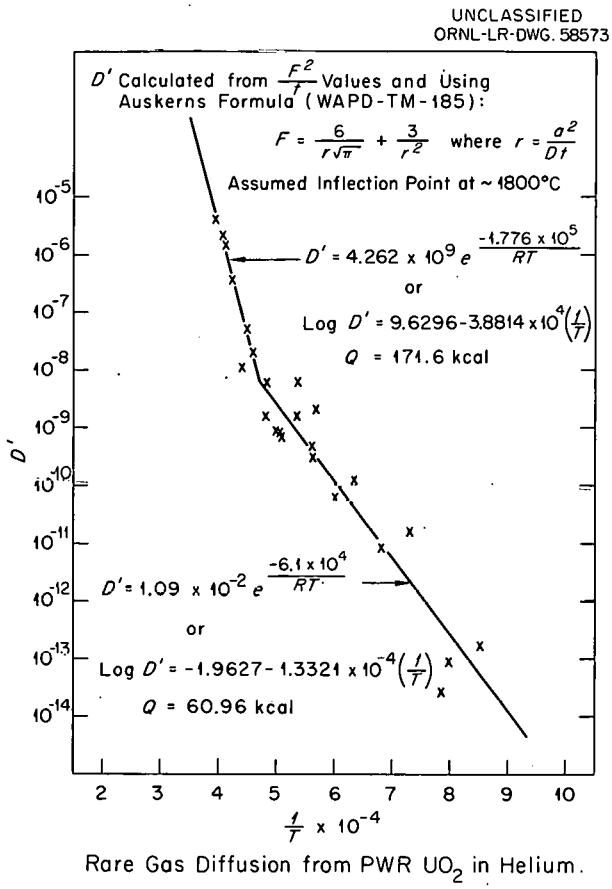

Rare Gas Diffusion from PWR UO_2 in Helium.

Fig. 8.4. Rare-Gas Diffusion from PWR UO_2 in Helium.

Table 8.1. Comparison of the Release of Fission Products from UO_2 by Diffusion in Pure Helium After a Trace Irradiation and After a 1000-Mwd/ton Irradiation

Temperature (°C)	Irradiation Level	Percentage of Individual Fission Products Released						
		Xe-Kr	I	Te	Cs	Ru	Sr	Ba
1400	Trace	0.8	4.0	3.9	0.02	0.02	0.001	
	1000 Mwd	0.8	0.9	0.8	2.6	0.001	0.1	
1610	Trace	2.7	6.5	12.1	1.7	1.5	0.1	
	1000 Mwd	2.6	3.7	12.0	12.0		2.0	17.0
1780	Trace	3.7	11.7	21.0	3.2	6.9	1.0	
	1000 Mwd	12.0	24.0	67.0	27.0	11.0	9.0	39.0
1980	Trace	12.3	41.0	75.0	15.0	13.4	4.2	8.7
	1000 Mwd	29.0	53.0	74.0	84.0		15.0	57.0

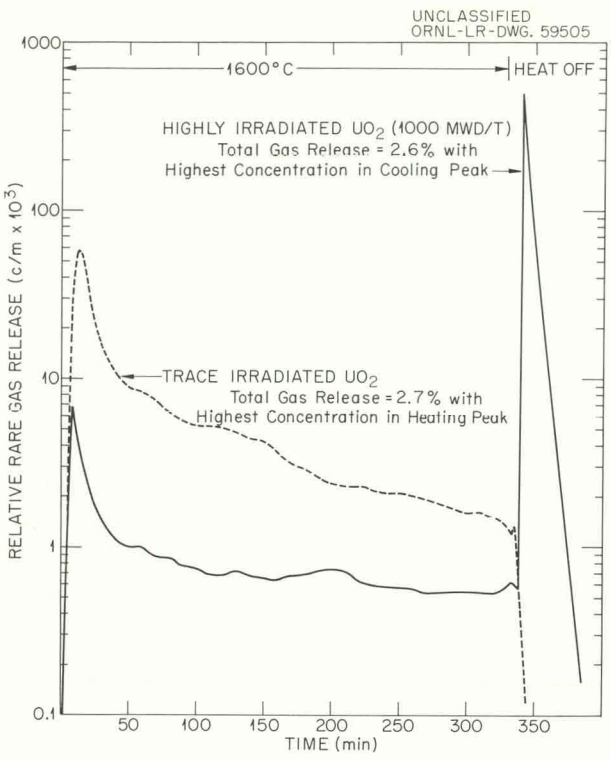

Fig. 8.5. Comparison of the Rates of Fission Gas Release from Trace-Irradiated and Highly Irradiated UO_2.

the enhanced cooling peak in the more highly irradiated process material suggests a different trapping process, such as that caused by a closed porosity that developed by plastic deformation during irradiation and which is subject to fracture on cooling.

Release of Fission Products on Melting UO_2 in Impure Helium, in Air, and in CO_2

Uranium dioxide meltdown may be postulated to occur as a result of a serious loss-of-coolant accident in large, non-gas-cooled reactors. In a series of experiments involving the melting of small UO_2 specimens by the carbon-arc-image method, high release rates were experienced for most of the so-called "volatile" fission products: rare gases, iodine, tellurium, cesium, and ruthenium. Sample size had an effect, apparently indicating incompleteness of melting in all but the smallest samples. On the other hand, atmospheric environment (helium, air, or CO_2) did not seriously differ in its effect on volatility. Table 8.2 shows a slightly lower release rate at trace-level irradiation for a CO_2 atmosphere; however, at higher irradiation levels, only ruthenium remains below the release rate in helium and air.

Table 8.2. Comparison of the Release of Fission Products on Melting UO_2 in Impure Helium, in Air, and in CO_2 After a Trace Irradiation and After a 2800-Mwd/ton Irradiation

Used GCR UO_2, with O/U ratio of 2.04 and density 95% of theoretical

Atmosphere	Irradiation Level	Weight of Sample (g)	Number of Results Averaged	Percentage (Averaged) of Individual Fission Products Released								Percentage of UO_2 Vaporized
				Xe-Kr	I	Te	Cs	Ru	Sr	Ba	Rare Earths	
Helium (impure)	Trace	0.22	2	99.5	89.7	92.0	91.3	61.0	2.1	4.6	2.2	
	2800 Mwd	0.03	3	99.9	92.2	98.2	98.5	90.4	2.1	6.6	5.1	21.2
Air	Trace	0.2	2	98.4	94.9	79.1	37.7	67.7	0.2	0.5	0.5	
	2800 Mwd	0.04	3	100.0	99.7	93.6	92.5	95.0	0.4	1.8	3.0	
CO_2	Trace	0.2	3	80.6	76.8	71.2	60.9	44.9	0.3	1.1	0.85	14.1
	2800 Mwd	0.02	3	99.9	98.7	98.6	90.2	74.3	0.5	2.5	2.8	
	11,000 Mwd	0.05	3	99.9	99.9	99.0	96.6	79.1	0.6	2.9	2.3	

Size of Particles Released from UO_2 Melted in Air and Helium

By means of the shadowed-carbon-replica process, particles collected on Millipore filters were photographed (Fig. 8.6) in the electron microscope.[8] The range of sizes of such particles as

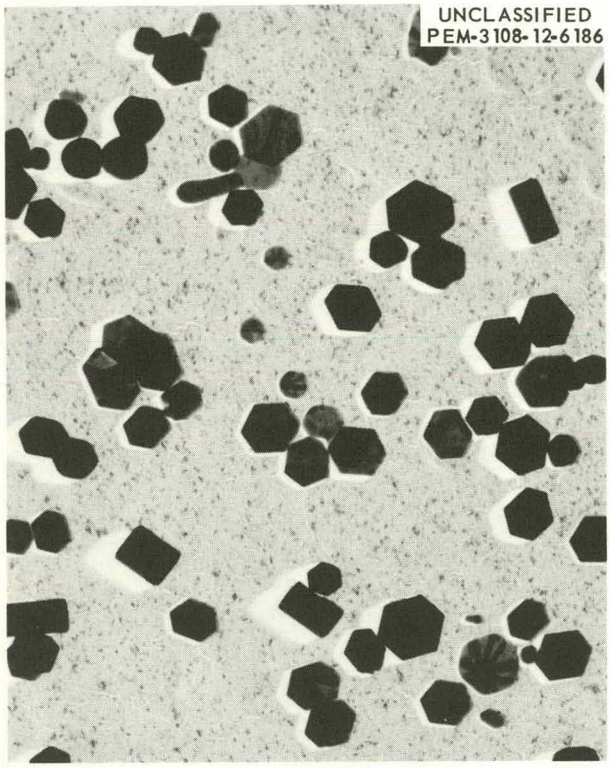

Fig. 8.6. Replica of Crystalline U_3O_8 Particles Vaporized from UO_2 Melted in Air (Particle Diameters 0.02 to 0.2 μ). 40,000X.

well as their identification as U_3O_8 (from the melting done in air) and as UO_2 (from the melting done in helium) was established. The average diameter of the crystalline U_3O_8 was 0.1 μ, while the spherical particles from helium melts averaged about 0.01 μ. The released fission products were all uniformly adsorbed on the vaporized uranium oxides (U_3O_8 or UO_2), with some variations, according to the distance that the particle traveled before plating out.

[8] T. E. Willmarth and T. G. Harmon, ORNL, private communication.

ELECTRICAL CONDUCTIVITY OF SOLUTIONS OF SOME ALKALINE- AND RARE-EARTH METALS IN THEIR MOLTEN CHLORIDES

A. S. Dworkin H. R. Bronstein
M. A. Bredig

Previous attempts to extend the capillary-cell measurements of the electrical conductivity of solutions of metals in their molten halides to the alkaline-earth and rare-earth systems were unsuccessful due to reaction between the solutions and the ceramic capillary cell. Therefore, a conductivity apparatus was developed in which no contact between the solutions and ceramic insulators occurs.

The apparatus (see Fig. 8.7) employed two rigidly mounted parallel electrodes of molybdenum immersed in a melt which was contained in a molybdenum cup. This parallel-electrode assembly yielded data of excellent quality with the metal–metal halide solutions discussed here; excessive polarization at the electrodes precluded use of this apparatus with pure salts. Accordingly, a sapphire capillary cell[9] was used to confirm the previously established conductivity behavior of Cd-$CdCl_2$ solutions,[10] and these solutions were employed as standards to determine the cell constant for the parallel-electrode assembly. In addition, the cell of synthetic sapphire was used to establish the conductivity of the pure salts. A short extrapolation of the metal–metal halide conductivities to that of the pure salts gives good agreement with the values determined for the pure salts by use of the sapphire cell. This constitutes an excellent verification of the cell constant obtained from the Cd-$CdCl_2$ solutions.

The conductivity apparatus and experimental procedure are described in detail in two papers now in press.[11,12]

Figures 8.8 and 8.9 show the results obtained with these systems as compared with the Na-NaCl and K-KCl systems.[9] (Those for Sr-$SrCl_2$ are of a preliminary nature, since only three points were

[9] H. R. Bronstein and M. A. Bredig, *J. Am. Chem. Soc.* 80, 2077 (1958).

[10] A. H. W. Aten, *Z. physik. Chem.* 73, 578 (1910).

[11] H. R. Bronstein, A. S. Dworkin, and M. A. Bredig, *Journal of Physical Chemistry* (in press).

[12] A. S. Dworkin, H. R. Bronstein, and M. A. Bredig, *Discussions of the Faraday Society* (in press).

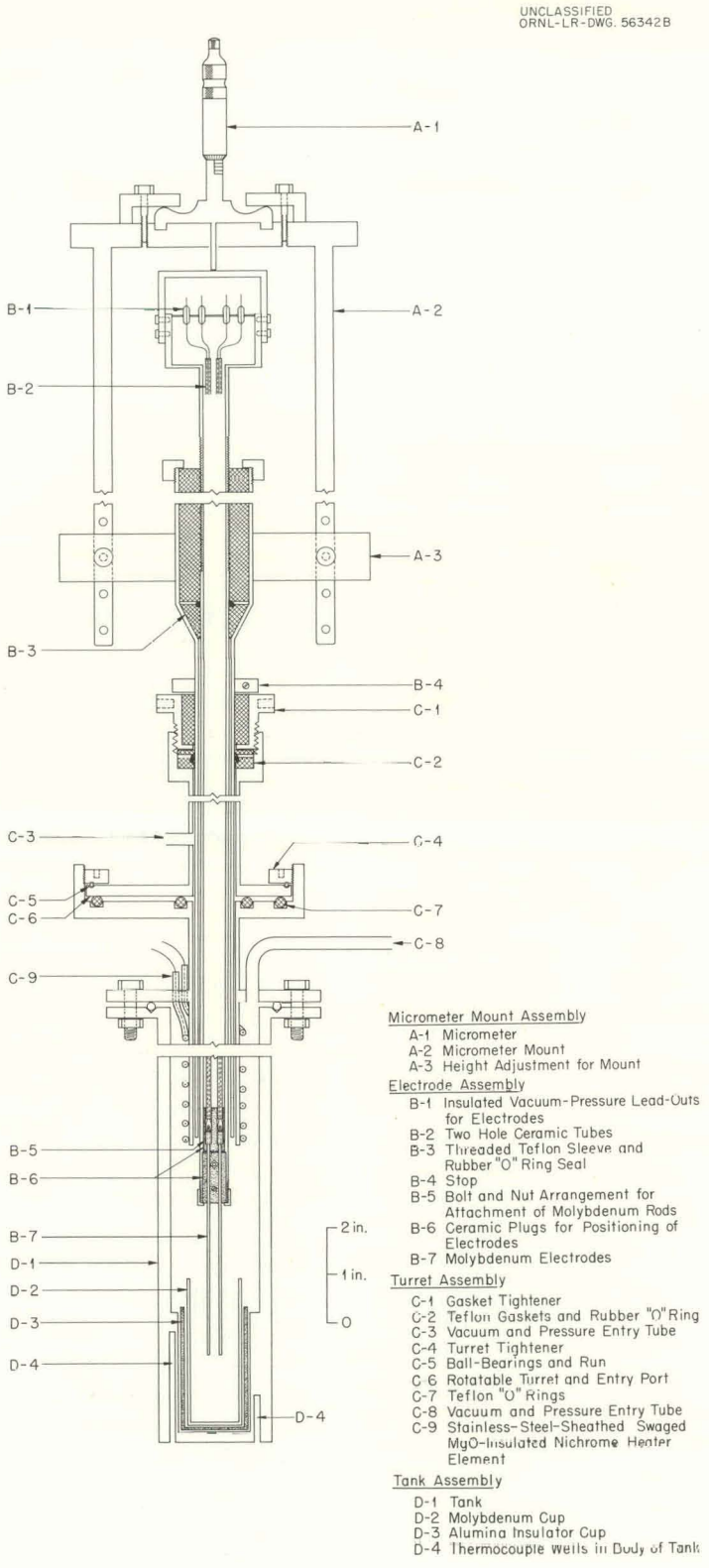

Fig. 8.7. All-Metal, Parallel-Electrode Conductivity Apparatus.

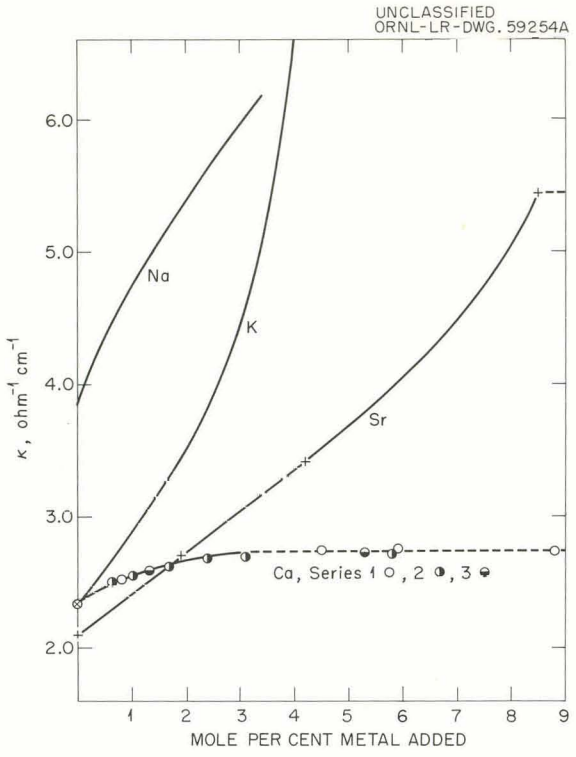

Fig. 8.8. Specific Conductivity of Solutions of Ca and Sr in Their Molten Chlorides.

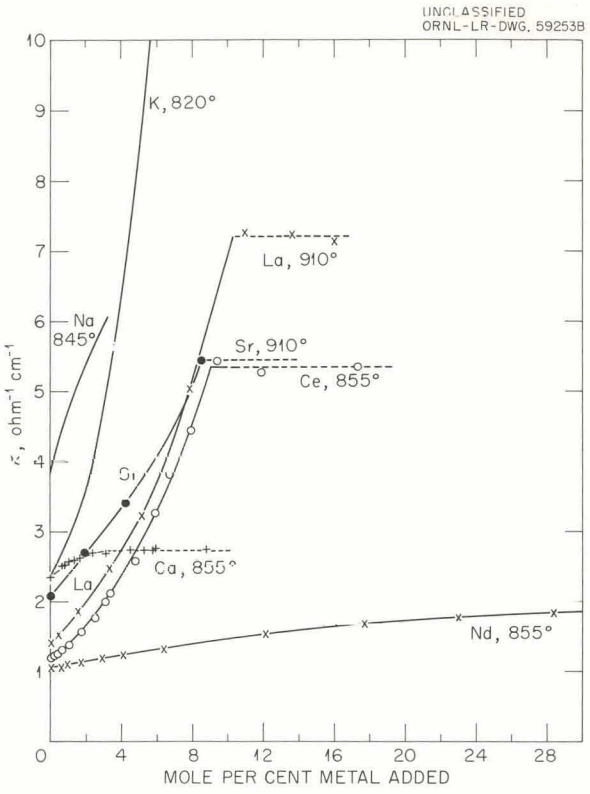

Fig. 8.9. Specific Conductivity of Solutions of Some Alkaline-Earth and Rare-Earth Metals in Their Molten Salts.

obtained due to experimental difficulties.) The specific conductivity κ of pure $CaCl_2$ and $SrCl_2$ as measured with the sapphire capillary cell agreed with the measurements of Bockris *et al.*[13] to ±1%. The temperature dependence of the conductance of the rare-earth trichlorides was found to be

$$\kappa_{LaCl_3} = -0.940 + 2.564 \times 10^{-3}t \qquad (880 \text{ to } 920^{\circ}C),$$

$$\kappa_{CeCl_3} = -5.300 + 12.38 \times 10^{-3}t - 5.596 \times 10^{-6}t^2 \qquad (820 \text{ to } 940^{\circ}C),$$

$$\kappa_{NdCl_3} = -3.854 + 9.200 \times 10^{-3}t - 4.000 \times 10^{-6}t^2 \qquad (800 \text{ to } 900^{\circ}C).$$

As in the Na-NaCl system,[9] the rate of increase in the specific conductivity of the Ca-$CaCl_2$ system decreases rather sharply with metal concentration. On the other hand, in the Sr-$SrCl_2$ system, the conductivity increases linearly to approximately 4 mole % metal, whereupon it starts to increase as in the K-KCl system.[9] The equivalent conductance of the metal solute Λ_{Ca} (calculated as in the alkali-metal systems[9]) drops rapidly from 800 ohm^{-1} cm^2 equiv^{-1} at infinite dilution to 450 at saturation (2.95 mole % Ca), while Λ_{Sr} rises from 950 at infinite dilution to 1250 ohm^{-1} cm^2 equiv^{-1} at 8.5 mole % Sr.

Figure 8.9 reveals a striking dissimilarity in the electrical behavior of lanthanum and cerium on the one hand and neodymium on the other when they are dissolved in their molten trichlorides. The La-$LaCl_3$ and Ce-$CeCl_3$ systems show an accelerating rise in conductivity with increasing metal concentration, while the conductivity of Nd-$NdCl_3$ rises much more slowly, the rate of increase decreasing with increasing metal concentration. From infinite dilution to saturation, Λ_{La} and Λ_{Ce} rise from 800 and 450 to above 2000 and 1000 ohm^{-1} cm^2 equiv^{-1}, and Λ_{Nd} decreases from 130 to 40 ohm^{-1} cm^2 equiv^{-1}. The

[13] J. O'M. Bockris *et al.*, *Proc. Roy. Soc.* (*London*) **A255**, 558 (1960).

latter is in the range of ionic rather than electronic conductivities.

In the Na-NaX systems, the decrease in solute conductance was attributed to an equilibrium $2e^- + 2Na^+ \rightleftharpoons Na_2$, according to which mobile electrons are immobilized by being trapped in the covalent bonds of neutral sodium molecules. A similar mechanism is proposed for the Ca-$CaCl_2$ solutions, except that the electron-trapping species postulated is a single-bonded molecule ion $(Ca_2)^{2+}$ in equilibrium with mobile electrons and normal cations, Ca^{2+}, according to $2e^- + 2Ca^{2+} \rightleftharpoons (Ca_2)^{2+}$. For Sr-$SrCl_2$, the initial straight portion of the specific conductance curve corresponding to nearly constant Λ_{Sr} indicates a situation for $(Sr_2)^{2+}$ ions intermediate between that of the relatively stable Na_2 molecules in the Na-NaX system and the rather unstable K_2 molecules in K-KX.

The rapid increase in both specific and equivalent conductances in the Ce-$CeCl_3$ and La-$LaCl_3$ systems, the rate of which also increases, indicates a large proportion of conductance by electrons. Whether a lower-valent ionic species such as Ce^{2+} (or La^{2+}) exists in the molten solution or, in other words, what the extent of the equilibrium $Ce^{2+} \rightleftharpoons Ce^{3+} + e^-$ is, cannot be deduced from the present data. The electronic conductance could be entirely due to the presence of mobile electrons from the reaction $M \longrightarrow M^{3+} + 3e^-$. However, M^{2+} ions could be assumed to contribute electronic conductance at a rate increasing with concentration, due to overlap of their electronic orbitals, as discussed previously[9] for alkali-metal atoms or molecule ions.

For the Nd-$NdCl_3$ system, where the stability of the M^{2+} ion is demonstrated by the existence of an electrically insulating solid $NdCl_2$, the very small increase in conductivity on addition of metal indicates very little (or no) electronic conductance. An exchange of an electron between two adjacent valence states such as Nd^{2+} and Nd^{3+} may be thought of as a possible source of electronic conduction. If both $NdCl_2$ and $NdCl_3$ conduct only ionically, any nonionic fraction of the conductance of the solutions of $NdCl_2$ in $NdCl_3$ should show a maximum at or near 50 mole % $NdCl_2$. A plot of the difference between the total equivalent conductance of the solution and the additive ionic conductances of $NdCl_3$ and $NdCl_2$ shows such a maximum of approximately 10 $ohm^{-1}\ cm^2\ equiv^{-1}$ close to 50 mole % $NdCl_2$. It remains to be determined whether this can be taken as true evidence for the presence of an electron exchange mechanism in the conductance of these solutions, or whether the positive deviation from additive behavior could be ascribed to purely ionic conductance, as it must be in the mixtures of $MgCl_2$ with $BaCl_2$ or $CaCl_2$, where positive deviation was also observed.[14]

ELECTRICAL CONDUCTANCE OF SOLUTIONS OF SALTS IN LIQUID METALS: KF-K, KBr-K, KI-K

H. R. Bronstein A. S. Dworkin
M. A. Bredig

The high degree of solubility of the alkali halides KX, RbX, and CsX in their corresponding liquid metals,[15] with the attainment of complete miscibility in all proportions at or slightly above the melting temperatures of the salts, affords the opportunity to investigate the continuous change in the properties of these solutions from a molten salt to a molten metal. Previous measurements of the electrical conductivity in the salt-rich KX-K solutions[16] exhibited an increasing conductivity with increasing metal content. An apparatus essentially similar to that described earlier[16] was modified to permit measurements of the conductivity of the metal-rich mixtures, or solutions of salts in liquid metals. The electrode arrangement was modified to be used with a dc Mueller bridge for accurately measuring very low resistances in the absence of polarization effects. The electrode inserted in the cup of the synthetic sapphire capillary dip cell was a hollow stainless steel tube welded closed at the bottom. Running axially inside the tube was a ceramic-insulated wire welded to the inner bottom of the tube. The tube and inner wire are thus two leads. Penetrating into the bottom of the tank just below the capillary end of the dip cell was the junction of two other lead wires. This arrangement afforded the four terminal leads necessary to measure the

[14] R. W. Huber, E. V. Potter, and H. W. St. Clair, *Bureau of Mines Report of Investigations*, No. 4858 (1952).

[15] M. A. Bredig and J. W. Johnson, *J. Phys. Chem.* 64, 1899 (1960), and earlier papers.

[16] H. R. Bronstein and M. A. Bredig, *J. Am. Chem. Soc.* 80, 2077 (1958), and *Journal of Physical Chemistry* (August 1961).

resistance of the liquid in the capillary. The cell constant was determined as previously.[16] The accuracy of the method was checked by measuring the resistivity of liquid mercury.

Figure 8.10 shows the rapid decrease in the specific conductivity upon dissolution of salt in the liquid metal at 700°C for KF and KI and at 740°C for KBr. It also illustrates the manner in which the specific conductivity of the metal-rich solutions approaches the previous measurements of the salt-rich solutions.[16] Of significance is the observation that the resistivity ρ of the metal-rich solutions increases linearly with increasing salt concentration. With an average deviation of ±2.5%, the data can be expressed by the equation

$$\rho = aN + b \,, \qquad (1)$$

where N is the concentration of the salt in mole per cent. The parameter b equals the resistivity of the pure metal, 58 microhm-cm at 700°C, the test temperature for KF and KI, and 64 microhm-cm at 740°C, the temperature in the case of KBr. The slope a was a constant 4.20, 7.43, and 9.20 microhm-cm per mole per cent of KF (up to 12 mole %, the solubility limit), of KBr, and of KI (both up to 20 mole %) respectively.

Thus the resistivity of the metallic liquid seems to be essentially a linear function of the concentration of the electron-scattering centers introduced by the addition of the salt. As can be seen from Fig. 8.10 and the relative values of the slope a of Eq. (1), an increase in the size of the anion is reflected in a decrease in the specific conductivity or an increase in the resistivity.

The data for KI-K have been published.[17]

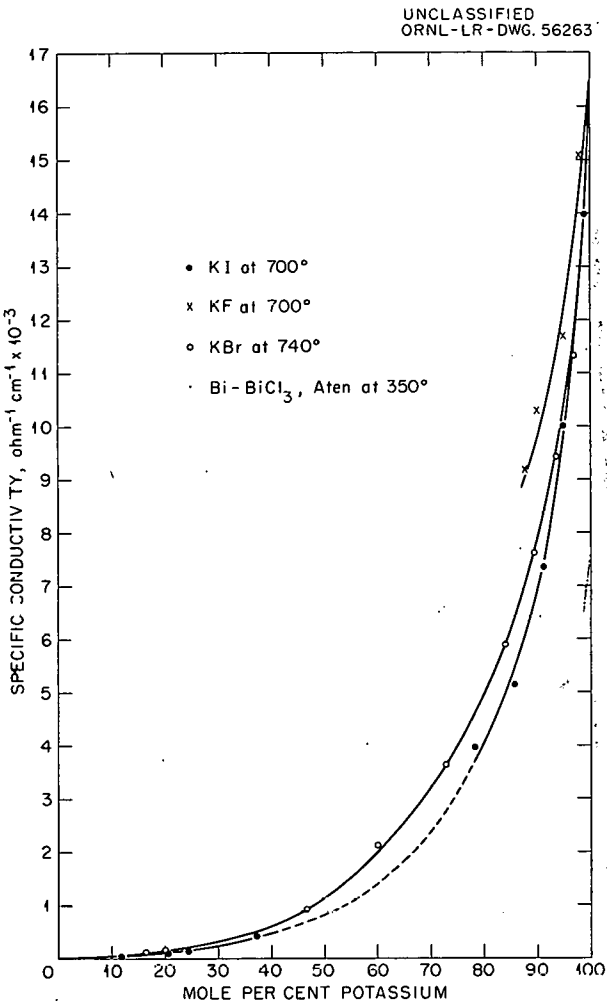

Fig. 8.10. Specific Conductivity of Solutions of Potassium Halides in Liquid Potassium Metal.

[17] H. R. Bronstein, A. S. Dworkin, and M. A. Bredig, *J. Chem. Phys.* 34, 1843 (1961).

9. CHEMICAL PHYSICS

MICROWAVE AND RADIO-FREQUENCY SPECTROSCOPY

Paramagnetic Resonance Study of Irradiated Single Crystals of Potassium Nitrate

Henry Zeldes

Paramagnetic resonance measurements were completed on the spectra of two species appearing in single crystals of gamma-irradiated KNO_3. For each species there are large N^{14} hyperfine splittings, and the data are accurately described by a spin-Hamiltonian with electron spin of $\frac{1}{2}$ of the form

$$\mathcal{H} = -\beta H \cdot g \cdot S - S \cdot A \cdot I,$$

where H is the applied field, S and I are spin operators respectively for the electron and for N^{14} in units of $\hbar$, β is the Bohr magneton, and g and A are symmetric tensors respectively for the spectroscopic splitting factor and the hyperfine coupling.

For one of the species, the g and A tensors are diagonal in the orthorhombic crystal axis system. The principal values of these tensors are:

$\lvert g_a \rvert = 2.0057$	$\lvert A_a \rvert / h = 89.0$ Mc
$\lvert g_b \rvert = 2.0057$	$\lvert A_b \rvert / h = 89.0$ Mc
$\lvert g_c \rvert = 2.0015$	$\lvert A_c \rvert / h = 177.6$ Mc

(h is Planck's constant, and the a, b, and c axes of the crystal unit cell are, respectively, 5.43 A, 9.17 A, and 6.45 A)

These parameters are close in value to those attributed[1] to NO_3^{2-} in x-irradiated crystals of KCl, KBr, and KI which had been doped with nitrate.

For the other species, the g and A tensors have different principal axes. For the hyperfine tensor the direction cosines between the principal axes, labeled 1, 2, and 3, and the crystal axes are:

	1	2	3
a	1	0	0
b	0	0.9483	−0.3177
c	0	0.3177	0.9483

and the principal values of A/h are:

$$\lvert A_1 \rvert / h = 176.3 \text{ Mc}$$
$$\lvert A_2 \rvert / h = 141.1 \text{ Mc}$$
$$\lvert A_3 \rvert / h = 136.6 \text{ Mc}$$

For the g tensor the direction cosines between the principal axes, labelled 1′, 2′, and 3′, and the crystal axes are:

	1′	2′	3′
a	1	0	0
b	0	0.9997	−0.0231
c	0	0.0231	0.9997

and the principal values of g are:

$$\lvert g_{1'} \rvert = 1.9996$$
$$\lvert g_{2'} \rvert = 1.9932$$
$$\lvert g_{3'} \rvert = 2.0055$$

This species is believed to be NO_2, although the parameters differ considerably from those of NO_2 in $NaNO_2$ (ref 2). A striking similarity is that in both crystals, KNO_3 and $NaNO_2$, the g and A tensors of NO_2 differ markedly from being axially symmetric. A significant finding is that the trace of each tensor is accurately the same in both lattices. This is strong evidence that the paramagnetic species is the same in the two lattices. It is also good evidence that the differences in the parameters are due to motional effects. Large amplitudes of torsional oscillations of NO_2 would modify the principal components of each tensor,

[1] Claude Jaccard, Argonne National Laboratory, private communication.

[2] H. Zeldes and R. Livingston, *Chem. Div. Ann. Progr. Rept. June 20, 1960*, ORNL-2983, p 77.

making the largest component smaller and the smallest component larger, but would not modify the trace. Comparison of the extreme principal parameters for each tensor in the two lattices indicates that NO_2 in KNO_3 is undergoing torsional oscillations of large amplitude at 77°K. The electronic structures of NO_2 in the two lattices are not seen to be different since the traces of g and of A are the same in the two lattices.

Paramagnetic Resonance Study of Gamma-Irradiated Single Crystals of Sodium Nitrite and of Sodium Nitrite Containing Silver Nitrite

Henry Zeldes Ralph Livingston

Paramagnetic resonance measurements of gamma-irradiated single crystals of $NaNO_2$ indicated the spectrum is the same as that previously reported[3] in irradiated single crystals of $NaNO_2$ containing $AgNO_2$. The spectra are much weaker in crystals not containing $AgNO_2$. It is believed that the spectrum arises from NO_2. From the spectrum and the known symmetry of $NaNO_2$, it was determined that in both cases NO_2 occupies a position of *mm* symmetry in the $NaNO_2$ lattice. The hyperfine parameters are in accord with a molecular orbital for the unpaired electron of NO_2 which has σ-symmetry and comprises the $2s$ orbital of nitrogen, the $2p$ orbital of nitrogen directed along the intersection of the two mirror planes, and orbitals of oxygen. These findings have been prepared for publication in the *Journal of Chemical Physics.*

A Paramagnetic Resonance Study of Irradiated Potassium Chlorate

R. W. Holmberg

A paramagnetic resonance study of the radiation decomposition of single crystals of $KClO_3$ was undertaken. A very complex spectrum is seen when the crystals are gamma irradiated and observed in a paramagnetic resonance spectrometer at 77°K. In addition to lines from free radicals with no detectable hyperfine splittings, at least three non-equivalent species exhibiting chlorine hyperfine structure have been seen. Two of these show large hyperfine couplings characteristic of a single chlorine; the third most probably contains two chlorines.

[3]H. Zeldes and R. Livingston, *Chem. Div. Ann. Progr. Rept. June 20, 1960*, ORNL-2983, p 77.

Detailed measurements are now being made in an attempt to characterize the more prominent of the one-chlorine centers. Although the measurements are not yet complete, approximate values of the hyperfine coupling parameters strongly suggest that this species is the stable free radical ClO_2 trapped at a ClO_3^- ion position in the lattice.

STUDIES OF ANOMALOUS NEUTRON SCATTERING

S. W. Peterson H. G. Smith

Studies of anomalous scattering of neutrons from CdI_2 single crystals were continued over an energy range including the cadmium resonance peak at 0.178 ev. The complete $(h0l)$ zone of reflections was measured at one wavelength (1.075 A) in order to permit a structure refinement which would simultaneously give a precise measurement of the complex scattering amplitude of cadmium at this wavelength. Selected reflections were also measured at several other wavelengths. In addition a single crystal of $Cd^{113}I_2$ was grown, and Bragg intensities were measured for several reflections at 1.075 A.

The results of the least-squares refinement of the $(h0l)$ zone data are listed in Table 9.1. The ideal values of the iodine z parameters for a close-packed arrangement are $\frac{3}{8}$ and $\frac{5}{8}$. The close experimental agreement with those values is some indication of the accuracy of the refinement. The cadmium scattering amplitude determined is in remarkably good agreement with that calculated with the aid of the Breit-Wigner formulation for a single resonance.

Analysis of the measured reflections at the several wavelengths resulted in the imaginary components of the scattering amplitude for cadmium which are shown in Fig. 9.1, given for the Cd^{113}

Table 9.1. Least-Squares Analysis of CdI_2

$f_{Cd} = (0.38 \pm 0.01) + (0.120 \pm 0.007)i$

$f_I = 0.52$ (fixed)

	x	y	z	$4B_{11}/b_1^2$	$4B_{33}/b_3^2$
Cd	$\frac{1}{3}$	$\frac{2}{3}$	0	2.01 ± 0.36	3.51 ± 0.21
I_1	$\frac{1}{3}$	$\frac{2}{3}$	0.376 ± 0.001	1.65 ± 0.23	1.70 ± 0.32
I_2	0	0	0.625 ± 0.001	1.80 ± 0.15	1.80 ± 0.35

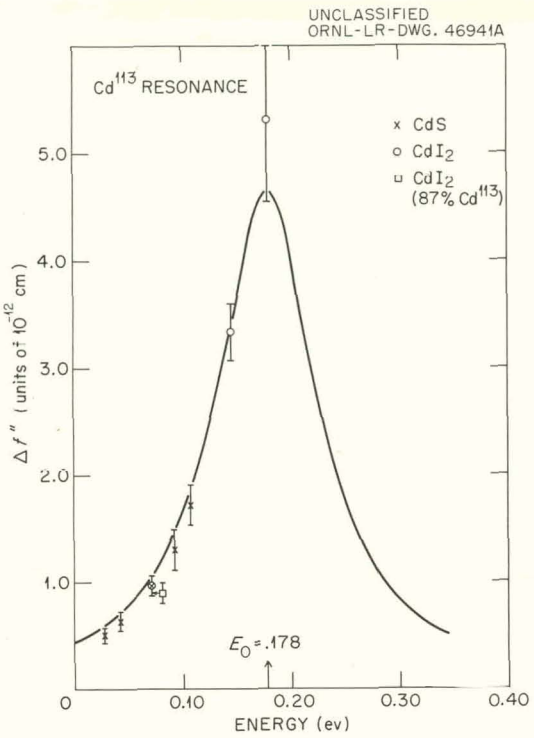

Fig. 9.1. Energy Dependence of Imaginary Component of the Amplitude of Neutron Scattering from Cd^{113}.

isotope as a function of neutron energy. The scattering amplitude is expressed in the form $f_{Cd^{113}} = f_0 + \Delta f' + i\Delta f''$. The smooth curve in the figure represents the Breit-Wigner theory prediction, making use of the neutron and gamma widths determined for cadmium by Brockhouse.[4] The accuracy of each of the plotted points, which include data from both CdI_2 and CdS crystals, is indicated by the height of the vertical line. In Fig. 9.2 the real components are plotted as a function of energy. The smooth curve is again the theoretical curve based on application of the Breit-Wigner formalism. Since the real components are determined with less certainty than the imaginary ones, only values obtained as a result of least-squares analyses are used.

Measurements made on CdI_2 crystals enriched in Cd^{113}, although difficult to make because of extremely high absorption, were analyzed primarily to give the scattering amplitude. The resulting value for the 87.3% Cd^{113}-enriched sample was

[4]B. N. Brockhouse, *Can. J. Phys.* 31, 432 (1953).

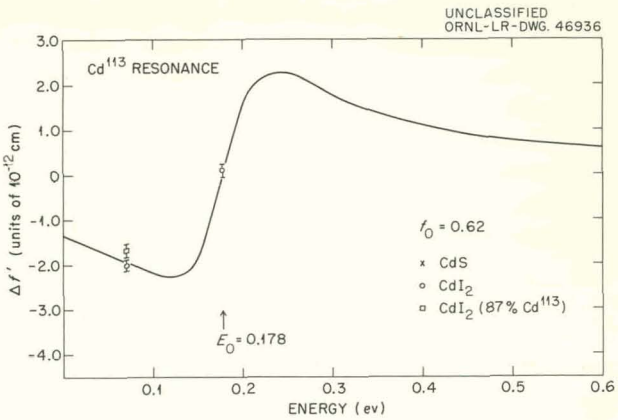

Fig. 9.2. Energy Dependence of Real Resonance Component of the Amplitude of Neutron Scattering from Cd^{113}.

$f = -0.80 + 0.75i$. This value is interesting in that the resonance contribution to the real component is large enough to outweigh the positive potential scattering term and give a negative real term contrary to the case with ordinary cadmium.

The present results thus strongly confirm the existence of anomalous coherent neutron scattering effects, give substantial support to the Breit-Wigner single level formulations, and indicate that the anomalous scattering terms may be calculated with considerable confidence from certain parameters.

PHOTOGRAPHIC TECHNIQUES IN NEUTRON DIFFRACTION

H. G. Smith

The recording of neutron diffraction patterns by photographic techniques has not previously received wide application in crystal structure analysis for two main reasons: (1) low intensity of neutron beams and (2) inefficient photographic methods. With the advent of appreciable increases in neutron flux from present higher-flux reactors and more efficient neutron phosphors (ZnS-B^{10} of Sun *et al.*,[5] and more recently ZnS-Li^6 of Stedman[6]), plus the use of high-speed Polaroid film, photographic methods in thermal-neutron detection are now practical and useful.

[5]K. H. Sun, P. R. Malmberg, and F. A. Pecjak, *Nucleonics* 14, 46 (1956).

[6]R. Stedman, *Rev. Sci. Instr.* 31, 1156 (1960).

The present report describes a device assembled to record neutron diffraction patterns of rotating single crystals and powder specimens, and also to investigate the uniformity of the monochromatic beam from the monochromator.

A Polaroid film holder (type 500) that uses individual 4- × 5-in. film packets was used in conjunction with a neutron-sensitive phosphor, prepared by mixing equal quantities of ZnS and Li^6F and suspending the mixture in a viscous Lucite-acetone mixture. The resulting mixture was poured in a dish, allowed to settle, and most of the excess liquid was syphoned off. When the acetone evaporated, the remaining Lucite solidified and acted as a binder for the ZnS-Li^6F. The result was an essentially flat disk 1 mm thick and about 100 mm in diameter. The disk was further flattened by compressing it between two flat plates at about 250°C.

The phosphor was attached to the holder with light-tight flexible materials and was pressed against the film during exposure. The neutrons traveled through the back of the film holder and film and impinged on the front surface of the phosphor. To facilitate removal of the film packet it is necessary to pull the phosphor slightly away from the film packet. Photographs that previously required several hours of exposure can now be taken in a few minutes. Several neutron photographs taken by the author are shown in Fig. 9.3.

X-ray diffraction photographs have also been obtained by replacing the neutron-sensitive phosphor with a high-speed x-ray phosphor. The present method is about twice as fast as the conventional x-ray methods, and the development time is only 10 sec.

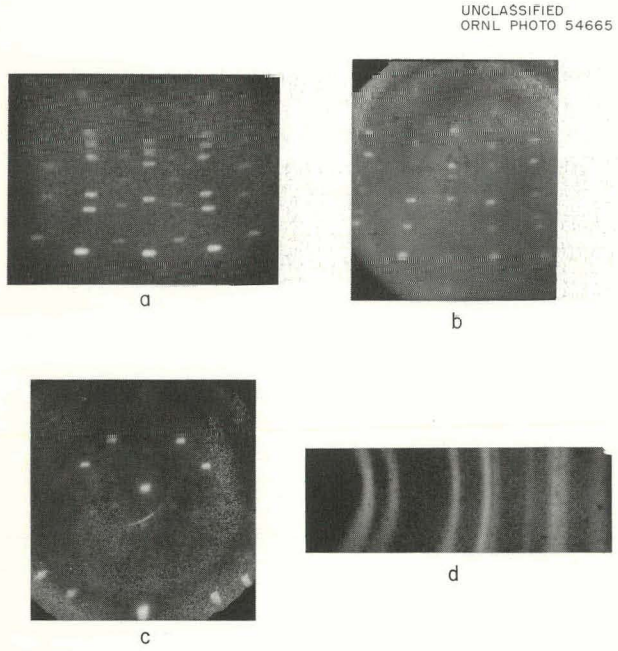

Fig. 9.3. Neutron Diffraction Photographs. *(a)* NaCl, 60° rotation, 30-min exposure; *(b)* $Li_2SO_4 \cdot H_2O$, 30° rotation, 2-hr exposure; *(c)* NaCl, Laue photograph, 2-min exposure; *(d)* Ni powder pattern, 7-min exposure. Photographs *(a)* and *(d)* were made with dry phosphor; *(b)* and *(c)* were made with Lucite phosphor.

NEUTRON DIFFRACTION STUDY OF $Li_2SO_4 \cdot H_2O$

H. G. Smith S. W. Peterson
H. A. Levy

There is disagreement in the literature concerning the positions of the hydrogen atoms and the nature of the hydrogen bonding in $Li_2SO_4 \cdot H_2O$, both in the x-ray investigations[7,8] and in the nuclear magnetic resonance studies.[9,10]

Ketudat and Pound[11] studied the quadrupole splitting of the deuteron resonance in $Li_2SO_4 \cdot D_2O$ and concluded that the deuterium positions are as postulated by Larson and Helmholz.[8] Recently McGrath, Silvidi, and Carroll[12] made an extensive NMR study on single crystals of $Li_2SO_4 \cdot H_2O$ in order to study the details of the Pake curves. Although their results for the proton-proton vectors are in agreement with the positions of the hydrogen atoms proposed by Larson and Helmholz, they were not able to give a quantitative explanation of the Pake curves. It was decided that a determination of the hydrogen positions by the more direct method of neutron diffraction would be very useful and interesting.

[7] G. E. Ziegler, *Z. Krist.* **89**, 456 (1934).

[8] A. C. Larson and L. Helmholz, *J. Chem. Phys.* **22**, 2049 (1954).

[9] M. Soutif and Y. Ayant, *J. chim. phys.* **50**, C107 (1953).

[10] E. Hirahara and M. Murakami, *J. Phys. Soc. Japan* **11**, 239 (1956).

[11] S. Ketudat and R. V. Pound, *J. Chem. Phys.* **26**, 708 (1957).

[12] J. W. McGrath, A. A. Silvidi, and J. C. Carroll, *J. Chem. Phys.* **31**, 1444 (1959).

Neutron diffraction intensities were obtained for about 300 ($h0l$), ($0kl$), and ($hk0$) reflections, although the ($hk0$) data have not yet been analyzed.

Nuclear density maps were calculated, with the phases determined by the sulfur and oxygen atom parameters of Larson and Helmholz[8] and Larson.[13] The peaks of negative density which represent the lithium and hydrogen atoms were clearly discernible. The hydrogen atoms were then located more precisely by difference maps.

The position parameters of all the atoms and most of the thermal parameters were refined by an anisotropic least-squares analysis. Only the position parameters are listed in Table 9.2, for a complete determination of the anisotropic temperature factors will soon be made. A few of the prominent bond distances and bond angles are given in Table 9.3. They have not been corrected for thermal motion. The R factor (for F^2) based on 240 ($h0l$) and ($0kl$) reflections is 7.1%.

A perspective view of the atomic arrangement in the crystal is shown in Fig. 9.4. The long O–H··O distances (2.86 A and 2.95 A) and their large deviations from linearity (O–H–O′ = 151° as compared to 180° for a linear hydrogen bond) suggest that the water molecule is only weakly hydrogen-bonded to its neighbors. The coordination of the two nonequivalent types of lithium atoms shown by dotted lines indicates that they play a dominant role in holding the crystal together.

[13]A. C. Larson, private communication.

The determination of the hydrogen positions does not reveal any need for a drastic reinterpretation of the NMR data of McGrath *et al.*,[12] for his proton-proton vectors are essentially in agreement with the present study. However, because of the neighboring hydrogen and lithium atoms (2.38 A–2.64 A), it would appear necessary to include their effects in giving a quantitative explanation of the Pake curves.

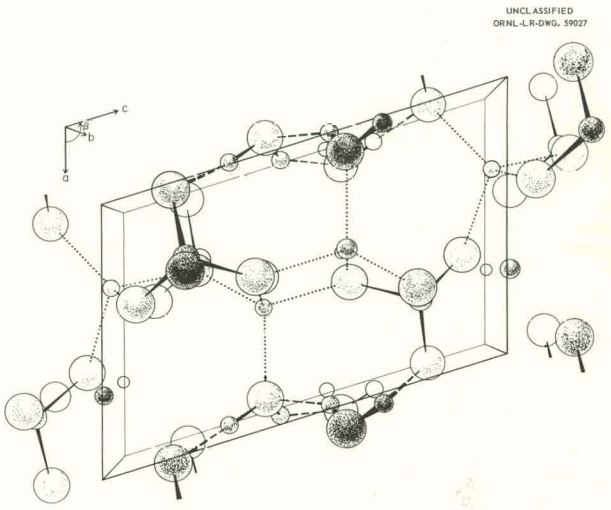

Fig. 9.4. Perspective Drawing of the Unit Cell of $Li_2SO_4 \cdot H_2O$, Looking Along the b Axis.

Table 9.2. Position Parameters for $Li_2SO_4 \cdot H_2O$

	x	y	z
Li_1	0.303 ±0.001	0.498 ±0.004	0.993 ±0.001
Li_2	0.560 ±0.002	0.485 ±0.004	0.394 ±0.001
S	0.288 ±0.003	0	0.208 ±0.001
O_1	0.0221 ±0.0004	0.071 ±0.003	0.1704 ±0.0003
O_2	0.4347 ±0.0005	0.114 ±0.003	0.3784 ±0.0002
O_3	0.3999 ±0.0005	0.124 ±0.003	0.0785 ±0.0003
O_4	0.3330 ±0.0017	0.702 ±0.002	0.2104 ±0.0007
O_5	0.9123 ±0.0007	0.470 ±0.003	0.3967 ±0.0005
H_1	0.9668 ±0.0014	0.393 ±0.007	0.3082 ±0.0010
H_2	0.0060 ±0.0027	0.638 ±0.009	0.4379 ±0.0022

Table 9.3. Bond Distances and Bond Angles

Bond	Bond Distance (A)	Angle	Value (deg)
$S-O_1$	1.43 ± 0.02	$H_1-O_5-H_2$	110.4 ± 2.1
$S-O_2$	1.49 ± 0.01	$O_5-H_2-O_5'$	150.9 ± 1.1
$S-O_3$	1.50 ± 0.01	$O_5-H_1-O_1$	151.8 ± 2.8
$S-O_4$	1.47 ± 0.01	$Li_2-O_5-H_1$	123.7 ± 0.8
O_5-H_1	0.94 ± 0.02	$Li_2-O_5-H_2$	113.4 ± 1.3
O_5-H_2	0.97 ± 0.04	$O_5-H_2-O_2$	120.0 ± 2.3
$O_5'-H_2$	2.07 ± 0.03	O_1-S-O_2	109.8 ± 0.9
O_1-H_1	2.00 ± 0.03	O_1-S-O_3	110.6 ± 0.8
O_5-O_1	2.86 ± 0.01	O_1-S-O_4	113.2 ± 1.2
O_5-O_5'	2.95 ± 0.01	O_2-S-O_3	107.0 ± 1.0
O_5-O_2	3.09 ± 0.01	O_2-S-O_4	108.3 ± 1.0
H_1-H_2	1.56 ± 0.04	O_3-S-O_4	107.7 ± 1.1
H_2-H_2'	2.64 ± 0.01		
$H_1'-H_2$	2.38 ± 0.04		
Li_2-H_1	2.56 ± 0.01		
Li_2-H_2	2.46 ± 0.02		
Li_1-O_3	1.96 ± 0.01		
Li_1-O_3	1.98 ± 0.01		
Li_1-O_4	1.99 ± 0.01		
Li_1-O_1	1.91 ± 0.01		
Li_2-O_5	1.92 ± 0.01		
Li_2-O_2	1.92 ± 0.01		
Li_2-O_4	1.95 ± 0.01		
Li_2-O_2'	1.95 ± 0.01		

A SINGLE CRYSTAL NEUTRON DIFFRACTION STUDY OF HYDRAZINE

W. R. Busing Marcello Zocchi[14]
H. A. Levy

A single crystal neutron diffraction study of hydrazine, N_2H_4, is in progress. The projection based on measurements of the $h0l$ reflections has been described previously.[15] The intensities of 62 reflections of the type lkl, $lk\bar{l}$, $2l\ k\ l$, and $2l\ k\ \bar{l}$ have now been measured in an effort to determine the complete structure.

Eight possible trial structures are consistent with the $h0l$ projection since each hydrogen atom may have a y parameter either greater or less than that of the nitrogen to which it is bonded. Unfortunately, all eight of these structures are approximately homometric, because they have almost the same N-N and N-H vectors. Since the scattering

[14]Guest scientist from Comitato Nazionale per l'Energia Nucleare, Rome, Italy.

[15]W. R. Busing, M. Zocchi, and H. A. Levy, *Chem. Div. Ann. Progr. Rept. June 20, 1960*, ORNL-2983, p 75.

factors for N and H are 0.94 and −0.378, respectively, the H-H vectors do not make an important contribution to the intensity. Least squares and Fourier methods have failed to distinguish unequivocally among the eight models. At present a structure in which the molecule has an approximately eclipsed configuration appears to be the most reasonable on the basis of R factor and symmetry of the molecule. Further work using N_2D_4 is planned.

THE CRYSTAL STRUCTURE OF HYDRAZINE HYDRATE, $N_2H_4 \cdot H_2O$

Marcello Zocchi[16] R. D. Ellison
W. R. Busing H. A. Levy

In the course of a study of the configuration of the N_2H_4 molecule in the solid state, the crystal structure of $N_2H_4 \cdot H_2O$ has been investigated with x rays. Crystals (mp about −50°C) were grown and kept at about 10° below their melting point for the period of the experiment by using an apparatus similar to that described by Abrahams *et al.*[17]

Zero and first-layer precession photographs were taken, using Mo$K\alpha$ radiation, and the intensities of ten reflections were estimated visually by comparison of several films with different exposures.

The cell dimension of the face-centered cubic crystal is $a_0 = 6.75 \pm 0.01$ A. With 4 $N_2H_4 \cdot H_2O$ units per cell, the calculated density is $\rho_c = 1.07_5$ g/cm^3, in reasonable agreement with the density of 1.03 g/cm^3 for the liquid at 21°C.[18] The space group is $Fm3m$, and the structure appears to be that of NaCl with freely rotating or disordered H_2O and N_2H_4 molecules replacing Na^+ and Cl^- ions, respectively. Further refinement is in progress.

COHERENT AND TOTAL THERMAL NEUTRON CROSS SECTIONS OF RUBIDIUM AND CHLORINE ISOTOPES

P. A. Agron H. A. Levy

An interest in the thermal cross sections of rubidium and chlorine isotopes stems from the molten-state studies of rubidium chloride in progress here.

The neutron diffraction patterns of powdered samples of RbCl and enriched $Rb^{87}Cl$ (98.25% Rb^{87}) were measured, using monochromatic neutrons with $\lambda = 1.075$ A. Unnormalized squared structure amplitudes derived from integrated intensity measurements of the even (hkl) reflections as a function of $\sin^2\theta$ are given in Table 9.4. Normalizing with a powdered nickel sample ($f_{coh} = 1.025$ fermi units) and utilizing the coherent scattering amplitude reported for normal chlorine ($f_{coh} = 0.98$ fermi unit), one obtains $f_{coh} = 0.71 \pm 0.03$ and $f_{coh} = 0.69 \pm 0.03$ fermi unit for normal rubidium and Rb^{87}, respectively. The former is significantly higher than an earlier reported value of $f_{coh} = 0.55$ fermi unit. The only odd index reflection observable, (111), was consistent with the foregoing value.

Reflections from a single crystal of normal RbCl were examined as a further check of the coherent scattering amplitude of rubidium. The integrated intensities for both even and odd (hkl) reflections about the [110] zone were measured. Table 9.5 gives the unnormalized squared structure amplitudes as a function of $\sin^2\theta$. Upon extrapolating the values for reflections of even and odd index sums to zero scattering angle and again assuming the reported value for the scattering amplitude for chlorine, one obtains $f_{coh} = 0.69 \pm 0.03$ fermi unit for rubidium. This agrees well with the value obtained from the powder measurement. Thus it appears that there is no significant difference in the coherent scattering amplitude for Rb^{85} and Rb^{87}. The corresponding coherent scattering cross sections are 6.3 ± 0.3 and 6.0 ± 0.3 barns.

Total cross sections were derived from transmission measurements of 1.114-A neutrons made on powdered samples of normal RbCl and on several preparations isotopically enriched in Rb^{87}, Cl^{35}, and Cl^{37}. Cadmium differences were applied to each measurement. Table 9.6 lists the observed total cross sections (σ_T) at an energy $E = 0.066$ ev. Using $\sigma_T = 37.0$ barns for normal chlorine at this energy, and assuming that the total cross sections are additive in the compound, one obtains the following consistent set of total cross sections

[16] Guest scientist from Comitato Nazionale per l'Energia Nucleare, Rome, Italy.

[17] S. C. Abrahams *et al.*, *Rev. Sci. Instr.* 21, 396 (1950).

[18] T. Curtius and H. Schulz, *J. prakt. Chem.* 42(2), 521 (1890); *Handbook of Chemistry and Physics*, 42nd ed., p 580, 1960-61.

Table 9.4. Coherent Scattering of Powdered Rubidium Chloride

hkl	$\sin^2\theta$	$Rb^{87}Cl$ KF^2	Standard Deviation (%)	N-RbCl $K'F^2$	Standard Deviation (%)
200	0.0267	45.36	0.82	34.03	0.70
220	0.0534	40.69	0.85	30.94	0.71
222	0.0801	34.29	1.37	26.71	0.38
400	0.1068	36.33	2.14	25.95	0.62
420	0.1334	29.77	0.83	23.53	0.25
422	0.1601	26.37	0.90	20.78	0.89
440	0.2135	24.02	2.31		
600,442	0.2402	21.58	1.06	17.09	0.36
620	0.2669	19.75	0.57	14.92	0.65
622	0.2936	16.48	0.63	14.18	0.76
444	0.3203	17.31	2.23	11.62	1.96
640	0.3470	15.01	0.74	10.60	0.84

Table 9.5. Coherent Scattering of a Single Crystal of Rubidium Chloride (Normal)

hkl	$\sin^2\theta$	$K''F^2$	Standard Deviation (%)
002	0.0267	31,543	0.34
220	0.0534	31,630	0.41
222	0.0801	27,541	0.49
004	0.1068	23,633	0.56
440	0.2135	17,557	0.83
006	0.2402	15,634	0.80
444	0.3203	11,541	1.1
008	0.4271	8,600	1.2
660	0.4804	5,938	1.8
00, 10	0.6673	3,930	1.9
666	0.7203	2,365	3.1
111	0.0200	1,060	3.1
113	0.0734	764	4.8
331	0.1268	694	6.6
115	0.1802	461	5.6
333	0.1802	396	11.5
335	0.2870	252	4.3
337	0.4470	159	10.7
337	0.4470	105	38.0

(in barns) for the individual isotopes and normal element: Rb(normal), 7.8; Rb^{87}, 8.7; Rb^{85}, 7.45 (by difference); Cl^{35}, 47.45; Cl^{37}, 3.9.

Table 9.6. Total Cross Sections of Normal and Enriched RbCl at $\lambda = 1.114$ A ($E = 0.066$ ev)

Sample	Isotopic Enrichment (%)	σ_T (barns)
N-RbCl	Normal	44.8
$Rb^{87}Cl$*	98.25	45.7
$RbCl^{35}$*	96.8	55.25
$RbCl^{37}$*	96.37	11.7

*Enriched samples obtained from ORNL Isotopes Division.

CELL PARAMETERS AND SPACE GROUPS OF POTASSIUM, RUBIDIUM, AND CESIUM ACID CHLOROMALEATES

R. D. Ellison H. A. Levy
S. W. Peterson

The cell parameters and space groups of the potassium, rubidium, and cesium acid chloromaleates grown from aqueous solution were determined from single crystal diffraction data taken on the precession camera. The values of the cell parameters were refined by least-squares methods, using powder diffraction data taken in a Debye-Scherrer camera.

Potassium acid chloromaleate was found to be orthorhombic with space group *Pbcn* and cell dimensions $a = 15.815 \pm 0.015$ A, $b = 10.928 \pm 0.006$

A, $c = 7.707 \pm 0.005$ A. The density calculated on the basis of this cell and assuming 8 molecules per unit cell is 1.881 g/cc; the pycnometrically measured density is 1.868 g/cc.

The space group of the two isomorphous monoclinic salts, rubidium and cesium acid chloromaleate, was not uniquely determined. Of the three space groups Im, $I2$, and $I\frac{2}{m}$ that are consistent with the systematic absences noted on the precession camera pictures, the last is considered unlikely because it requires that two chloromaleate ions lie in mirror planes in the approximately 5- by 8-A face of the cell. The cell parameters are listed in Table 9.7. The more usual C-centered cell is included, but the body-centered cell with β close to 90° is retained for convenience. The calculated densities shown are based on 4 molecules/cell; the observed densities were measured pycnometrically.

Table 9.7. Crystallographic Data for Cesium and Rubidium Acid Chloromaleates

The errors listed are least-squares standard deviations

	Rubidium		Cesium	
	Body-Centered Cell	C-Centered Cell	Body-Centered Cell	C-Centered Cell
a	8.112 ± 0.003 A	9.61 A	8.352 ± 0.007 A	9.87 A
b	16.638 ± 0.011 A	16.64 A	17.325 ± 0.014 A	17.33 A
c	5.090 ± 0.003 A	5.09 A	5.152 ± 0.004 A	5.15 A
β	90°28′ ⊥ 4′	122°26′	90°45′ ± 5′	122°12′
Calculated density	2.272 g/cc		2.516 g/cc	
Observed density	2.246		2.515	

THE STRUCTURE OF CALCIUM CARBIDE AT HIGH TEMPERATURE

M. D. Danford M. A. Bredig
H. A. Levy

Two of the four crystal modifications of calcium carbide,[19] namely the tetragonal, low-temperature and the cubic, high-temperature forms, have structures which are prototypes for a number of dicarbides, among them the metallic uranium dicarbide and rare earth dicarbides.[20,21] While the tetragonal structure is known in detail,[20] the present investigation is the first attempt to elucidate the structure of the cubic form stable only above 450°C. The compound is of particular interest also because of the speed of the transformation, which is instantaneous at a temperature almost 2000°C below the melting point, indicating an unusual mobility of the component ions.

The x-ray diffractometer for liquids,[22] which has been described previously, was used for obtaining diffraction patterns of the powder at 477°C. The sample of CaC_2 was prepared in a dry box, with the particle size being kept to less than 44 μ by screening. Special precautions were taken to ensure against preferred orientation in loading the sample, which was enclosed in a vacuum-tight beryllium cup.

The diffraction pattern is similar to that which would be obtained from a NaCl type of structure, with observed reflections having indices all odd or all even. The unit cell size obtained from the positions of Bragg reflections is 5.88 ± 0.01 A. Because the sample was contaminated by a small amount of CaO (about 5%), a sample of pure CaO was prepared, and the intensities of nine Bragg reflections were measured at 477°C.

A least-squares refinement of these intensities resulted in temperature factor coefficients $2B = 2.08 \pm 0.13$ and 2.34 ± 0.12 for calcium and oxygen,

[19] M. A. Bredig, *J. Phys. Chem.* **46**, 801 (1942).

[20] M. A. Bredig, *Phys. Div. Quart. Progr. Rept. Sept. 20, 1950*, ORNL-865, p 81; *Chem. Div. Quart. Progr. Rept. Dec. 31, 1951*, ORNL-1260, p 105.

[21] M. Atoji and R. C. Medrud, *J. Chem. Phys.* **31**, 332 (1959).

[22] P. C. Sharrah *et al.*, *Chem. Div. Semiann. Progr. Rept. June 20, 1955*, ORNL-1940, p 39.

respectively, with an agreement factor of 1.7%. The unit cell size at 477°C is 4.84 ± 0.01 A. The measured CaO intensities were used to correct the CaC_2 pattern for contamination by CaO.

Twelve Bragg reflections from the CaC_2 pattern were analyzed in terms of five possible structures, four of them disordered. These comprised the ordered pyrite structure, a model with a freely rotating C_2^{2-} ion, a disordered pyrite structure in which the C_2^{2-} ion assumes four possible orientations along the cube diagonals (3*m* symmetry), a model in which the C_2^{2-} ion assumes three possible orientations parallel to the cube edge (4*mm* symmetry), and a model in which the C_2^{2-} ion assumes six possible orientations parallel to the cube-face diagonals (*mm* symmetry). In each case, the center of the randomly oriented C_2^{2-} ion occupies one set of NaCl-like positions of space group $Fm3m$. The ordered pyrite model is considered unsatisfactory because non-face-centered reflections, which are calculated to have observable intensities, were unobserved. All the other models gave equally good agreement with the observed intensities, although the separation of opposite carbon sites (apparent C-C distance) obtained from the least-squares refinements were different for each model: the models for free rotation, 3*m* symmetry, 4*mm* symmetry, and *mm* symmetry gave 1.06 ± 0.20 A, 0.96 ± 0.48 A, 0.98 ± 0.27 A, and 1.34 ± 0.10 A, respectively, none of them in agreement with the literature value[21] of 1.20 A. For all models, the temperature-factor coefficient, 2*B*, was approximately 12.5 for calcium, with a somewhat larger but rather poorly defined coefficient for carbon. Although measurements by neutron diffraction showed only four reflections, they are considered significant as they gave no evidence for non-face-centered reflections which would result from an ordered pyrite structure.

In a different approach to the problem, the total scattering was subjected to a radial distribution analysis, after the measurement of intensities by x-ray diffraction had been extended to $\theta = 65°$. The background scattering in the crystal powder pattern exhibits a very pronounced sinusoidal character, typical of scattering from liquids, where only short range structure exists.

The radial distribution curve contained well-defined peaks at 4.18 A, 6.01 A, and 7.15 A, corresponding to the distances in the face-centered lattice. In addition, a small peak appears at 1.40 A and a broad, unresolved "doublet" at 2.65 to 3.44 A. The former suggests that the C-C distance has the unexpectedly large value of 1.40 A, apparently confirming the value obtained from refinement of the Bragg intensities according to the *mm* model. The "doublet" may be interpreted as the shortest Ca-C interaction. According to the *mm* model with the C-C distance at 1.34 A, it should consist of three equal components at 2.51 A, 3.02 A, and 3.45 A; the observed curve is resolvable into three roughly equal components at 2.57 A, 3.00 A, and 3.43 A. An equally satisfactory interpretation, however, can be made in terms of the 3*m* model (again with the C-C distance at 1.34 A), but the 4*mm* and free-rotation models seem incompatible with the observed curve.

Thus, the evidence for the nature of the high-temperature CaC_2 structure must be considered at present to be inconclusive. Work on the problem is continuing.

CALORIMETRY

Thermodynamic Properties of Potassium Hexachlororhenate(IV)

R. H. Busey R. B. Bevan, Jr.
R. A. Gilbert

This report is a summary of an article on the low-temperature heat capacity of K_2ReCl_6, which is in preparation for publication.

Heat capacity measurements reported previously[23] on K_2ReCl_6 from 15 to 300°K revealed the existence of three cooperative transitions at 76, 103, and 111°K. Further heat capacity measurements made this year below 15°K gave the results presented in Fig. 9.5. The cooperative transition shown is the transition to an antiferromagnetic state below 11.9°K.[24]

An estimate of the entropy associated with each of the anomalies at 76, 103, and 111°K has been made by utilizing the entropy of the diamagnetic compound K_2PtCl_6 (ref 25), which is isomorphous with the rhenium compound. The excess entropy

[23] R. H. Busey, H. H. Dearman, and Q. V. Larson, *Chem. Div. Ann. Progr. Rept. June 20, 1956*, ORNL-2159, p 11.

[24] R. H. Busey and E. Sonder, *Journal of Chemical Physics* (in press).

[25] L. V. Coulter, K. S. Pitzer, and W. M. Latimer, *J. Am. Chem. Soc.* 62, 2845 (1940).

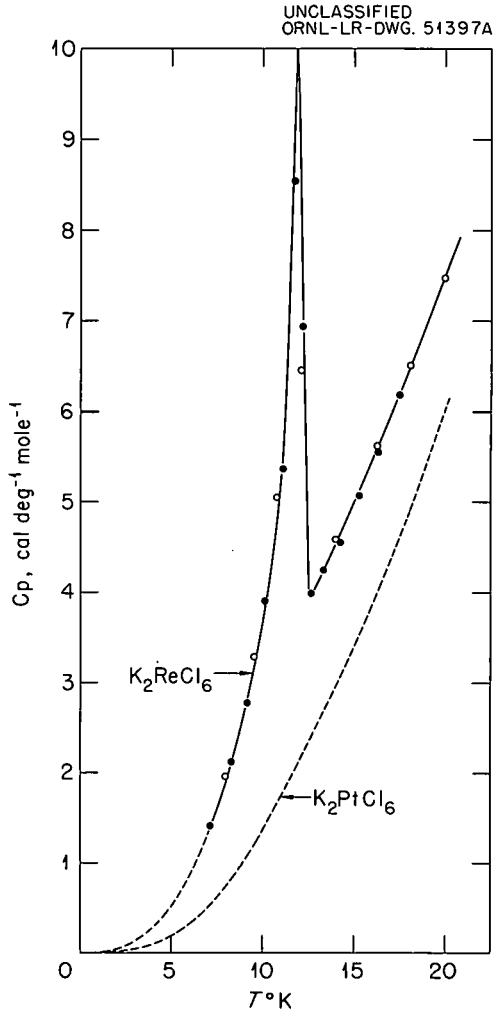

Fig. 9.5. Cooperative Transition of K_2ReCl_6 with Heat-Capacity Maximum at 11.9°K. The transition is from an antiferromagnetic, ordered state below 11.9°K to the paramagnetic state above this temperature. Two series of measurements are presented.

of K_2ReCl_6 above that of K_2PtCl_6 is 9.06 cal deg^{-1} $mole^{-1}$ at 300°K. This difference becomes 6.31 cal deg^{-1} $mole^{-1}$ when the magnetic entropy of R ln 4 is subtracted. A portion of this remaining entropy difference is accounted for by a low-energy vibrational state within the $ReCl_6^{2-}$ ion. The visible spectrum of $ReCl_6^{2-}$ in 1 M HCl shows vibrational fine structure with an average energy separation of 150 cm^{-1} superimposed upon the ligand field bands. This also represents the energy separation in the electronic ground state, since the electronic ground state and the excited electronic states exhibiting the vibrational fine structure all have the same electronic structure, namely, a $d\epsilon^3$ configuration in terms of crystal field theory. The low-energy vibrational state of 150 cm^{-1} gives rise to 2.68 cal deg^{-1} $mole^{-1}$ vibrational entropy at 300°K, assuming a simple harmonic oscillator. This leaves an entropy of 3.63 cal deg^{-1} $mole^{-1}$ as an estimate of the entropy associated with the anomalies at 76, 103, and 111°K. If one assumes equal division of this entropy between the three transitions, there results 1.21 cal deg^{-1} $mole^{-1}$ for each anomaly, a value reasonably close to R ln 2 = 1.38 cal deg^{-1} $mole^{-1}$, considering the uncertainties involved in the lattice and vibrational entropy estimates. An entropy of R ln 2 associated with each of the transitions is strongly suggestive that these are order-disorder types of cooperative transitions. The interpretation of these transitions requires more knowledge of any crystal symmetry change and/or change in symmetry of the chloride ions surrounding the Re^{4+}.

The revised entropy of K_2ReCl_6 at 298.15°K is 88.84 ± 0.18 cal deg^{-1} $mole^{-1}$. This entropy, together with the heat of solution and solubility determinations,[26] and a good estimate of the mean molal activity coefficient ($\gamma_\pm$ = 0.36 ± 0.01) of K_2ReCl_6 in a saturated solution at 25°C, permits the calculation of the entropy of the $ReCl_6^{2-}(aq)$. The estimate of $\gamma_\pm$ is based upon considerations of the temperature coefficient of the solubility and the heat of solution. At 25°C the entropy of $ReCl_6^{2-}(aq)$ is 59.8 ± 0.2 cal deg^{-1} $mole^{-1}$, and the entropy of formation is −140.2 cal deg^{-1} $mole^{-1}$.

High-Temperature Heat-Content Measurements

R. H. Busey R. A. Gilbert

The extension of calorimetric measurements, using the Bunsen ice calorimeter, to systems involving fused fluorides led to the discard of the Nichrome V screw-top sample capsule previously employed. Experience, both here and at the National Bureau of Standards, showed that capsules with this type of closure tend to leak after

[26] R. H. Busey and R. B. Bevan, Jr., *Chem. Div. Ann. Progr. Rept. June 20, 1960*, ORNL-2983, p 8.

high-temperature operation. A new capsule, also made of Nichrome V but designed to be sealed by Heliarc welding, has been tested and found satisfactory for use with molten salts.

By use of this capsule, the heat of fusion of Li_3ThF_7 was determined.[27] In addition, it was found possible to calculate the liquid-soluble, solid-insoluble impurity content of the sample from careful measurements in the premelting region of the curve for heat content vs temperature. It was necessary to equilibrate the capsule in the furnace for as long as 24 hr in order to allow all the impurity to be "washed out" of the solid into the liquid phase. This long period was necessary because it was not possible to agitate the capsule during equilibration.

In Fig. 9.6, $1/r$ (r = fraction melted) for Li_3ThF_7 is plotted against the equilibrium temperature, and the best straight line has been calculated for the points up to $1/r = 11.68$. From this line the

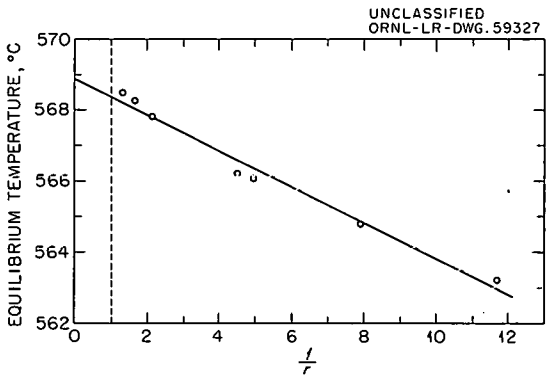

Fig. 9.6. Temperature of the Liquid-Solid Equilibrium for Li_3ThF_7 as a Function of the Reciprocal of the Fraction of Sample Melted.

melting point of the sample (temperature at $1/r = 1$) is found to be 568.4°C. The melting point of a pure sample of Li_3ThF_7 is 568.9° (temperature at $1/r = 0$), giving a freezing-point lowering of 0.5°C. By using the relationship

$$N_2 = \frac{\Delta H_f}{R(T_1^*)^2}(T_1^* - T),$$

where

N_2 = mole fraction of impurity,

ΔH_f = heat of fusion of major component,

R = gas constant (1.987 cal/deg),

T_1^* = melting point of the pure major component in °K,

T = melting point of the actual sample in °K,

the impurity content of the sample was calculated to be 0.5 mole %. The uncertainty in this value is estimated to be ±0.1 mole %.

The value agrees well with that obtained from R. E. Thoma of the Reactor Chemistry Division, who furnished the sample. He indicated a maximum impurity content from petrographic examination of 0.5 mole %.

MOLECULAR BEAM STUDIES OF CHEMICALLY REACTIVE COLLISIONS

Reactions of Atomic Hydrogen

S. Datz R. E. Minturn
E. H. Taylor

The construction of an apparatus for studying the reactions of a high-temperature atomic hydrogen beam was completed. The atomic hydrogen is formed by thermal dissociation of molecular hydrogen in a tungsten furnace which can be heated to *ca.* 3000°K, and the beam is formed by effusion through a slit in the furnace. After one stage of differential pumping, the beam is modulated at 1.08 kc by a mechanical chopper consisting of a slotted disk driven by a synchronous motor. Following a second stage of differential pumping, the modulated beam is collimated. Two different types of reaction zone are available. First, homogeneous gas reactions can be studied by intersecting the atomic beam with a molecular beam formed at an effusion source in which the temperature can be varied from room temperature to 20°K. Second, surface reactions can be studied by the introduction of a metallic surface at the beam intersection. The surface temperature and the beam-surface intersection angle can be varied.

The detector is a 135°-sector magnetic mass spectrometer with a radius of curvature of 2.5 cm. The mass spectrometer utilizes a modified Fricke ion source[28] and a permanent analyzer magnet (3000 gauss). Mass selection is achieved by varying the ion acceleration energy. The analyzed ion beam is focused onto the first dynode of a

[27] R. A. Gilbert and R. E. Thoma, *Reactor Chem. Div. Ann. Progr. Rept. Jan. 31, 1961*, ORNL-3127, p 23.

[28] G. Fricke, *Z. physik* 141, 166 (1955).

14-stage electron multiplier, and the output signal is coupled to the external system through a cathode follower. The modulated signal is then passed through a high-Q preamplifier[29] and into a phase-sensitive detector-integrator. The synchronizing signal is supplied by a light beam modulated by the beam chopper. The use of modulated beams and phase-sensitive detection allows better discrimination of beam signals from those arising from background gas. In addition, the choice of *ca.* 1 kc allows the observation of time shifts ranging from 50 to 500 μsec. These time shifts are caused, in crossed-beam experiments, by time-of-flight changes due either to mass or energy changes, and, in beam-surface reactions, by reaction time or adsorption time effects.

Preliminary experiments have been carried out on the gas phase reactions:

$$H + D_2 \longrightarrow HD + D ,$$

$$D + H_2 \longrightarrow HD + H ,$$

and on the catalytic hydrogen-deuterium exchange reaction on platinum.

Reactions of Alkali Metals

R. E. Minturn S. Datz
E. H. Taylor

A new apparatus for the study of chemical kinetics by the crossed-molecular-beam technique was designed and constructed. The vacuum box, 38 × 22 × 16 in. high, is of stainless steel and consists of a framework enclosed by flanges which permit complete accessibility to the interior working mechanisms. The box is divided into three vacuum chambers, each of which can be isolated from the others and from the vacuum pumps, so that minor adjustments can be made in a given chamber without interference with the rest of the system. As a result, downtime during operation due to such things as detector failure, beam source depletion, and the like can be kept to a minimum. Care was taken in design to provide considerable flexibility in the choice of the chemical system to be studied and in the type of beam source or detector to be utilized. Pressures of the order of 1×10^{-7} mm Hg or less are routinely obtained.

Construction has begun on a multidisk mechanical velocity selector designed to operate from 3000 to 24,000 rpm. When completed and installed, the selector will intercept one molecular beam so as to allow only molecules with a selected energy to reach the reaction center.

Collision Mechanics in Crossed Maxwellian Molecular Beams

S. Datz D. R. Herschbach[30]
E. H. Taylor

A general theoretical treatment of the mechanics of collision between two Maxwellian molecular beams was developed and was accepted for publication by the *Journal of Chemical Physics*. Expressions were obtained for the distribution in collision energy, for the elastic and reactive collision rates, and for the angular distribution of the center-of-mass vectors for beams colliding at any angle. The treatment can accommodate any reaction cross section which can be expressed as a step function multiplied by a linear combination of powers of the relative energy.

The recoil momentum which affects the product distribution in the laboratory system was discussed, and the treatment was applied to some experimental data on the reaction of potassium with HBr.

MASS SPECTROMETRY AND RELATED TECHNIQUES

Positive-Ion Intermediates in the Beta-Particle Radiolysis of Ethylene

C. R. Baldock T. W. Martin[31]

Positive ions induced in ethylene by beta particles have been identified and measured with a mass spectrometer. The relative proportions of primary and secondary ions thus produced were compared with the ions induced by 75-ev electrons as well as with the previously reported ions induced by alpha particles.[32] The results obtained

[29] F. T. May and R. A. Dandl, *Rev. Sci. Instr.* 32, 387 (1961).

[30] Department of Chemistry and Lawrence Radiation Laboratory, University of California.

[31] Summer employee from Vanderbilt University; present address: Department of Chemistry, Vanderbilt University, Nashville 5, Tennessee.

[32] C. E. Melton and P. S. Rudolph, *J. Chem. Phys.* 32, 1128 (1960); abstracted in *Chem. Div. Ann. Progr. Rept. June 20, 1960*, ORNL-2983, p 86.

for the secondary ions, using all three ionizing sources, are remarkably similar.

This work follows previous studies in the Laboratory of the ionization induced by alpha particles in the mass spectrometer[32-34] and is a part of our general program for investigating the ionization phenomena initiated by various modes of radiation.

The essential features of our research mass spectrometer[35] and the experimental techniques used in this type of study have been described previously.[32,34] The ion source was modified in a manner very similar to that employed in the alpha-particle study.[33] The present modification permitted us to study (1) ions produced by beta particles alone, or (2) ions produced by both the electrons from a thoria-iridium filament and beta particles, combined. For this investigation, 23 μg of Ni^{63} (β^- max = 0.063 Mev) was plated out on a 0.5-cm^2 nickel sheet which covered the bottom of the ion repeller. The Ni^{63} had a decay rate of approximately 10^6 dis/sec and produced a measured $C_2H_4^+$ parent-ion beam intensity of 200 ions/sec, or 4×10^{-17} amp, at a pressure of 0.01 mm Hg in the ionization chamber.

The general dependence of the parent and secondary ion abundance on pressure in the range 0.01 to 0.12 mm Hg for ethylene is shown in Fig. 9.7. As deduced from pressure studies, the three ions shown are interrelated by the interesting consecutive ion-molecule reactions which are displayed in the figure. The three curves, which show the variation in per cent abundance for ions involved in a series of consecutive reactions, completely corroborate the earlier study by the two previous investigators using alpha particles.[32] The only noticeable difference occurs in the parent-ion curve at low pressure, where the beta particles give about 20% fewer parent ions and, consequently, 20% more degradation ions (masses 26 and 27) than do the alpha particles (see Table 9.8). Further comparison of the data in Table 9.8 reveals the striking similarity between the ionization produced by the Ni^{63} beta particles and 75-ev electrons. This similarity may well be due in

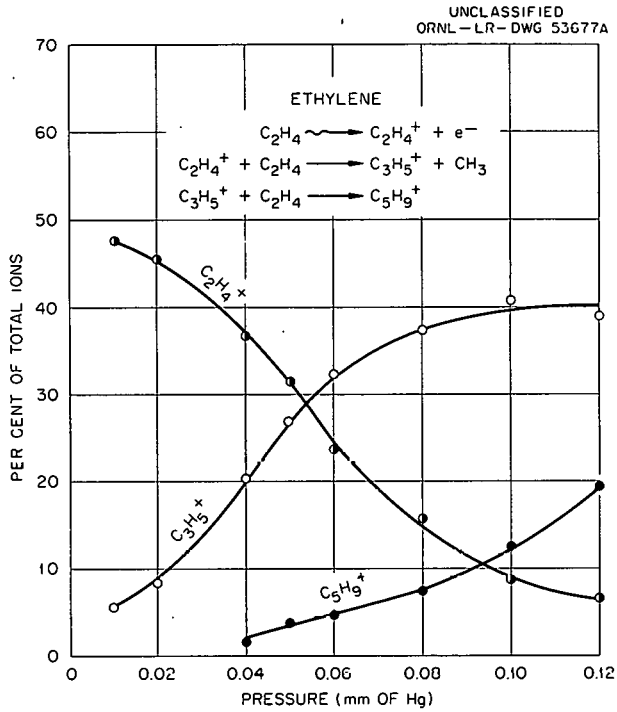

Fig. 9.7. Typical Curves Showing the Variation in Per Cent Abundance for Ions Involved in a Series of Consecutive Reactions.

Table 9.8. Percentage Abundance of Positive Ions Induced in Ethylene by Various Ionizing Sources ($p \cong 0.01$ mm Hg)

Mass (m/e)	Probable Ion	Po^{208} Alpha Particles[a]	Ni^{63} Beta Particles	75-ev Electrons
24	C_2^+			0.4
25	C_2H^+			1.6
26	$C_2H_2^+$	9.9	15.5	13.9
27	$C_2H_3^+$	21.6	26.6	22.1
28	$C_2H_4^+$	59.3	47.7	48.6
29	$C_2H_5^+$		5.0	6.6
41	$C_3H_5^+$	9.3	5.2	6.0

[a]Data obtained by Melton and Rudolph (ref 32).

[33]C. E. Melton and P. S. Rudolph, *J. Chem. Phys.* 30, 847 (1959).

[34]P. S. Rudolph and C. E. Melton, *J. Phys. Chem.* 63, 916 (1959).

[35]G. F. Wells and C. E. Melton, *Rev. Sci. Instr.* 28, 1065 (1957).

part, at least, to the fact that secondary electrons produced by beta particles striking the walls of the ionization chamber have contributed to the ion spectrum produced by the beta particles. Ions at masses 24 and 25, although observed, are not reported for the beta spectrum because of their low intensities.

This work further demonstrates the applicability of mass spectrometric studies in evaluating the effects of different ionizing radiation sources. It also represents the first direct use of beta particles as an ionizing source in the mass spectrometer. The general similarities in the ionic patterns of the parent ion and of the secondary ions produced from ethylene and initiated by entirely different radiation sources should be of interest to radiation chemists.

Ionization Processes in Argon, Krypton, and the C_2 Hydrocarbons Produced by 3.1-kev Electrons and Other Modes of Excitation[36]

C. E. Melton

Positive argon and krypton ions ranging in charge from one through eight were observed in our research mass spectrometer[37] when the respective neutral gases were bombarded with 3.1-kev electrons. For this study, the ion source of the instrument was modified by inserting electron accelerating plates between the thoria-iridium electron filament and the ionization chamber, as shown in Fig. 9.8. Marked similarities are manifest in the relative proportions of multiply charged argon and krypton ions produced by 3.1-kev electrons and those resulting from the β^- nuclear transitions in these gases, as shown in Tables 9.9 and 9.10. In Table 9.11, the relative proportions of argon ions of charge 3 and greater that are produced by 3.1-kev electrons are compared with those resulting from the electron capture–nuclear transition $Ar^{37} \rightarrow Cl^{37}$. The close agreement in the relative proportions of the multiply charged ions in these three tables suggests that the mode of ionization leading to multiple charges following initial excitation of the neutral molecules is the same. Namely, the atom loses an inner orbital electron in the primary ionization process: the resulting inner-shell vacancy is filled by an electron from the next outer shell by a secondary Auger process, and the energy from this radiationless transition results in the ejection of another

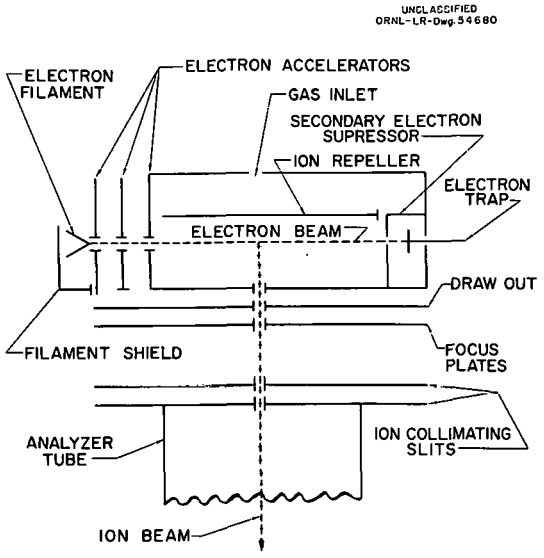

Fig. 9.8. Schematic Diagram of Mass Spectrometer Ion Source Employing High-Energy Ionizing Electrons.

[36] *Journal of Chemical Physics* (to be published).

[37] G. F. Wells and C. E. Melton, *Rev. Sci. Instr.* 28, 1065 (1957).

Table 9.9. Multiple Ionization in Argon

Charge	Mode of Excitation	
	3.1-kev Electrons,[a] Ar^{40}	β^- Decay,[b] $Ar^{39} \rightarrow K^{39}$
1	90.8%	86%
2	7.1%	10.5%
3	1.7%	2.5%
4	0.3%	0.8%
5	0.04%	0.3%
6	0.006%	<0.005%
7	0.003%	
8	0.0004%	
Average charge	1.11	1.19

[a] This study.

[b] T. A. Carlson, A. H. Snell, and F. Pleasonton, *IAEA Symposium on Chemical Effects of Nuclear Transformations, Prague, Czechoslovakia, Oct. 24–27, 1960.*

electron from the atom. Subsequent Auger processes accompanied by electron ejection continue until all inner-shell vacancies are filled, thus leaving the atom multiply charged.

In general, the relative proportions of fragment ions produced from either of the C_2 hydrocarbons by 3.1-kev electrons are not significantly different from those produced in the same compound by 75-ev electrons, as shown by the results in Tables 9.12–9.14. However, the abundances of the ions produced by intramolecular decomposition[38] (e.g., mass 24.1, Table 9.14) are from two to four times greater for the high-energy excitation. This observation is not in accord with that expected on the basis of the statistical theory[39] of intramolecular decomposition, wherein the rate of decomposition depends upon the random distribution of

Table 9.10. Multiple Ionization in Krypton

Charge	Mode of Excitation	
	3.1-kev Electrons,[a] Kr^{86}	β^- Decay,[b] $Kr^{85} \rightarrow Rb^{85}$
1	81.77%	79.25%
2	10.38%	10.95%
3	4.79%	3.91%
4	1.93%	3.12%
5	0.84%	1.51%
6	0.23%	0.66%
7	0.05%	0.40%
8	0.005%	0.19%
Average charge	1.13	1.14

[a]This study.

[b]A. H. Snell and F. Pleasonton, *Phys. Rev.* 107, 740 (1957).

[38]C. E. Melton, *Mass Spectrometry of Organic Ions* (ed. by F. W. McLafferty), Academic Press, New York, 1962.

[39]H. M. Rosenstock *et al.*, *Proc. Natl. Acad. Sci. U.S.* 38, 667 (1952).

Table 9.12. Ionization and Dissociation of Acetylene

m/e	Positive Ion	Relative Abundance	
		75 ev	3100 ev
12	C	1.45	1.29
12.5	C_2H^{2+}	0.02[a]	0.01
13	CH	3.70	3.53
14	CH_2	0.20	0.18
24	C_2	5.97	4.01
25	C_2H	21.13	19.60
26	C_2H_2	100.00	100.00

[a]Values underlined are significantly different.

Table 9.11. Multiple Ionization Processes in Argon

Charge	Mode of Excitation			
	β Decay,[a] $Ar^{39} \rightarrow K^{39}$	*K* Capture; $Ar^{37} \rightarrow Cl^{37}$		3.1-kev Electrons,[d] Ar^{40}
		Exp.[b]	Exp.[c]	
3	100	100	100	100
4	24	64	47	18
5	8.0	24	10	2
6	< 1.3	4	~3	0.3
7		0.5		0.2

[a]T. A. Carlson, A. H. Snell, and F. Pleasonton, *IAEA Symposium on Chemical Effects of Nuclear Transformations, Prague, Czechoslovakia, Oct. 24–27, 1960.*

[b]A. H. Snell and F. Pleasonton, *J. Phys. Chem.* 62, 1377 (1958).

[c]O. Kofoed-Hansen, *Phys. Rev.* 96, 1045 (1954).

[d]This study.

energy rather than the mode of excitation. It is possible that intramolecule decomposition of ions excited by high-energy electrons proceeds by a different path from that for ions excited by low-energy electrons.

Table 9.13. Ionization and Dissociation of Ethylene

m/e	Positive Ion	Relative Abundance	
		75 ev	3100 ev
12	C	0.94	0.76
13	CH	1.73	1.31
13.5	$C_2H_3^{2+}$	0.18[a]	0.10
14	CH_2	3.81	3.59
15	CH_3	0.39	0.37
24	C_2	3.09	1.80
24.1	$C_2H_4^+ \rightarrow C_2H_2^+ + H_2$	0.06	0.12
25	C_2H	9.60	5.81
26	C_2H_2	52.29	51.46
27	C_2H_3	62.12	64.99
28	C_2H_4	100.00	100.00

[a]Underlined values indicate significant differences.

Table 9.14. Ionization and Dissociation of Ethane

Mass	Positive Ion	Relative Abundance	
		75 ev	3100 ev
12	C	0.27	0.26
13	CH	0.50	0.40
13.5	C_2H_3	0.04[a]	0.03
14	CH_2	1.77	1.31
14.5	C_2H_5	0.39	0.23
15	CH_3	2.97	2.97
24	C_2	1.32	0.48
24.1	$C_2H_4^+ \rightarrow C_2H_2^+ + H_2$	0.04	0.10
25	C_2H	3.24	1.99
25.1	$C_2H_5^+ \rightarrow C_2H_3^+ + H_2$	0.05	0.13
26	C_2H_2	19.76	14.33
26.1	$C_2H_6^+ \rightarrow C_2H_4 + H_2$	0.17	0.39
27	C_2H_3	29.40	28.10
28	C_2H_4	100.00	100.00
29	C_2H_5	22.10	21.57
39	C_2H_6	29.55	29.20

[a]Underlined values are significantly different.

PUBLICATIONS

NUCLEAR CHEMISTRY

H. W. Schmitt and J. Halperin, "$Al^{27}(n,\alpha)Na^{24}$ Cross Sections as a Function of Neutron Energy," *Phys. Rev.* **121**, 827 (1961).

N. R. Johnson, E. Eichler, G. D. O'Kelley, J. W. Chase, and J. T. Wasson, "Decay of I^{134}," *Phys. Rev.* **122**, 1546 (1961).

R. L. Robinson, E. Eichler, and N. R. Johnson, "Decay of I^{132}," *Phys. Rev.* **122**, 1791 (1961).

ISOLATION AND CHEMICAL PROPERTIES OF SYNTHETIC ELEMENTS

G. E. Boyd and Q. V. Larson, "Solvent Extraction of Heptavalent Technetium," *J. Phys. Chem.* **64**, 988 (1960).

CHEMICAL SEPARATION OF ISOTOPES

G. M. Begun and W. H. Fletcher, "Partition Function Ratios for Molecules Containing Nitrogen Isotopes," *J. Chem. Phys.* **33**, 1083–85 (1960).

D. A. Lee, "The Enrichment of Lithium Isotopes by Ion Exchange. III. The Influence of the Nature of the Solution Phase on the Separation Factor," *J. Am. Chem. Soc.* **83**, 1801 (1961).

A. A. Palko and J. S. Drury, "Separation of Boron Isotopes. IV. The Methyl Sulfide–BF_3 System," *J. Chem. Phys.* **33**, 779 (1960).

L. L. Brown and J. S. Drury, "The Single-Stage Fractionation Factor for the System Oxygen vs Cobalt Di(Salicylal)-Ethylenediimine–Oxygen," *J. Chem. Phys.* **33**, 1889–90 (1960).

H. H. Garretson and J. S. Drury, "Isotopic Separation Factor for the System Potassium Amalgam–Aqueous Potassium Hydroxide," *J. Chem. Phys.* **34**, 1957–58 (1961).

J. S. Drury, R. H. Guymon and E. F. Joseph, "The Production of Low-Tritium Deuterium," *Chem. & Process Eng.* **42**, 220–24 (1961).

RADIATION CHEMISTRY

C. J. Hochanadel, "Radiation Chemistry of Water," pp 151–85 in *Comparative Effects of Radiation*, ed. by M. Burton, J. S. Kirby-Smith, and J. L. Magee, Wiley, New York, 1960.

C. J. Hochanadel, "Irradiation Effects in Aqueous Solutions," pp 384–88 in *Reactor Handbook*, 2d ed. vol I, ed. by C. R. Tipton, Interscience, New York, 1960.

C. J. Hochanadel, "Water Decomposition and Nitrogen Fixation," ibid, 878–81.

A. O. Allen and C. J. Hochanadel, "Suppression of Water Decomposition," U.S. Patent 2,937,981, 1960.

R. L. Durfee, "Energy Transfer in the Gamma Radiolysis of Isolated Nitrate and Nitrite Ions," doctoral thesis, Virginia Polytechnic Institute, 1960.

H. A. Mahlman, "The $G(OH)$ in the Co^{60} Radiolysis of Aqueous $NaNO_3$ Solutions," *J. Phys. Chem.* **64**, 1598 (1960).

P. S. Rudolph and S. C. Lind, "Kinetics of the Alpha Radiolysis of Carbon Monoxide," *J. Chem. Phys.* **33**, 705 (1960).

C. E. Melton and P. S. Rudolph, "Transient Species in the Radiolytic Polymerization of Cyanogen," *J. Chem. Phys.* **33**, 1594 (1960).

G. A. Ropp, C. E. Melton, and P. S. Rudolph, "Mass Spectrometric Test for an Intermediate in a Photochemical Reaction Involving Chlorine," *J. Chem. Phys.* **34**, 688 (1961).

S. C. Lind, *Radiation Chemistry of Gases*, Reinhold, New York, 1961.

ORGANIC CHEMISTRY

C. J. Collins, "The Pinacol Rearrangement," *Quart. Revs. (London)* **14**, 357 (1960).

C. J. Collins, "Some Aspects of Deuterium Isotope Effects in Mechanism Studies," *Ann. N. Y. Acad. Sci.* **84**(Art. 16), 603–7 (Nov. 1960).

V. F. Raaen and J. F. Eastham, "The Reaction of Cyanogen with Arylmethylmagnesium Halides," *J. Am. Chem. Soc.* **82**, 1349 (1960).

V. F. Raaen, A. K. Tsiomis, and C. J. Collins, "A Secondary Isotope Effect in the Formation of a Derivative of Acetophenone-β-C^{14}," *J. Am. Chem. Soc.* **82**, 5502 (1960).

M. M. Staum, *The Deamination and Rearrangement of erythro-1-Amino-1-phenyl-2-o-tolyl-2-propanol*, ORNL-3057 (June 1961).

J. H. Stocker, Padet Sidisunthorn, B. M. Benjamin, and C. J. Collins, "The Effect of Changing Reagent Upon Stereoselectivity," *J. Am. Chem. Soc.* **82**, 3913 (1960).

W. Davis, Jr., W. H. Baldwin, and A. B. Meservy, "Chemistry of the Intercycle Evaporator Incident of Nov. 20, 1959," ORNL 2979 (Nov. 9, 1960).

C. E. Higgins and W. H. Baldwin, "The Thermal Decomposition of Tributyl Phosphate," *J. Org. Chem.* **26**, 846 (1961).

CHEMISTRY OF AQUEOUS SYSTEMS

J. S. Johnson, K. A. Kraus, and G. Scatchard, "Activity Coefficients of Silicontungstic Acid; Ultra-Centrifugation and Light Scattering," *J. Phys. Chem.* **64**, 1867 (1960).

M. Eigen (Max Planck Institute for Physical Chemistry) and J. S. Johnson, "Kinetics of Reactions in Solution," *Ann. Rev. Phys. Chem.* **11**, 307 (1960).

F. Nelson, R. A. Day, Jr., and K. A. Kraus, "Anion Exchange Studies XXX. A Number of Elements in Ethylenediaminetetraacetic Acid Solutions," *J. Inorg. & Nuclear Chem.* **15**, 140 (1960).

K. A. Kraus and R. J. Raridon, "Anion Exchange Studies XXXI. Adsorption of Zn(II) and Ga(III) from HCl Solutions in the Temperature Range 25 to 150°," *J. Am. Chem. Soc.* **82**, 3271 (1960).

K. A. Kraus, "Some Applications of Radioisotopes in Physical Chemistry – Two-Phase Equilibria and Packed Column Techniques," *Proc. Intern. Atomic Energy Agency Conf. Use Radioisotopes in Phys. Sci. and Ind.*, Paper RICC-177, Copenhagen, Denmark, Sept. 6–17, 1960.

G. E. Boyd, S. Lindenbaum, and G. E. Myers, "A Thermodynamic Calculation of Selectivity Coefficients for Strong-base Anion Exchangers," *J. Phys. Chem.* **65**, 577 (1961).

M. H. Lietzke and R. W. Stoughton, "The Solubility of Silver Sulfate in Electrolyte Solutions. Part 7. Solubility in Uranyl Sulfate Solutions," *J. Phys. Chem.* **64**, 816 (1960).

R. S. Greeley, W. T. Smith, Jr., M. H. Lietzke, and R. W. Stoughton, "Electromotive Force Measurements in Aqueous Solutions at Elevated Temperatures. II. Thermodynamic Properties of Hydrochloric Acid," *J. Phys. Chem.* **64**, 1445 (1960).

M. B. Towns, R. S. Greeley, and M. H. Lietzke, "Electromotive Force Studies in Aqueous Solutions at Elevated Temperatures. III. The Standard Potential of the Silver–Silver Bromide Electrode and the Mean Ionic Activity Coefficient of Hydrobromic Acid," *J. Phys. Chem.* **64**, 1861 (1960).

R. S. Greeley, "An Operationally Defined pH Scale from 25° to 275°C," *Anal. Chem.* **32**, 1717 (1960).

ELECTROCHEMISTRY OF CORROSION

G. H. Cartledge, "Cathodic Processes in Corrosion," *Proc. AEC-Euratom Conf. Aqueous Corrosion Reactor Materials, Brussels, Belgium, October 1959*, TID-7587, pp 12–19 (1960).

G. H. Cartledge, "Chemische und elektrochemische Aspekte der Korrosion im Kernreaktor," *Korrosion 12, II Kongr. europ. Föderation Korrosion Frankfurt/Main, 1958* pp 1–11 (1960).

G. H. Cartledge, "The Comparative Roles of Oxygen and Inhibitors in the Passivation of Iron. I. Non-Oxidizing Inhibitors," *J. Phys. Chem.* **64**, 1877 (1960).

G. H. Cartledge, "The Comparative Roles of Oxygen and Inhibitors in the Passivation of Iron. II. The Pertechnetate Ion," *J. Phys. Chem.* **64**, 1882 (1960).

G. H. Cartledge, "Report on Conference on the Use of Radioisotopes in the Physical Sciences and Industry – Copenhagen, Denmark," ORNL Cf-60-10-22 (October 1960).

R. E. Meyer, "Cathodic Processes on Passive Zirconium," *J. Electrochem. Soc.* **107**, 847 (1960).

R. E. Meyer, "Self Diffusion of Liquid Mercury," *J. Phys. Chem.* **65**, 567 (1961).

NONAQUEOUS SYSTEMS AT HIGH TEMPERATURE

G. W. Parker, G. E. Creek, W. J. Martin, and C. J. Barton, "Fuel Element Catastrophe Studies: Hazards of Fission Product Release from Irradiated Uranium," ORNL CF-60-6-24 (June 30, 1960).

G. W. Parker, G. E. Creek, and W. J. Martin, "Fission Product Release from UO_2 by High Temperature Diffusion and Melting in Helium and Air," ORNL CF-60-12-24 (February 14, 1961).

G. W. Parker, "Fission Gas Release from Reactor Fuels," *Nuclear Safety* 2(4), 20 (1960).

M. A. Bredig, "Fused-Salt Equilibria. Metal-Metal Halide Systems," p 582 in *McGraw-Hill Encyclopedia of Science and Technology*, vol. 5, McGraw-Hill, New York, 1960.

M. A. Bredig, "The High-Temperature Cubic Phases of Uranium and Lanthanum Dicarbides," *J. Am. Chem. Soc.* **43**, 493 (1960).

M. A. Bredig and J. W. Johnson, "Miscibility of Metals with Salts. V. The Rubidium–Rubidium Halide Systems," *J. Phys. Chem.* **64**, 1899 (1960).

M. A. Bredig, "Reply to the Comments by W. Pfab and R. Nast on the paper, 'Polymorphism of Calcium Carbide,'" *Z. anorg. allg. Chem.* **304**, 98 (1960).

M. A. Bredig, H. A. Levy, F. J. Keneshea, and D. Cubicciotti, "The Volume of Dimeric Bismuth Monohalide Dissolved in Molten Bismuth Trihalide," *J. Phys. Chem.* **64**, 191 (1960).

H. A. Levy, M. A. Bredig, M. D. Danford, and P. A. Agron, "Trimeric Bismuth(I): An X-Ray Diffraction Study of Solid and Molten Bismuth(I) Chloroaluminate," *J. Phys. Chem.* **64**, 1959 (1960).

H. A. Levy, P. A. Agron, M. D. Danford, and R. D. Ellison, "Cell Dimensions and Space Group of Bismuth(I) Chloroaluminate," *Acta Cryst.* **14**, 549 (1961).

A. S. Dworkin, R. B. Escue, and E. R. Van Artsdalen, "Self Diffusion in Molten Nitrates," *J. Phys. Chem.* **64**, 872 (1960).

H. R. Bronstein, A. S. Dworkin, and M. A. Bredig, "Solutions of Metals in Molten Salts. Cerium in Cerium Trichloride," *J. Phys. Chem.* **64**, 1344 (1960).

H. R. Bronstein, A. S. Dworkin, and M. A. Bredig, "The Electrical Conductance of Solutions of Salts in Liquid Metals; Potassium Iodide in Potassium," *J. Chem. Phys.* **33**, 1843 (1961).

CHEMICAL PHYSICS

Ralph Livingston and A. J. Weinberger, "Atomic and Molecular Hydrogen Yields from Irradiated Acids," *J. Chem. Phys.* **33**, 499 (1960).

R. W. Holmberg, Ralph Livingston, and W. T. Smith, Jr., "Paramagnetic Resonance Study of Hyperfine Interactions in Single Crystals Containing α,α-Diphenyl-β-Picrylhydrazyl," *J. Chem. Phys.* **33**, 541 (1960).

Henry Zeldes and Ralph Livingston, "Paramagnetic Resonance Study of Irradiated Single Crystals of Calcium Tungstate," *J. Chem. Phys.* **34**, 247 (1961).

R. W. Holmberg, "A Paramagnetic Resonance Study of Hyperfine Interactions in Single Crystals Containing α,α-Diphenyl-β-Picrylhydrazyl," ORNL-3052 (Jan. 24, 1961).

W. R. Busing and H. A. Levy, "An IBM 704 Program for Interpreting the Results of Crystal Structure Refinements," *Computing Methods, Report of a Conference held at Glasgow*, pp 140–45, Pergamon, New York, 1961.

W. R. Busing and H. A. Levy, "Least Squares Refinement Programs for the IBM 704," *Computing Methods, Report of a Conference held at Glasgow*, pp 146–49, Pergamon, New York, 1961.

S. W. Peterson and H. G. Smith, "Anomalous Neutron Diffraction in α-Cadmium Sulfide," *Phys. Rev. Letters* **6**, 7 (1961).

E. H. Taylor, H. W. Kohn, and G. E. Moore, "The Use of Ionizing Radiation in Heterogeneous Catalysis," p 119 in *Large Radiation Sources in Industry*, International Atomic Energy Agency, Vienna, 1960.

H. W. Kohn, "Paramagnetic Studies of Radiation Damage in Silica Gel," *J. Chem. Phys.* **33**, 1588 (1960).

S. Datz, W. T. Smith, Jr., and E. H. Taylor, "Molecular Association in Alkali Halide Vapors," *J. Chem. Phys.* **34**, 558 (1961).

H. W. Kohn and B. M. Benjamin, "Radiation Coloration of Silica Minerals," *Am. Mineralogist* **46**, 218 (1961).

S. Datz, R. E. Minturn, and E. H. Taylor, "Multiple Aperture Slits for Molecular Beam Sources," *Rev. Sci. Instr.* **32**, 210 (1961).

S. Datz, "The Application of Molecular Beam Techniques to Chemically Reactive Collisions," *Proceedings of the Atomic and Molecular Beams Conference*, University of Denver, Denver, Colo. (1960).

C. E. Melton, T. W. Martin, and G. A. Ropp, "Evidence for Hydrogen Migration in a Negative Ion-Molecule Reaction," *J. Phys. Chem.* **64**, 1577 (1960).

C. E. Melton, "Charge Transfer Reactions Producing Intrinsic Chemical Change: Methyl, Methylene, and Hydrogen Radicals from Argon and Methane Reactions," *J. Chem. Phys.* **33**, 647 (1960).

C. E. Melton and P. S. Rudolph, "Transient Species in the Radiolytic Polymerization of Cyanogen," *J. Chem. Phys.* **33**, 1594 (1960).

G. A. Ropp, C. E. Melton, and P. S. Rudolph, "Mass Spectrometric Test for an Intermediate in a Photochemical Reaction Involving Chlorine," *J. Chem. Phys.* **34**, 688 (1961).

PAPERS PRESENTED AT SCIENTIFIC AND TECHNICAL MEETINGS

NUCLEAR CHEMISTRY

R. W. Stoughton,* J. Halperin, R. E. Druschel, F. J. Johnston, P. M. Lantz, J. H. Oliver, and G. W. Parker, "Measurements of Thermal Cross Sections and Resonance Integrals Using Pile Neutrons and Activation Techniques," International Atomic Energy Agency Symposium on Pile Neutron Research in Physics, Vienna, Austria, October 17–21, 1960.

E. Eichler,* R. L. Robinson, G. D. O'Kelley, and N. R. Johnson, "Decay of As^{74}," American Physical Society, Washington, D.C., April 24–27, 1960 [*Bull. Am. Phys. Soc.* [2]6, 228 (1961)].

E. Eichler, "Studies of Nuclear Level Schemes in the Medium-Weight Region," ORINS Traveling Lecture, Physics Journal Club, Cornell University, Ithaca, New York, April 10, 1961.

E. Eichler, "Nuclear Spectroscopy of Short-Lived Fission Products," ORINS Traveling Lecture, Chemistry Department Seminar, University of Buffalo, Buffalo, New York, April 12, 1961.

N. R. Johnson, "Decay of Re^{184} Isomers," American Physical Society, New York, New York, February 1–4, 1961 [*Bull. Am. Phys. Soc.* [2]6, 73 (1961)].

W. N. Bishop,* R. L. Wolke, E. Eichler, N. R. Johnson, and G. D. O'Kelley, "Ranges and Energy Loss of Tritons in Various Substances," American Physical Society, New York, New York, February 1–4, 1961 [*Bull. Am. Phys. Soc.* [2]6, 36 (1961)].

G. D. O'Kelley, "Decay Scheme Studies of Short-Lived Activities," Gordon Research Conference on Nuclear Chemistry, New London, New Hampshire, June 29, 1960.

G. D. O'Kelley, "Special Topics in Scintillation Counting," ORINS Radioisotopes Training School, Oak Ridge, Tennessee, August 5, September 16, 1960; January 23, March 17, May 12, 1961.

CHEMICAL SEPARATION OF ISOTOPES

A. A. Palko and J. S. Drury,* "Isotope Fractionation in BF_3 Systems," Gordon Research Conference on the Chemistry and Physics of Isotopes, New Hampton, New Hampshire, July 4–8, 1960.

G. M. Begun* and W. H. Fletcher, "Partition Function Ratios for Molecules Containing Nitrogen and Boron Isotopes," Gordon Research Conference on the Chemistry and Physics of Isotopes, New Hampton, New Hampshire, July 4–8, 1960.

J. S. Drury, "Separation of Isotopes," Eleventh Annual Nuclear Sciences Seminar, ORINS, Oak Ridge, Tennessee, November 30–December 13, 1960.

G. M. Begun* and L. Landau, "Mass Spectra and Metastable Transitions in Isotopic Nitrous Oxides," American Physical Society, Monterey, California, March 22, 1961.

RADIATION CHEMISTRY

C. J. Hochanadel, "Radiation Chemistry," ORINS Industrial Radioisotopes Training Course, Oak Ridge, Tennessee, August 22, 1960.

C. J. Hochanadel, "Radiation Chemistry," ORNL Biology Division, Oak Ridge, Tennessee, December 9, 1960.

---

*Denotes speaker.

C. J. Hochanadel, "The Nature of the Intermediates in Irradiated Water," Conference of the Subcommittee on Effects of Ionizing Radiations, Committee on Nuclear Science, NRC, Laboratoire Curie, Paris, France, April 27, 1961.

C. J. Hochanadel, "Radiation Chemistry," Colloquium on Radiation and Tracer Research Techniques, 14th Annual Reciprocal Meats Conference, University of Tennessee, Knoxville, Tennessee, June 22, 1961.

J. W. Boyle, "Radiation Chemistry of Aqueous Sulfuric Acid Solutions," Conference on Radiation Chemistry of Water, University of Notre Dame, Notre Dame, Indiana, March 23–25, 1961.

E. H. Taylor* and H. W. Kohn, "The Effect of Ionizing Radiation on Surface Properties of Silica Gel," 2nd International Congress on Catalysis, Paris, France, July 4–9, 1960.

H. W. Kohn* and E. H. Taylor, "Modification of Surface Properties of Silica Gel by Radiation," American Chemical Society, New York, New York, September 11–16, 1960.

ORGANIC CHEMISTRY

C. J. Collins, "The Use of Carbon-14 in Mechanism Studies," Midland, Michigan, Section of the American Chemical Society, March 20, 1961.

C. J. Collins, "Stereochemistry and Radiochemistry of Deamination Reactions," 8th Conference on Reaction Mechanisms, Princeton, New Jersey, September 7, 1960

C. J. Collins, "Stereochemistry and Radiochemistry of Deamination Reactions," (1) Conference on the Use of Radioisotopes in the Physical Sciences and Industry, Copenhagen, Denmark, September 15, 1960, (2) Imperial College, London, England, October 4, 1960, (3) Institut für Organische Chemie, der Universität, Munich, Germany, September 26, 1960, (4) Institut für Organische Chemie, der Universität, Heidelberg, Germany, September 27, 1960.

C. J. Collins, "Some Configurational Relationships," Institute for Chemistry, The University of Paris, Paris, France, September 31, 1960.

W. H. Baldwin, "P^{32} Labeled Organic Phosphorus Compounds," (1) Science Institute, Colorado State University, Fort Collins, Colorado, August 11, 1960, (2) Chemistry Seminar, Knoxville College, Knoxville, Tennessee, November 9, 1960.

W. H. Baldwin, "Natural Radiocarbon Dating," (1) Science Institute, Colorado State University, Fort Collins, Colorado, August 10, 1960, (2) East Tennessee Archeological Society, Knoxville, Tennessee, April 27, 1961.

W. H. Baldwin, "Reactions of Trialkyl Phosphates," Americal Chemical Society, Southeastern Regional Meeting, Birmingham, Alabama, November 3, 1960.

CHEMISTRY OF AQUEOUS SYSTEMS

J. S. Johnson,* K. A. Kraus, and G. Scatchard, "Activity Coefficients of Silicotungstic Acid: Ultracentrifugation and Light Scattering," American Chemical Society, New York, New York, September 11–16, 1960.

R. M. Rush, "The Ultracentrifuge," ORINS Lecture, Phi Beta Chi Scientific Fraternity, Centre College of Kentucky, Danville, Kentucky, April, 1961

K. A. Kraus, "Ion Exchange Chromatography," Purdue Summer Conference on Chromatography, Purdue University, Lafayette, Indiana, July 18–20, 1960.

K. A. Kraus, "Some Applications of Radioisotopes in Physical Chemistry – Two-Phase Equilibria and Packed Column Techniques," Paper RICC-177, International Atomic Energy Agency Conference on Use of Radioisotopes in the Physical Sciences and Industry, Copenhagen, Denmark, September 6–17, 1960.

K. A. Kraus, "Ion Exchange Separations," (1) Pittsburgh Conference on Analytical Chemistry and Applied Spectroscopy, American Chemical Society, February 27, 1961, Pittsburgh, Pennsylvania, (2) Chemistry Division Seminar, National Chemical Laboratory, Teddington, England, April 27, 1961, (3) Chemistry Division Seminar, National Chemical Laboratory, Teddington, England, May 4, 1961.

K. A. Kraus, "Physical Chemistry of Ion Exchange Resins," Chemistry Division Seminar, National Chemical Laboratory, Teddington, England, May 18, 1961.

K. A. Kraus, "Ion Exchange Properties of Hydrous Oxides," Chemistry Division Seminar, National Chemical Laboratory, Teddington, England, May 26, 1961.

K. A. Kraus, "Hydrolysis of Metal Ions," Chemistry Division Seminar, National Chemical Laboratory, Teddington, England, June 1, 1961.

G. E. Boyd, Co-Chairman of Panel Discussion on "Important Unsolved Problems in Ion Exchange," Gordon Research Conference on Ion Exchange, Tilton, New Hampshire, June 1961.

S. Lindenbaum, "Liquid Ion Exchangers," Gordon Research Conference on Ion Exchange, Tilton, New Hampshire, June 1961.

W. C. Waggener, "Spectrophotometry of Aqueous Solutions at High Temperatures and Pressures," (1) Department of Chemistry, Georgia Institute of Technology, January 26, 1961, (2) Department of Chemistry, University of Louisville, Louisville, Kentucky, February 23, 1961.

M. H. Lietzke, "High Temperature Solution Chemistry" and "The Use of High Speed Computers in Chemistry," Southwestern Louisiana Institute, Lafayette, Louisiana, November 21, 1960.

M. H. Lietzke, "The Use of High Speed Computers in Chemistry," Hamline University, St. Paul, Minnesota, February 27, 1961.

M. H. Lietzke, "High Temperature Solution Chemistry," University of Wisconsin, Madison, Wisconsin, March 3, 1961.

M. H. Lietzke and R. W. Stoughton,* "A Study of Eauilibria in Uranyl Sulfate Solutions at Elevated Temperatures from Solubility Data," American Chemical Society, New York, New York, September 11–16, 1960.

ELECTROCHEMISTRY OF CORROSION

G. H. Cartledge, "Effects of Iodide ons and Other Inhibitors in the Polarization of Iron," Gordon Research Conference, New London, New Hampshire, July 1960.

G. H. Cartledge, "Radioisotopes in the Physical Chemistry of the Corrosion Process and Its Inhibition," International Conference on the Uses of Radioisotopes in the Physical Sciences and Industry, Copenhagen, Denmark, September 1960.

G. H. Cartledge, "Electrochemical Studies on the Corrosion of Iron and Its Inhibition," (1) Central Institute for Industrial Research, Oslo, Norway, September 1960, (2) United States Steel Applied Research Laboratory, Monroeville, Pennsylvania, February 1961.

G. H. Cartledge, "Recent Studies with the XO_4^{n-} Inhibitors of Corrosion," Max-Planck-Institut für Metallforschung, Stuttgart, Germany, September 1960.

G. H. Cartledge, "Adsorption and Ion Exchange at the Corrosion Interface," Electrochemical Society, Houston, Texas, October 1960.

F. A. Posey, "Potentiostatic and Galvanostatic Studies on Passive Stainless Steel," Gordon Research Conference on Corrosion, New London, New Hampshire, July 1960.

R. E. Meyer, "Effects of Corrosion Films on Cathodic Properties," Electrochemical Society Meeting, Houston, Texas, October 1960.

NONAQUEOUS SYSTEMS AT HIGH TEMPERATURE

G. W. Parker,* G. E. Creek, and W. J. Martin, "Fission Product Release from UO_2 Under Simulated Reactor Accident Conditions," Conference on Nuclear Reactor Chemistry, Gatlinburg, Tennessee, October 12–14, 1960.

G. W. Parker,* C. E. Creek, W. J. Martin, and C. J. Barton, "Fuel Element Catastrophe Studies: Hazards of Fission Product Release from Irradiated Uranium," Conference on Aerosol Problems of Nuclear Reactors, AERE, Harwell, England, December 7–8, 1960.

M. A. Bredig, "Metal-Salt Solutions," Symposium on Recent Advances in the Chemistry of Fused Salts of the Division of Chemical Education, American Chemical Society, St. Louis, Missouri, March 27, 1961.

CHEMICAL PHYSICS

S. W. Peterson, "Anomalous Neutron Scattering in α-CdS," International Crystallographic Congress, Cambridge, England, August 1960, and Seminar in Modern Methods in Crystallography, Manchester, England, September 1960.

S. W. Peterson, "Neutron Diffraction and Structural Chemistry," Ohio State University, Columbus, Ohio, November 1960.

R. H. Busey,* R. B. Bevan, Jr., and R. A. Gilbert, "Low Temperature Heat Capacities and Magnetic Susceptibilities of K_2ReCl_6 and K_2ReBr_6," 15th Annual Calorimetry Conference, Gatlinburg, Tennessee, September 7–10, 1960.

C. R. Baldock* and T. W. Martin, "Positive Ion Intermediates in the Beta Particle Radiolysis of Ethylene," Tennessee Academy of Science, Knoxville, Tennessee, December 2–3, 1960.

C. R. Baldock, "The Investigation of Gas Phase Reactions by Means of a Mass Spectrometer," Auburn University, Auburn, Alabama, November 3, 1960.

C. E. Melton, "Studies of Reaction Rates, Free Radicals, and a Stable Intermediate from Catalytic Reactions of $CO_2 + D_2$ and $1\text{-}C_4H_8$," Symposium on Heterogeneous Reactions, American Chemical Society, New York, New York, September 11–16, 1960.

C. E. Melton, "Studies of Ionization, Excitation, and Charge Transfer Induced by High Energy Electrons in a Mass Spectrometer," International Conference on the Physics of Electronic and Atomic Collisions, Boulder, Colorado, June 12–15, 1961.

C. E. Melton, "Mass Spectrometric Studies of Transient Species Formed During Catalytic Reactions," (1) Vanderbilt University, Nashville, Tennessee, October 14, 1960, (2) Tennessee Academy of Science, Knoxville, Tennessee, December 2–3, 1960, (3) University of Louisville, Louisville, Kentucky, January 12, 1961, (4) Johns Hopkins University, Baltimore, Maryland, May 23, 1961.

THIS PAGE

WAS INTENTIONALLY

LEFT BLANK

ORNL-3176
UC-4 – Chemistry
TID-4500 (16th ed., Rev.)

INTERNAL DISTRIBUTION

1. C. E. Center
2. Biology Library
3–5. Research Library
6–26. Laboratory Records Department
27. Laboratory Records, ORNL R.C.
28. Reactor Division Library
29. A. M. Weinberg
30. J. P. Murray (K-25)
31. R. G. Jordan (Y-12)
32. J. A. Swartout
33–42. E. H. Taylor
43. E. D. Shipley
44. S. C. Lind
45. M. L. Nelson
46. W. H. Jordan
47. F. L. Culler
48. A. H. Snell
49. A. Hollaender
50. M. T. Kelley
51. W. D. Manly
52. K. Z. Morgan
53. T. A. Lincoln
54. A. S. Householder
55. C. S. Harrill
56. C. E. Winters
57. H. E. Seagren
58. D. Phillips
59. J. A. Lane
60. G. E. Boyd
61–68. M. A. Bredig
69. R. W. Stoughton
70. R. B. Briggs
71. G. W. Parker
72. C. J. Borkowski
73. G. H. Jenks
74. K. A. Kraus
75. H. A. Levy
76. R. S. Livingston
77. T. E. Willmarth
78. C. H. Secoy
79. C. J. Hochanadel
80. W. H. Baldwin
81. A. R. Brosi
82. R. N. Lyon
83. S. A. Reynolds
84. P. F. Thomason
85. E. G. Bohlmann
86. C. D. Susano
87. R. Livingston
88. G. H. Cartledge
89. E. R. Van Artsdalen
90. E. Lamb
91. R. W. Johnson
92. J. R. McNally, Jr.
93. G. D. O'Kelley
94. M. J. Skinner
95. D. S. Billington
96. H. G. MacPherson
97. J. L. Gabbard
98. R. H. Busey
99. J. J. Pinajian
100. D. W. Sherwood
101. C. R. Baldock
102. F. F. Blankenship
103. C. J. Collins
104. J. S. Drury
105. W. R. Grimes
106. J. S. Johnson
107. W. L. Marshall
108. H. F. McDuffie
109. G. J. Nessle
110. S. W. Peterson
111. G. A. Ropp
112. G. M. Watson
113. R. F. Newton
114. R. E. Thoma
115. D. R. Cuneo
116. P. S. Rudolph
117. J. D. Roberts (consultant)
118. G. T. Seaborg (consultant)
119. C. E. Larson (consultant)
120. E. P. Wigner (consultant)
121. B. Crawford (consultant)
122. T. H. Davies (consultant)

EXTERNAL DISTRIBUTION

123. H. Miller, Office of Isotope Development, AEC, Washington
124. R. H. Schuler, Radiation Research Laboratories, Mellon Institute, 4400 Fifth Ave., Pittsburgh 13, Pa.
125. Division of Research and Development, AEC, Washington
126. Division of Research and Development, AEC, ORO
127. Boeing Airplane Company
128. Union Carbide and Carbon Chemical Company (South Charleston)
129. North American Aviation, Inc.
130–709. Given distribution as shown in TID-4500 (16th ed. Rev.) under Chemistry category (75 copies – OTS)